



UNIVERSITÉ DE STRASBOURG

ÉCOLE DOCTORALE DE PHYSIQUE ET CHIMIE-PHYSIQUE

Institut Charles Sadron, CNRS UPR 22

THÈSE présentée par :

Eirini SKOUFA

Soutenance prévue le 17 Février 2022

Pour obtenir le grade de : **Docteur de l'Université de Strasbourg**

Discipline : *Génie des procédés*

Spécialité : *Procédés d'émulsification et de polymérisation*

Poly(thioether) micro- and nanoparticles produced by low energy emulsification devices and continuous-flow photopolymerization

Directeur de Thèse :	Christophe SERRA	Professeur, Université de Strasbourg
Rapporteur externe :	Eric FAVRE	Professeur, Université de Lorraine
Rapporteuse externe :	Nida SHEIBAT-OTHMAN	Directrice de Recherche, CNRS - Université Claude Bernard Lyon
Examinatrice interne :	Madeline VAUTHIER	Maîtresse de conférences, Université de Strasbourg

Sometimes words are not enough to describe how grateful I am for all the support I received from so many people during these three years. However, I will do my best to acknowledge all the people that were there for me during my Ph.D. journey.

Starting with a huge thank you to my three SUPERvisors, Christophe A. Serra, Madeline Vauthier and Michel Bouquey, who did not give up on me and they support me from the beginning till the end. Christophe said several times that “I am very resilient” and I could not believe it. But now that the end has come, I do realize that despite the difficulties I never gave up. All three of them were there to remind me that they believe in me and gave me courage every single moment.

In addition, I would like to thank my ITN project partners, especially Abraham Chemtob and Cuong M-Q Le (IS2M, Mulhouse, France), Michael Wörner and Iris Perner-Nochta (KIT, Karlsruhe, Germany) and Alexander Peschl (Mainz, Germany) for taking the time to discuss and advise me.

I also want to thank the people from administration and characterization platforms, who helped me to settle down, shared their knowledge with me and guided me during my experiments. And of course, I want to thank the two people who helped to build up the new device, Patrick Allgayer and Marc Basler.

Then I would like to thank all the CMP group in which I was part of. A special thank you to Laurence Oswald, who always had a solution for any problem that I encountered. Additionally, I would like to thank Delphine Chan-Seng, Wiebke Drenckhan, Leondro Jacomine and René Muller for the countless hours of scientific conversations and advices.

I could never forget to thank my beloved friends Imen, Andrea, Wasif, Eulalie, Javid and Ricardo, who were patient enough to listen to me every time when I was happy, crying or screaming.

Finally, I want to thank my family, my mom, Zoi, my sister, Elpida, and my uncle, Kostas, who believed in me more than anyone else and always stand next to me no matter what. And the most important person in my life, Vasilis, who was, is and will be my “happy place”, where all the difficulties seem so small and easy to overcome.

*“Nothing in life is to be feared, it is only to be understood.
Now is the time to understand more, so that we may fear less”*

Marie Curie

Thank you

RESUME DE THESE

TABLE DES MATIERES

Introduction	7
La réaction thiol-ène.....	7
Développement de nouveaux dispositifs d'émulsification.....	8
L'émulsifieur pneumatique à flux élongationnel (pRMX)	8
S'affranchir des problèmes de polymérisation pendant l'émulsification.....	10
Vers une production continue de nanoparticules de poly(thioéther).....	11
Production de particules de taille microscopique.....	12
Conclusion	13
Références	14

Introduction

Une miniémulsion huile-dans-eau (o/w) est un système hétérophasique contenant des nanogouttelettes (phase huile) dispersées dans une phase continue, aqueuse, non-miscible [1]. Les dispositifs conventionnels utilisés pour obtenir ces miniémulsions type rotor-stator et homogénéisateur haute pression, appliquent des forces de cisaillement au système et la taille des gouttelettes obtenues varie généralement de 100 à 500 nm, mais au prix d'un mauvais contrôle de la taille (dans le premier cas) ou d'une pression élevée (~2 000 bar, dans le second) [2,3].

Dans ce projet, de nouveaux dispositifs d'émulsification à faible énergie, fonctionnant à des pressions modérées (< 6 bar) ont été développés pour produire des micro- et nanoparticules de poly(thioéther) de tailles contrôlées grâce à la photopolymérisation de (mini)émulsions de thiol-ène.

La réaction thiol-ène

Le mécanisme réactionnel de synthèse de poly(thioéther) qui nous a intéressé dans ce projet est un processus de croissance par étapes à radicaux libres entre un alcène (R=CH₂) et un thiol (R-SH) et est résumé dans le Schéma 1 [4].

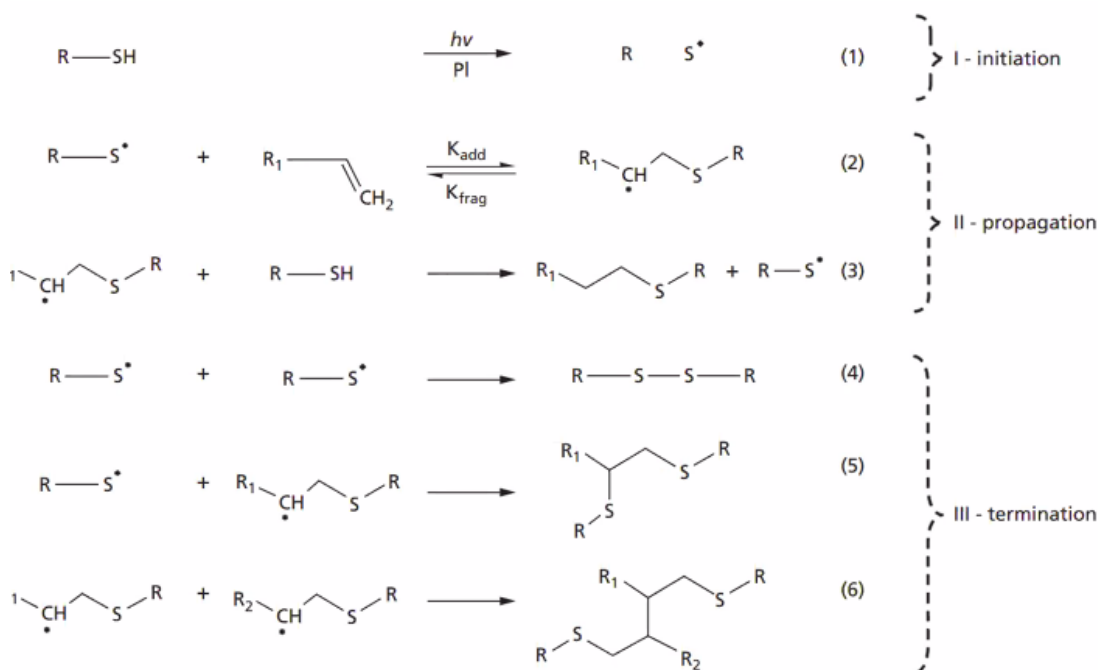


Schéma 1: Mécanisme de réaction thiol-ène [5]

Dans ce projet, il a été décidé de se focaliser sur le couple 2,2'-(ethylenedioxy)diéthanethiol (EDDT) / diallyl phtalate (DAP), tous deux difonctionnels. En effet, le but principal de ces travaux de thèse ne consiste pas à étudier la réactivité chimique de plusieurs couples thiol/alcène mais bien de développer, d'étudier et d'optimiser des procédés permettant la production de micro- et nanoparticules thiol-ène en grande quantité et avec un contrôle de taille (et de dispersité en taille).

L'hexadécane (HD, un agent anti-murissement d'Oswald), l'oxyde de diphenyle (2,4,6-triméthylbenzoyl) phosphine (DTPO, un photoamorceur organique) ou le phenyl-2,4,6-triméthylbenzoylphosphinate de lithium (LAP, photoamorceur aqueux), le 2,5-di-tert-butylhydroquinone (DBHQ, inhibiteur), le sodium dodécyl sulfate (SDS, surfactant) et l'eau distillée viennent s'ajouter à la constitution des phases dispersées et continues comme représenté dans le Tableau 1.

Tableau 1: Composition de référence (C₀) des phases dispersées et continues [5].

Phase Dispersée		Phase continue	
Composés	Concentration massique	Composés	Concentration massiques
Monomères : EDDT + DAP	20 w%	Eau	80 w%
HD	4 w%/monomères	SDS	3,5 w%/monomères
DTPO	2 w%/monomères	LAP	2 w%/monomères
DBHQ	1,05 w%/monomères		

Développement de nouveaux dispositifs d'émulsification

Dans tous les cas, avant d'introduire la solution dans le dispositif d'émulsification, les deux phases ont été mélangées par agitation magnétique pour obtenir une pré-émulsion. Une première mise sous vide de 10 min a été appliquée, suivie de 10 min de barbotage d'azote dans la solution afin d'éliminer l'oxygène dissout pour éviter le début de la polymérisation par l'oxydation du thiol.

L'émulsifieur pneumatique à flux élongationnel (pRMX)

Une grande partie de ces travaux de thèse visait à développer un nouveau dispositif d'émulsification à faible énergie fonctionnant à basse pression (6 bar) et

capable de produire des nanogouttelettes de manière contrôlée : l'émulsifieur pneumatique à flux élongationnel (pRMX) [6].

Le pRMX (Figure 1.a) se compose de deux pistons se déplaçant chacun dans une chambre en acier inoxydable de 35 mL toutes deux reliées entre elles par un élément de mélange en acier inoxydable, possédant un trou de 1 mm de diamètre. Les pistons fonctionnent en opposition de phase (1 cycle = 1 aller/retour des pistons). Ce système permet donc de générer un fort flux élongationnel au passage du trou, conduisant à une émulsification efficace, même pour des solutions très visqueuses. Après récupération de l'émulsion, la polymérisation des gouttelettes a été réalisée par irradiation UV à 365 nm dans un photoréacteur helicoidal [7] (Figure 1.b) pour établir un latex de poly(thioéther).

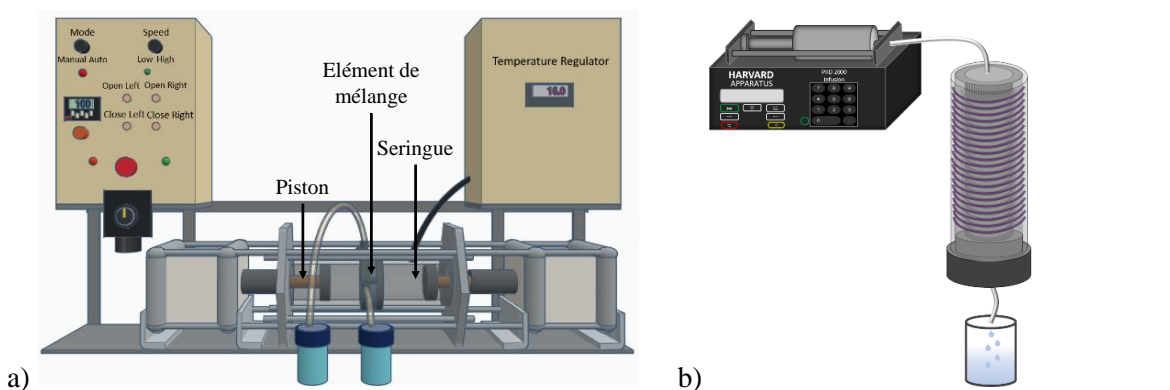


Figure 1: Schéma a) de l'émulsifieur pneumatique à flux élongationnel et b) du photoréacteur.

L'influence des paramètres de fonctionnement du pRMX (Figure 2.a) ainsi que la concentration relative des différents composés chimiques (Figure 2.b) sur la taille et la dispersité des gouttelettes a été étudiée par diffusion dynamique de la lumière (DLS).

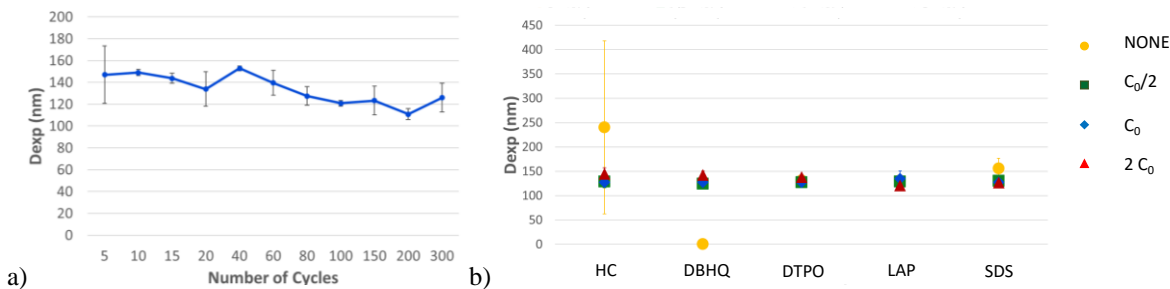


Figure 2 : Tailles des gouttelettes (avant polymérisation) en fonction a) du nombre de cycles réalisés avec le pRMX pour une concentration des composés chimiques égale à C₀ et b) de la concentration des composés chimiques pour un nombre de cycles égal à 100.

Une légère diminution du diamètre des nanogouttelettes, de 150 nm à 110 nm, est observée lors de l'augmentation due au nombre de cycles de 50 à 300. Il est

également intéressant d'observer qu'aucun des paramètres chimiques n'a une influence significative sur la taille des gouttelettes de plus de 100 nm. Ceci montre donc la puissance du pRMX: ses paramètres de fonctionnement ont bien plus d'influence sur le contrôle de la taille des gouttelettes que la composition chimique des phases.

Cependant, l'étude du rendement de la réaction de polymérisation, par résonance magnétique nucléaire du proton (^1H RMN), a révélé qu'il s'élevait déjà à 40% en sortie du pRMX. Ceci est probablement dû à la formation d'oligomères stables lors de l'émulsification. Ce point reste à optimiser, en introduisant par exemple une phase dispersée à base de poly(thioéther) et non à base de monomères.

S'affranchir des problèmes de polymérisation pendant l'émulsification

La nouvelle méthode développée dans cette partie est basée sur la dissolution des monomères (EDDT et DAP) dans un solvant avec lequel ils ne réagissent pas (acétone) afin de réaliser la photopolymérisation (Figure 1.b) avant l'émulsification. Cette méthode offre plusieurs avantages, mais le plus important est le contrôle de la réaction chimique, c.-à-d. le contrôle de la vitesse de polymérisation, et permet de surcroît de s'affranchir de la potentielle élévation de température dans le pRMX consécutive à un démarrage incontrôlé de la réaction de polymérisation.

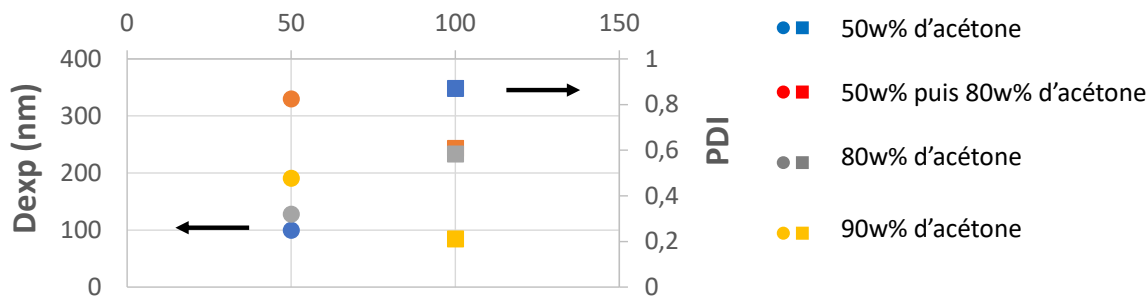


Figure 3 : Diamètre et PDI des particules de latex de poly(thioéther) préparées par photopolymérisation en solution. Nombre de cycles : 100.

La Figure 3 montre une variation du diamètre des particules de latex et de l'indice de polydispersité avec la concentration d'acétone introduite lors de la photopolymérisation. Les valeurs de PDI sont supérieures à 0,6 dans la plupart des expériences, ce qui n'est pas satisfaisant car cela reflète une polymodalité élevée de la distribution en taille du latex obtenu. En revanche, augmenter le pourcentage de solvant semble permettre d'avoir des nanoparticules plus petites

(200 nm de diamètre pour 90% d'acétone) avec un PDI très bas (proche de 0,2), ce qui est très encourageant et valide la viabilité de cette approche.

Ce système semble prometteur et reste à étudier avec de plus grandes quantités d'acétone.

Vers une production continue de nanoparticules de poly(thioéther)

Lors de ces trois ans, un dernier dispositif a été construit : le cpRMX. Le principe est le même que le pRMX à ceci près que le cpRMX doit fonctionner de façon continue, afin de pouvoir passer à des quantités de production supérieure (Figure 4). Il représente en soi une montée en échelle du procédé de production de nanoparticules de poly(thioéther).

Il se distingue du cpRMX par les faits i) qu'il est entièrement supervisé (température, pression) et contrôlé (démarrage, pression, température, arrêt d'urgence, nombre de cycles) par ordinateur, ii) que le débit d'émulsification est à présent asservi par la régulation de pression), iii) que les phases continues et dispersées sont injectées continuellement dans le dispositif via l'élément de mélange dont la conception très particulière autorise cette injection quelque soit la chambre qui se vide.

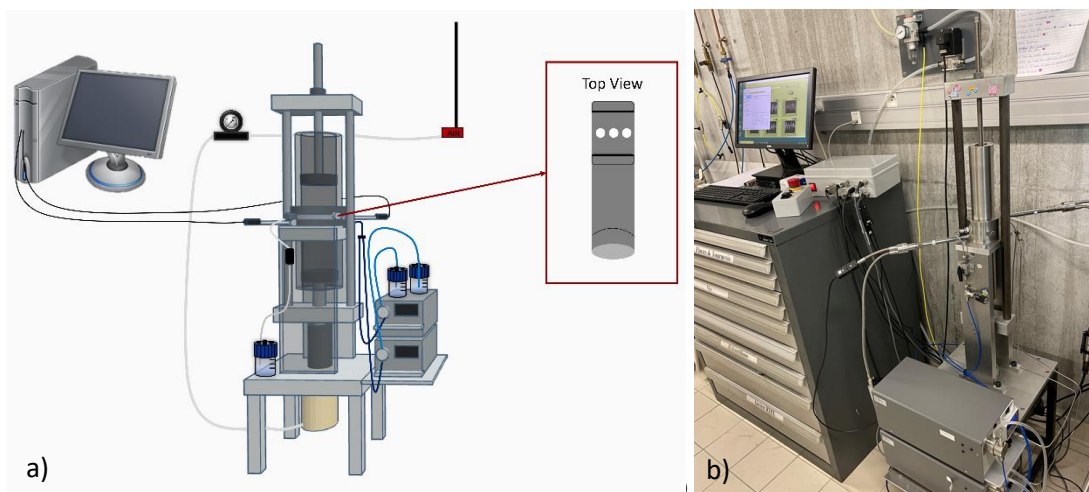


Figure 4: a) Schéma et b) photographie de l'émulsifieur pneumatique continu à flux élongationnel (cpRMX) et de l'élément de mélange (insert de droite du schéma a).

Production de particules de taille microscopique

Afin d'aller plus loin, il est également intéressant d'étudier la production en flux de microparticules de poly(thioéther) (Figure 5). Dans cette partie, il a été décidé de changer le EDDT (thiol difonctionnel) pour le triméthylpropane tris(3-mercaptopropionate) (TMPTMP, thiol trifonctionnel). En effet, ce système permettra de promouvoir des réticulations lors de la polymérisation et, donc, des microparticules plus solides et plus stables dans le temps. L'idée principale était de connaître l'effet de différents paramètres influençant la taille des particules produites (i) en faisant varier le débit de la phase dispersée (solution thiol-ène) tout en maintenant constant le débit de la phase continue (solution aqueuse de viscosité variable) et (ii) en faisant varier le débit de la phase continue tout en maintenant constant le débit de la phase dispersée. Dans les deux cas, l'influence de la viscosité de la phase continue (15 à 800 mPa.s) sur la taille et la dispersité en taille des microparticules a été étudiée (Figure 6).

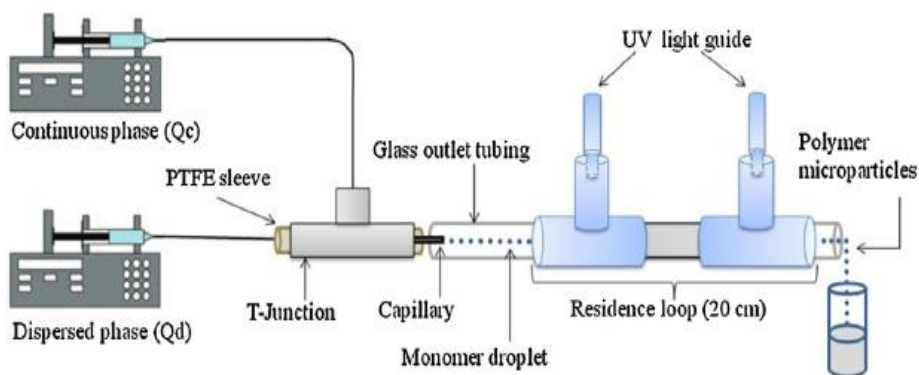


Figure 5 : Système microfluidique (jonction en T) utilisée pour la production en flux de microparticules de poly(thioéther) [8].

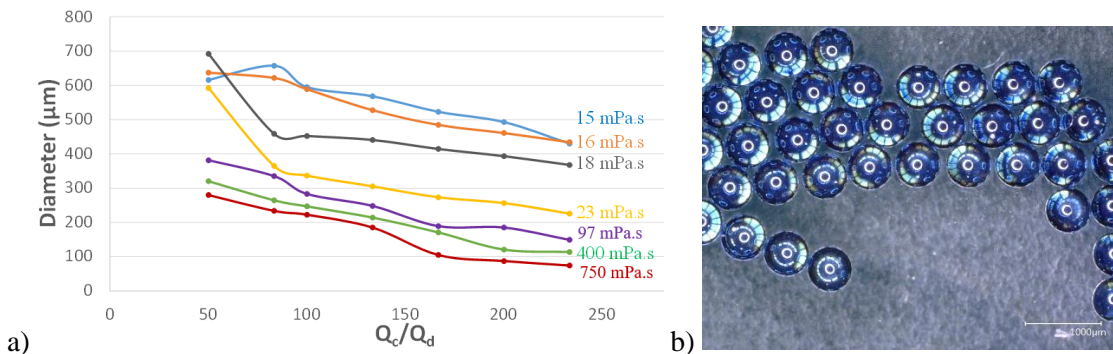


Figure 6 : a) Variation de la taille des microparticules de poly(thioéther) en fonction des rapports des débits pour différentes viscosités de la phase continue et b) microparticules obtenues pour un rapport de débit de phase continu et dispersée $Q_c/Q_d = 167$ et une viscosité de la phase dispersée de $\eta = 18$ mPa.s.

Ces résultats ont permis de confirmer que, peu importe les valeurs de débit des phases dispersées et continues (Q_d et Q_c respectivement), seul le rapport de débit Q_c/Q_d et la viscosité de la phase continue influencent la taille des microparticules. En revanche, les particules obtenues dans les différentes conditions sont toutes monodisperses, prouvant la fiabilité et la praticité de ce type d'appareillage.

Conclusion

Des miniémulsions de thiol-ène avec des tailles de gouttelettes nanométriques contrôlées ont été préparées en utilisant des dispositifs de miniémulsification à faible énergie. Ces dispositifs microfluidiques, dont un (cpRMX) fut développé pendant ces travaux de thèse, forment des nano-objets par allongement des gouttelettes. La modification des paramètres de procédé et chimiques a permis de déterminer les conditions optimales pour la production de latex thiol-ène et de contrôler leur taille et leur dispersité en taille ($PDI < 0,2$).

De plus, une nouvelle méthode pour produire des particules de latex, basée sur la photopolymérisation en solution, a été développée. Cette méthode a permis de s'affranchir des problèmes de pré-polymérisation du système lors de l'émulsification. Les résultats préliminaires sont prometteurs car ils montrent qu'une quantité élevée de solvant pendant la photopolymérisation (supérieure à 80%) peut fournir des nanoparticules monomodales d'environ 200 nm.

Enfin, des particules microscopiques (100-700 μm) ont également été produites en flux par microfluidique, démontrant l'importance des débits des phases dispersées et continues et de la viscosité de la phase continue sur la taille de ces objets.

A la suite de ce projet de thèse, il s'agira de continuer les essais de production de latex basée sur la photopolymérisation en solution en augmentant la quantité de solvant, de passer à une production continue des latex et de produire des microparticules de morphologies différentes (bâtonnets, cœur-écorce, Janus etc.).

Références

[1] S. Slomkowski *et al.*, "Terminology of polymers and polymerization processes in dispersed systems (IUPAC recommendations 2011)," *Pure and Applied Chemistry*, vol. 83, no. 12, pp. 2229–2259, 2011, doi: 10.1351/PAC-REC-10-06-03.

[2] S. Hall, M. Cooke, A. El-Hamouz, and A. J. Kowalski, "Droplet break-up by in-line Silverson rotor-stator mixer," *Chemical Engineering Science*, vol. 66, no. 10, pp. 2068–2079, 2011, doi: 10.1016/j.ces.2011.01.054.

[3] N. Thakur, G. Garg, P. K. Sharma, and N. Kumar, "Nanoemulsions: A Review on Various Pharmaceutical Application," *Global Journal of Pharmacology*, vol. 6, no. 3, pp. 222–225, 2012, doi: 10.5829/idosi.gjp.2012.6.3.65135.

[4] B. H. Northrop and R. N. Coffey, "Thiol-ene click chemistry: Computational and kinetic analysis of the influence of alkene functionality," *Journal of the American Chemical Society*, vol. 134, no. 33, pp. 13804–13817, 2012, doi: 10.1021/ja305441d.

[5] F. Jasinski *et al.*, "Thiol-Ene Linear Step-Growth Photopolymerization in Miniemulsion: Fast Rates, Redox-Responsive Particles, and Semicrystalline Films," *Macromolecules*, vol. 49, no. 4, pp. 1143–1153, 2016, doi: 10.1021/acs.macromol.5b02512.

[6] I. Souilem *et al.*, "A Novel Low-Pressure Device for Production of Nanoemulsions," *Chemical Engineering and Technology*, vol. 35, no. 9, pp. 1692–1698, 2012, doi: 10.1002/ceat.201100676.

[7] D. Parida *et al.*, "Coil flow inversion as a route to control polymerization in microreactors," *Macromolecules*, vol. 47, no. 10, pp. 3282–3287, 2014, doi: 10.1021/ma5001628.

[8] Z. Chang, C. A. Serra, M. Bouquey, L. Prat, and G. Hadziioannou, "Co-axial capillaries microfluidic device for synthesizing size- and morphology-controlled polymer core-polymer shell particles," *Lab on a Chip*, vol. 9, no. 20, pp. 3007–3011, 2009, doi: 10.1039/b913703c.

TABLE OF CONTENTS

GENERAL INTRODUCTION

Background Overview And Context..... 23

CHAPTER I. BACKGROUND LITERATURE

A A General Overview of Emulsions..... 31

1. Definition of Important Terms..... 31

2. Types of Emulsion 33

2.1 Water-in-Oil Emulsions (W/O)..... 34

2.2 Oil-in-Water Emulsions (O/W)..... 36

2.3 Multiple Emulsions 40

3. Stability of Emulsion 42

3.1 Gravitational Separation (Creaming/Sedimentation)..... 43

3.2 Flocculation..... 44

3.3 Coalescence 45

3.4 Ostwald Ripening..... 46

B The Thiol-Ene Reaction: A Crucial Reaction In Chemistry..... 47

1. General Information 47

2. Thiol-ene reactions that can occur..... 49

2.5 Thiol-Michael Addition Click Reaction 52

2.6 Self-Initiated Thiol-Ene Click Reaction..... 53

3. Applications 53

C Emulsification Methods 58

1. High-Energy Emulsification Methods 59

1.1 Ultrasound Generator..... 61

1.2 Rotor-Stator Mixer..... 65

1.3 High-Pressure Homogenizer..... 69

Table of Contents

1.4 Static Mixer	74
1.5 Membrane.....	79
2. Low-Energy Emulsification Methods.....	84
2.1 Spontaneous Emulsifications	84
2.2 Phase Inversion Temperature.....	85
2.3 Phase Inversion Composition	87
3. Microfluidics	87
<i>D</i> Conclusion	92
<i>E</i> Bibliography	93
 CHAPTER II. MATERIALS AND METHODS	
Preface.....	117
<i>A</i> Emulsification Devices	117
1. Some Theoretical and Historical Aspects of the Elongational-Flow Emulsification	117
2. Micro Elongational-Flow Reactor and Mixer (μ RMX).....	121
3. Pneumatic Elongational-Flow Reactor and Mixer (pRMX).....	125
4. Rotor-Stator Mixer	130
<i>B</i> Thiol-Ene Miniemulsion Formulation	131
1. Coarse Emulsion Preparation.....	133
1.1 Ambient Atmosphere.....	133
1.2 Inert Atmosphere.....	133
2. Miniemulsion Preparation	134
<i>C</i> Thiol-Ene Miniemulsion Photopolymerization	134
1. Linear Photoreactor (LP).....	135

Table of Contents

2.	Coiled Tube Photoreactor (CTP)	137
<i>D</i>	Characterization Techniques	139
1.	Dynamic Light Scattering (DLS).....	139
2.	Proton Nuclear Magnetic Resonance (¹ H NMR).....	140
<i>E</i>	Bibliography	141
 CHAPTER III. FROM THIOL-ENE MINIEMULSION TO THIOETHER LATEX NANOPARTICLES		
	Preface.....	147
<i>A</i>	Introduction	147
<i>B</i>	Thiol-Ene Miniemulsification and Photopolymerization	149
1.	Proton Nuclear Magnetic Resonance (¹ H NMR): Spectra Interpretation 149	
2.	Miniemulsions With Tetra-Functional Thiol And Bi-Functional Alkene .	154
2.1	Pneumatic Elongational-Flow Reactor and Mixer: Effect of Process Parameters and Surrounding Atmosphere	155
2.1.1	Four-Holes Static Mixing Element and Ambient Atmosphere	156
2.1.2	One-Hole Static Mixing Element and Inert Atmosphere	160
2.2	Pneumatic Elongational-Flow Reactor and Mixer: Effect of Chemical Parameters.....	162
2.3	System Stability.....	166
2.4	Rotor-Stator Mixer.....	168
3.	Bi-Functional Thiol and Bi-Functional Alkene	170
3.1	1,2-Ethanedithiol (EDT) and Diallyl phthalate (DAP)	170
3.1.1	Micro Elongational-Flow Reactor and Mixer (μRMX).....	172
3.1.2	Pneumatic Elongational-Flow Reactor and Mixer (pRMX).....	174

Table of Contents

3.1.3 Rotor-Stator Mixer	175
3.2 2,2'-(Ethylenedioxy)diethanethiol (EDDT) and Diallyl phthalate (DAP) 176	
3.2.1 Pneumatic Elongational-Flow Reactor and Mixer: Effect of Process Parameters	178
3.2.2 Pneumatic Elongational-Flow Reactor and Mixer: Effect of Chemical Parameters	180
3.2.3 System Stability	185
3.2.4 Pneumatic Elongational-Flow Reactor and Mixer: Temperature Control 187	
3.2.5 Rotor-Stator Mixer	189
3.3 Thiol-Ene Photopolymerization and Miniemulsification	191
<i>C</i> Conclusions	193
<i>D</i> Bibliography	195
CHAPTER IV. DEVELOPMENT OF A CONTINUOUS PNEUMATIC ELONGATIONAL-FLOW REACTOR AND MIXER	
Preface	201
<i>A</i> Continuous Pneumatic Elongational-Flow Reactor and Mixer (cpRMX) .	201
<i>B</i> Forecasted Experiments	205
<i>C</i> Operating Software Manual	208
<i>D</i> Bibliography	213
CHAPTER V. MICROFLUIDIC DEVICE FOR THIOETHER MICRON SIZE PARTICLES	
Preface	217
<i>A</i> Introduction	217

Table of Contents

<i>B</i>	Materials and Methods.....	219
1.	Co-Flow Microfluidic Device for Production of Microparticles	219
2.	Co-Flow Microfluidic Device for Production of Microrods.....	221
3.	Control of particle size	222
4.	Thiol-Ene Solution Formulation and Particles Characterization	223
<i>C</i>	Results and Discussion.....	224
1.	Thioether Microparticles.....	225
2.	Thioether Microrods.....	232
<i>D</i>	Conclusion	233
<i>E</i>	Bibliography	235
CONCLUSIONS AND PERSPECTIVES		
<i>A</i>	Context and Objectives	239
<i>B</i>	Results	240
1.	Chapter 3: From Thiol-Ene Miniemulsion To Thioether Latex Nanoparticles	240
2.	Chapter 4: Development Of A Continuous Pneumatic Elongational-Flow Reactor And Mixer.....	243
3.	Chapter 5: Microfluidic Device For Thioether Micron Size Particles	243
<i>C</i>	Perspectives	244
SCIENTIFIC PRODUCTION		
<i>A</i>	Articles	247
<i>B</i>	Oral Communications.....	247
<i>C</i>	Science Dissimination	247

GENERAL INTRODUCTION

Background overview and context

Polymers are present in life with many different fields, such as in polymer chemistry and physics, materials science as well as engineering. They can either be of natural or synthetic origin. Both categories are of a great importance in everyday life and can be found in cosmetics, food, drugs, implants, human body, etc. This wide range of applications is emanated from the very broad properties that polymers provide, that can be tailored according to the final application. Nowadays, there is an increased interest of the polymer industries on developing environmentally friendly processes.

Then, the fast reactivity along with the absence of side products of thiol-ene click reactions led to a very high demand on this chemistry. Indeed, these are of great interest to minimize the energy needed to obtain the thiol-ene based product as compared to other acrylate products that might need longer process times.

In this context, the present work is part of the European-funded Innovative Training Network (ITN) project of the H2020 program called PHOTO-EMULSION that has as a main goal the development of new eco-friendly polymerization technologies based on thiol-ene chemistry (Figure 1). The goal is to create a wide range of products and properties as well as to develop processes that need the least consumption of energy to provide more efficient products. To achieve this, two main processes that are widely used are established: the emulsification and photopolymerization. An emulsion consists of two liquids that are immiscible, such as water and oil, and depending on the droplet size and can be classified in macro- or mini-emulsions. Representative example of emulsion can be mayonnaise, where oil is mixed with vinegar and egg yolk, which plays the role of the emulsifier. Photopolymerization is used to obtain the final product called latex. It is worth mentioning that photopolymerization in dispersed media is the second largest polymerization process that has zero volatile organic compounds (zero-VOC). This means that the reduction of VOC by using ultraviolet light can improve the air quality, thus contributing to acquire a greener environment for the planet.

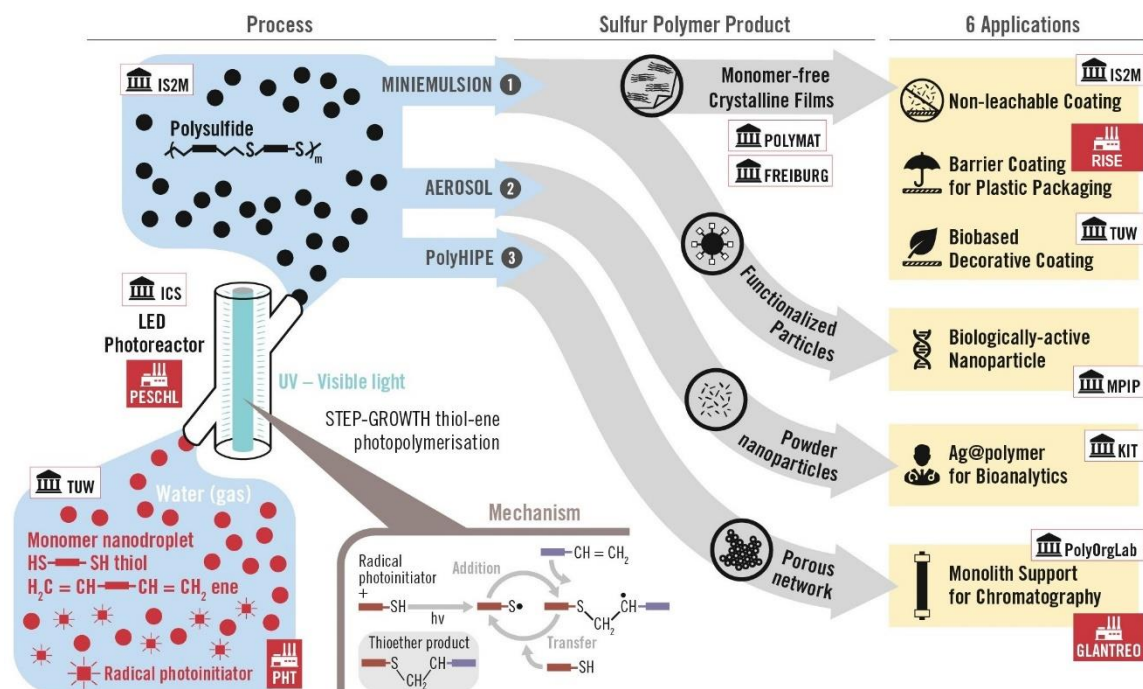


Figure 1. Overall schematic representation of ITN PHOTO-EMULSION (<https://www.photo-emulsion.uha.fr/>).

Variety of emulsification processes are used worldwide such as rotor-stator mixers and high-pressure homogenizers, but they have a bad impact on the environment since they use a big amount of energy. On account of this a novel device is developed, under the scope of this Ph.D. research, that works with the lowest amount of energy and is able to provide well defined thiol-ene miniemulsions. Regarding photopolymerization, a novel flow photoreactor is developed in this project, in order to use the UV light to polymerize the thiol-ene emulsion.

This manuscript comprises of five chapters, including a bibliographic section, a section where all devices used for this research will be described and three experimental sections.

In **Chapter 1**, the **literature background** is presented where a review on emulsions, its types, stabilization mechanisms and emulsification devices are described. Additionally, focus is also given on the thiol-ene reaction that is the chemistry that was used for the whole research of this project.

In **Chapter 2**, the **materials and methods** used for this research are delineated. Two innovative elongational-flow devices are used for the production of size-controlled thiol-ene miniemulsion. Additionally, a conventional rotor-stator device is used for comparison purposes. Another important point addresses the development of two flow photoreactors, where all the characteristics are described.

In **Chapter 3**, scrutinizes all the results obtained using the elongational-flow devices and flow photoreactors. Process parameters, such as number of cycles and mixing element, along with chemical parameters, such as the composition of the **miniemulsion** are assessed. The influence on the droplet size under the changes of the different parameters is thoroughly discussed. Comparison with conventional emulsification device is performed and the evaluation of the elongational-flow devices on the droplet diameter control is studied.

Chapter 4 is devoted to the depiction of the novel **continuous elongational flow device** that we developed. The aim is to obtain thioether latex in a continuous flow and with the least energy consumption by simply pumping monomer solution, emulsifying and photopolymerizing in a single process that is operating by a software.

In **Chapter 5**, instead of nano-objects, micro-objects are produced using microfluidic devices. The micro-objects that are developed are **thioether micro-particles** and microrods by slightly changing the experimental setup. The effect of the flow rate along with the viscosity of the continuous phase on the particle diameter control are investigated.

CHAPTER I
BACKGROUND LITERATURE

OUTLINE

<i>A</i>	A General Overview of Emulsions.....	31
1.	Definition of Important Terms.....	31
2.	Types of Emulsion	33
2.1	Water-in-Oil Emulsions (W/O).....	34
2.2	Oil-in-Water Emulsions (O/W).....	36
2.3	Multiple Emulsions	40
3.	Stability of Emulsion	42
3.1	Gravitational Separation (Creaming/Sedimentation).....	43
3.2	Flocculation.....	44
3.3	Coalescence	45
3.4	Ostwald Ripening.....	46
<i>B</i>	The thiol-ene reaction: a crucial reaction in chemistry	47
1.	General information	47
2.	Thiol-ene reactions that can occur.....	49
2.5	Thiol-Michael Addition Click Reaction	52
2.6	Self-initiated Thiol-Ene Click Reaction	53
3.	Applications	53
<i>C</i>	Emulsification Methods	58
1.	High-Energy Emulsification Methods	59
1.1	Ultrasound Generator.....	61
1.2	Rotor-Stator Mixer.....	65
1.3	High-Pressure Homogenizer.....	69
1.4	Static Mixer	74
1.5	Membrane.....	79

2.	Low-Energy Emulsification Methods.....	84
2.1	Spontaneous Emulsifications	84
2.2	Phase Inversion Temperature.....	85
2.3	Phase Inversion Composition	87
3.	Microfluidics	87
∂	Conclusion	92
ℰ	Bibliography	93

A A General Overview of Emulsions

1. Definition of Important Terms

A system in which distributed particles of one material are dispersed in a continuous phase of another material is called dispersion [1]. According to the International Union of Pure and Applied Chemistry (IUPAC), dispersion is a material comprising more than one phase where at least one of the phases consists of finely divided phase domains, often in the colloidal size range, dispersed throughout a continuous phase [1]. There are three major classes of dispersions based on the particle size: suspensions, colloids, and solutions [1]. A suspension is a heterogeneous mixture of solid particles that are spread throughout the liquid without dissolving in it. Typical particle size diameter is greater than 1000 nm which makes them sufficiently large for sedimentation [2]–[6]. On the contrary, a colloid is a heterogeneous mixture in which the dispersed particles do not settle out. The insoluble particles in the mixture have sizes between 1 and 1000 nm [4]–[10]. Finally, a solution constitutes a homogeneous mixture of two or more substances, where the one is dissolved in another. In this case the particles will not settle unlike to the suspension [11], [12].

On the other hand, dispersions can also be classified by the combination of the dispersed phase and the medium phase where the particles are suspended in [11]. First type is the gel, which is defined as a non-fluid colloidal network or polymer network that is expanded throughout its whole volume by a fluid [10], [13]. Second is the emulsion, which is a mixture of two or more liquids that are normally immiscible (unmixable or unblendable) [14]. Last class of dispersions is the aerosol, which consists of fine solid particles or liquid droplets in air or another gas [10], [15].

For the purpose of this chapter, focus will be given in emulsions. More specifically, an emulsion is defined as a biphasic system consisting of two immiscible liquids, with one of them being dispersed as small spherical droplets in the other liquid [16]–[20]. Emulsions are thermodynamically unstable, and consequently tend to collapse over time in order to minimize the interfacial area between the aqueous

and oil phase [19]. [21]. Due to this phenomenon, destabilization of emulsion can happen due to various physicochemical mechanisms, including gravitational separation, flocculation, coalescence, Ostwald's ripening and phase separation [19], [22]. There are two essential phases in order to form a stable emulsion; i) continuous phase, where the droplets are dispersed, and ii) dispersed phase, which are the dispersed droplets [17], [18], [23]–[25]. The use of an emulsifying agent, usually introduced in the continuous phase is essential to obtain a stable emulsion, by forming a thin film around the globules of dispersed phase [20], [26]. This agent is called surfactant. Depending on the type of the emulsion, surfactants vary. The selection of the appropriate surfactant is based on the Hydrophilic-Lipophilic Balance (HLB) of it [27]. HLB is a value to determine the hydrophilic or lipophilic degree of the surfactant as described by Griffin in 1945 [28] and 1954 [29] (Figure 1.1). Therefore, to enhance emulsions long-term stability, different stabilizers are incorporated in emulsion formulations apart from emulsifier, such as texture modifiers, ripening inhibitor and weighting agents.

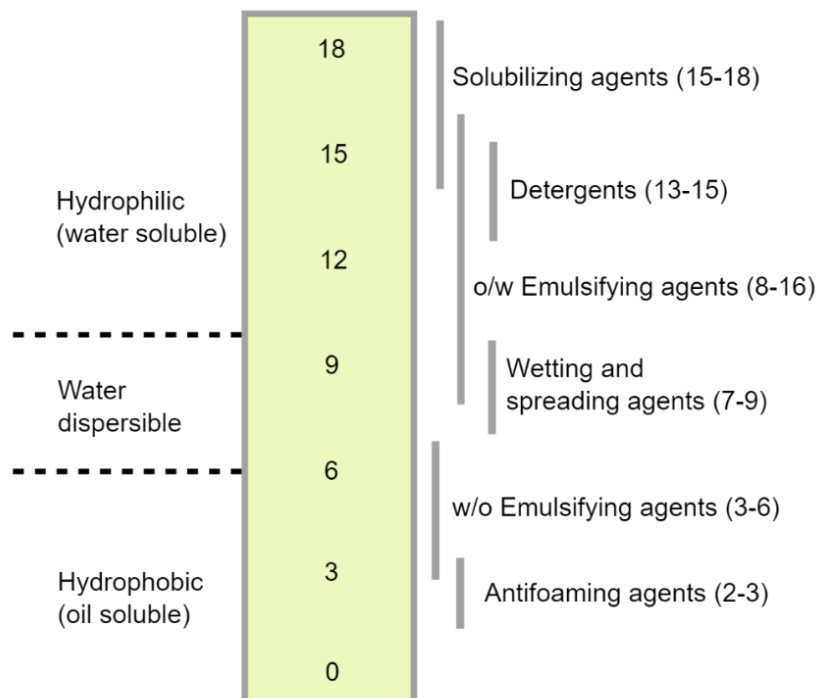


Figure 1.1. Hydrophilic-Lipophilic Balance (HLB) [30].

2. Types of Emulsion

Emulsions can be classified according to the relative spatial distribution of the different phases. First type of emulsions is oil-in-water (O/W), where oil droplets are dispersed in an aqueous phase, e.g. milk, mayonnaise, and ice-cream [31], [32]. Second type is water-in-oil (W/O) emulsion, in which water droplets are dispersed in an oil phase, e.g. butter and margarine [16][19]. The material that constitutes the droplets is usually referred as dispersed phase, internal phase or discontinuous phase, while the material that makes up the surrounding liquid is referred as continuous phase, external phase or dispersing phase. In addition of these two types of emulsions, multiple emulsions are also possible to create, such as oil-in-water-in-oil (O/W/O), water-in-oil-in-water (W/O/W), oil-in-water-in-water (O/W/W) (Figure 1.2). Regardless of their importance, multiple emulsions have limitations because of thermodynamic instability and their complex structure [26], [33].

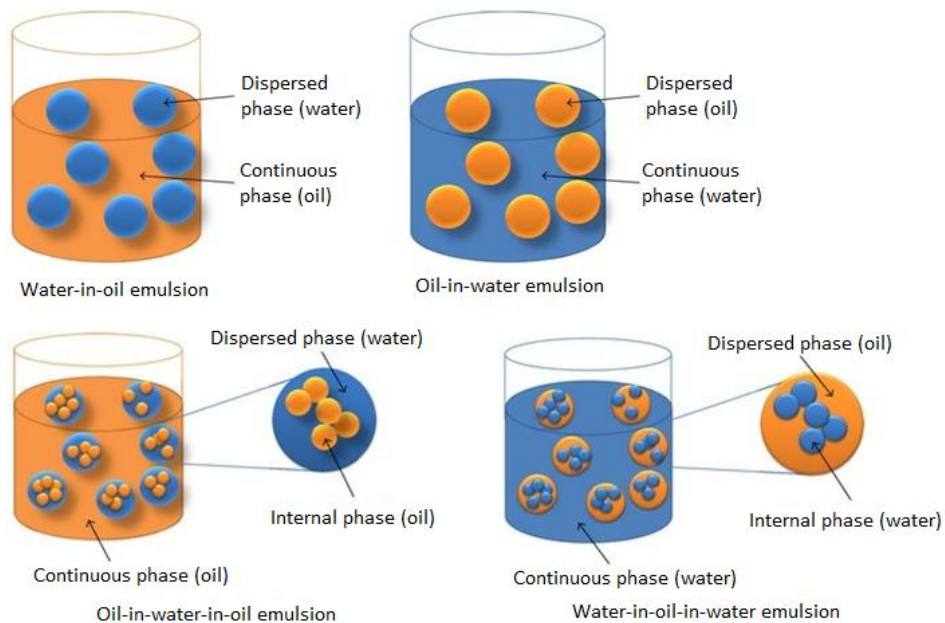


Figure 1.2. Types of emulsion [34].

Details about the different types of emulsions will be discussed in the following sections. This will lead to a better understanding of their main differences.

2.1 Water-in-Oil Emulsions (W/O)

A water-in-oil emulsion is the type of emulsion in which the continuous phase is usually composed of hydrophobic materials such as oil and the dispersed phase is usually water. These emulsions contain three substances: a solvent, a surfactant and water. The specific composition plays a very important role in the formation of W/O emulsions. According to the literature, emulsion stability is the most important asset. In the case of W/O emulsion, the appropriate surfactant to stabilize it has a low Hydrophilic-Lipophilic Balance (HLB), between 3 and 6 [35]–[37].

Since the last decade researchers focused on the influence of the emulsifier type and concentration in water-in-oil emulsion formation. The main characteristics that can change by varying the amount emulsifier are the droplet size, viscosity, interfacial tension between oil and water phases, etc. [38] Nesterenko *et al.* [39] investigated how the concentration of surfactant effects the droplet size. They prepared water-in-oil emulsion by using paraffin oil as the continuous phase mixed with a combination of two emulsifiers, hydrophobic silica particles and a non-ionic surfactant (Span 80). The continuous phase (70%) was first homogenized using a high-speed homogenizer (Ultra-Turrax) at maximum speed (24000 rpm) for 3 min. Then the dispersed phase (30%) was added drop wise and finally mixed with the same device for 5 min. After varying the concentration of surfactant between 0.1 and 1.8 wt%, they observed that the droplet size was decreased by increasing the amount of surfactant, while aggregates were formed in lower surfactant concentrations (0.1-0.2 wt%). This behavior was explained by the fact that the amount of surfactant was not enough to cover all the droplets and stabilize the emulsion. Moreover, Colucci *et al.* [40] made water in oil emulsions using natural oil, such as almond oil in order to prepare vesicles of aqueous cinnamon extract. Cinnamon extract is well known as a natural extract that has antimicrobial properties. The produced emulsions could be used in encapsulation of hydrophilic medicines, immobilizing enzymes or loading protein drugs. They prepared a 40/60 (v/v) water in oil emulsions to assure the high-volume fraction of water. During their experiments they varied the composition of the surfactant that was used so as to evaluate the stability of the different emulsions produced. They used different

mixtures of Span 80 (hydrophobic) with Tween 80 (hydrophilic) as well as Span 85 with Tween 80 so as to evaluate the droplet stability when the ratio between the two surfactants was changing. It was shown that by changing the ratio of concentrations of Span80/Tween80 from 54/46 to 80/20 smaller droplets were obtained while changing from Span80/Tween 80 to Span 85/Tween 80 for the same 80/20 concentrations, it was observed an increase in the droplet size of the emulsion. All of the different base emulsions were found to be not stable for more than two days. For this reason, they developed a high-pressure homogenizer (HPH) to increase the stability. It was found that a decrease on the droplet size was observed by increasing the number of cycles in the HPH but there is a limit since coalescence can occur by increasing the emulsification time (Figure 1.3). By using HPH they managed to obtain water in oil emulsions stable for up to 180 days, since it is lowering the collision efficiency.

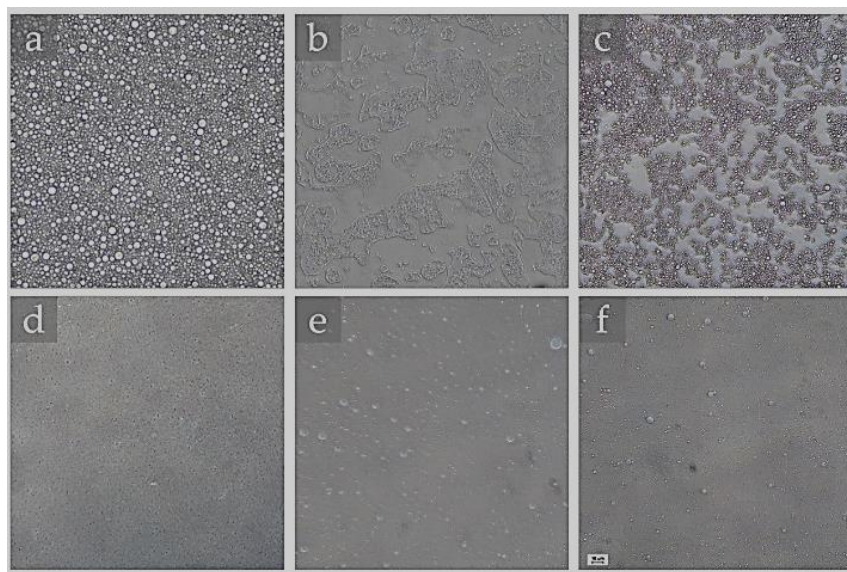


Figure 1.3. Optical microscopy of the produced 40/60 water-in-oil (W/O) emulsions. Primary emulsions: (a) S80/T80 54/46; (b) S80/T80 80/20; (c) S85/T80 80/20. After 12 high-pressure homogenizer HPH cycles: (d) S80/T80 54/46; (e) S80/T80 80/20; (f) S85/T80 80/20. Bar = 10 μm , 200 \times magnification [40].

Finally, Viswanathan *et al.* [41] worked on increasing the effectiveness of encapsulation of macromolecules by mobilizing them in non-aqueous medium. They prepared (water-in-oil)-in-oil emulsions by mixing water with different proteins and add it in a first oil solution of acetonitrile, dichloromethane, and lactic or glycolic acid by using sonicator. Then this first emulsion was combined with the second oil phase, which was liquid paraffin and Span 80 as surfactant. The volume ratios for

(w/o₁)/o₂ were 1:8:100. It was found that increasing the amount of the polymer in the first oil solution gave rise to a droplet size higher than 100 nm, but all the different samples were monomodal in distribution. Referring to the effect of polymer molecular weight to the droplet size, they show that increasing the molecular weight of the polymer led to the growth of the droplet size even by decreasing the polymer concentration in the emulsion. Also, they observed that for molecular weights higher than 170,000 g/mol aggregates started to form, which indicated the maximum limit on this parameter. In contrary, by decreasing the molecular weight, the droplet size was decreasing, and they had to increase the polymer concentration in the emulsion up to 31% to reach a higher droplet size, which was the desired. Their main target was a droplet size between 100 and 200 μm , so as to ensure maximum microencapsulation. Finally, some of their samples were monitored to have high loading efficiency by decreasing the molecular weight of the polymer.

Water in oil emulsions have a wide range of applications. Many research groups were focused on controlling the size of the droplets produced. The variation of different chemical properties such as, the ratio between the oil and water phase, showed a diameter change that was tuned depending on the different applications. On the other hand, oil in water emulsions show also an increased interest and some researchers tried with many ways to obtain stability over time along with droplet size control.

2.2 Oil-in-Water Emulsions (O/W)

An oil-in-water emulsion is formed when the oil is the dispersed phase and the water the dispersion medium or continuous phase. Typically to obtain an O/W emulsion the continuous phase occupies 45% of the total volume of the emulsion. Another key factor for as stable O/W emulsion is the use of an emulsifier which is soluble in the water phase and the HLB is high, between 8 and 16 [24], [35].

There was always an increased interest on oil-in-water miniemulsion formation and on the control of the droplet diameter according to the application. Huge amount of research is based on the biomedical field, for instance Delmas *et al.* [42], aimed

at extending the stability of miniemulsion produced from soybean oil mixed with water, using ultrasounds. Basically, they detected the droplet size and distribution while emulsifying and found that between 2 and 5 minutes of emulsification, a strong decrease on the droplet size of 120 nm occurred while the distribution was very broadened (Figure 1.4). Both dispersity and diameter decreased after 5 min of emulsification and remained constant from 12 to 30 min. Furthermore, they changed the power of the sonicator and discovered that the droplet size decreased with an increase of energy the first approximately 10 min and then it reached a plateau value. It is worth mentioning that this decrease was sharper in high powers. After evaluating the emulsification, they observed the storage time of the emulsion by applying different temperatures, ranging from 25°C to 70 °C and concluded that the temperature gave rise to the diameter of the droplets after almost 4 days. However, keeping the temperature constant at 25°C allowed the droplet size to remain almost the same through the 4 days of storage.

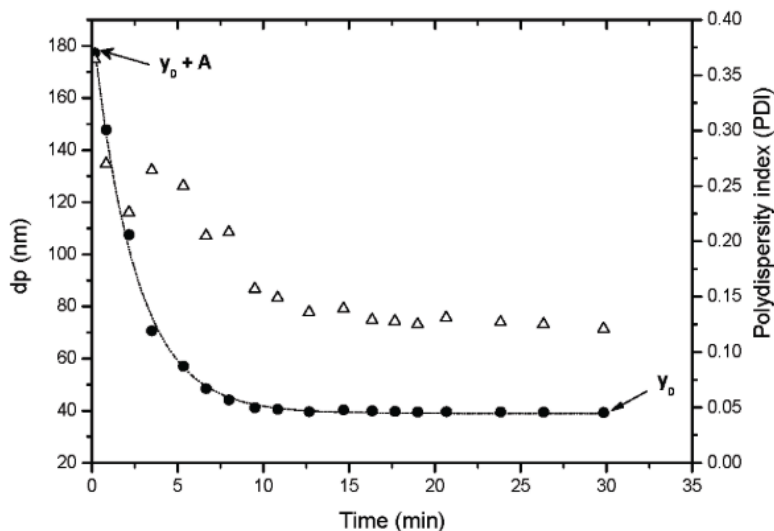


Figure 1.4. Complete monitoring during emulsification by ultrasonication: particle mean diameter (black disks), and polydispersity index (open triangles) [42].

Another very important field in which O/W emulsions are used is the food industry. A research group in Australia used again a sonicator to emulsify flax seed oil with water and monitor the droplet size [43]. Initially, they examined the impact of the surfactant (Tween 40) concentration, ranging from 1.5 wt% to 6.5 wt%, on the droplet diameter and observed a drop size ranging from 0.15 μm to 0.12 μm by increasing Tween 40 concentration. It can be explained by the area where the surfactant can be adsorbed (Figure 1.5): when the amount of Tween 40 is not

enough to cover and stabilize the droplets their coalescence led to an increase of the size. Thus, when the surfactant concentration was increased up to 2wt%, the surfactant molecules were enough to cover and stabilize the oil droplets. However, when the amount of surfactant was above 5 wt% no further decrease on the droplet size was observed. Moreover, they figured out that even though the droplet diameter was decreasing by applying more time of mixing, there was an overprocessing effect happening that when the energy applied to the system increased more than 200 W the diameter of the droplets increased too. This overprocessing effect occurred in many different devices during emulsification and will be explained later on this Chapter.

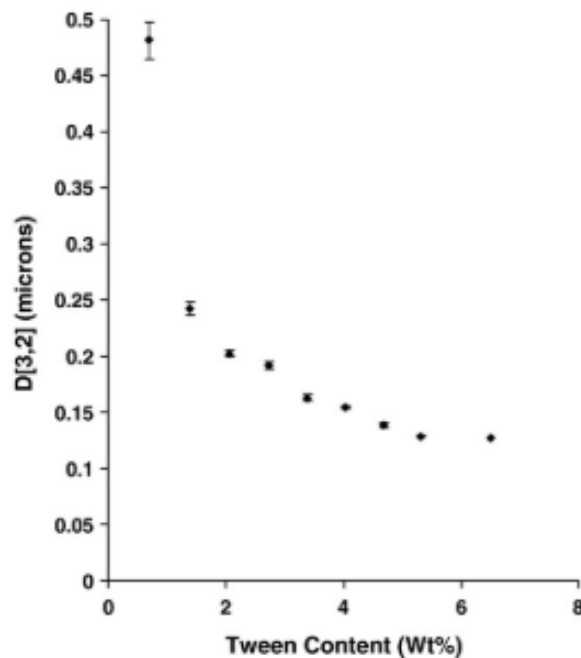


Figure 1.5. The effect of Tween 40 content on the particle size [43].

Another research group tried to strengthen the droplet growth by evaluating the influence of the oil phase concentration as well as the existence of a co-surfactant [44]. The emulsion produced was composed of sunflower oil with water and Tween 80, while Span 80 was the co-surfactant. Sonicator was applied for 10 min and the oil amount was slowly increased from 1.5 wt% up to 15 wt%. A slight initial decrease was obvious when the amount of oil was close to 2.5wt%, whereas a further increase led to a 100 nm increase on the droplet size at 15wt% of oil content (Figure 1.6).

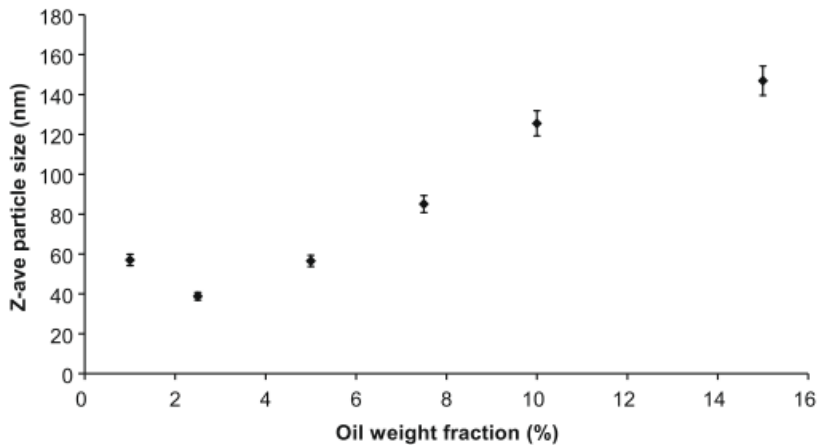


Figure 1.6. The effect of oil concentration on the average droplet diameter of emulsions [45].

Based on this study, Ashokkumar's team decided to keep the oil concentration at 15 wt% and add different amounts of co-stabilizer. The droplet size was measured with an initial concentration of Span 80 at 1.5wt% (diameter equal to 160 nm) but the further addition until 6 wt% revealed a diameter decrease down to 150 nm (Figure 1.7). More increase of Span 80 content started to show an increase of the droplet size which can be attributed to the fact that Span 80 is a hydrophobic emulsifier, and the higher amount did not allow the oil-in-water droplets to stabilize.

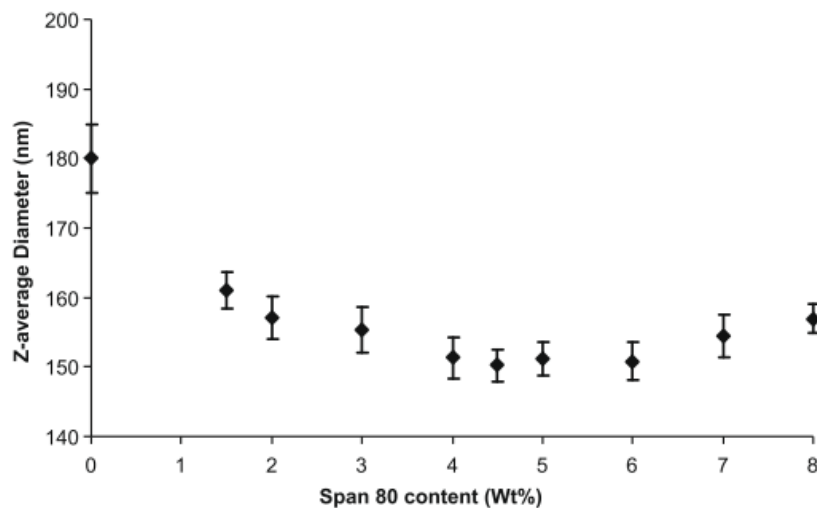


Figure 1.7. The effect of increasing Span 80 content on the average droplet diameter of emulsions [45].

Research has shown that the amount of surfactant added to the system is capable of stabilizing the emulsion and provide droplet control. Oil-in-water emulsions as well as water-in-oil emulsions both can be stabilized by using a single surfactant, either water or oil soluble respectively. In contrast, multiple emulsions need two

types of surfactants in order to stabilize, one water soluble (high HLB) and one oil soluble (low HLB) and details will be discussed in the following chapter.

2.3 Multiple Emulsions

Complex or multiple emulsions such as water-in-oil-in-water (W/O/W) and oil-in-water-in-oil (O/W/O) can also be formed. Most common way of stabilizing these emulsions is by using a combination of hydrophilic, high HLB, and hydrophobic, low HLB, surfactants, whose ratio plays the most important role in their stability. Generally, multiple emulsions are often called liquid membrane systems considering that the internal phase can be miscible with the continuous phase and the immiscible phase works as a thin semi-permeable film [46]. They illustrate several advantages as compared to the simple emulsions, such as the fact that the encapsulated compounds can be both hydrophilic and hydrophobic and they are protected from undesired or premature release. This allows higher amounts of material to be enclosed [46]. The aforementioned advantages provide many applications such as in pharmaceutical [47], [48] and food industries[49], [50].

There are three fundamental methods that are widely used for producing multiple emulsions: , phase inversion [51], [52], one- [53], [54] and two-stage emulsification [55], [56]. The latter is the one that is mostly used and provides stable, well-defined and low polydisperse multiple emulsions [49], [57]–[59]. In the late 90s, Matsumoto *et al.* [60] were the first one to display a simple two stage emulsification process. Several years later, Okochi & Nakano, [61], developed further the two-stage emulsification process by producing stable W/O/W emulsions that would work as carriers of different peptides and exhibit great drug entrapment effectiveness. They used castor oil derivatives for the oil phase and saline for the aqueous phase and mixed them primarily using a rotor-stator device for 10 min. Basically, the internal water phase containing the drug was mixed first with the oil phase and on the second step the derived emulsion was mixed with the continuous phase. They demonstrated a drastic droplets' size decrease, from 100 μm down to 7 μm , when the rotational speed increased from 1000 rpm up to 75000 rpm, while a further increase did not provide that big drop in the diameter (Figure 1.8). For speed higher

than 10,000 rpm the droplet size reached a plateau value of approximately 5 μm . Sadly they observed that the entrapment efficiency from 100% in 1000 rpm was diminished down to 70% when the speed was at max 20,000 rpm.

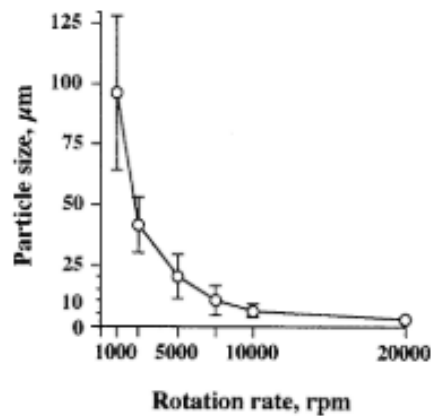


Figure 1.8. Relationship between rotation rate and particle size, $t = 10$ min [62].

Later in 2005, a research group in Germany produced W/O/W with a two-stage emulsification, that can be used in the food industry [63]. The main goal was to amplify an automated image analysis in order to estimate the droplet size and distribution. First, they encapsulated a water-soluble polymeric dye in sunflower oil by using a rotor-stator system to obtain W_1/O emulsion. Then they used a membrane emulsification to produce the multiple $W_1/O/W_2$ emulsions, where whey protein isolate was used as surfactant so as to stabilize the final product. In membrane emulsification there are several factors that influence the droplet size, but a detailed overview is given later on this Chapter. A very important factor is the wall shear stress, which is based on the velocity of the continuous phase. In Figure 1.9, the decrease of droplet size was evaluated under the increase of the wall shear stress.

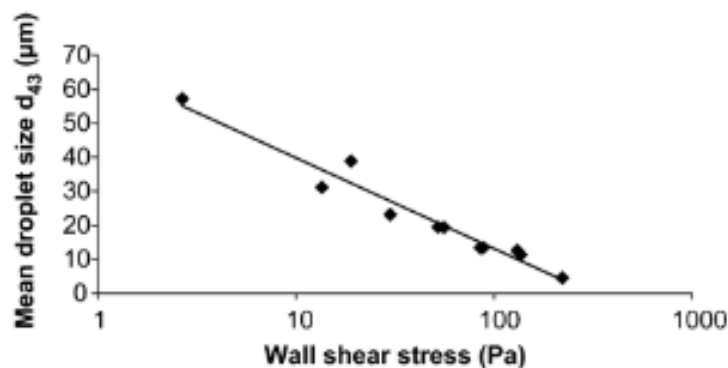


Figure 1.9. Development of the oil droplet size of multiple emulsions on wall shear stress [63].

From the data given in their work, it also becomes evident that an increase of viscosity and velocity of the outer aqueous phase led to a lowering of the droplet size from 55 μm down to 5 μm . Finally, they managed to confirm that the results obtained by their newly developed automated image processing were similar with the ones of the lighting microscopy referring in the droplet characteristics. As it was evocated in the beginning of this chapter, the stability of the emulsion plays the most crucial role. Researchers tried different types of surfactants and evaluated the stability as well as the droplet size of the different emulsions. In the following section the different mechanism that can influence the stability of the emulsion will be described in detail.

3. Stability of Emulsion

The most important criterion for producing emulsions is their stability [26]. Emulsion's stability is defined as the ability of the system to resist in physicochemical changes over time [16]. It is crucial to obtain stable emulsions for many applications including food products [64], [65], cosmetics [66], [67] or pharmaceuticals [68], [69] for instance. In order to reach thermodynamic stability, four major factors need to be taken into account: flocculation, creaming/sedimentation, coalescence and Ostwald ripening (Figure 1.10) [19], [70], [71].

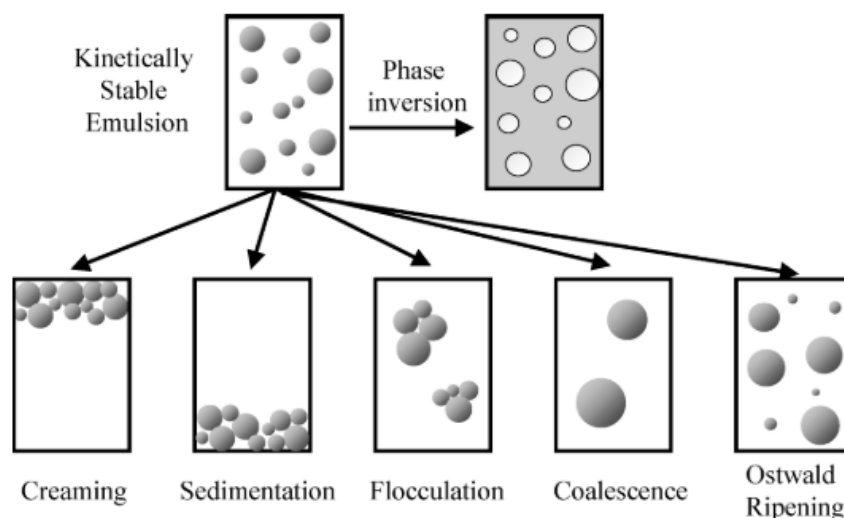


Figure 1.10. Schematic diagram of most common instability mechanisms that occur in food emulsions: creaming, sedimentation, flocculation, coalescence, Ostwald ripening and phase inversion [16].

In case one of the aforementioned phenomena occurred then a thermodynamically unstable emulsion will be recovered [70]. An unstable system means that there is a spontaneous predilection of the two liquids to separate and reduce the interfacial area, and therefore the interfacial energy between the two phases [19], [72]. The destabilization factors involve either changes in primary droplet size, e.g. coalescence and ripening, or spatial rearrangement of droplets with respect to each other and with respect to an external frame of reference, e.g. flocculation and aggregation [19], [73]. The physical and chemical parameters that can be tuned to control destabilization of the emulsions are the droplet size distribution, the amount of the dispersed phase, the viscosity of the continuous phase, the temperature, the pH of the solution but most importantly is the class of emulsifier that would be chosen to stabilize the system [19].

3.1 Gravitational Separation (Creaming/Sedimentation)

Gravitational separation is one of the most important types of destabilization in emulsion-based products, such as food [74], [75], cosmetics [76], [77], pharmaceuticals [78], [79] etc. During this process, a destabilization of the emulsion occurs, which is due to different forces applied to the system, such as gravity, centrifugal acceleration or electromagnetism [80]. This happens on account of the density difference between the droplets and the surrounding liquid, meaning that if the droplets have lower density than the continuous phase they will tend to go up, which will lead to a creaming of emulsion [81], while if they are heavier they will move downwards, where sedimentation will be formed [16], [80], [82]–[85]. Additionally, this separation is influenced by hydrodynamic and colloidal interactions between droplets, the physical state of the droplets, the rheology of the continuous phase, the electrical charge on the droplets and the nature of the interfacial membrane [80], [81], [83].

Emulsions that comprise of a big variation of droplet sizes are more likely to destabilize. In the case of creaming, the bigger droplets will go on the upper surface much faster than the smaller ones. This will lead to visible creamier layer on the top of the solution, while on the bottom may still the small droplets be dispersed. This means that the creaming formation might not be so obvious in

some cases as compared to others. In case of an emulsion system where flocculation is already observed, it is more likely that the droplets will undergo a gravitational separation too, while the ones that are not flocculated will form a turbid layer at the bottom [16]. On the contrary, in a monodisperse emulsion if the droplets are highly charged or coated with an effective surfactant, they repulse each other, and they cream as individual particles [73].

Creaming and sedimentation are temporary phases in some extent. They can be reversed by simply shaking or stirring the emulsion and the emulsion will be homogeneous again [24]. Gravitational separation depends on various factors such as the density difference between the dispersed and continuous phase, the diameter of the droplets while it is inversely proportional to the viscosity of the dispersed phase [24].

3.2 Flocculation

Flocculation appears when at least two droplets attach together yet without changing their distinctive characteristics [16]. This causes the droplets to come out of the suspension in the form of floc or flake, either spontaneously or due to the addition of clarifying agent [86][87]. Flocculation can be favored when attractive forces prevail over the repulsive forces. Attractive forces can be van der Waals, depletion or hydrophobic forces, while repulsive forces can be either electrostatic or steric forces [88]. In other words, when the repulsive forces are superior to attractive forces, the droplets stay close to each other without getting combined to start coalescence [16], [26], [82], [89]. These aggregates could be compact or may form an expanded gel-like structure. However, the individual droplets remain separated by a layer of the continuous phase - thin liquid film. The formation of such configuration is due to an attractive interaction but the stability of the film between the interfaces proves that at shorter distances repulsive force is present [82].

Flocculation is the initial step leading to further aging of the emulsion, as coalescence and phase separation [26], [86]. This can happen due to the presence of excess surfactant in the continuous phase of the emulsion, which can cause flocculation of the emulsion droplets. The aforementioned phenomenon is called

depletion effect and is used to describe a system which contains excess of surfactant in the form of micelles. This occurs when the dispersed emulsion droplets approach each other to distances smaller than the diameter of the surfactant micelles, leading micelles from the interparticle space to separate due to the loss of configurational entropy of the micelles. This depletion mechanism results in an attractive force between the droplets due to the lowering of the osmotic pressure in the region between the droplets [26].

Nowadays, scientists tried to find ways to improve the stability of the emulsion against flocculation since the latter can be due to the oil volume fraction, the mean droplet size, and pH [90]. One solution among many could be the decrease of the droplet diameter, which can languish the attractive Van der Waals forces between the droplets and prevent flocculation. On the other hand, choosing a surfactant whose molecule will occupy bigger area in the droplet space, can lead to a thicker interfacial layer of the droplet and hence decrease the possibility of coalescence [91]. Various techniques, such as microscopy and particle size analysis can determine flocculation in an emulsion [16].

3.3 Coalescence

Coalescence is another very typical destabilization mechanism of emulsions. It basically describes the moment at which two or more droplets came in contact for a time long enough to merge and form one bigger droplet [82]. Coalescence can be enhanced when the system undergoes flocculation, meaning that the droplets are in a very small distance where only a very thin film of the continuous phase separates them [92]. The aforementioned liquid film is the major driving force for coalescence since its characteristics can determine the merging of the droplets [93]. This thin film can collapse unprompted, especially when the droplets are already big which means that the film area is large, while the thinner the film the stronger the attracting force between the oil droplets which leads to the merging of the two droplets. Another factor that can promote coalescence is the low interfacial tension between oil and water phases, which highly relies on the emulsifier that is used for the preparation of the emulsion [92].

Coalescence happens in different steps. The first step is the proximate approach of the two oil droplets, which occurs during flocculation and simultaneously coagulation between the two. This step is associated by the formation of a thin film, as mentioned before, which after a while undergoes a rupture. This film rupture is the characteristic of coalescence and is irreversible. Basically, once the liquid film reaches a critical point a hole is originated that is growing and upon a precarious size, the two droplets get unified forming a bigger one [94].

3.4 Ostwald Ripening

Wilhelm Ostwald was the first one to report the Ostwald ripening phenomenon in 1896 [95]. It is a destabilization phenomenon that happens in emulsions that are not in a thermodynamic equilibrium, which indicates that the system is polydisperse. Ostwald ripening strongly relies on the solubility of the droplets in the continuous phase [96]. In more detail, in an emulsion where there are multiple sizes of droplets and they are slightly soluble in the continuous phase, the molecules of the small droplets tend to diffuse through the continuous phase to feed the larger droplets [97]. When this happens the mean droplet size of the emulsion is drastically increasing with time [98] and it might lead to the deterioration of it [99]. The droplet size plays a crucial role on the Ostwald ripening process. When the droplets are very small, their chemical potential is higher than the one of the bigger droplets which promotes the transfer across the continuous phase of molecules from the smallest to the biggest droplets [82], [100].

According to IUPAC, the official definition of Ostwald ripening is the “dissolution of small crystals or sol particles and the redeposition of the dissolved species on the surfaces of larger crystals or sol particles” [101]. Moreover, they clarify that this phenomenon is happening due to the higher surface energy, thus the total Gibbs energy of the smaller droplets alike the larger ones, which grows the solubility of the first ones [101].

Another important factor that impacts Ostwald ripening is the properties of the interfacial layer around the droplets [97]. One of those characteristics is the width of this layer, which means that the thinner it is, the easier the molecule diffusion can be, so the smaller droplets will disappear in favor of the bigger ones. Another

important aspect is the permeability of this layer, while high permeability leads to an easier spreading of molecules through the continuous phase, hence the appearance of Oswald ripening.

All the previous destabilization phenomena can occur despite the composition of the dispersed and continuous phases. In this project, focus will be given on the production of stable and monomodal miniemulsion using thiol-ene click chemistry to produce droplets in an aqueous continuous phase.

➤ The thiol-ene reaction: a crucial reaction in chemistry

1. General information

Thiol-ene reaction was first communicated in 1950 by Posner [102] and describes the reaction of a thiol with an alkene that form a thioether [103] (Figure 1.11).

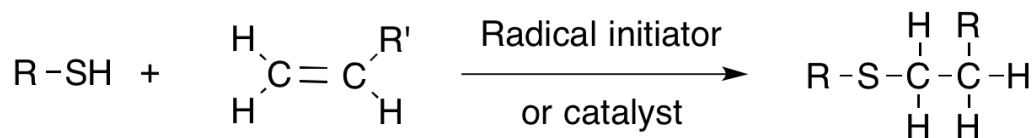


Figure 1.11. Schematic representation of the thiol-ene reaction [104].

Thiol-ene polymerization is often mentioned in the literature as click-chemistry reaction, which refers to a process where simple, efficient reactions that yield in a single product are required. Kolb and his coworkers were the first ones to establish the term 'click-chemistry' by combining small heteroatom units in order to produce modular "blocks" for both small- and large-scale applications [105]. These reactions possess several characteristics, among which the high polymerization yield with no side products, the insensibility to water and oxygen, provided that the amount of oxygen is less than the amount of thiol, the abstention of solvents since most of the time water is used as well as the stereospecificity and regiospecificity. The later refers to the formation of a unique structural isomer during the reaction [106].

There are two different categories of thiol-ene reactions, the one that involves free-radical thiol-ene click reaction and the one mentioned as thiol-Michael additions click reaction, and both provide various advantages [104]. In more detail, thiol-ene reactions have very fast reaction rates with quantitative polymerization yields

where most of the time no side-products are produced. Another important advantage is the wide range of monomers, thiols and alkenes, that are available on the market while in the case of thiol-Michael additions, a small amount of catalyst is required for the reaction to start [104] (Figure 1.12 and 1.13).

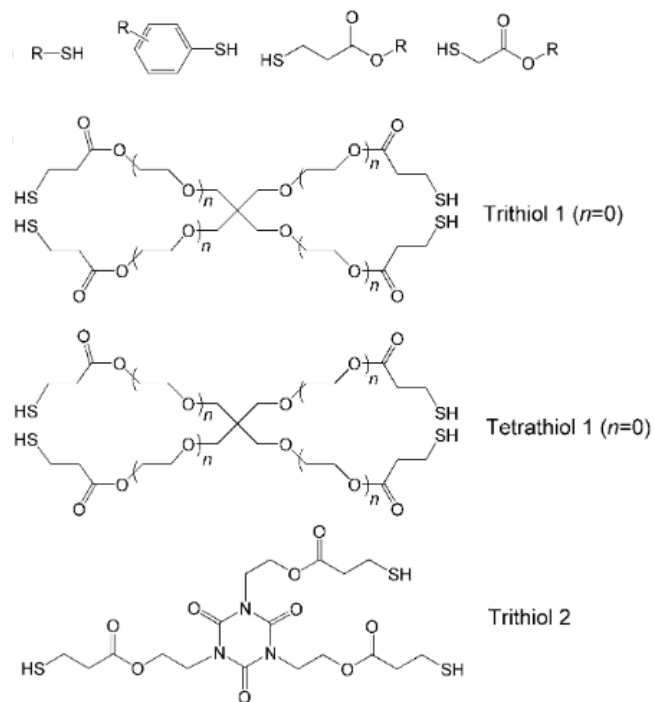


Figure 1.12. Common thiols [104].

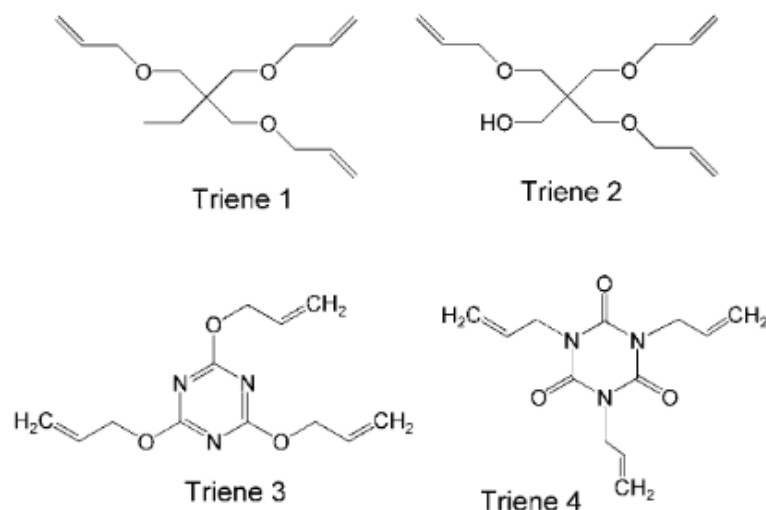


Figure 1.13. Common alkenes [104].

On the other hand, thiol-ene chemistry has some restrictive disadvantages. One of the most important pitfalls is the very strong odor of the thiol which can be an

obstacle in some cases, while at the same time the monomer can be toxic for human beings. Even though in China, researchers patented a method to remove the strong smell of thiols by adding a masking agent, which worked as parfum to cover the sulfur odor [107], the aforementioned limitation has to be strongly considered before manipulating the thiols.

Another important issue when thiol is combined with alkene is the poor stability over time since certain thiol-ene mixtures have low thermal stability when they are stored at room temperature. This can be a limiting factor in some applications where long storage time is desired. Researchers have reported some reasons of destabilization of the system such as decomposition of potential impurities that can initiate a thermal free-radical reaction or a spontaneous polymerization initiation by charge transfer interaction in the ground-state between thiol and alkene [108].

However, thiol-ene reactions have plenty advantages as compared to other acrylate reactions. Acrylate radical-based photopolymerization is more sensitive to oxygen, as compared to thiol-ene reactions, and this can initiate the polymerization [109]. Also, in acrylate systems the use of initiator is mandatory, while thiol-ene can also polymerize by the absence of photoinitiator [109]. Overall, thiol-ene chemistry is known to form rapidly a homogeneous polymeric network since the polymerization step can be tailored by step- and chain-growth mechanism [104].

Therefore, the fields that thiol-ene click chemistry is used are versatile and they will be described in the following part. As an example, thiol-ene chemistry is used in biomedical [110], optical [111] and sensing fields [112].

2. Thiol-ene reactions that can occur

The kinetics of the reaction between thiol and alkene is very rapid, which is attributed to the exothermic reaction of the chain transfer. This chain transfer happens when the thiyl radicals, RS^{\bullet} , react with the double bond of the alkene. This results to low molecular weight polymers with high gel point conversions [113]. The gel point refers to the moment when all monomers are connected to the polymeric network by at least one chemical bond.

2.4 Free-Radical Thiol-Ene Click Reaction

Radical mediated thiol-ene click reaction can be either step- or chain-growth. Referring to the first one, it is also called condensation polymerization and the first to be formed are the oligomers which later combine with each other to form longer polymeric chains. On the contrary, chain-growth is also known as addition polymerization where the polymer chain is formed, and monomers are added only to the ends of this chain. Free radical polymerization has chain-growth mechanism, divided in three steps: initiation, propagation and termination (Figure 1.14) [114].

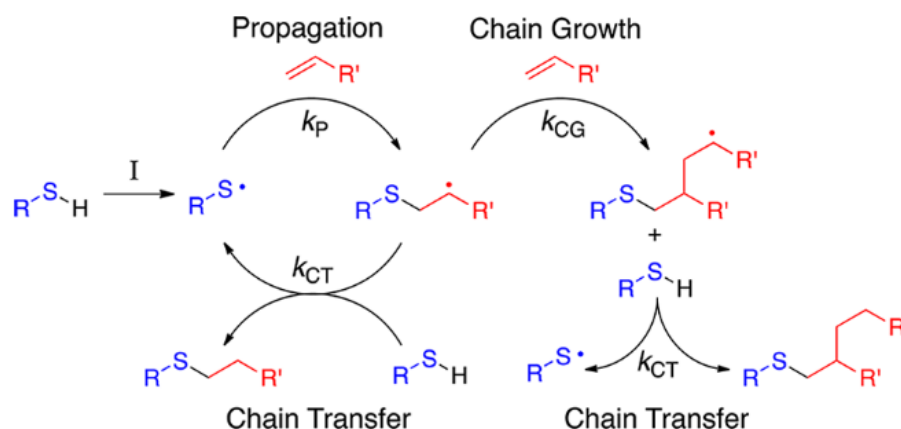


Figure 1.14. Propagation, chain-transfer and chain growth steps that occur during free-radical thiol-ene click reaction ("I" refers to initiator) [115].

In the beginning thiol and initiator come in contact and once energy is given to the system, the proton of the thiol is absorbed by the initiator and the thiyl radical $RS\cdot$ is formed. Free-radical thiol-ene click reaction can be initiated either by heat or light. Especially, the photopolymerization is widely used in this chemistry since it provides several advantages such as the controlled reaction rate, light intensity or small residence time [116].

As a second step, propagation occurs when the alkene is added to the system: the covalent reaction of thiol with the double bond of the alkene results to a carbon-centered radical intermediate. This formed radical intermediate can evolve in two different ways: (i) the step-growth, during which a chain transfer from a hydrogen of another thiol occurs and one thioether oligomer is formed, while at the same time a new thiyl radical is generated, and the cycle continuous, or (ii) the chain-growth, where the carbon-centered radical intermediate undergoes

homopolymerization, which means that it reacts with a double bond of another alkene and a new carbon-centered radical intermediate is generated. The latter can either react with a new thiol-radical and follow the step-growth mechanism or react again with a new alkene and follow chain-growth polymerization [115]. An ideal thiol-ene polymerization, where no impurities exist in the solution, only step-growth thiol-ene polymerization happens, while the chain-growth, meaning the homopolymerization of the carbon-centered radical of the alkene, is not favored, *i.e.* $k_{CG} \ll k_P$, k_{CT} (k_{CG} : chain growth rate, k_P : propagation rate, k_{CT} : chain transfer rate). Simply thiol functional group reacts with the alkene functional group and results to a thioether [117]. However, ideal conditions are very challenging to be achieved. For this reason, the path that will be followed for the reaction of thiol with the alkene can be determined by the relative kinetics of the two steps, chain-transfer and homopolymerization, and strongly depends on the functionality of the alkene. When the alkene is electron-rich, such as vinyl ether ($\text{CH}_2=\text{CH}-\text{O}-\text{CH}=\text{CH}_2$), it is more reactive and step-growth is favored, while an electron-poor alkene, such as acrylonitrile ($\text{CH}_2=\text{CH}-\text{C}\equiv\text{N}$), is less reactive, thus both mechanisms occur [118].

The thiol-ene kinetics is strongly affected by the propagation and chain-transfer rates, k_P and k_{CT} respectively (Figure 1.15).

$$k_P/k_{CT} \begin{cases} \gg 1; & R_P \propto [\text{SH}]^1 & (1) \\ \approx 1; & R_P \propto [\text{SH}]^{1/2}[\text{C}=\text{C}]^{1/2} & (2) \\ \ll 1; & R_P \propto [\text{C}=\text{C}]^1 & (3) \end{cases}$$

Figure 1.15. Thiol-ene radical addition reaction rate relationship [103]. R_P is the overall reaction rate, $[\text{SH}]$ is the concentration of thiol and $[\text{C}=\text{C}]$ the concentration of alkene [119].

In the case where the $k_P \gg k_{CT}$, which means that $k_P/k_{CT} \gg 1$, the concentration of the thiol dictates the reaction rate. This also indicates that the chain growth mechanism is the slowest step thus is the one to determine the overall reaction rate (R_P). On the contrary, when the $k_P \ll k_{CT}$ ($k_P/k_{CT} \ll 1$), alkene concentration and propagation mechanism take over the control of the R_P . Finally, in the case where $k_P \approx k_{CT}$, meaning $k_P/k_{CT} \approx 1$, consequently both chain transfer and propagation mechanisms influence the overall reaction rate.

2.5 Thiol-Michael Addition Click Reaction

Another way that thiol can react with alkene to obtain a thioether is called thiol-Michael addition (Figure 1.16). There are two ways to obtain the thiolate anion, RS^- , that will further participate in the Michael-addition reaction [120]. The first is called base-catalyzed mechanism (Figure 16.a), where a base, such as amine (RNH_2), to abstract a proton from the thiol and a thiolate anion is generated as well as a conjugated acid, HB^+ [121]. The thiolate anion initiates the propagation step during which an electron withdrawing alkene group (EWG) abstracts the anion and results to an intermediate carbon-centered anion, and becomes a strong base, which can absorb the hydrogen of the conjugated acid that was formed in the beginning. The final thioether product is generated. This base catalyst is regenerated, and the propagation step is repeated, like a cycle reaction.

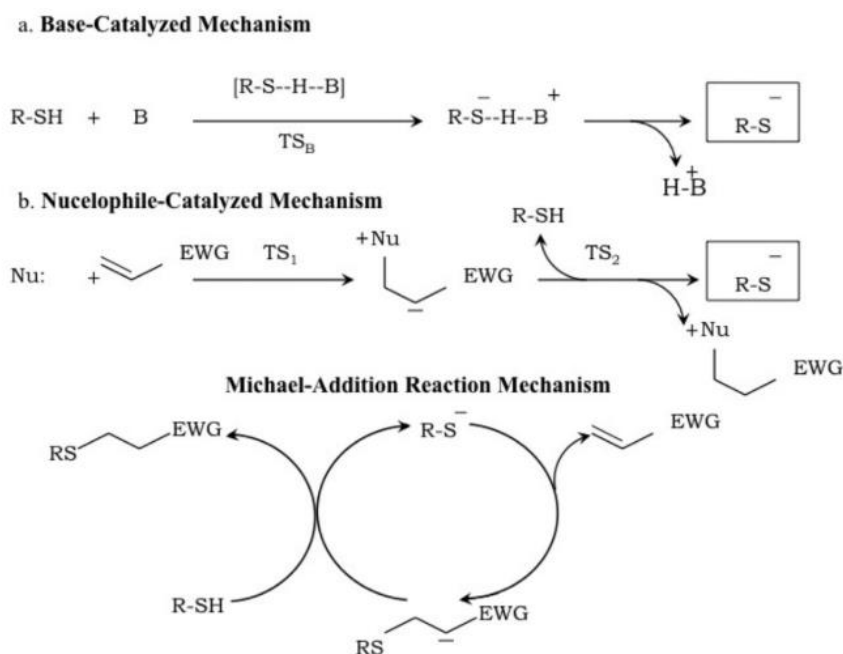


Figure 1.16. The base-catalyzed thiol-Michael addition reaction pathway shows the hydrothiolation of an activated $\text{C}=\text{C}$ bond via the addition of the anion across the electron-deficient beta-carbon of the ene [122].

The second way to generate a thiolate anion is called nucleophile-catalyzed thiol-Michael addition (Figure 16.b) [123]. A nucleophile is a molecule with a free pair of electrons, such as Br^- , which reacts with an EWG alkene, and a strong base is formed that reacts with the thiol to obtain the thiolate anion to start the propagation

step. The propagation is the same as described before for the base-catalyzed mechanism.

2.6 Self-initiated Thiol-Ene Click Reaction

A last way to achieve thiol-ene polymerization is called self-initiated thiol-ene click reaction, where no initiator is used to start the reaction. This method is not so common but there are still few research groups that have reported it. Since it is not widespread, the initiation mechanism is not so clearly described. It is believed that a thiol-ene charge-transfer complex is responsible for the initiation, while the different monomer impurities could also potentially start the reaction by producing thiyl radicals under UV [108]. Cramer *et al.* [109] used stoichiometric ratios of variety of vinyl polymers and thiols to polymerize under UV with no added photoinitiator. They observed an increased alkene homopolymerization than thiol-ene reaction but when the amount of thiol functional groups was four times higher than the double bonds of the alkene, they observed an equivalent consumption of both monomers. Another possible reaction that can initiate the polymerization without using initiator is the atmospheric oxygen [124]. Le *et al.* [125] recently show that a thiol can be oxidized by the oxygen to form acids with a sulfide oxygen bond (e.g. RSOH), or homopolymerized thiol, which is called disulfide (RSSR).

In this project, particular focus will be given on the free-radical thiol-ene reaction. More specifically, different types of thiols bearing multifunctional SH groups will be investigated. The main goal is to achieve droplet and particle control by using different emulsification devices. The choice of the free-radical thiol-ene reaction was done due to the high reactivity between the thiol and alkene that is also combined by a simple experimental procedure and without the addition of a catalyst. The simplicity of this method provides a broad area of applications that will be discussed in the following section.

3. Applications

A very big field where thiol-ene chemistry is widely used is the drug delivery systems. Drug delivery refers to the transportation of a pharmaceutical compound

to a specific place in the body in a controlled time and duration in order to cure the pain or disease [126].

In 2013 [127] a research group used this chemistry to produce thiol-ene nanoparticles where their surface was covered with either thiol or alkene functional groups that could be further functionalized by attaching proteins. They used a tetra functional thiol called, pentaerythritol tetrakis(3-mercaptopropionate) (PETMP) combined with a four functional alkene, pentaerythritol tetraacrylate (PETA) and added deionized water to produce nanoparticles by simple mechanical stirring for 24 hours (Figure 1.17). They proved that when they did not use stoichiometric ratios of thiol and alkene functional groups, the surface of the nanoparticles was covered with functional groups of the monomer that was in excess amount. The size of the nanoparticles was between 250 and 555 nm with quite low polydispersity, below 0.3, while the zeta potential measured was negative, which allowed the nanoparticles to resist against aggregation. The overloaded surface with functional groups was determined by using proton nuclear magnetic resonance (^1H NMR), where either the thiol or the alkene characteristic peaks were determined.

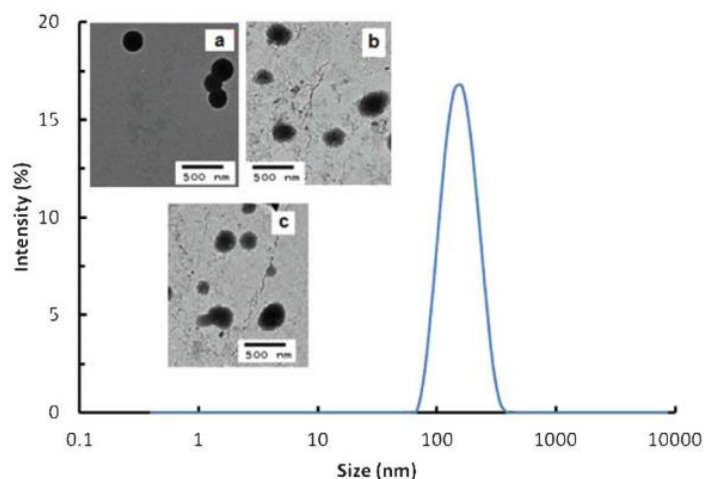


Figure 1.17. DLS size distribution for PETMP–PETA (1:1) nanoparticles. Inserts: TEM images [127].

Later, Durham team produced thiol-ene miniemulsions with controllable droplet size that can be used as drug carriers [128]. The main goal was to tune the particle size by varying some chemical parameters such as the initiator, surfactant, and monomer concentrations. Different number of functional groups of thiol and alkene were used to produce either linear or cross-linked particles using water-soluble

thermal initiator. Focus was given to a tetra-functional thiol and a tri-functional alkene. Starting with the effect of the surfactant concentration on the particle size, a range of 2 to 80 mM of sodium dodecyl sulfate concentration was used. It can be clearly seen in Figure 18.a that the higher the amount of surfactant the smaller was the particle diameter, with the lower value to be a bit below 100 nm and the polydispersity close to 0.2. The same trend was followed by varying the amount of thermal initiator where the highest particle size was 500 nm and the lowest a bit above 200 nm (Figure 18.b).

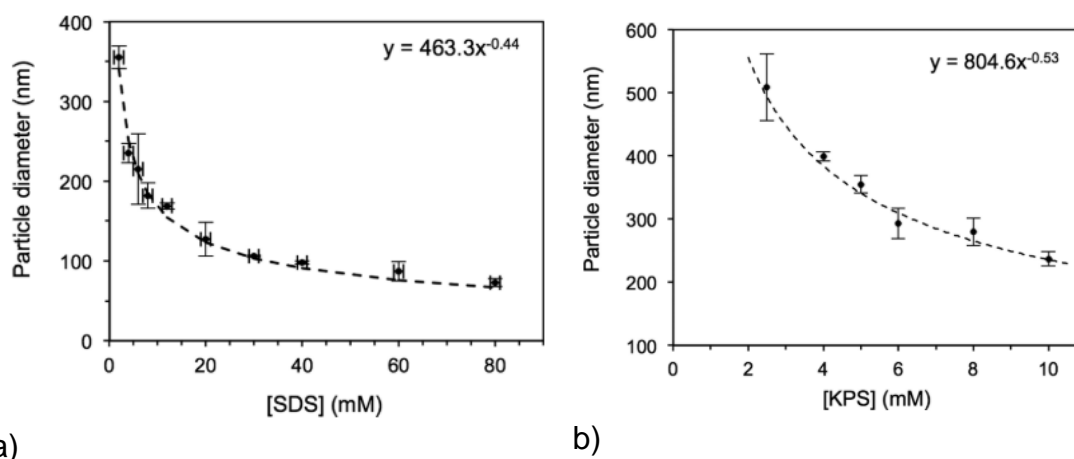


Figure 1.18. Dependence of Z-average particle diameter in the PETMP/ TTT thiol-ene latexes a) on surfactant concentration and b) on initiator concentration [128].

Another way to use thiol-ene click chemistry in drug delivery is by preparing a high internal phase emulsion (HIPE). These emulsions consist of more than 74% of internal phase volume and the droplets are dispersed and covered with a very thin layer of a continuous phase, which after polymerization evaporates and allows the porous structure to appear [129]. This year, 2021, Hobiger *et al.* [130], developed an oil-in-water HIPE using thiol-ene chemistry and photopolymerization as a fast-curing mechanism. They simply used a mechanical stirrer to mix and obtain the HIPE and then a UV-chamber of 320-580 nm wavelength to recover the final poly(HIPE), which is also called monolith. It is shown that adding a tri-functional thiol in a poly(ethylene glycol)-based monomer solution can significantly improve the mechanical properties of the material and provide better degradation properties due to the extra ester bonds created. It is also proven that step and chain-growth polymerization mechanisms that occur during polymerization lead to a strong increase in the toughness of the resulting material. Finally, the addition of tri-

functional thiol to the system allowed the opening of porous and thus the enhancement of the mechanical properties, while the drug release appeared to be burst for the first one hour, due to the open porous, and then a slower release profile was followed (Figure 1.19).

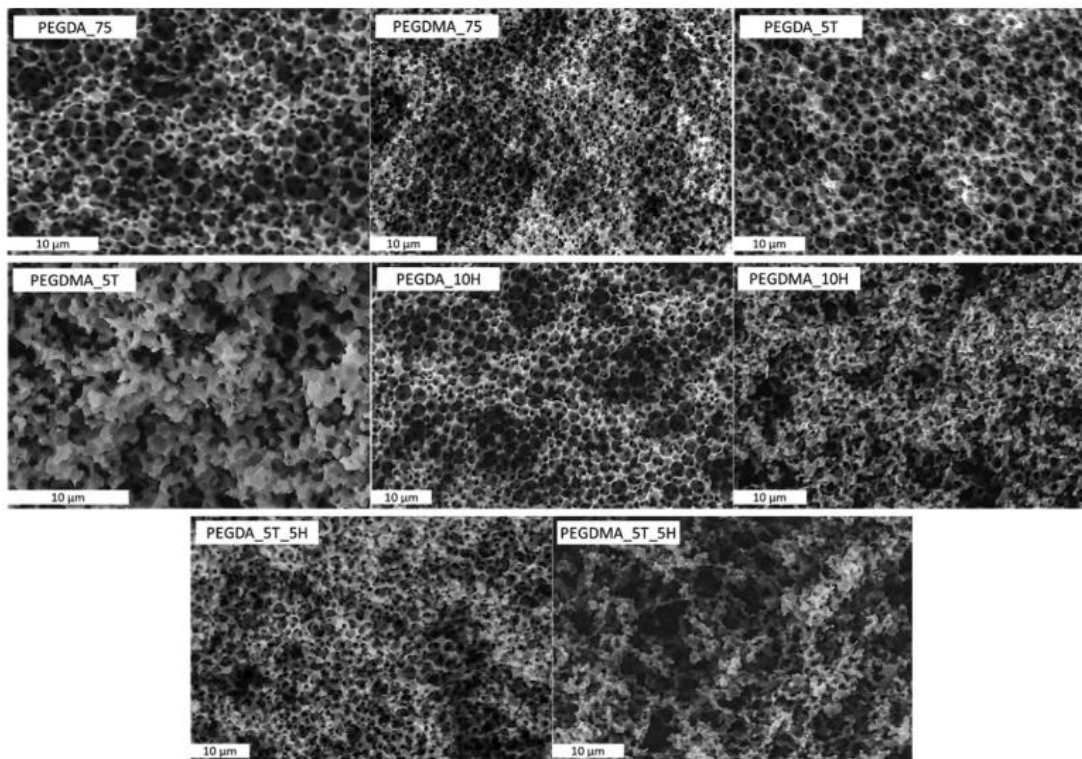


Figure 1.19. SEM micrographs of poly(ethylene glycol) diacrylate (PEGDA), poly(ethylene glycol)dimethacrylate(PEGDMA) of 75 vol%, 5T: 5wt% of thiol, 10H: 10wt% of (Hydroxyethyl)methacrylate (HEMA) and 5T_5H: 5wt% of thiol and 5wt% of HEMA [130].

As previously evocated, since thiols and alkenes can have more than one functional group, they can easily form polymeric networks. These networks can be used as scaffolds for the human cells to grow since the networks behave like the human tissues. Last year, Michel *et al.* [131], used thiol-ene click chemistry and produced hydrogels, hydrophilic polymer networks that swell in water. Chitosan was the main material and different thiolated poly(ethylene glycol) cross-linkers were used to evaluate the properties of the final photopolymerized hydrogels. The first observation was that all materials were honeycomb-like structures with the pore sizes to vary almost 100 nm (Figure 1.20). In terms of mechanical properties, they prove that the longer the cross-linker chain the more elastic the hydrogels appear since the distance between the polymer chains is long enough to enable the chains to rearrange when shear is applied to the material.

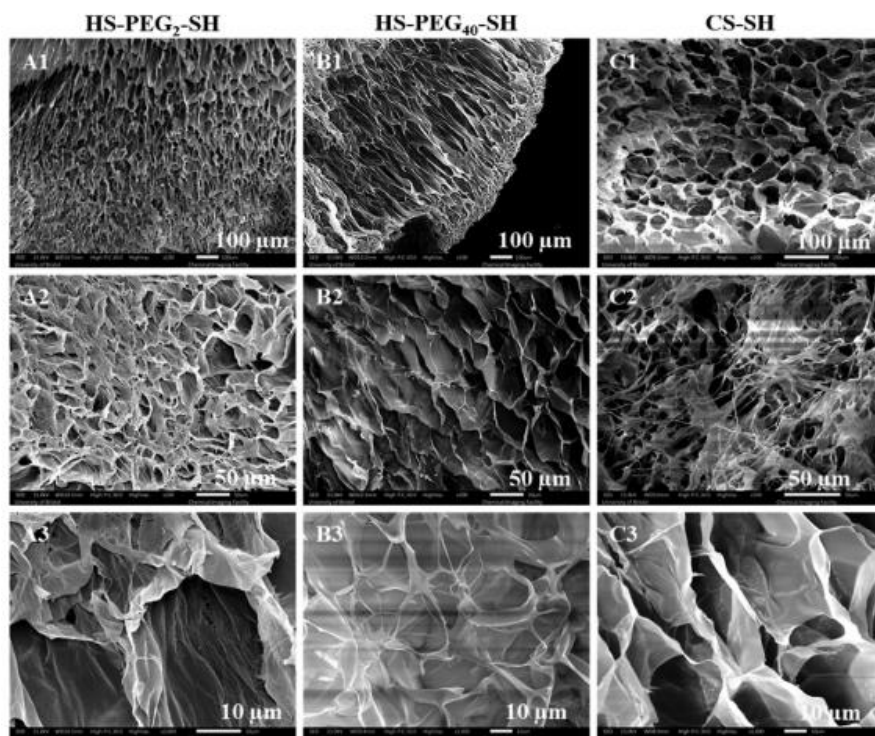


Figure 1.20. SEM images under different magnifications of cross-linked chitosan- thiolated poly(ethylene glycol) hydrogels [131].

Do *et al.* also used the thiol-ene chemistry for making neuroprosthetic implants [132]. The main goal was to produce shape-memory polymers that change shape when an external stimulus is applied on them. This stimulus can be either pH, temperature, solvent or electricity related. In this case, the implant prepared need to be stiff when the temperature was close to the one of the human body, while it was expected to change when it comes in contact with the body fluids. They used a tri-functional thiol and a bi- and tri-functional alkenes and compared between casting and spin-coating methods presented in Figure 1.21. It was shown that with casting process overall the material is thicker thus the UV cannot be evenly distributed in the middle of the material and lead to a more flexible structure where the shape change needed lower temperature than the thin spin-coated sample.

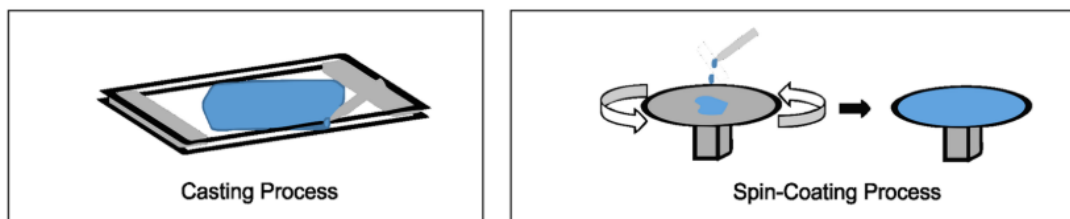


Figure 1.21. Casting and spin-coating processes [132].

Thiol-ene shape memory polymers can also be used in producing flexible electronics. In 2019, Frewin *et al.* mixed two different tri-functional thiols with a tri-functional alkene to UV polymerize them and to obtain flexible thin film transistors with great electrical properties [133].

A last versatile application of thiol-ene click chemistry is in the production of microfluidic devices. More specifically, in microfluidic devices so far poly(dimethylsiloxane) (PDMS) is by far the most common material that is used. But PDMS can swell in contact with organic solvents and its hydrophobic, thus small molecules can be absorbed on the surface. Thiol-ene on the other hand are known for the excellent resistance to any chemical or even to high temperatures. In this context, Bonabi *et al.* [133], used tri-functional thiol and alkene without any photoinitiator to produce a microchip by UV irradiation (Figure 1.22). The storage time was evaluated, and it turned out that thiol-ene with a ratio 2:3 is more stable through time as compared to thiol-ene with ratio 1:1 and PDMS microchip.

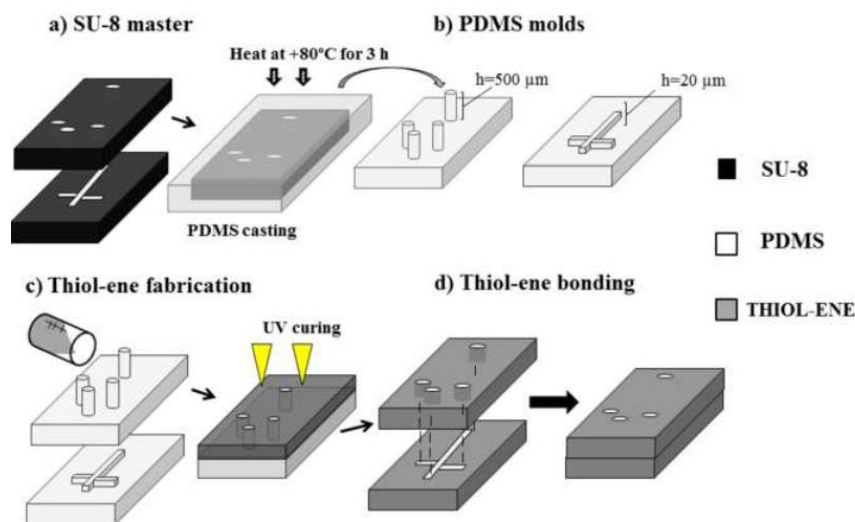


Figure 1.22. Chip fabrication process [134].

🔄 Emulsification Methods

There are several ways to produce a kinetically stable emulsion, for instance by making appropriate choice of the oil phase, by achieving a controlled size of the dispersed droplets, or by maintaining a relative low concentration of suitable surfactants, cosurfactants and finally by finding the ideal conditions of manufacturing [135]–[138]. However, emulsion droplet size plays a key role in

many emulsion properties such as stability, texture and rheology [139], [140]. Usually, the aim of emulsification is to produce as small droplets as possible, for this purpose assorted emulsification techniques can be used. They can be classified in high-energy or low-energy emulsification methods [135]. High-energy approaches utilize mechanical devices (ultrasonic methods [141], high pressure homogenizers [142], static mixers [143] or membranes [144]) that generate intense forces capable of forming very fine oil droplets. While low-energy methods involve complex interfacial hydrodynamic phenomena which depend on the system composition properties (phase inversion, solvent displacement, spontaneous emulsification [145], [146]).

There are several factors that play a significant role in the choice of the emulsification method, such as the application of the resulting emulsion, the apparent viscosity, the amount of mechanical energy required, and the heat-exchange demands [147].

1. High-Energy Emulsification Methods

In high-energy emulsification methods, large disruptive forces are provided by using mechanical devices such as ultrasound generators, microfluidizers and high-pressure homogenizers, which are able to produce small diameter droplets [135], [142]. These methods are traditionally used in industrial operations because of the flexible control of emulsion droplet size distribution and the ability to produce fine emulsions from a wide variety of materials. Moreover, an advantage of this category is the direct control of the process parameters, such as quantity of mechanical energy input and residence time in the equipment [148]. The parameters that play significant role on the droplet size are (i) the choice of the equipment, (ii) the production conditions, such as temperature and time, and (iii) the properties of the composition of the sample, in the manner of surfactant concentrations or viscosity of the phases.

Different high-energy emulsification devices used different mechanisms for the droplet breakup, closely linked to the Reynolds number. The Reynolds number Re , defined in Equation 1.1, is the ratio of the inertial to viscous forces in a fluid system.

According to Equation 1.1, when the characteristic dimensions of the system change, the Re also changes in a linear way.

$$Re = \frac{\rho v D}{\mu} \quad (1.1)$$

where ρ is the density of the fluid, V the mean velocity of the fluid, D the characteristic dimension of the flow and μ is the dynamic viscosity of the fluid.

In the case where Re is below 2000, the regime is laminar and simple shear forces are applied to the emulsion, which means that it undergoes no rotational flow, where the droplets flow along streamlines but also rotate around their own axis. On the contrary, in the case of Re above 4000, the flow becomes turbulent and elongational forces are applied to the droplets, which experience an irrotational flow, meaning that the droplets flow along the streamlines but do not rotate around their own axis. On this subject, Grace summarized Taylor's theory about the influence on the droplet breakup when the viscosity ratio (value of the dispersed phase viscosity divided by the continuous phase viscosity) increases for both rotational and irrotational shear fields [149]. In Figure 1.23, the viscosity ratio of dispersed and continuous phase for the simple shear and the elongational flow is shown. It demonstrates that the energy required for the droplet breakup in the elongational flow is less as compared to the simple shear for low and high viscosity ratios. Moreover, for viscosity ratios higher than 4 the droplets cannot bear breakup in the simple shear case, while in the elongational flow droplets can still become smaller.

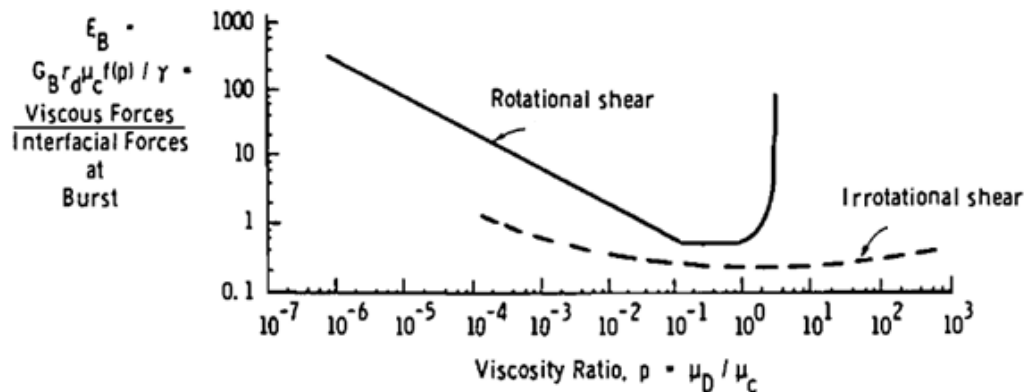


Figure 1.23. Comparison of effect of viscosity ratio on critical shear in rotational and irrotational shear fields [149].

1.1 Ultrasound Generator

The ultrasound generator, also called sonicator, is a widely used high-energy emulsification method that was first communicated by Wood and Loomis in 1927 [150]. It carries a sonotrode (sonicator probe), which is providing the energy input to the system, containing a piezoelectric quartz crystal that can expand and contract depending on the alternating electrical voltage [139]. Ultrasound can be generated either mechanically, whistle, siren, or electrically, reverse piezoelectric effect or magnetostrictive transducers, which is the most widely used type of apparatus [139]. The latter is using a piezoelectric material, such as quartz, to convert a high frequency oscillating electric field into mechanical vibrations of the same frequency [151]. Depending upon viscosity and conductivity of the medium, sound waves dissipate part of the acoustical energy into heat energy while passing through the medium [152].

During the time that the sonicator probe is in contact with the liquid, mechanical vibrations are generated and thus cavitation occurs. Cavitation is the main phenomenon responsible for ultrasonically induced effects [135], [139], [153]. More specifically, cavitation is a phenomenon in which rapid changes of pressure in a liquid lead to the formation of small vapor-filled cavities in places where the local pressure is reduced to that of the vapor at the temperature of the flowing liquid because of local velocity changes [139], [154], [155]. When the pressure is high, the cavities (in that case called bubbles or voids), collapse and may generate a strong shock wave very close to the bubble, but rapidly becomes weak as it propagates away from the bubble [154]. During emulsification, the collapse of these cavities causes powerful shock waves to radiate throughout the solution in proximity to the radiating face of the tip, leading to the braking of the dispersed droplets [139].

Cavitation, associated with the power dissipation, is considered as the driving force in sonochemical processing [156] and in particular, the essential mechanism of droplet breakup occurring during ultrasound emulsification [157], [158]. Moreover, the cavitation threshold, that happens when a liquid is irradiated by ultrasound and the pressure amplitude of the applied sound source reaches a certain minimum so that cavitation occurs, plays a significant role in emulsification [159]. Indeed, to

initiate the emulsification, it is essential the cavitation threshold to be attained: there is a corresponding maximum limit in concentration of emulsion (% of dispersed phase hold-up) that can be produced and remain stable when the intensity reaches a higher point compared to the threshold [155]. This limiting concentration of emulsion increases by increasing the ultrasound intensity. The aforementioned limited concentration appears when equilibrium between the two conflicting processes of emulsification and coagulation (coalescence) is obtained [160]. On the other hand, to achieve the formation of cavitation low frequency (f) is required, between 20 and 24 kHz, since it is inversely depending on the generated power (P) ($P \propto 1/f^2$) [161]. However, when the frequency is higher, close to 100 kHz, cavitation occurrence is reduced. When the generated ultrasound waves interact with matter, physical and chemical changes are caused [155], [162]. This means that longitudinal waves are generated, which propagate into the surrounding liquid medium [162]. These waves activate a motion in the medium particles through a series of compressions and rarefactions under fluctuating pressure, hence leading to acoustic cavitation phenomena [163]

Ultrasound can directly produce emulsions, starting from separate phases, but since breaking an interface requires a large amount of energy, it is preferable to prepare first a coarse emulsion before applying acoustic power [164].

As for all emulsification devices, various parameters are responsible for the control of the droplet/particles size. These parameters can be either process or chemical parameters. Referring to the last one, many changes can be done in the emulsion composition to control the droplet size. Such changes can be the amount of surfactant, the oil content and the Oswald's ripening inhibitor. In 2020, in Hernández-Giottonini *et al.* [165] conducted using poly(lactic-co-glycolic acid) (PLGA) to tune the nanoparticles' size to be applied in pharmaceutical or food industries. They changed monomer, surfactant and solvent concentrations to observe the evolution of the particle diameter. Starting with the PLGA concentration they discovered, alike other researchers [166], [167], that the increased concentration of PLGA during emulsification method does not really affect the particles of the emulsion. This can potentially be attributed to the small range of variation of the concentration of PLGA. Further the surfactant

concentration has been increased from 1 wt% to 5 wt% and a significant decreased particle diameter from 187 nm down to 159 nm occurred. Indeed, when the surfactant amount increased, the system was better stabilized against coalescence, hence the smaller particle size. Ultimately, the volume of the organic solvent has been alternated from 0.2 v% to 0.5 v%, exhibiting an increase of particle diameter from 167 nm up to 242 nm.

When it comes to process parameters, amplitude/intensity/power (how vigorously the particles vibrate), frequency (how fast the particles vibrate), time on and off, and duration can be some of those who determine the size [168], [169]. Also, the type of the sonicator as well as the tip and the bicker used play a significant role on the droplet formation. Sui *et al.* [170] investigated the effect of power and emulsification time on the particle size and polydispersity of an emulsion containing soybeans (Figure 1.24).

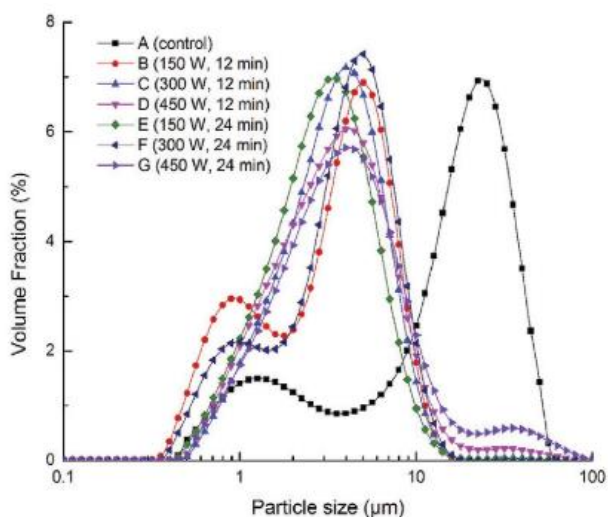


Figure 1.24. Particle size distribution regarding to emulsification time and power with an ultrasound generator [170].

On one hand, three different power values were compared, and the results show that (i) the system is bimodal (appearance of two different particle sizes at the same time) in low sonicator energy, (ii) an increase of power led to monomodal narrow distribution of the particles, and (iii) a further increase broadens the monomodal pick while the particle size slightly decreased. On the other hand, they examined the particle characteristics under the increase of time from 12 to 24 minutes, and the sample that was treated for 24 min (under 150 W, low power) was the one who gave the most encouraging results. This means, the smaller

particle size and the narrowest monodispersed pick. In contrary samples that were prepared using higher powers and longer times exhibit a bimodal behavior as well as an increase on the mean particle size. This can be attributed to the coalescence that might happen under long emulsification times, which many researchers call “over-processing” effect and will be discussed later in this chapter.

Another research group in Japan, Atobe *et al.* [171], used ultrasounds to produce stable, size-controlled methylmethacrylate (MMA) emulsions without adding surfactant. They claim that these emulsions are less pricey due to the absence of surfactant and can be used in many fields in electronics, photonics, and biotechnology. Just like Sui *et al.* [170] did with the effect of ultrasound generator power on the droplet’s properties, Atobe *et al.* [171] increased the frequency of the device which led to the formation of smaller droplets (ten times smaller when the frequency is multiplied by 100) and to a sharper and narrower polydispersity peak (Figure 1.25).

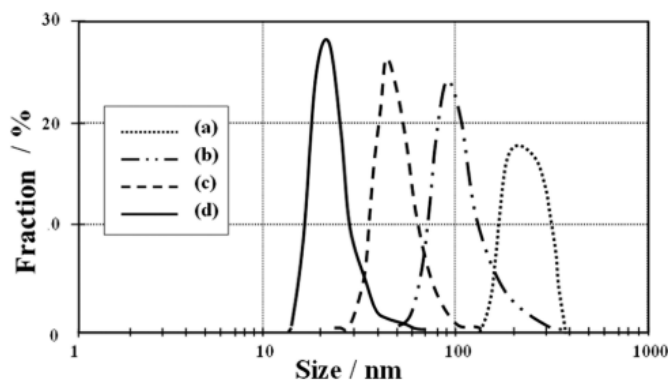


Figure 1.25. Size distributions of MMA droplets in acoustically emulsified aqueous solutions. a) 20 kHz, 8 min, b) 20 kHz, 8 min then 500 kHz, 10 min, c) 20 kHz, 8 min then 500 kHz, 10 min, 1.6 MHz, 10 min and d) 20 kHz, 8 min then 500 kHz, 10 min then 1.6 MHz, 10 min then 2.4 MHz, 10 min [171].

In 2018, Li *et al.* [172], decided to associate the droplet size of a sunflower oil emulsion with three major parameters: emulsification time, amplitude (which correlates with the power intensity) and processing volume (Figure 1.26).

As it could be expected, the increase of the sonicator energy input allows the droplets to break into smaller ones. The initial diameter was 10 μm for the least time and energy and decreased down to 7 μm when the energy increased. Referring to the sonication time it was proven that longer times tend to smaller droplet sizes until a steady state was reached. This state is characterized of the appearance of a plateau in the droplet diameter when the time is increasing

(triangular data points), which means that the droplet breaking was happening in a much lower level. Finally, in Figure 1.26.b, the processing volume is presented regarding the sonication time. It is shown that the bigger the volume the harder the droplets break so in 60 mL the droplets appear to have the lowest diameter above all.

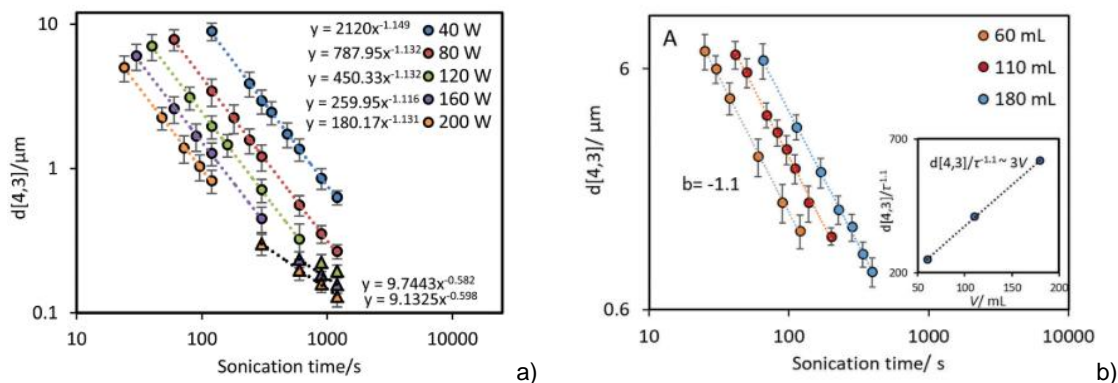


Figure 1.26. Volume mean droplet diameter as a function of sonication time a) for different power intensities at a constant volume (60 mL) and b) for different volumes at constant power intensities (200W) [172].

Considering all the work conducted using ultrasound generators, it is a very useful technique to achieve a diameter control regarding the desired application. However, it was very often reported that longer emulsification times not always lead to smaller droplet or particle diameters. Researchers attribute that to the “overprocessing” effect that occurs for increased emulsification time. This also follows a strong increase of the temperature during emulsification. This temperature rise in most of the cases needs to be avoided since it can decompose the emulsion.

1.2 Rotor-Stator Mixer

One of the main equipment widely employed in the preparation of liquid-liquid dispersions is the rotor-stator mixer, which have numerous industrial fields including food [173], [174], cosmetic [175], [176] and pharmaceutical products [177], [178]. In rotor-stator devices, oil and water phases are mixed at high rotation speeds (above 1000 rpm) in a narrow gap (50-3000 μm) between the static disk (stator) and a rotating disk (rotor) [148], [179]. The rotors generally rotate at an order of magnitude higher speed than conventional impellers in a stirred tank [179].

While the rotor rotates, generation of low pressure occurs, and the liquid is circulated, producing coarse emulsions with small droplets [139], [148], [177]. The distribution of the concentrated energy and shear by rotor-stator devices accelerate physical processes such as mixing, dissolution, emulsification and deagglomeration [179]. The mechanism that is promoted is the break-up of the droplets by mechanical and shear stress in the turbulent flow between the rotor and the stator [148]. The main advantage of using these mixers is due to the creation of very high energy dissipation rates as the kinetic energy generated by the rotor is dissipated in the small stator volume, and high shear rates in the rotor-stator gap [177].

Although there is a big variety on rotor-stator designs, they can broadly be classified into two groups based on the rotor type: teeth-designs and blade-designs (Figure 1.27). The former carries a rotor either extending all the way from the shaft or with both blades mounted on a plate attached to the rotor. Concerning the teeth-design, it accommodates a circular plate-mounted rotor [180].

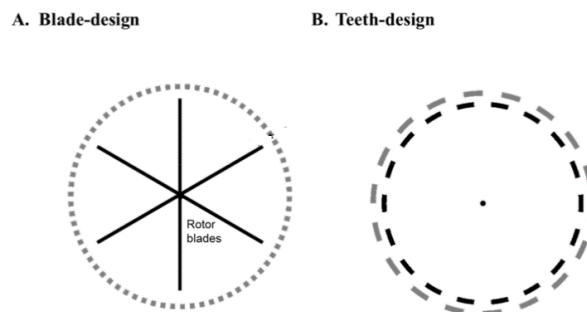


Figure 1.27. Schematic representation of a rotor-stator head with a) blade-design and b) teeth-design [180].

There are two major forces that can reduce the droplet size of the emulsion. First comes the mechanical impingement against the wall of the vial due to high fluid acceleration. Another force is the shear stress in the gap between the rotor and stator, which is generated by the rapid rotation of the rotor. The intensity of the shear stress can be adjusted by differing the thickness of the gap, the rotation speed or by using disks that have toothed surfaces or interlocking teeth [139]. Three main parameters can be controlled during this process: emulsification time and intensity as well as the design of the rotor/stator.

In the very late 90s, Maa and Hsu [133] analyzed the consequences of the operating parameters on the droplet diameter of poly(methyl methacrylate)

(PMMA) emulsion that can find application in food or pharmaceutical industries. At the same time comparison was done using two different tips: one micro-tip and one macro-tip. The main difference relies on the number of blades in the rotor, 4 and 2 blades respectively. In Figure 1.28, both tips provide smaller droplet diameters when the rotation speed was increasing.

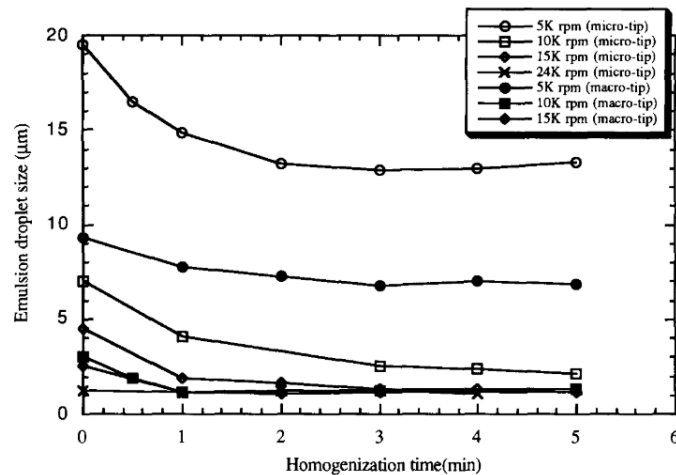


Figure 1.28. Emulsion droplet size regarding to homogenization time. The different phases were homogenized by a micro and a macro-tip at different rotational speeds [181]

The emulsification time is also represented with respect to the droplet size, showing a decreasing trend in the droplet diameter when the homogenization time increases but after approximately 2 min of emulsification the diameter reaches a plateau in almost all cases. Nevertheless, an equilibrium emulsion droplet size is observed for both tip designs. This equilibrium arises when the homogenization speed, even if its high, is not able to create the so-called turbulent eddies of sizes below a critical value that determines that droplet breakup [182]. In their system this equilibrium is reached for the micro-tip at 15,000 rpm and for the macro-tip at 10,000 rpm. Later, in 2009, El-Jaby's team [183] compared three emulsification devices: ultrasonicator, two rotor-stator blades, one with 5.5 cm and one with 7.5 cm head length, and static mixer. The later will be described later. Their main goal was to differentiate the power and energy consumption, droplet characteristics and shear rates using an oil mixture of acrylates and changing the emulsification time. It can be clearly seen that rotor-stator shows the bigger droplet for the higher amount of time, as compared to the others, while no significant difference between the two designs can be observed (Figure 1.29).

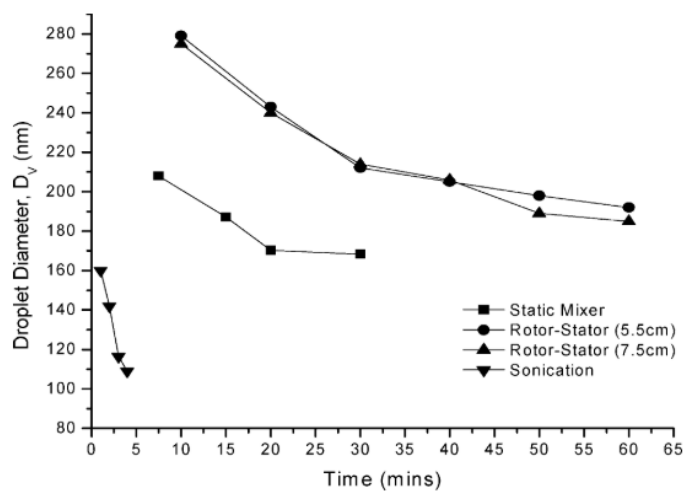


Figure 1.29. Droplet diameter evolutions for miniemulsions generated using the rotor-stator (5.5 and 7.5 cm stator head), static mixer, and sonicator [183].

Further, the diameter decreased using static mixer and followed by sonication with the smallest diameter 110 nm after 4 min of sonicator. Referring to the polydispersity of the systems all of them show monomodal distribution, values were below 0.15. The polydispersity values of the rotor-stator and the static mixer are quite close but former produces bigger droplets as compared to the latter, the droplet rupture is less effective which results to broader droplet size distributions alike the static mixer. In the case of sonicator a huge population of small droplets appears which leads to a quite broad size distribution. Last comparison was done concerning the energy consumptions of the three devices. It is proven that sonication is the method that requires less amount of energy to produce droplets. Even though static mixer needs energy input close to the one on the rotor-stator it is proven to be the most suitable technique to produce miniemulsions, since the system undergoes a bit less shear, hence less chances of increased temperature during emulsification.

It has been described that the rotor-stator mixers show the poorest droplet control as compared to ultrasound generators. This can be explained also by the Taylor theory that was described in the beginning of this chapter. In the case of simple shear, the droplet breakup is limited up to viscosity ratios $\mu_d/\mu_c = 4$. A further increase of the viscosity will severely impede the rupture the droplets further, thus emulsions produced with rotor-stator usually produced higher droplet/particle diameter.

1.3 High-Pressure Homogenizer

This method is widely used for the production of emulsions and several forces are employed such as hydraulic shear, intense turbulence and cavitation. The high-pressure homogenizer (HPH) is the most widely used high-energy device in the food industry and typically consists of a high-pressure pump and a homogenizing valve [135], [148]. The working principle is based on two immiscible liquids, which move through a small orifice of piston homogenizer under high pressure (500-5000 psi) in order to produce emulsions [184]. In the beginning, a coarse emulsion with large volume fraction of dispersed phase is formed, which can be diluted in a later procedure. HPH can be classified based on the nozzle geometry and design and depending on the flow guidance (Figure 1.30) [139]. There are four major categories: standard nozzles, microfluidizers, jet dispersers and orifice plates according to the emulsifying nozzle [148] [139]. The main difference between the first and the last two is that during the former turbulent flow is applied to the solution while on the other case is laminar elongation flow forces that generate the droplets and provide the mixing [185].

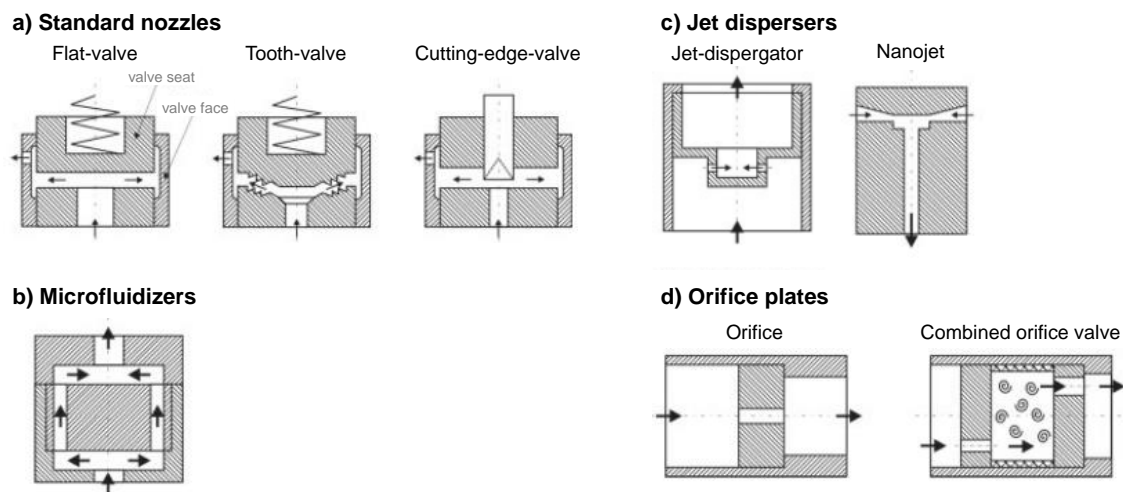


Figure 1.30. Different types of high-pressure homogenization systems [139].

The standard nozzles are also called valves and are the most common high-pressure systems used in industrial production (Figure 1.30.a) [139]. A coarse emulsion is first produced using a rotor-stator device, this emulsion is pumped through a central inlet bore, diverted by 90°, and urged through the radial gap between the valve seat and the valve plug [186]. These nozzles are also called

radial diffusers due to the radial flow that they experience. As the crude emulsion passes through the valve, it accelerates a very short distance to a very high velocity, and the resulting strong pressure gradient between the inlet and outlet of the valve generates a combination of intense shear forces, extensional stress through the valve as well as cavitation and turbulent flow [187]. The pressure energy that is applied on the system is the one responsible for the generation of the kinetic energy, which leads to particle disruption to the submicron range [188]. With other words, kinetic energy causes the large droplets to break down into smaller ones. The homogenizing pressure, for a given throughput, is determined by the force acting on the axially movable valve plug and the size of the gap resulting from this.

However, as described by Desrumaux and Marcand in 2002 [189] for sunflower oil-in-water emulsions, the droplet size decreases when the pressure increases until a given pressure threshold (Figure 1.31), after which a strange fluctuation on the droplet diameter can occur due to a temperature increase (from 5°C up to approximately 50°C). Indeed, increase of the heat, means increase of the Brownian motion in the emulsion, which gives rise to the possibility of coalescence.

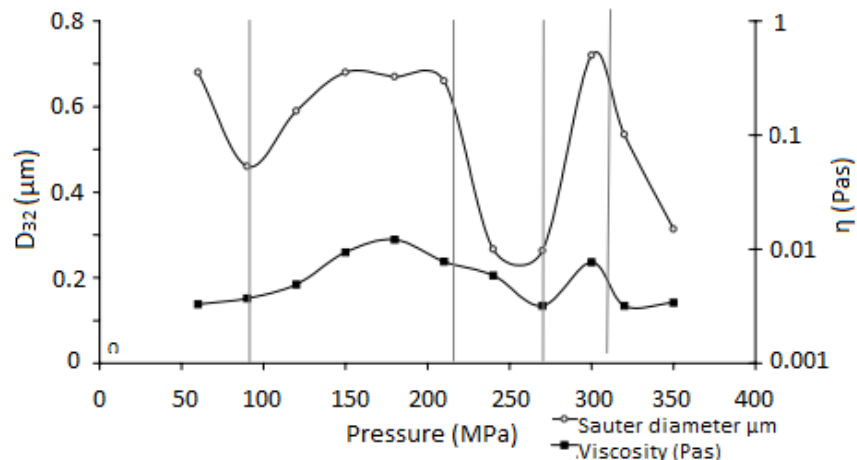


Figure 1.31. Effect of the pressure of homogenization on the droplet's diameter and on the viscosity of the emulsions [189].

The same conclusions were made by another research group [190] by varying process parameters such as homogenization pressure, number of homogenization cycles and homogenization temperature. Figure 1.32.a shows the decrease on the droplet diameter by increasing the pressure and the number of cycles, the passing of the emulsion through the nozzle of the homogenizer. When the pressure was

even higher at 160 MPa during one cycle the droplet size was smaller than the previous pressures but by increasing the number of cycles they observed an increase on the droplet diameter and distribution. This was followed by a significant increase in temperature at 60°C (Figure 1.32.b).

This phenomenon is actually observed very often in the literature, and it is called overprocessing [191]–[194]. During this stage there are two mechanisms competing each other. On the one hand is the breaking bigger droplets into smaller ones and on the other hand is the coalescence of the droplets. It is reported that during the droplet formation the new interfaces of the droplets get in contact with the surfactant molecules in order to stabilize the system. If the surfactant needs more time to adsorb on the surface than the two droplets to coagulate this will form an unstable system which will lead to coalescence [195].

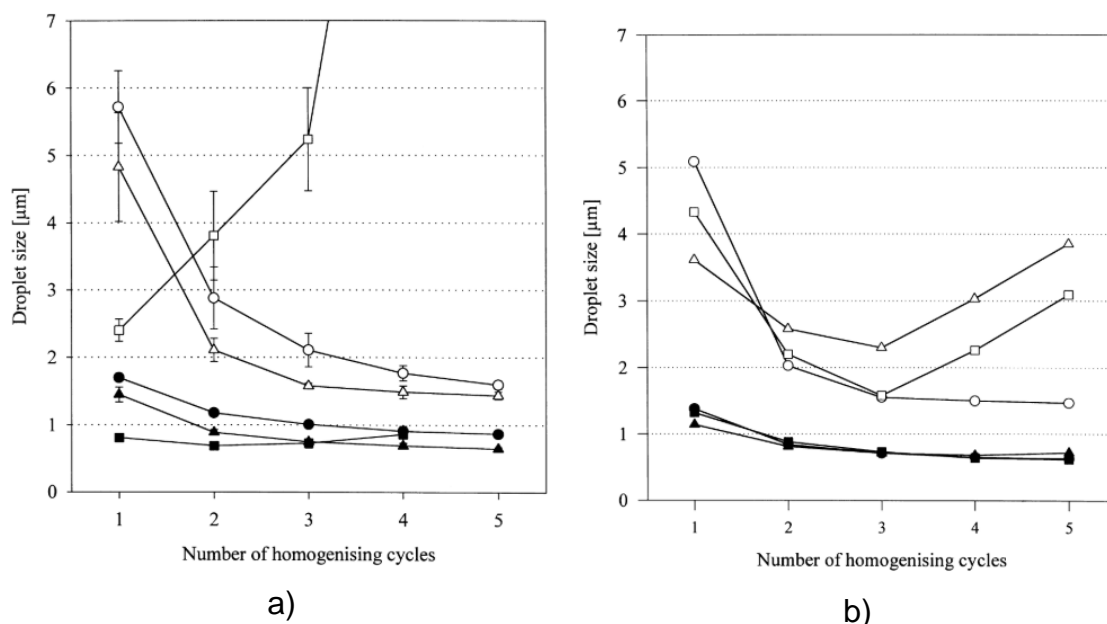


Figure 1.32. a) Influence of the homogenization pressure and the number of homogenization cycles and b) influence of the processing temperature on the droplet size (D (50%)) of emulsions processed at 50 MPa (●), 90 MPa (▲) and 160 MPa (■), D(90%) of emulsions of emulsions processed at 50 MPa (○), 90 MPa (△) and 160 MPa (□), [190].

The second family of HPH concerns the microfluidizers (Figure 1.30.b). Here, a coarse emulsion is forced by a pneumatically powered pump, and two jets of crude emulsion from two opposite channels collide with one another, as a result of a sudden decrease in the diameter of the pipe [196]. This pneumatically driven pump is able to pressurize the in-house compressed air (150-650 kPa) up to about 150

MPa [139]. In more details, a flow stream is pushed by high pressure through microchannels against an impingement area. This creates an enormous shearing action, which is able to provide a very fine emulsion [135]. Furthermore, the main mechanisms that are responsible for the droplets' disruption are the internal forces in turbulent flow along with cavitation [139]. When the emulsion has a high viscosity there is an opportunity to disrupt the laminar elongational flow [139], [148], [197], [198]. Concerning the droplet size control, the homogenization pressure plays a significant role, meaning that by increasing the pressure, the droplet size of the dispersed phase of the emulsions is decreasing. Also decrease of the size can be achieved by increasing the number of passages through the microchannel devices [135]. One hindrance that microfluidization has is that when it comes in the production of large amounts of emulsions it becomes very expensive [135], [199], [200]. In Germany, in 2017 [201], experiments were conducted using biopolymers, such as polysaccharides to obtain nanocarriers with tunable size. The increase of the pressure from 30 MPa to 103 MPa gave much smaller droplets (from 300 nm to 180 nm). Although there was no obvious decrease on the diameter above 69 MPa, the polydispersity index became higher due to the so-called overprocessing phenomenon.

The third class of HPH is the jet disperser (Figure 1.30.c). In this case also two or more jets or coarse emulsions, coming from opposing bore, collide with one another but in a different design [139], [185]. The bore diameters in the jet dispersers are usually 0.3-0.5 mm. The jet disperser has the same order of magnitude as the diameter of the orifice bore and the inlet head diameter of the of the orifice plate is typically 10-60 mm [185][139].

The last class is the based on the nozzle design and it is called orifice plate (Figure 1.30.d). It can be placed either in the center of the inlet or in the outlet of the channel, where the oil is passing through and generate in the outlet of the orifice [202]. The oil droplets undergo laminar elongational flow and they break in the water phase where they are collected. Nair *et al.* [203] prepared acrylate double emulsions and made effort to vary the droplet diameter by increasing the pressure

during homogenization from 6 to 10 MPa. They display that the diameter decreases by the pressure increase yet the size dispersity is significantly increasing which was consequence of a belligerent homogenization (Figure 1.33). Finally, in 2021, Mutsch *et al.* [204] compared two different Reynolds numbers, $Re = 2000$ (laminar flow) and $Re = 5700$ (turbulent flow) and evaluated the droplet variations. It was explained that both mean diameters were approximately the same, whereas the polydispersity was higher in the case of low Reynolds number due to the absence of such high stress forces (Figure 1.33).

In jet dispersers and orifice plates, droplets are mostly disrupted by cause of laminar elongational flow along the bores [139], [148], [185], [189], [198], [205]–[208].

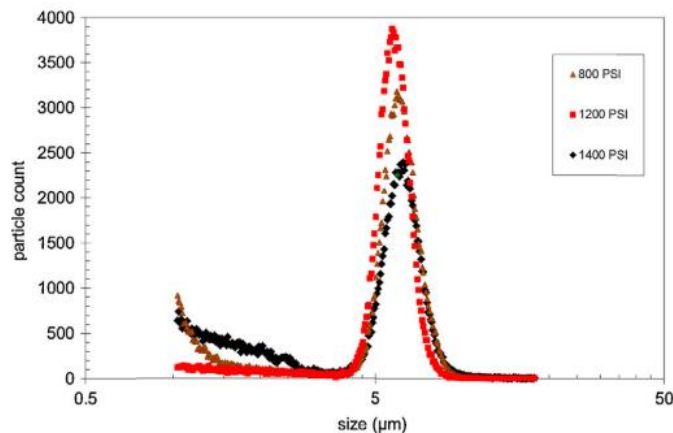


Figure 1.33. Particle size distributions of the final solidified porous particles as a function of orifice back pressure used during $W_1/O/W_2$ homogenization [203].

HPH is a highly efficient method, which makes it available at laboratory and industrial scale [209]. They are used to produce emulsions with droplet diameters smaller than $1.0 \mu\text{m}$ and a narrow droplet distribution [210]. However, two of the major disadvantages are that a big amount of energy is required in order to operate and usually there is an increase on the temperature during processing which might deteriorate the components [135]. This is why, some studies aim to obtain emulsions with rotor-stator mixer as efficient as the ones obtained with high-pressure homogenizers. For instance, in 2020, the production of triglyceride oil-in-water emulsion [211] has been done with these two methods. In Figure 1.34, both devices enable to provide smaller droplet sizes with longer emulsification time. Moreover, rotor-stator mixer displays bigger mean volume diameter in lower speed

but when the speed is maximum the results are comparable with the ones obtained from high-pressure homogenizer. The lowest diameter was a bit higher than 300 nm for both devices. When it comes to the emulsion polydispersity, results show that rotor-stator has lower polydispersity opposed to the high-pressure homogenizer.

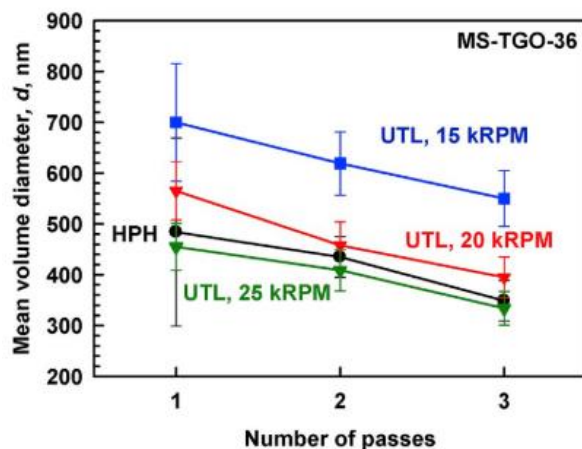


Figure 1.34. Mean diameters of emulsion droplets in relation with the number of passes through each equipment, realized with rotor-stator mixer (UTL) at different rotational speeds and with high-pressure homogenizer (HPH) [211].

So, both rotor-stator and high-pressure homogenizer can be used to obtain monodispersed emulsions, but there is still a need to scale-up these processes in order to have an industrial/continuous production of droplets or particles.

1.4 Static Mixer

In chemical process industries, mixing is the most common and essential procedure in many different aspects [212]. Liquid-liquid dispersions is a widely used method that can take place in various processes such as liquid-liquid extraction, or reactions concerning an emulsification step. It is also comprised in every-day used products such as food, cosmetics, or drug industries. In all the applications, it is crucial to be able to control the droplet size distribution and the average diameter which determine the final properties of the product [213]. Static mixers are being increasingly comprehended in pharmaceutical, chemical, food processing, polymer synthesis, paint and resin, pulp and paper, water treatment and petrochemical industries [214]. It is a device used for continuous mixing of fluid materials where there are motionless elements placed in a pipe or channel [215],

[216]. The only driving force is the pressure difference between the inlet and outlet of the tube [217]. Mainly it is used to provide mixing to two liquids, miscible and immiscible, as well as to mix gas streams, or disperse gas into liquid [215]. There is no requirement for external power apart from the energy needed to pump and flow the fluids through the mixer [216]. However, it should be mentioned that the usual energy required should be highly effected of the length of the tube as well as the design of the static mixers and may vary upon large range of decades.

In 1965 Armeniades *et al.* [218], discovered a new way of mixing two liquids or one liquid with one gas, by installing a hollow cylindrical tube containing several thin flat and curved sheets that fit in the inner tube diameter. Depending on the fluid to be mixed, these elements can be twisted in different angles, between 30° and 210° , to offer better dispersion. Their main use was to blend two viscous liquids that react with each other and create either a viscous or solid product, for example synthetic resin. Static mixing is claimed to be a cost-effective technique that provides in-depth mixing and low pressure drop.

Since then, different geometries of static mixers were established and sold by the most popular brands, Kenics® and Sulzer®, and are able to provide laminar or turbulent blending depending on the application. Both companies develop different geometries that can fulfill all the various demands of the market and research (Figure 1.35). Static mixers are keen to promote secondary transverse flows that elevate the mass and heat transfer in the cross-section [214]. An additional design of a static mixer is the insert-type configuration, where the typical design is a series of identical, stationary inserts named elements, which can be positioned in pipes, channels or ducts [162].



Figure 1.35. Different static mixers designs [219].

High demand of static mixers is observed in continuous processes instead of conventional agitation or batch processes due to the lower cost and sometimes better performance [214]. Using motionless mixers can provide plenty of advantages such as low energy consumption as well as the lower maintenance requirements due to the absence of moving parts [214], [220]. Other crucial benefits are the low cost of the equipment, the small space to place it along with the absence of power apart from pumping [214].

Majority of research that was conducted is based on computational fluid mixing (CFM) to forecast the mixing behavior using a static mixer. This method provides several advantages to research such as the low-cost, the easiness on alternation of the parameter of the system and also allows experimentalists to predict an outcome. Sulzer® SMRX static mixers were on high interest of several researchers. In this static mixer there are several solid crossing tubes in the inner part of the tube that provide high-efficiency cooling or heat of viscous media. In this way the fluid undergoes a compelling radical mixing combined with controlled heat transfer [221]. In 1996 a research group from Switzerland and Canada [222], compared experimental and numerical results to allow the understanding of flow in static mixers as well as to numerically develop an ideal design for an SMRX static mixer. They tested different crossing angles, 10° to 150° and compared an SMRX with one or two elements placed in the inner tube. During the simulations it was shown that 90° crossing angles are sufficient enough since smaller ones did not provide efficient mixing since the obstacles in the flow path were not enough. On the contrary, larger angles disrupt the flow and trigger high pressure drops. The bigger the cross angle the more intense pressure drop was observed. It was also shown that adding a second element in the tube increases the pressure drop by a factor of two, which can be a limit in depending on the application. Finally, they summarized that even though small deviations from numerical to experimental approach can occur, numerical simulations results can serve as a reasonable model of the experimental ones.

Later, Hobbs and Muzzio [223] numerically developed a 6-element Kenics static mixer so as to detect and assess micromixing performance. The main goal was to

vary the Reynolds number from very low up to $Re = 1000$ but still the mixed solution to be in the laminar regime. They discovered that in $Re \leq 10$ the fluid was in the creeping flow condition, where the advective inertial forces are smaller than the viscous forces. In other words, the velocity was very slow and the viscosity too high in that low Reynolds number [224]. On the contrary, by increasing $Re = 100$ and $Re = 1000$ they observed the formation of small islands that did not participate in the mixing process, while at the same time the fluid was entering the chaotic state of mixing. This led to the conclusion that in smaller Reynolds number, the mixing performance is much more effective than in higher where the mixing is poorer.

On the other hand, researchers experimentally evaluated micromixing ability of the widely used continuous flow stirred tank reactor (CSTR) and compared with static mixers. For example, in 2013, investigation was carried out on corn oil-in-water emulsion using a helical type of static mixer equipped with 20 elements [225]. It was shown that even in the beginning of the mixing, static mixer induced smaller and more uniform droplet sizes than the mechanical mixer (Figure 1.36). However, static mixer was more prone to higher reaction rates than the mechanical stirring. This means that in cases that reaction between the two fluid is desired, static mixer can provide this in less time and with much less power consumption.

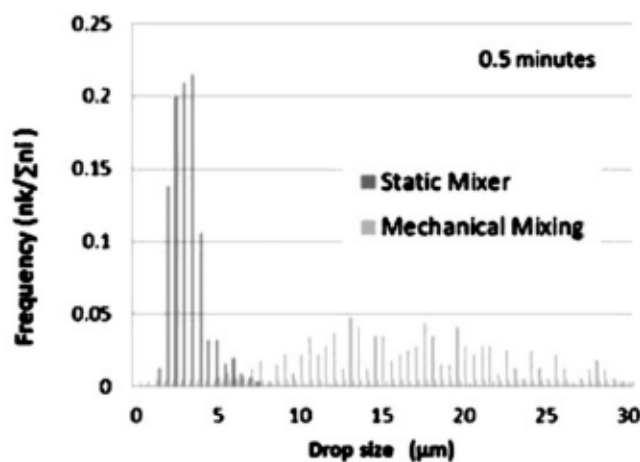


Figure 1.36. Droplet size distribution of methanol in oil when static mixer or mechanical mixing was used for 0.5 min of reaction time [225].

The famous Kenics mixer was developed from different scientific groups and by using various number of elements, e.g. 6, 12 or 24. In the late 90s experimentalists

from Canada [226] used a KM Kenics static mixer equipped with 6 elements and proved that working at low Reynolds numbers ($Re = 2000$, laminar flow) is advantageous due to the decreased energy inputs needed to operate the mixer. During the experiments, streamlines number and thickness were the main characteristics to evaluate the micromixing efficiency. They showed that low or high Reynold numbers had approximately the same striation characteristics after the fluid was passing the 4th or 5th element. This was a great understanding on the fact that high feeding energy does not always cause better mixing. Finally, it was also established that even if the viscosity ratio is high, up to 1, and the streamline widths are bigger, the mixing is more consistent than at lower values of the ratio. This is consequence of the shear rate applied in a less viscous material that causes it to elongate and lead to less thick striations and providing poorer mixing efficiency to the fluid.

Research has also been conducted on the Sulzer SMX static mixer. Recently has been investigated the influence of different parameters on the vegetable oil-in-water emulsion using a 9 element SMX static mixer (Figure 1.37) [227].

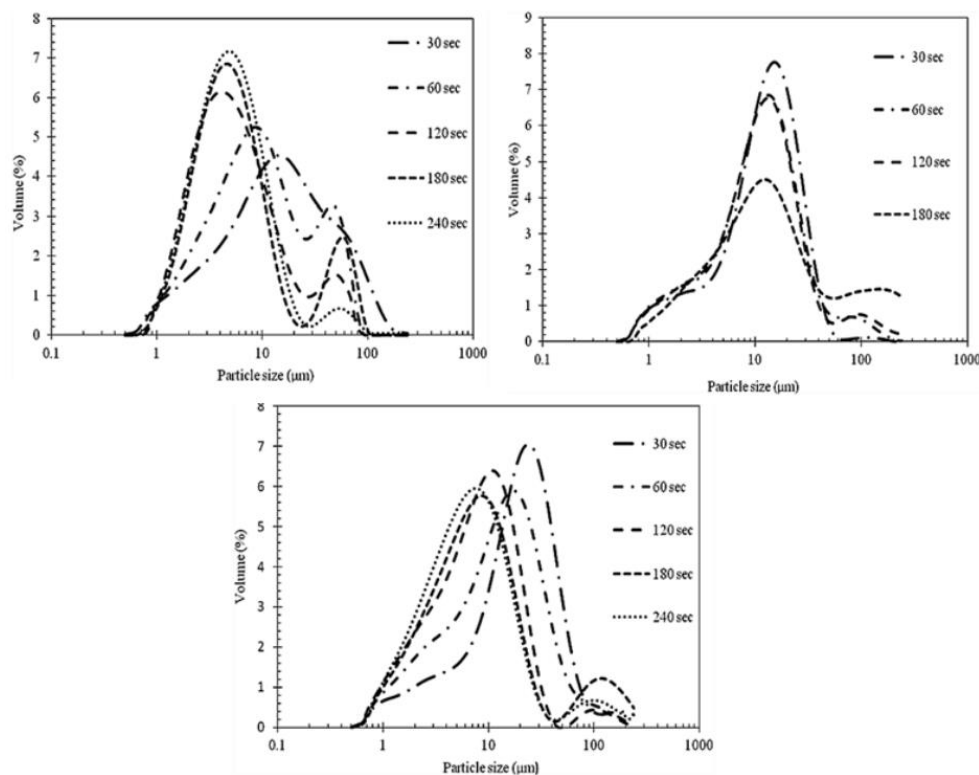


Figure 1.37. Particle size distribution obtained with a Sulzer SMX static mixer, for different ratios of o/w emulsion (top left) 1:100; (top right) 1:50; (bottom) 1:25, at constant flow rates equal to 1250 L/h and for increased emulsification times (30 sec to 3 min) [227].

It was remarked that for a constant flow rate, $q = 1250$ L/h, the increase of the oil content caused the diameter of the oil droplets to increase, while a second peak arise due to instant coalescence of the droplets. Contrastingly, a rise on the flow rate, from 750 to 12500 L/h, improved the droplet size below 10 μm . Finally, the operating time was investigated, and it appears that the droplet size enhanced by longer mixing time. Unfortunately, in all the experiments coalescence of the oil droplets was observed that could not be avoided.

As a partial conclusion, the previously evocated devices (ultrasound generators, rotor-stator mixers, HPH and static mixers), that are the most widely used to produce emulsions [147], [228] use high shear stress to deform and disrupt large droplets [228], [229]. Therefore, high-energy inputs are required in order to operate, limiting their use for shear-sensitive ingredients, such as proteins and starch, that can lose their properties resulting in a poorer system stability [228], [230]. Additionally, using these devices does not allow to easily control the droplet size and the droplet size distribution. This is caused due to the shear stress that is not uniformly distributed, because it is collectively applied near the mixing element, while leaving dead volume areas [231]. Consequently, they can show low reproducibility and quality of the product due to the variations per batch on the same manufacturing scale [232]. Thus, there is a need to develop other methods, such as membrane emulsification, to get rid of these disadvantages.

1.5 Membrane

Contrary to ultrasound generators, rotor-stator mixers, HPH and static mixers, during membrane emulsification the shear stress is allocated evenly over the membrane surface and the droplet size as well as the distribution are more controlled [231]. Besides, the previously mentioned high-energy emulsification devices apply high shear and energy which give rise to the temperature [233]. This temperature increase is attributed to the mechanical energy that is transformed to heat because of the viscous dissipation [234]. On the contrary, during membrane emulsification the shear applied is mild and allows the temperature to have a constant value [233]. Control of temperature is one of the major factors that enable

temperature-sensitive compounds to stay flawless [231]. Over the last 20 years, membrane emulsification received an increasing attention as an alternative method to produce emulsions and particles. It is used in different fields such as food industries and pharmaceuticals where highly consistent droplets with tunable diameters are demanded, such as targeted chemotherapy.

The membrane emulsification method to fabricate monodispersed emulsions was first introduced in 1986 by Nakashima and Shimuzu [235]. In the recent years, there is an increase of interest concerning membrane emulsification used as an alternative method to produce emulsions and particles [236]–[239]. The operating principle, drawn in Figure 1.38, is quite easy to understand. In more details, there are two phases (the continuous and dispersed one) that are separated with a porous membrane that can be hydrophilic or hydrophobic depending on the type of emulsion.

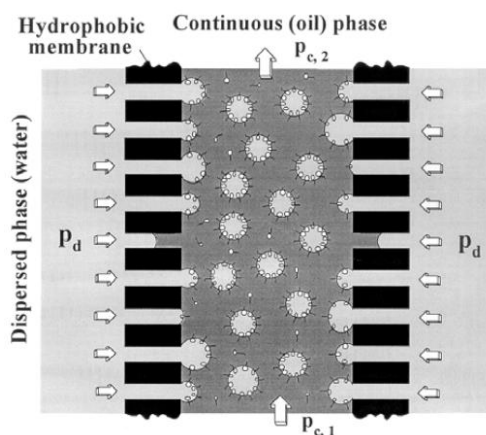


Figure 1.38. Schematic diagram of the preparation of W/O emulsion by membrane emulsification [240].

Usually, the dispersed phase is surrounding the continuous phase that is running through the center of the membrane. Basically, the dispersed phase is pushed with the help of a pump to flow inside the membrane where the continuous phase flows to form the droplets [240], [241]. It is very important to mention that the membrane should not be wetted by the dispersed phase, since it can cause polydisperse emulsions [242]. Once the droplets start to form, surfactant molecules from the continuous phase are attached on their surface so as to stabilize them. This adsorption kinetics dictates the time required to stabilize the droplets against coalescence [240].

There are several factors that influence the droplet size and can be divided in three categories [243]. First, are the properties of the membrane: the porosity of the membrane is a crucial parameter since it can influence the appearance of coalescence. It is believed that the higher the porosity the more likely the droplets in the exit of pores will come in contact and coalesce. Whereas the low porosity can cause the decrease of the dispersed phase flux, which is not desired in a larger-scale emulsion production [240]. Additionally, there is reported a linear relationship between the mean droplet diameter of the emulsion and the mean pore diameter of the membrane [241]. This means that increasing the later tends to increase the droplet size. In 2002, researchers prepared vegetable oil-in-water emulsions by using Shirasu-Porous-Glass (SPG) membrane and obtained a 3.5 times higher mean droplet size compared to the pore size of the membrane [244]. A second category that plays an important role on the droplet size is the process parameters. Two parameters distinguish among others, the transmembrane pressure and the crossflow velocity of the continuous phase. The former refers to the amount of force that is required to push the dispersed phase through the membrane [245]. Increasing this, leads to an obvious increase of the dispersed phase flux through the membrane which causes bigger droplet sizes since the emulsifier molecules do not have enough time to stabilize the newly formed droplets, thus the polydispersity is also increasing. Wu *et al.* [246] prepared water-in-oil kerosene emulsions by using a multiple ceramic membrane. As presented in Figure 1.39, they confirmed that high transmembrane pressure brought an increase on the dispersed phase flux, hence an increase on the mean droplet diameter and polydispersity, that showed a linear dependence on the transmembrane pressure.

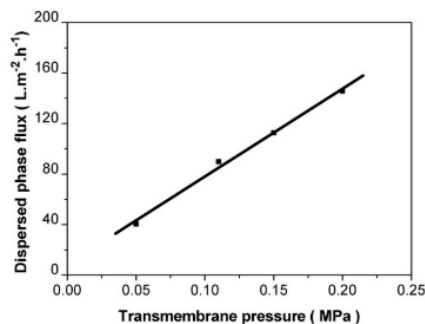


Figure 1.39. Influence of transmembrane pressure on the flux of the dispersed phase [246].

On the other hand, the increase of the cross-flow velocity of the continuous phase allows the formation of smaller droplets, while decreasing the shear forces applied to the formed droplets causes the droplet size and polydispersity to increase [240]. Last category is the physical properties of the fluids to be mixed. One of the major factors that plays a role on the size of the droplets is the surfactant. Its choice has to be done carefully since the polar groups that are attached on the ends can react with the membrane, if they are opposite charged, and adsorb on the surface. This can cause polydisperse emulsions [242]. Moreover, the adsorption time of the surfactant molecules on the droplets surface affects the droplet size. The more rapid the adsorption the smaller the droplets [247]. Finally, the diffusion of the emulsifier molecules determines the size of the newly formed droplets. This means that a rise on the continuous phase viscosity will lead to lower diffusion of the molecules thus to higher droplet diameters [240]. While on the contrary, Vladislavljvic and Schubert [244] showed that an increase on the concentration of the dispersed phase up to 20 vol% has no obvious impact on the mean droplet size (Figure 1.40).

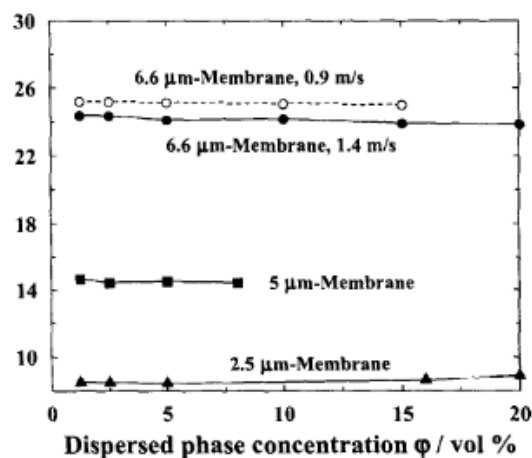


Figure 1.40. The influence of dispersed phase content on mean droplet size for different mean pore sizes [244].

As a summary, all the high-energy emulsification methods evocated in this part, and summarized in Table 1.1, are widely used to produce emulsions. However, the increased energy consumption when these devices are used led to the development of low-energy emulsification devices. This way the emulsification process becomes less expensive as well as more friendly for the environment.

These low-energy emulsification processes will be discussed in more detail in the following chapter.

Table 1.1. High-energy emulsification (HEE) methods.

HEE Methods	Forces driving the droplet formation	Pros and cons
Ultrasound generators	Mechanical vibrations (cavitation)	Pros: <ul style="list-style-type: none"> • Fast method • Small diameters (even below 100 nm) • Narrow size distributions (PDI<0.2) Cons: <ul style="list-style-type: none"> • High energy consumption • Heat increase • Small volume (not possible to scale-up)
Rotos-stator mixers	Mechanical and shear stress forces	Pros: <ul style="list-style-type: none"> • Rapid • Already used on industrial scale Cons: <ul style="list-style-type: none"> • Lack of diameter control • High polydisperse emulsions
High-pressure homogenizer	Intense shear and extensional stress forces	Pros: <ul style="list-style-type: none"> • Improved droplet size control Cons: <ul style="list-style-type: none"> • High energy consumption • Heat increase • Difficult to obtain monomodal emulsions and diameter below 100 nm
Static mixers	Shear and extensional stress forces	Pros: <ul style="list-style-type: none"> • Low cost • Compact device • Rapid • Low pressure drop¹ Cons: <ul style="list-style-type: none"> • High pressure drop² • Heat increase
Membrane	Mild shear forces	Pros: <ul style="list-style-type: none"> • Improved temperature control • Low energy consumption • Narrow size distributions Cons: <ul style="list-style-type: none"> • Low productivity • Low production rate • Relatively diluted emulsions (dispersed phase up to 30 vol%) • High pressure drop

1: Short tube, few static mixers, 2: Long tube, more static mixers

2. Low-Energy Emulsification Methods

Low-energy emulsification occurs under laminar and low-energy conditions. The important advantage using this method is from an economic perspective and as a potential matrix to encapsulate fragile molecules. Low-energy methods are primarily controlled by the physicochemical behavior of the surfactants and requires careful selection of surfactant and cosurfactant combinations [148].

2.1 Spontaneous Emulsifications

Spontaneous emulsification has received an increased interest during the last years since the energy input required is much less compared to the high-energy emulsification techniques [248]. Therefore, they are used in different fields such as pharmaceuticals, food, and agricultural industries. Johannes Gad was the one who described spontaneous emulsification in 1879 [249]. Theoretically, to form an emulsion using this method there is no requirement of external energy feeding just an oil phase as well as an aqueous phase that are not in thermodynamic equilibrium to come in contact. In a realistic sense, to spontaneously form the emulsion energy is required, such as temperature increase, which can help a thermosensitive system to form emulsion [250]. A very characteristic phenomena for the spontaneous emulsification is the “Ouzo effect”. The first to describe this were Vitale and Katz [251]. The term “ouzo” origins from a Greek alcoholic beverage containing star-anis. Basically the “ouzo effect” occurs when water is added in a mixture of ethanol containing anise oil. Once the anis oil is dissolved, small droplets spontaneously nucleate and the emulsion is formed [252], [253]. Anton *et al.* [254] described a physicochemical mechanism where the two liquids are mixed at room temperature. Particularly, the dispersed phase is composed of oil, surfactant and a solvent that is miscible in water, and it is mixed with water. When these two phases come in contact the surfactant, if water soluble, with the solvent are diffusing to the aqueous phase, which causes a high turbulence at the oil-water interface. This fast diffusion leads the oil-water interfacial area to grow and allow the spontaneous development of the oil droplets in the aqueous phase.

Three categories play a very important role on the control of the particle size. The most obvious one is the thoughtful choice of the composition of organic and aqueous phases. For example, in 2021, researchers tried to tune the morphology of porous particles that could be used as biomaterials in tissue engineering [255]. They were the first ones to prove that varying the amount of the organic solvent that is added in the continuous phase can change the porous formation (Figure 1.41).

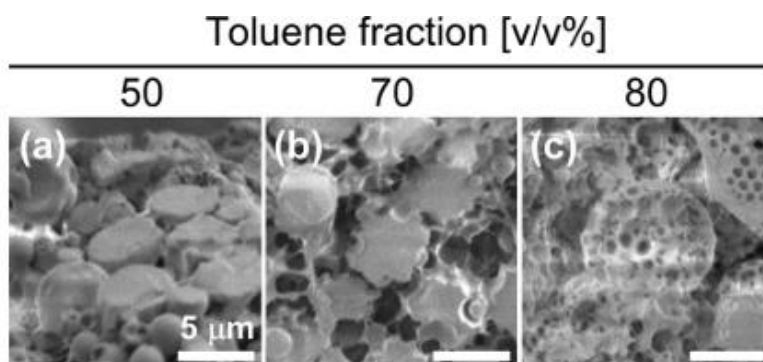


Figure 1.41. Scanning electron microscopy images of particle cross-sections. The particles were produced by changing the amount of organic solvent (toluene) that is added in the continuous phase. Extracted from [255].

Another way to tune the particle size is the changes of the experimental environment, such the temperature, pH and ionic strength are some important conditions for this [256]. Finally, the mixing step is also important, which means that the stirring speed need to be controlled, along with the sequence of addition of the two phases, as well as the speed with which the second phase is added to the first one [256], [257].

Several advantages distinguish this technique. Starting with the minimum energy input which is necessary to form the emulsion, while at the same time the use of compounds that do not harm encapsulated molecules [254]. On the contrary, a big drawback is the fact that large amounts of synthetic surfactants are required in many cases, which can be a restrictive factor in biocompatibility and most importantly the increased cost of production [256].

2.2 Phase Inversion Temperature

The phase inversion temperature (PIT) process involves the recording of changes of the emulsion properties according to the HLB of the emulsifier used, when

temperature is provided to the system [258], [259]. Practically, the PIT occurs when the emulsion from oil-in-water becomes inversed and forms water-in-oil emulsion, and vice versa [260]. Shinoda and Saito were the first to introduce the low-energy phase inversion temperature method in 1968 [261]. They simply mixed oil with water and non-ionic surfactants at room temperature under low stirring and progressively increased the temperature. They observed that the oil-in-water emulsion that was initially prepared, experienced phase inversion to form a water-in-oil emulsion. This spontaneous emulsification method involves both oil-in-water and water-in-oil emulsions that can be inversed. The driving force for this change is the physicochemical properties of the surfactant.

This means that a nonionic surfactant can undergo changes in its hydrophilic-lipophilic balance (HLB) which influences also the solubility in oil and water phases depending on the temperature [262]. It is well known that the head group of a nonionic surfactant is soluble in water, and this is due to the increased moisture that is trapped in between the molecules. When the temperature is low, the water solubility of the surfactant is high. Increasing the temperature results in the dehydration of its head which lower its solubility in water. A further increase in the temperature will reaches a critical point, called PIT, where the surfactant is almost equally soluble in water and oil phases. Above PIT, the solubility of the surfactant is higher in the oil than in the water phase. Some researchers refer this PIT to a change in the curvature of the non-ionic surfactant molecules [256].

It is worth to mention that a stable oil-in-water emulsion in ambient temperature can be obtained when the PIT happens at higher temperatures [261]. Control of this temperature can be achieved by controlling the amount of surfactant used for the experiment. Researchers in Japan reported that the higher the hydrophilicity of the surfactant, the higher was the PIT, meaning above 25 - 70°C higher than the storage temperature [263]. Another important parameter is the hydrophilic-hydrophobic properties of the emulsifier. When the surfactant chosen is more hydrophobic, the PIT decreases and the opposite [264]. Finally, a careful selection of the oil that is used to emulsify is required. Indeed, Förster *et al.* [264], observed a lower PIT when the oil they used was less polar.

2.3 Phase Inversion Composition

The phase inversion composition (PIC) process has some common points with the phase inversion temperature (PIT). However, the main difference relies on the absence of heat input to the system. This unfolds a big variation of surfactants alike PIT where the surfactant system has to be thermosensitive [265]. PIC is conducted at room temperature, however emulsification occurs when the composition of the system changes [256]. Most of the time a big amount of water is added to a water-in-oil system in order to dilute and exceed the critical point above which an oil-in-water emulsion will be formed. This allows the surfactant micelles of the water phase to swell while the water is diffusing inside and form a sponge like phase. The addition of more water will eventually lead to the phase inversion when the oil droplets nucleate in this sponge phase, but they still stay there while the rest of the sponge composition eventually forms cylindrical or spherical micelles that are soluble in water. Finally, the oil droplets and micelles separate and disperse in the aqueous phase and the resulting emulsion has a bimodal size distribution [265].

3. Microfluidics

Microfluidics is the field where small amount of fluids, between 10^{-9} – 10^{-18} liters, flow in small channels having tens or hundreds of micrometers dimensions [266]–[269]. Even though it seems that is a quite new method, the first time that this concept was discussed was in microelectronics in 1947 [270]. There is an extensive range of applications since microfluidics get involved in different fields, such as microtechnology, biotechnology, engineering, chemistry, physics and so on [210]. Researchers rely on the plenty advantages of microfluidics. Starting with the fact that very small amounts of reagents can be used in order to run an experiment, which rises from their small internal volume. This also is a big benefit since the production time is very short. The budget required for the experiment can be very low thanks to the use of common laboratory equipment, such as plastic syringes and tubes, in some cases. Microfluidics offers a better control of the parameters of the system, process or chemical parameters, as well as of the size,

shape, and morphology of the material to be produced [168], [272], [273]. Finally, it turns out to be a method where contamination of the products can hardly happen [271]. On the contrary, there are several disadvantages as well. The main restrictions of microfluidics are the low production rates and the process scale-up. In addition, the need of syringe pump is essential and can increase the set-up costs [272].

Among many different subcategories of microfluidics is the so-called droplet-based microfluidics and can be used in different applications such as individual chemical microreactors, or emulsions, etc. [274], [275]. Main focus will be given on the formation of micron size emulsions. Generally, in droplet-based microfluidics immiscible fluids of specific volumes are used to form droplets that are mainly in the range of micrometers with very narrow size distributions [276]. There are two important classes of droplet generators: the microchannel- and capillary-based devices. In the former, microfluidic chips composed of different microchannels allow to put in contact both continuous and dispersed phases (Figure 1.42.a-c), while for the second assembly of tubing and capillary are used for the same (Figure 1.42.d-f) [277] [278].

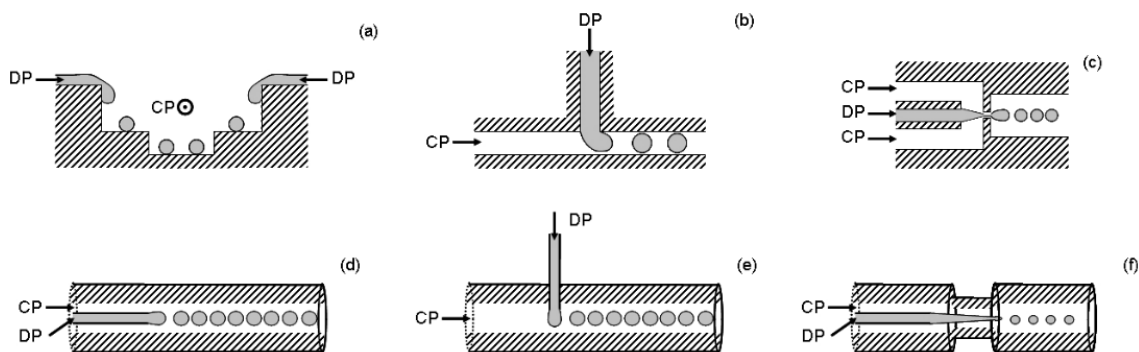


Figure 1.42. Different microfluidic devices for the emulsification of a liquid monomer. Microchannel-based devices: (a) terrace-like device, (b) T-junction device, (c) flow-focusing device. Capillary-based devices: (d) co-flow device, (e) crossflow device, (f) flow-focusing device. CP and DP are respectively the continuous and the dispersed phases [275]

In both classes, the main driving force for droplet production is the shearing force imposed to the forming droplets. This force happens when the droplet that is formed undergoes shear due to the flow of the continuous phase and gets detached and dispersed into the continuous phase [277]. Different strategies can be used to put the two fluids (Figure 1.42), among which the co-flow devices where the continuous and disperse phase flow in the same direction. The review of the

literature concerning the co-flow devices will allow the better understanding of the diameter control using those systems, which will also be used in the present dissertation.

To have a better understanding on the system there are two dimensionless numbers that play a crucial role on the particle diameter. The first one is the Reynolds number Re , which is the ratio of the inertial to viscous forces in a fluid system (Part D.1, Equation 1). Since the characteristic dimension of these droplet generators is in the micron range, the Re is expected to be low ($Re < 2000$) and, thus, the system evolves under a laminar flow regime. In this regime, the system does not mix alike the turbulent flow but only by diffusion [279]. The second dimensionless number is called the capillary number Ca (Equation 1.2), which depicts for a shear flow the ratio between the viscous and interfacial forces of the fluid system [279]:

$$Ca = \frac{\mu v}{\sigma} \quad (1.2)$$

where σ is the interfacial tension between the two fluids, v is the mean velocity of the fluid and μ is the dynamic viscosity of the fluid.

Control of the particle size can be achieved by controlling the parameters that influence those two dimensionless numbers [275]. Over the years, researchers developed a big variety of particle shapes that are produced using microfluidics, such as spheres [280], [281], discs [282] and rods [283]. In view of these possibilities, Nie *et al.* [284] developed a polyurethane elastomer microfluidic reactor allowing the continuous production of core-shell droplets to be used in data storage (Figure 1.43).

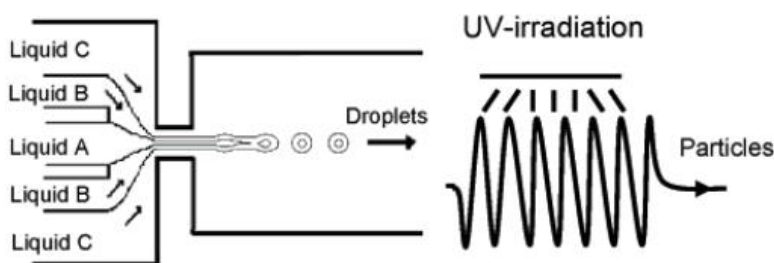


Figure 1.43. Schematic of production of droplets by laminar co-flow of silicone oil (A), monomer (B), and aqueous (C) phases followed by schematic of the wavy channel used for photopolymerization of monomer in core-shell droplets [284].

They used three immiscible fluids the continuous phase fluid was an aqueous solution with of sodium dodecyl sulfate as surfactant, the core fluid was silicon oil mixed with another surfactant, Span 80, and finally the shell was a mixture of two acrylate monomers and the photoinitiator. They obtained the solid particles using a wavy channel which was under UV irradiation at 360 nm wavelength. Among the different parameters that influence the particle size, they paid attention to the flow rate of the continuous phase as it can change the particle size. In Figure 1.44, the average diameter of the core-shell droplets is presented as the flow rate of the continuous phase increases and keeping the other two flow rates constant. A decrease of the diameter from 100 μm down to 70 μm has been observed when the flow rate of the continuous phase was increased from 20 mL/h to 50 mL/h. Moreover, the coefficient of variation, determined as the standard deviation divided by the mean droplet size, and when this value is below 5% the particles are considered to be monodisperse, which is the case in this research (CV below 1.5%).

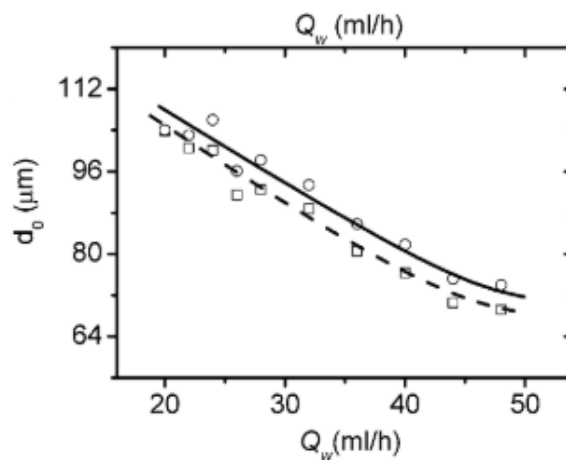


Figure 1.44. Average diameter of core-shell droplets plotted as a function of flow rate of the continuous phase [284].

Another particle morphology that was introduced in 2008 by Serra *at al.* [285] using co-flow microfluidics (Figure 1.45) is the polymeric beads that stick together to form a necklace looking shape. They used methyl methacrylate mixed with a cross-linker and a photoinitiator to form the dispersed phase. For the continuous phase they mixed distilled water with methyl cellulose. Once the droplets were formed, they used in-line UV polymerization, at 365 nm wavelength, to obtain the particles. Then they linked the particles using an aqueous solution and pushing the droplets

in a tube so as the one touches the other in a line. Finally, the system was heated for 1 h at 80°C in order for the particles to stick together and form a necklace shape.

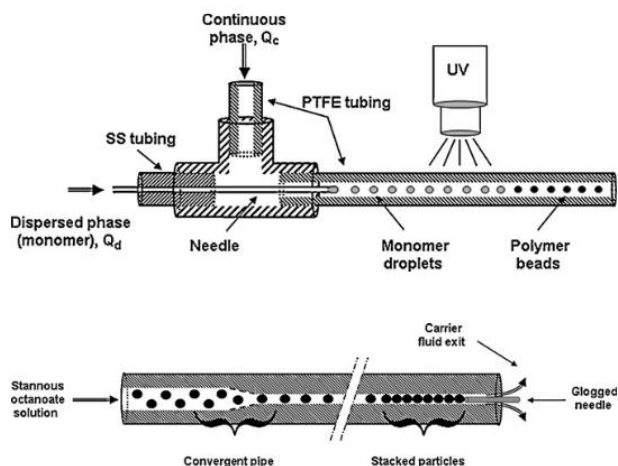


Figure 1.45. Schematic of needle/tubing microfluidic device and particles stacking [285].

In another work [286] they evaluate the influence of material and operating parameters on the droplet size. Figure 1.45 shows that for a fixed ratio of continuous and disperse phase flow rates, Q_c / Q_d , the viscosity of the continuous phase is inversely proportional to the particle size. This means that in higher viscosities the obtained particle size is becoming smaller, since the shear applied to the dispersed phase is much higher. At higher viscosities, more than 1050 cP, a plateau was observed when the Q_c / Q_d was higher than 150. This can be explained by the fact that the needle used to produce the droplets had an inner diameter of 260 μm , and the droplets could not be formed below this value.

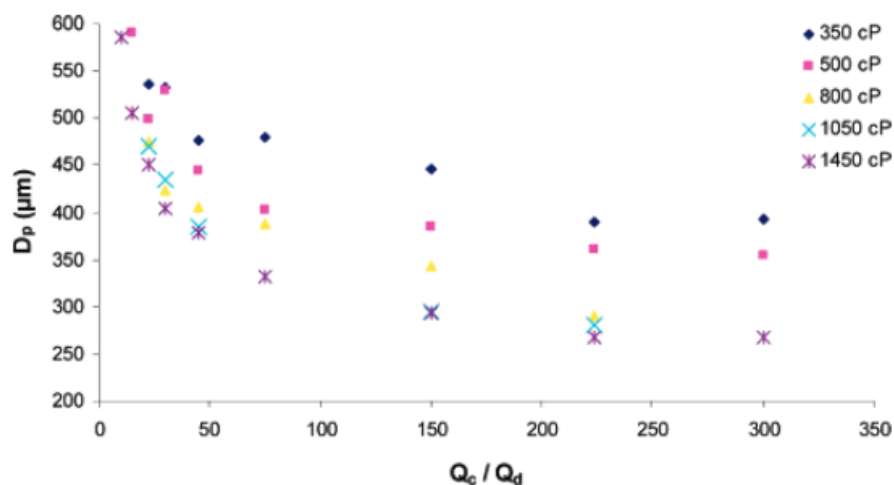


Figure 1.46. Average diameters of polymer particles produced by varying the continuous phase viscosity [286].

D Conclusion

To summarize what was described in this chapter, an overview about emulsion types (w/o, o/w and multiple) and stabilization mechanisms along with their wide variety of applications were discussed in detail. This was followed by an extensive report on the thiol-ene chemistry, and its use in many applications including miniemulsions. Finally, several emulsification devices were detailed for the production of nanometer and micron size droplets and polymeric particles. For the production of nanodroplets, high-energy emulsification devices, containing rotor-stator mixers and high-pressure homogenizers show several disadvantages such as lack of droplet diameter control and increased energy consumption. Regarding microdroplets, microfluidic-based droplet generators were appeared as elements of choice to produce monodisperse micron size droplets whose diameter can be easily varied upon changes in operating and material parameters.

The literature review revealed the need for the development of low-energy emulsification device in order to produce thiol-ene based miniemulsions. The goal of this thesis is to develop an elongational-flow based device so as to produce monomodal miniemulsion whose droplet size can be tuned with the least amount of energy required to operate. Since thiol-ene click chemistry has several advantages and applications that were described before, the miniemulsion that will be produced will be based on this thiol-ene chemistry using different monomers. This way the droplet diameter can be tuned depending on the desired application. Different emulsification devices will be investigated to produce different poly(thioether) nano- and microparticles.

Ξ Bibliography

- [1] S. Slomkowski *et al.*, "Terminology of polymers and polymerization processes in dispersed systems (IUPAC recommendations 2011)," *Pure and Applied Chemistry*, vol. 83, no. 12, pp. 2229–2259, 2011, doi: 10.1351/PAC-REC-10-06-03.
- [2] Ph. D. Helmenstine, Anne Marie, "Suspension Definition in Chemistry," 2020. thoughtco.com/definition-of-suspension-605714
- [3] C. Dictionary, "Definition of Suspension." <https://www.chemicool.com/definition/suspension.html>
- [4] Byju's, "Suspensions." <https://byjus.com/chemistry/suspension/>
- [5] D. H. Everett and L. Butterworths, "Manual of Symbols and Terminology for Physiocochemical Quantities and Units, Appendix II: Definitions, Terminology and Symbols in Colloid and Surface Chemistry PART I Prepare." 1971.
- [6] Brady Senese, *Chemistry: Matter and Its Changes*, 4th ed.
- [7] Ph. D. Helmenstine, Anne Marie, "Colloid Definition - Chemistry Glossary," 2020. thoughtco.com/definition-of-colloid-chemistry-glossary-605840
- [8] C. Dictionary, "Definition of Colloid." <https://www.chemicool.com/definition/colloid.html>
- [9] Jacob N. Israelachvili, *Intermolecular and surface forces*, 3rd ed. Academic Press, 2011.
- [10] R. G. Jones *et al.*, "Compendium of Polymer Terminology," *International Union of Pure and Applied Chemistry (IUPAC)*, 2008.
- [11] S. Slomkowski *et al.*, "Terminology of polymers and polymerization processes in dispersed systems (IUPAC Recommendations 2011)", [Online]. Available: [https://en.wikipedia.org/wiki/Dispersion_\(chemistry\)](https://en.wikipedia.org/wiki/Dispersion_(chemistry))
- [12] IUPAC. Compendium of Chemical Terminology (The "Gold Book"), *Solution*, 2nd ed. Oxford: Blackwell Scientific Publications, 1997. doi: <https://doi.org/10.1351/goldbook>.
- [13] D. U. Khademhosseini A, *Gels Handbook: Fundamentals, Properties and Applications*. World Scientific Pub Co Inc.
- [14] Harper Douglas, "Online Etymology Dictionary." www.etymonline.com (accessed Jan. 12, 2022).
- [15] W. C. Hinds, *Aerosol Technology*, 2nd ed. Wiley-Interscience, 1999.
- [16] D. J. McClements, "Critical review of techniques and methodologies for characterization of emulsion stability," *Critical Reviews in Food Science and Nutrition*, vol. 47, no. 7, pp. 611–649, 2007, doi: 10.1080/10408390701289292.
- [17] S. Akbari and A. H. Nour, "Emulsion types, stability mechanisms and rheology: A review," *International Journal of Innovative Research and Scientific Studies*, vol. 1, no. 1, pp. 14–21, 2018.
- [18] J. S. Lim, S. F. Wong, M. C. Law, Y. Samyudia, and S. S. Dol, "A Review on the Effects of Emulsions on Flow Behaviours and Common Factors Affecting the Stability of

- Emulsions,” *Journal of Applied Sciences*, vol. 15, no. 2. pp. 167–172, 2015. doi: 10.3923/jas.2015.167.172.
- [19] B. Novales, P. Papineau, A. Sire, and M. A. V. Axelos, “Characterization of emulsions and suspensions by video image analysis,” *Colloids and Surfaces A: Physicochemical and Engineering Aspects*, vol. 221, no. 1–3, pp. 81–89, 2003, doi: 10.1016/S0927-7757(03)00102-X.
- [20] M. M. Robins, A. D. Watson, and P. J. Wilde, “Emulsions - Creaming and rheology,” *Current Opinion in Colloid and Interface Science*, vol. 7, no. 5–6, pp. 419–425, 2002, doi: 10.1016/S1359-0294(02)00089-4.
- [21] H. Butt, K. Graf, and M. Kappl, *Physics and Chemistry of Interfaces*. Wiley, 2003. doi: 10.1002/3527602313.
- [22] D. J. McClements and S. M. Jafari, “Improving emulsion formation, stability and performance using mixed emulsifiers: A review,” *Advances in Colloid and Interface Science*, vol. 251, pp. 55–79, 2018, doi: 10.1016/j.cis.2017.12.001.
- [23] A. W. Thomas, “A review of the literature of emulsions,” *Industrial and Engineering Chemistry*, vol. 12, no. 2, pp. 177–181, 1920, doi: 10.1021/ie50122a031.
- [24] V. Madaan, A. chanana, M. K. Kataria, and A. Bilandi, “Emulsion Technology and Recent Trends in Emulsion Applications,” *International Research Journal of Pharmacy*, vol. 5, no. 7, pp. 533–542, 2014, doi: 10.7897/2230-8407.0507108.
- [25] M. E.-S. Abdel-Raouf, *Crude Oil Emulsion-Composition Stability and Characterization*. 2012. doi: 10.5772/35875.
- [26] B. A. Khan *et al.*, “Basics of pharmaceutical emulsions: A review,” *African Journal of Pharmacy and Pharmacology*, vol. 5, no. 25, pp. 2715–2725, 2011, doi: 10.5897/AJPP11.698.
- [27] W. C. Griffin, “Classification of Surface-Active Agents by ‘HLB,’” *J Soc Cosmet Chem*, vol. 1, no. 5, pp. 311–326, 1949.
- [28] W. C. Griffin, “Classification of Surface-Active Agents by ‘HLB,’” *J Soc Cosmet Chem*, vol. 1, pp. 311–326, doi: 10.1155/2012/187421.
- [29] W. C. Griffin, “Calculation of HLB Values of Non-Ionic Surfactants,” *Journal of Pharmaceutical Sciences*, vol. 58, no. 12, pp. 1443–1449, 1969, doi: 10.1002/jps.2600581203.
- [30] W. C. Griffin, “Calculation of HLB Values of Non-Ionic Surfactants,” *J Soc Cosmet Chem*, vol. 5, no. 4, pp. 249–256, 1954.
- [31] A. Mandal, A. Samanta, A. Bera, and K. Ojha, “Characterization of oil-water emulsion and its use in enhanced oil recovery,” *Industrial and Engineering Chemistry Research*, vol. 49, no. 24, pp. 12756–12761, Dec. 2010, doi: 10.1021/ie101589x.
- [32] C. Gonglun and T. Daniel, “An experimental study of stability of oil–water emulsion,” *Fuel Processing Technology*, vol. 86, no. 5, pp. 499–508, 2005, doi: <https://doi.org/10.1016/j.fuproc.2004.03.010>.

- [33] E. M. Rodrigues, A. V. N. de Carvalho Teixeira, D. E. Cesar, and M. R. Tótola, "Strategy to improve crude oil biodegradation in oligotrophic aquatic environments: W/O/W fertilized emulsions and hydrocarbonoclastic bacteria," *Brazilian Journal of Microbiology*, no. February, 2020, doi: 10.1007/s42770-020-00244-x.
- [34] M. Khan, "Recent trends in water-indiesel emulsion as fuel," *The Scientific World Journal*, 2014.
- [35] Skinchakra, "W/O vs. O/W Emulsions," 2015. <https://skinchakra.eu/blog/archives/331-WO-vs.-OW-Emulsions.html>
- [36] A. I. A. Mohamed, A. S. Sultan, I. A. Hussein, and G. A. Al-Muntasheri, "Influence of Surfactant Structure on the Stability of Water-in-Oil Emulsions under High-Temperature High-Salinity Conditions," *Journal of Chemistry*, vol. 2017, 2017, doi: 10.1155/2017/5471376.
- [37] J. M. Williams, "High Internal Phase Water-in-Oil Emulsions: Influence of Surfactants and Cosurfactants on Emulsion Stability and Foam Quality," 1370. [Online]. Available: <https://pubs.acs.org/sharingguidelines>
- [38] Y. Morozumi and Y. Saito, "Effect of physical properties on microexplosion occurrence in water-in-oil emulsion droplets," *Energy and Fuels*, vol. 24, no. 3, pp. 1854–1859, 2010, doi: 10.1021/ef9014026.
- [39] A. Nesterenko, A. Drelich, H. Lu, D. Clause, and I. Pezron, "Influence of a mixed particle/surfactant emulsifier system on water-in-oil emulsion stability," *Colloids and Surfaces A: Physicochemical and Engineering Aspects*, vol. 457, no. 1, pp. 49–57, Sep. 2014, doi: 10.1016/j.colsurfa.2014.05.044.
- [40] G. Colucci, A. Santamaria-echart, S. C. Silva, I. P. M. Fernandes, C. C. Sipoli, and M. F. Barreiro, "Development of Water-in-Oil Emulsions as Delivery Vehicles and Testing with a Natural Antimicrobial Extract," pp. 5–7.
- [41] N. Badri Viswanathan, P. A. Thomas, J. K. Pandit, M. G. Kulkarni, and R. A. Mashelkar, "Preparation of non-porous microspheres with high entrapment efficiency of proteins by a (water-in-oil)-in-oil emulsion technique," *Journal of Controlled Release*, vol. 58, no. 1, pp. 9–20, 1999, doi: 10.1016/S0168-3659(98)00140-0.
- [42] T. Delmas *et al.*, "How to prepare and stabilize very small nanoemulsions," *Langmuir*, vol. 27, no. 5, pp. 1683–1692, 2011, doi: 10.1021/la104221q.
- [43] S. Kentish, T. J. Wooster, M. Ashokkumar, S. Balachandran, R. Mawson, and L. Simons, "The use of ultrasonics for nanoemulsion preparation," *Innovative Food Science and Emerging Technologies*, vol. 9, no. 2, pp. 170–175, 2008, doi: 10.1016/j.ifset.2007.07.005.
- [44] T. S. H. Leong, T. J. Wooster, S. E. Kentish, and M. Ashokkumar, "Minimising oil droplet size using ultrasonic emulsification," *Ultrasonics Sonochemistry*, vol. 16, no. 6, pp. 721–727, 2009, doi: 10.1016/j.ultsonch.2009.02.008.
- [45] T. S. H. Leong, T. J. Wooster, S. E. Kentish, and M. Ashokkumar, "Minimising oil droplet size using ultrasonic emulsification," *Ultrasonics Sonochemistry*, vol. 16, no. 6, pp. 721–727, 2009, doi: 10.1016/j.ultsonch.2009.02.008.

- [46] F. J. A. and R. K. K. Azhar Yaqoob Khan, Sushama Talegaonkar, Zeenat Iqbal, "An Overview on Multiple Emulsions," *Current Drug Delivery*, vol. 3, pp. 429–443, 2006, doi: 10.52711/2231-5713.2021.00026.
- [47] S. S. Davis and I. M. Walker, "Multiple Emulsions as Targetable Delivery Systems," 1987.
- [48] C. X. Zhao, "Multiphase flow microfluidics for the production of single or multiple emulsions for drug delivery," *Advanced Drug Delivery Reviews*, vol. 65, no. 11–12, pp. 1420–1446, Nov. 15, 2013. doi: 10.1016/j.addr.2013.05.009.
- [49] G. Muschiolik, "Multiple emulsions for food use," *Current Opinion in Colloid and Interface Science*, vol. 12, no. 4–5, pp. 213–220, Oct. 2007. doi: 10.1016/j.cocis.2007.07.006.
- [50] F. Jiménez-Colmenero, "Potential applications of multiple emulsions in the development of healthy and functional foods," *Food Research International*, vol. 52, no. 1, pp. 64–74, Jun. 2013. doi: 10.1016/j.foodres.2013.02.040.
- [51] J. M. Morais, P. A. Rocha-Filho, and D. J. Burgess, "Influence of phase inversion on the formation and stability of one-step multiple emulsions," *Langmuir*, vol. 25, no. 14, pp. 7954–7961, Jul. 2009, doi: 10.1021/la9007125.
- [52] F. Jahanzad, G. Crombie, R. Innes, and S. Sajjadi, "Catastrophic phase inversion via formation of multiple emulsions: A prerequisite for formation of fine emulsions," *Chemical Engineering Research and Design*, vol. 87, no. 4, pp. 492–498, Apr. 2009, doi: 10.1016/j.cherd.2008.11.015.
- [53] Y. Beldengrün *et al.*, "Formation and stabilization of multiple water-in-water-in-water (W/W/W) emulsions," *Food Hydrocolloids*, vol. 102, May 2020, doi: 10.1016/j.foodhyd.2019.105588.
- [54] P. B. O'Donnell and J. W. McGinity, "Properties of multiphase microspheres of poly(dl-lactic acid) or poly(dl-lactic-co-glycolic acid) produced by mechanical agitation, sonication, or potentiometric dispersion," *Journal of Microencapsulation*, vol. 13, no. 6, pp. 667–677, 1996, doi: 10.3109/02652049609026050.
- [55] S. Y. Tang and M. Sivakumar, "Design and evaluation of aspirin-loaded water-in-oil-in-water submicron multiple emulsions generated using two-stage ultrasonic cavitation emulsification technique," *Asia-Pacific Journal of Chemical Engineering*, vol. 7, no. SUPPL. 1, May 2012, doi: 10.1002/apj.664.
- [56] S. Y. Tang, M. Sivakumar, and B. Nashiru, "Impact of osmotic pressure and gelling in the generation of highly stable single core water-in-oil-in-water (W/O/W) nano multiple emulsions of aspirin assisted by two-stage ultrasonic cavitation emulsification," *Colloids and Surfaces B: Biointerfaces*, vol. 102, pp. 653–658, Feb. 2013, doi: 10.1016/j.colsurfb.2012.08.036.
- [57] W. Jing, J. Wu, W. Xing, W. Jin, and N. Xu, "Emulsions prepared by two-stage ceramic membrane jet-flow emulsification," *AIChE Journal*, vol. 51, no. 5, pp. 1339–1345, May 2005, doi: 10.1002/aic.10405.
- [58] X. Ying *et al.*, "Preparation and drying of water-in-oil-in-water (W/O/W) double emulsion to encapsulate soy peptides," *Food Research International*, vol. 141, Mar. 2021, doi: 10.1016/j.foodres.2021.110148.

- [59] V. Massel, Y. Fang, and M. Corredig, "Pectin nanoemulsions in multiple emulsions: Stability and encapsulation efficiency," *Food Research International*, vol. 139, Jan. 2021, doi: 10.1016/j.foodres.2020.109950.
- [60] S. Matsumoto, Y. Kita, and D. Yonezawa, "An Attempt at Preparing Water-in-Oil-in-Water Multiple-Phase Emulsions."
- [61] H. Okochi and M. Nakano, "Preparation and evaluation of w/o/w type emulsions containing vancomycin," *Advanced Drug Delivery Reviews*, vol. 45, no. 1, pp. 5–26, 2000, doi: 10.1016/S0169-409X(00)00097-1.
- [62] H. Okochi and M. Nakano, "Basic Studies on Formulation Method of Preparation and Characterization of Water-in-Oil-in-Water Type Multiple Emulsions Containing Vancomycin," *Chemical and Pharmaceutical Bulletin*, vol. 44, no. 1, pp. 180–186, 1996.
- [63] I. Scherze, R. Knöfel, and G. Muschiolik, "Automated image analysis as a control tool for multiple emulsions," *Food Hydrocolloids*, vol. 19, no. 3, pp. 617–624, 2005, doi: 10.1016/j.foodhyd.2004.10.029.
- [64] E. Dickinson and S. R. Euston, "Stability of Food Emulsions Containing both Protein and Polysaccharide," in *Food Polymers, Gels and Colloids*, Elsevier, 1991, pp. 132–146. doi: 10.1533/9781845698331.132.
- [65] K. P. Das and J. E. Kinsella, "Stability of food emulsions: Physicochemical role of protein and nonprotein emulsifiers," *Advances in Food and Nutrition Research*, vol. 34, 1990.
- [66] Y. Xie *et al.*, "The research about microscopic structure of emulsion membrane in O/W emulsion by NMR and its influence to emulsion stability," *International Journal of Pharmaceutics*, vol. 500, no. 1–2, pp. 110–119, Mar. 2016, doi: 10.1016/j.ijpharm.2016.01.032.
- [67] M. Kowalska, M. Ziomek, and A. Zbikowska, "Stability of cosmetic emulsion containing different amount of hemp oil," *International Journal of Cosmetic Science*, vol. 37, no. 4, pp. 408–416, Aug. 2015, doi: 10.1111/ics.12211.
- [68] Particle Sciences, "Emulsion Stability and Testing," *Drug Development Services*, vol. 2, 2011.
- [69] K. C. Powell, R. Damitz, and A. Chauhan, "Relating emulsion stability to interfacial properties for pharmaceutical emulsions stabilized by Pluronic F68 surfactant," *International Journal of Pharmaceutics*, vol. 521, no. 1–2, pp. 8–18, Apr. 2017, doi: 10.1016/j.ijpharm.2017.01.058.
- [70] P. Thanasukarn, R. Pongsawatmanit, and D. J. McClements, "Influence of emulsifier type on freeze-thaw stability of hydrogenated palm oil-in-water emulsions," *Food Hydrocolloids*, vol. 18, no. 6, pp. 1033–1043, 2004, doi: 10.1016/j.foodhyd.2004.04.010.
- [71] G. G. Palazolo, P. A. Sobral, and J. R. Wagner, "Freeze-thaw stability of oil-in-water emulsions prepared with native and thermally-denatured soybean isolates," *Food Hydrocolloids*, vol. 25, no. 3, pp. 398–409, 2011, doi: 10.1016/j.foodhyd.2010.07.008.
- [72] Petrowiki, "Stability of oil emulsions." https://petrowiki.org/Stability_of_oil_emulsions

- [73] M. M. Robins, "Emulsions - Creaming phenomena," *Current Opinion in Colloid and Interface Science*, vol. 5, no. 5–6, pp. 265–272, 2000, doi: 10.1016/S1359-0294(00)00065-0.
- [74] A. Seifert, M. Schultz, K. Strence, G. Muschiolik, and H. Schmandke, "Mechanical barrier preventing the centrifugal creaming of O/W food emulsions, stabilized by proteins," *Nahrung*, vol. 34, pp. 293–295, 1990.
- [75] D. I. Comas, J. R. Wagner, and M. C. Tomás, "Creaming stability of oil in water (O/W) emulsions: Influence of pH on soybean protein-lecithin interaction," *Food Hydrocolloids*, vol. 20, no. 7, pp. 990–996, Oct. 2006, doi: 10.1016/j.foodhyd.2005.11.006.
- [76] R. Chanamai and D. J. McClements, "Creaming stability of flocculated monodisperse oil-in-water emulsions," *Journal of Colloid and Interface Science*, vol. 225, no. 1, pp. 214–218, May 2000, doi: 10.1006/jcis.2000.6766.
- [77] R. Chanamai and D. J. McClements, "Dependence of creaming and rheology of monodisperse oil-in-water emulsions on droplet size and concentration," 2000. [Online]. Available: www.elsevier.nl/locate/colsurfa
- [78] T. Schmidts, P. Schlupp, A. Gross, D. Dobler, and F. Runkel, "Required HLB Determination of Some Pharmaceutical Oils in Submicron Emulsions," *Journal of Dispersion Science and Technology*, vol. 33, no. 6, pp. 816–820, Jun. 2012, doi: 10.1080/01932691.2011.584800.
- [79] Y. Osei *et al.*, "Investigation of the emulsifying and suspending potential of cashew tree gum in pharmaceutical formulations," *Article in International Journal of Pharmacy and Pharmaceutical Sciences*, 2011.
- [80] Oxford English Dictionary, "Sedimentation," *Oxford University Press*.
- [81] J. Bibette, D. Roux, and B. Pouligny, "Creaming of emulsions: the role of depletion forces induced by surfactant," *Journal de Physique II*, vol. 3, pp. 401–424, 1992, doi: 10.1051/jp2:1992141ff.ffjpa-00247641.
- [82] D. N. Petsev, "Theory of emulsion flocculation," *Interface Science and Technology*, vol. 4, no. C, pp. 313–350, 2004, doi: 10.1016/S1573-4285(04)80010-3.
- [83] T. K. Basaran, K. Demetriades, and D. J. McClements, "Ultrasonic imaging of gravitational separation in emulsions," *Colloids and Surfaces A: Physicochemical and Engineering Aspects*, vol. 136, no. 1–2, pp. 169–181, 1998, doi: 10.1016/S0927-7757(97)00338-5.
- [84] H. M. Princen, "Gravitational syneresis in foams and concentrated emulsions," *Journal of Colloid And Interface Science*, vol. 134, no. 1, pp. 188–197, 1990, doi: 10.1016/0021-9797(90)90266-Q.
- [85] A. M. Howe, A. R. Mackie, and M. M. Robins, "Technique to measure emulsion creaming by velocity of ultrasound," *Journal of Dispersion Science and Technology*, vol. 7, no. 2, pp. 231–243, 1986, doi: 10.1080/01932698608943457.
- [86] S. Slomkowski *et al.*, "Terminology of polymers and polymerization processes in dispersed systems (IUPAC Recommendations 2011)," *Pure and Applied Chemistry*, vol. 83, no. 12, 2011, doi: 10.1351/PAC-REC-10-06-03.

- [87] E. Dickinson, M. Golding, and M. J. W. Povey, "Creaming and flocculation of oil-in-water emulsions containing sodium caseinate," *Journal of Colloid and Interface Science*, vol. 185, no. 2, pp. 515–529, 1997, doi: 10.1006/jcis.1996.4605.
- [88] D. J. McClements, *Food Emulsions: Principles, particles and Techniques, Second Edition*, 2nd ed. Boca Taton: CRC Press, 2004. doi: <https://doi.org/10.1201/9781420039436>.
- [89] S. Slomkowski *et al.*, "Terminology of polymers and polymerization processes in dispersed systems (IUPAC recommendations 2011)," *Pure and Applied Chemistry*, vol. 83, no. 12, pp. 2229–2259, 2011, doi: 10.1351/PAC-REC-10-06-03.
- [90] E. Dickinson, "Flocculation of protein-stabilized oil-in-water emulsions," *Colloids and Surfaces B: Biointerfaces*, vol. 81, no. 1, pp. 130–140, 2010, doi: 10.1016/j.colsurfb.2010.06.033.
- [91] E. Dickinson, "Strategies to control and inhibit the flocculation of protein-stabilized oil-in-water emulsions," *Food Hydrocolloids*, vol. 96, no. May, pp. 209–223, 2019, doi: 10.1016/j.foodhyd.2019.05.021.
- [92] E. Fredrick, P. Walstra, and K. Dewettinck, "Factors governing partial coalescence in oil-in-water emulsions," *Advances in Colloid and Interface Science*, vol. 153, no. 1–2, pp. 30–42, 2010, doi: 10.1016/j.cis.2009.10.003.
- [93] Y. Yamashita, R. Miyahara, and K. Sakamoto, *Emulsion and emulsification technology*. Elsevier Inc., 2017. doi: 10.1016/B978-0-12-802005-0.00028-8.
- [94] S. J. Friberg Stig, Larsson Kare, *Food Emulsions, Fourth Edition, Revises and Expanded*, 4th ed. CRC Press, 2003.
- [95] IUPAC Compendium of Chemical Terminology (the "Gold Book"), *Ostwald ripening*, 2nd ed. Blackwell Scientific Publications, 1997. doi: <https://doi.org/10.1351/goldbook>.
- [96] A. Kabalnov, "Ostwald ripening and related phenomena," *Journal of Dispersion Science and Technology*, vol. 22, no. 1, pp. 1–12, 2001, doi: 10.1081/DIS-100102675.
- [97] D. J. McClements, *Biopolymers in Food Emulsions*, First Edit. Elsevier Inc., 2009. doi: 10.1016/B978-0-12-374195-0.00004-5.
- [98] P. Taylor, "Ostwald ripening in emulsions," *Advances in Colloid and Interface Science*, vol. 75, no. 2, pp. 107–163, 1998, doi: 10.1016/S0001-8686(98)00035-9.
- [99] A. S. Kabal'nov, A. V. Pertzov, and E. D. Shchukin, "Ostwald ripening in two-component disperse phase systems: Application to emulsion stability," *Colloids and Surfaces*, vol. 24, no. 1, pp. 19–32, 1987, doi: 10.1016/0166-6622(87)80258-5.
- [100] P. Taylor, "Ostwald ripening in emulsions," *Colloids and Surfaces A: Physicochemical and Engineering Aspects*, vol. 99, pp. 175–185, 1995.
- [101] J. Alemán *et al.*, "Definitions of terms relating to the structure and processing of sols, gels, networks, and inorganic-organic hybrid materials (IUPAC recommendations 2007)," *Pure and Applied Chemistry*, vol. 79, no. 10, pp. 1801–1829, 2007, doi: 10.1351/pac200779101801.
- [102] T. Posner, "Zum Schluss darf ich es nicht unterlausen, nieiuen Aasisteuteii Hrn. / In German," *Ber. Dtsch. Chem. Ges.*, vol. 38, no. 1, pp. 646–657, 1905.

- [103] Brian H. Northrop and Roderick N. Coffey, "Thiol-ene Click Chemistry: Computational and Kinetic Analysis of the Influence of Alkene Functionality," *American Chemical Society*, vol. 134, pp. 13804–13817, 2012, doi: [dx.doi.org/10.1021/ja305441d](https://doi.org/10.1021/ja305441d).
- [104] C. E. Hoyle and C. N. Bowman, "Thiol-ene click chemistry," *Angewandte Chemie - International Edition*, vol. 49, no. 9, pp. 1540–1573, 2010, doi: [10.1002/anie.200903924](https://doi.org/10.1002/anie.200903924).
- [105] H. C. Kolb, M. G. Finn, and K. B. Sharpless, "Click Chemistry: Diverse Chemical Function from a Few Good Reactions," *Angewandte Chemie - International Edition*, vol. 40, no. 11, pp. 2004–2021, 2001, doi: [10.1002/1521-3773\(20010601\)40:11<2004::AID-ANIE2004>3.0.CO;2-5](https://doi.org/10.1002/1521-3773(20010601)40:11<2004::AID-ANIE2004>3.0.CO;2-5).
- [106] "regiospecific," www.merriam-webster.com. <https://www.merriam-webster.com/medical/regiospecific>
- [107] HUBEI BENXING CHEMICAL CO, "Method for removing thiol smell in thiol organotin/ In Chinese," 2008
- [108] G. Kühne, J. S. Diesen, and E. Klemm, "New results of the self-initiation mechanism of SH/En addition polymerization," *Angewandte Makromolekulare Chemie*, vol. 242, pp. 139–145, 1996, doi: [10.1002/apmc.1996.052420109](https://doi.org/10.1002/apmc.1996.052420109).
- [109] N. B. Cramer, J. P. Scott, and C. N. Bowman, "Photopolymerizations of thiol-ene polymers without photoinitiators," *Macromolecules*, vol. 35, no. 14, pp. 5361–5365, 2002, doi: [10.1021/ma0200672](https://doi.org/10.1021/ma0200672).
- [110] T. O. Machado, P. B. Cardoso, P. E. Feuser, C. Sayer, and P. H. H. Araújo, "Thiol-ene miniemulsion polymerization of a biobased monomer for biomedical applications," *Colloids and Surfaces B: Biointerfaces*, vol. 159, pp. 509–517, 2017, doi: [10.1016/j.colsurfb.2017.07.043](https://doi.org/10.1016/j.colsurfb.2017.07.043).
- [111] J. Kumpfmüller, K. Stadlmann, Z. Li, V. Satzinger, J. Stampfl, and R. Liska, "Two-photon-induced thiol-ene polymerization as a fabrication tool for flexible optical waveguides," *Designed Monomers and Polymers*, vol. 17, no. 4, pp. 390–400, 2014, doi: [10.1080/15685551.2013.840515](https://doi.org/10.1080/15685551.2013.840515).
- [112] Y. Rong, S. Ali, Q. Ouyang, L. Wang, B. Wang, and Q. Chen, "A turn-on upconversion fluorescence sensor for acrylamide in potato chips based on fluorescence resonance energy transfer and thiol-ene Michael addition," *Food Chemistry*, vol. 351, no. January, p. 129215, 2021, doi: [10.1016/j.foodchem.2021.129215](https://doi.org/10.1016/j.foodchem.2021.129215).
- [113] O. Okay, S. K. Reddy, and C. N. Bowman, "Molecular weight development during thiol-ene photopolymerizations," *Macromolecules*, vol. 38, no. 10, pp. 4501–4511, 2005, doi: [10.1021/ma050080x](https://doi.org/10.1021/ma050080x).
- [114] Madhusha, "Difference Between Chain Growth and Step Growth Polymerization." <https://pediaa.com/difference-between-chain-growth-and-step-growth-polymerization/>
- [115] B. H. Northrop and R. N. Coffey, "Thiol-ene click chemistry: Computational and kinetic analysis of the influence of alkene functionality," *J Am Chem Soc*, vol. 134, no. 33, pp. 13804–13817, 2012, doi: [10.1021/ja305441d](https://doi.org/10.1021/ja305441d).

- [116] C. E. Hoyle, A. B. Lowe, and C. N. Bowman, "Thiol-click chemistry: A multifaceted toolbox for small molecule and polymer synthesis," *Chemical Society Reviews*, vol. 39, no. 4, pp. 1355–1387, 2010, doi: 10.1039/b901979k.
- [117] N. B. Cramer and C. N. Bowman, "Chapter 1. Thiol-ene and Thiol-yne Chemistry in Ideal Network Synthesis," no. 6, pp. 1–27, 2013, doi: 10.1039/9781849736961-00001.
- [118] C. E. Hoyle, T. Y. Lee, and T. Roper, "Thiol-enes: Chemistry of the past with promise for the future," *Journal of Polymer Science, Part A: Polymer Chemistry*, vol. 42, no. 21, pp. 5301–5338, 2004, doi: 10.1002/pola.20366.
- [119] S. K. Reddy, N. B. Cramer, and C. N. Bowman, "Thiol-vinyl mechanisms. 1. Termination and propagation kinetics in thiol-ene photopolymerizations," *Macromolecules*, vol. 39, no. 10, pp. 3673–3680, 2006, doi: 10.1021/ma060008e.
- [120] D. P. Nair *et al.*, "The Thiol-Michael addition click reaction: A powerful and widely used tool in materials chemistry," *Chemistry of Materials*, vol. 26, no. 1, pp. 724–744, 2014, doi: 10.1021/cm402180t.
- [121] Y. Sun *et al.*, "Thiol Michael addition reaction: a facile tool for introducing peptides into polymer-based gene delivery systems," *Polymer International*, vol. 67, no. 1, pp. 25–31, 2018, doi: 10.1002/pi.5490.
- [122] D. P. Nair *et al.*, "The Thiol-Michael addition click reaction: A powerful and widely used tool in materials chemistry," *Chemistry of Materials*, vol. 26, no. 1, pp. 724–744, 2014, doi: 10.1021/cm402180t.
- [123] F. Goethals, "Multistep reactions based on thiolactones for the synthesis of functionalized polymers," 2015.
- [124] H. H. Szmant, A. J. Mata, A. J. Namis, and A. M. Panthananickal, "The thiol-olefin co-oxidation (TOCO) Reaction—IV," *Tetrahedron*, vol. 32, no. 22, pp. 2665–2680, 1976, doi: 10.1016/0040-4020(76)80104-4.
- [125] C. M. Q. Le, F. Morlet-Savaryab, and A. Chemtob, "Role of thiol oxidation by air in the mechanism of the self-initiated thermal thiol-ene polymerization," *Polymer Chemistry*, 2021, doi: DOI <https://doi.org/10.1039/D1PY01301G>.
- [126] B. M. Rayaprolu, J. J. Strawser, and G. Anyarambhatla, "Excipients in parenteral formulations: selection considerations and effective utilization with small molecules and biologics," *Drug Development and Industrial Pharmacy*, vol. 44, no. 10. Taylor and Francis Ltd., pp. 1565–1571, Oct. 03, 2018. doi: 10.1080/03639045.2018.1483392.
- [127] A. Štorha, E. A. Mun, and V. v. Khutoryanskiy, "Synthesis of thiolated and acrylated nanoparticles using thiol-ene click chemistry: Towards novel mucoadhesive materials for drug delivery," *RSC Advances*, vol. 3, no. 30, pp. 12275–12279, 2013, doi: 10.1039/c3ra2093k.
- [128] O. Z. Durham, D. V. Chapman, S. Krishnan, and D. A. Shipp, "Radical Mediated Thiol-Ene Emulsion Polymerizations," *Macromolecules*, vol. 50, no. 3, pp. 775–783, 2017, doi: 10.1021/acs.macromol.6b02228.

- [129] T. Yang, J. Zheng, B. S. Zheng, F. Liu, S. Wang, and C. H. Tang, "High internal phase emulsions stabilized by starch nanocrystals," *Food Hydrocolloids*, vol. 82, pp. 230–238, 2018, doi: 10.1016/j.foodhyd.2018.04.006.
- [130] V. Hobiger, A. Zahoranova, S. Baudis, R. Liska, and P. Krajnc, "Thiol – Ene Cross-linking of Poly(ethylene glycol) within High Internal Phase Emulsions: Degradable Hydrophilic PolyHIPEs for Controlled Drug Release," 2021, doi: 10.1021/acs.macromol.1c01240.
- [131] S. E. S. Michel, S. E. Rogers, W. H. Briscoe, and M. C. Galan, "Tunable Thiol-Ene Photo-Cross-Linked Chitosan-Based Hydrogels for Biomedical Applications," *ACS Applied Bio Materials*, 2020, doi: 10.1021/acsabm.0c01171.
- [132] D. H. Do, M. Ecker, and W. E. Voit, "Characterization of a Thiol-Ene/Acrylate-Based Polymer for Neuroprosthetic Implants," *ACS Omega*, vol. 2, no. 8, pp. 4604–4611, 2017, doi: 10.1021/acsomega.7b00834.
- [133] D. Sticker, R. Geczy, U. O. Häfeli, and J. P. Kutter, "Thiol-Ene Based Polymers as Versatile Materials for Microfluidic Devices for Life Sciences Applications," *ACS Applied Materials and Interfaces*, vol. 12, no. 9, pp. 10080–10095, 2020, doi: 10.1021/acsmi.9b22050.
- [134] S. M. Tähkä, A. Bonabi, M. E. Nordberg, M. Kanerva, V. P. Jokinen, and T. M. Sikanen, "Thiol-ene microfluidic devices for microchip electrophoresis: Effects of curing conditions and monomer composition on surface properties," *Journal of Chromatography A*, vol. 1426, pp. 233–240, 2015, doi: 10.1016/j.chroma.2015.11.072.
- [135] J. Hadžiabdić, D. Orman, A. Elezović, E. Vranić, and E. Vranić, "Preparation of Nanoemulsion by High-Energy and Low-Energy Emulsification Methods," vol. 62, pp. 317–322, 2017, doi: 10.1007/978-981-10-4166-2.
- [136] D. Rousseau, "Fat crystals and emulsion stability - a review," *Food Research International*, vol. 33, pp. 3–14, 2000, [Online]. Available: www.elsevier.com/locate/foodres
- [137] L. Lobo, I. Ivanov, and D. Wasan, "Dispersion Coalescence: Kinetic Creamed Dispersions Stability of," *Materials, Interfaces and Electrochemical Phenomena*, vol. 39, no. 2, pp. 322–334, 1993.
- [138] R. A. W. Hill and J. T. Knight, "A Kinetic Theory of Droplet Coalescence with Application to Emulsion Stability," *Transaction of the Faraday Society*, vol. 61, pp. 170–181, 1965, doi: <https://doi.org/10.1039/TF9656100170>.
- [139] S. Mahdi, E. Assadpoor, Y. He, and B. Bhandari, "Re-coalescence of emulsion droplets during high-energy emulsification," *Food Hydrocolloids*, vol. 22, pp. 1191–1202, 2008, doi: 10.1016/j.foodhyd.2007.09.006.
- [140] J. Rondin, M. Bouquey, R. Muller, C. A. ; Serra, G. Martin, and P. Sonntag, "Dispersive mixing efficiency of an elongational flow mixer on PP/EPDM blends: morphological analysis and correlation with viscoelastic properties," *Polymer Engineering and Science*, vol. 54, 2014, doi: DOI:10.1002/pen.23667.
- [141] A. Taha *et al.*, "Ultrasonic emulsification: An overview on the preparation of different emulsifiers-stabilized emulsions," *Trends in Food Science and Technology*, vol. 105, pp. 363–377, Nov. 2020, doi: 10.1016/j.tifs.2020.09.024.

- [142] M. Stang, H. Schuchmann, and H. Schubert, "Emulsification in High-Pressure Homogenizers," *Engineering in Life Sciences*, vol. 1, no. 4, pp. 151–157, 2001, doi: 1618-0240/01/0410-0151.
- [143] Y. F. Maa and C. Hsu, "Liquid-liquid emulsification by static mixers for use in microencapsulation," *Journal of Microencapsulation*, vol. 13, no. 4, pp. 419–433, 1996, doi: 10.3109/02652049609026028.
- [144] H. Yuyama, T. Watanabe, G.-H. Ma, M. Nagai, and S. Omi, "Preparation and analysis of uniform emulsion droplets using SPG membrane emulsification technique," *Colloids and Surfaces A: Physicochemical and Engineering Aspects*, vol. 168, 2000.
- [145] A. U. Rehman *et al.*, "Spontaneous nano-emulsification with tailor-made amphiphilic polymers and related monomers," *European Journal of Pharmaceutical Research*, vol. 1, no. 1, pp. 27–36, Mar. 2019, doi: 10.34154/2019-ejpr.01(01).pp-27-36/eurass.
- [146] C. Solans, D. Morales, and M. Homs, "Spontaneous emulsification," *Current Opinion in Colloid and Interface Science*, vol. 22. Elsevier Ltd, pp. 88–93, Apr. 01, 2016. doi: 10.1016/j.cocis.2016.03.002.
- [147] S. M. Joscelyne and G. Trägårdh, "Membrane emulsification - A literature review," *Journal of Membrane Science*, vol. 169, no. 1, pp. 107–117, 2000, doi: 10.1016/S0376-7388(99)00334-8.
- [148] R. C. Santana, F. A. Perrechil, and R. L. Cunha, "High- and Low-Energy Emulsifications for Food Applications: A Focus on Process Parameters," *Food Engineering Reviews*, vol. 5, no. 2, pp. 107–122, 2013, doi: 10.1007/s12393-013-9065-4.
- [149] P. Taylor and H. P. Grace, "Dispersion Phenomena in High Viscosity Immiscible Fluid Systems and Application of Static Mixers As Dispersion Dispersion Phenomena in High Viscosity Immiscible Fluid Systems and Application O F Static Mixers As Dispersion Devices in Such Systems," *Science (1979)*, vol. 6445, no. 912873516, pp. 37–41, 2009, doi: 10.1080/00986448208911047.
- [150] J. D. N. Cheeke and J. D. N. Cheeke, *Fundamentals and Applications of Ultrasonic Waves*. 2010. doi: 10.1201/9781420042139.
- [151] B. Abismaïl, J. P. Canselier, A. M. Wilhelm, H. Delmas, and C. Gourdon, "Emulsification by ultrasound: Drop size distribution and stability," *Ultrasonics Sonochemistry*, vol. 6, no. 1–2, pp. 75–83, 1999, doi: 10.1016/S1350-4177(98)00027-3.
- [152] M. Ashokkumar, "The characterization of acoustic cavitation bubbles - An overview," *Ultrasonics Sonochemistry*, vol. 18, no. 4, pp. 864–872, 2011, doi: 10.1016/j.ultsonch.2010.11.016.
- [153] J. P. Canselier, H. Delmas, A. M. Wilhelm, and B. Abismaïl, "Ultrasound emulsification - An overview," *Journal of Dispersion Science and Technology*, vol. 23, no. 1–3, pp. 333–349, 2002, doi: 10.1080/01932690208984209.
- [154] C. E. Brennen, *Cavitation and Bubble Dynamics*. Oxford University Press, 1995.
- [155] S. G. Gaikwad and A. B. Pandit, "Ultrasound emulsification: Effect of ultrasonic and physicochemical properties on dispersed phase volume and droplet size," *Ultrasonics Sonochemistry*, vol. 15, no. 4, pp. 554–563, 2008, doi: 10.1016/j.ultsonch.2007.06.011.

- [156] T. G. Mason, J. N. Wilking, K. Meleson, C. B. Chang, and S. M. Graves, "Nanoemulsions: Formation, structure, and physical properties," *Journal of Physics Condensed Matter*, vol. 18, no. 41, 2006, doi: 10.1088/0953-8984/18/41/R01.
- [157] R. J. Wood, J. Lee, and M. J. Bussemaker, "A parametric review of sonochemistry: Control and augmentation of sonochemical activity in aqueous solutions," *Ultrasonics Sonochemistry*, vol. 38. Elsevier B.V., pp. 351–370, Sep. 01, 2017. doi: 10.1016/j.ultsonch.2017.03.030.
- [158] P. R. Gogate and P. N. Patil, "Sonochemical Reactors," *Topics in current chemistry (Cham)*, vol. 374, no. 5. p. 61, Oct. 01, 2016. doi: 10.1007/s41061-016-0064-9.
- [159] T. Hielscher, "Ultrasonic Production of Nano-Size Dispersions and Emulsions," *Dans European Nano Systems Workshop - ENS*, pp. 138–143, 2005, doi: <https://doi.org/10.48550/arXiv.0708.1831>.
- [160] E. Webster, "Cavitation," *Dictionary, Merriam-Webster*. <https://www.merriam-webster.com/dictionary/cavitation> (accessed Mar. 16, 2022).
- [161] D. Bermúdez-Aguirre, T. Mobbs, and G. v. Barbosa-Cánovas, "Ultrasound applications in food processing," in *Food Engineering Series*, Springer, 2011, pp. 65–105. doi: 10.1007/978-1-4419-7472-3_3.
- [162] S. Abbas, K. Hayat, E. Karangwa, M. Bashari, and X. Zhang, "An Overview of Ultrasound-Assisted Food-Grade Nanoemulsions," *Food Engineering Reviews*, vol. 5, no. 3, pp. 139–157, 2013, doi: 10.1007/s12393-013-9066-3.
- [163] T. J. Mason and P. Cintas, "Sonochemistry," *Handbook of Green Chemistry and Technology*, pp. 372–396, 2007, doi: 10.1002/9780470988305.ch16.
- [164] S. Kentish, T. J. Wooster, M. Ashokkumar, S. Balachandran, R. Mawson, and L. Simons, "The use of ultrasonics for nanoemulsion preparation," *Innovative Food Science and Emerging Technologies*, vol. 9, no. 2, pp. 170–175, 2008, doi: 10.1016/j.ifset.2007.07.005.
- [165] K. Y. Hernández-Giottonini *et al.*, "PLGA nanoparticle preparations by emulsification and nanoprecipitation techniques: Effects of formulation parameters," *RSC Advances*, vol. 10, no. 8, pp. 4218–4231, 2020, doi: 10.1039/c9ra10857b.
- [166] C. E. Astete and C. M. Sabliov, "Synthesis and characterization of PLGA nanoparticles," *Journal of Biomaterials Science, Polymer Edition*, vol. 17, no. 3. VSP BV, pp. 247–289, 2006. doi: 10.1163/156856206775997322.
- [167] S. Y. Xie, S. L. Wang, B. K. Zhao, C. Han, M. Wang, and W. Z. Zhou, "Effect of PLGA as a polymeric emulsifier on preparation of hydrophilic protein-loaded solid lipid nanoparticles," *Colloids and Surfaces B: Biointerfaces*, vol. 67, no. 2, pp. 199–204, Dec. 2008, doi: 10.1016/j.colsurfb.2008.08.018.
- [168] M. Vauthier and C. A. Serra, "One-step production of polyelectrolyte nanoparticles," *Polymer International*, vol. 70, no. 6, pp. 860–865, 2021, doi: 10.1002/pi.6178.
- [169] S. Ferri *et al.*, "Tailoring the size of ultrasound responsive lipid-shelled nanodroplets by varying production parameters and environmental conditions," *Ultrasonics Sonochemistry*, vol. 73, May 2021, doi: 10.1016/j.ultsonch.2021.105482.

- [170] X. Sui *et al.*, “Impact of ultrasonic treatment on an emulsion system stabilized with soybean protein isolate and lecithin: Its emulsifying property and emulsion stability,” *Food Hydrocolloids*, vol. 63, pp. 727–734, 2017, doi: 10.1016/j.foodhyd.2016.10.024.
- [171] K. Nakabayashi, M. Kojima, S. Inagi, Y. Hirai, and M. Atobe, “Size-controlled synthesis of polymer nanoparticles with tandem acoustic emulsification followed by soap-free emulsion polymerization,” *ACS Macro Letters*, vol. 2, no. 6, pp. 482–484, 2013, doi: 10.1021/mz4001817.
- [172] W. Li, T. S. H. Leong, M. Ashokkumar, and G. J. O. Martin, “A study of the effectiveness and energy efficiency of ultrasonic emulsification,” *Physical Chemistry Chemical Physics*, vol. 20, no. 1, pp. 86–96, 2017, doi: 10.1039/c7cp07133g.
- [173] P. Scholz and C. M. Keck, “Nanoemulsions produced by rotor-stator high speed stirring,” *International Journal of Pharmaceutics*, vol. 482, no. 1–2, pp. 110–117, Mar. 2015, doi: 10.1016/j.ijpharm.2014.12.040.
- [174] A. Håkansson, M. Askaner, and F. Innings, “Extent and mechanism of coalescence in rotor-stator mixer food-emulsion emulsification,” *Journal of Food Engineering*, vol. 175, pp. 127–135, Apr. 2016, doi: 10.1016/j.jfoodeng.2015.12.015.
- [175] R. Llinares, P. Ramírez, J. Carmona, F. Carrillo, and J. Muñoz, “Formulation and optimization of emulsions based on bitter fennel essential oil and EO/BO block copolymer surfactant,” *Colloids and Surfaces A: Physicochemical and Engineering Aspects*, vol. 536, pp. 142–147, Jan. 2018, doi: 10.1016/j.colsurfa.2017.07.027.
- [176] R. Nehme, W. Blel, A. Montillet, J. Bellettre, and L. Marchal, “Production of oil in water emulsions in microchannels at high throughput: Evaluation of emulsions in view of cosmetic, nutraceutical or pharmaceutical applications,” *Chemical Engineering and Processing - Process Intensification*, vol. 161, Apr. 2021, doi: 10.1016/j.cep.2021.108301.
- [177] S. Hall, M. Cooke, A. El-Hamouz, and A. J. Kowalski, “Droplet break-up by in-line Silverson rotor-stator mixer,” *Chemical Engineering Science*, vol. 66, no. 10, pp. 2068–2079, 2011, doi: 10.1016/j.ces.2011.01.054.
- [178] C. Albert, M. Beladjine, N. Tsapis, E. Fattal, F. Agnely, and N. Huang, “Pickering emulsions: Preparation processes, key parameters governing their properties and potential for pharmaceutical applications,” *Journal of Controlled Release*, vol. 309, Elsevier B.V., pp. 302–332, Sep. 10, 2019. doi: 10.1016/j.jconrel.2019.07.003.
- [179] J. James *et al.*, “Scale-up of batch rotor–stator mixers. Part 1—power constants,” *Chemical Engineering Research and Design*, vol. 124, pp. 313–320, 2017, doi: 10.1016/j.cherd.2017.06.020.
- [180] A. Håkansson, “Rotor-stator mixers: From batch to continuous mode of operation-A review,” *Processes*, vol. 6, no. 4, pp. 1–17, 2018, doi: 10.3390/pr6040032.
- [181] Y. F. Maa and C. Hsu, “Liquid-liquid emulsification by rotor/stator homogenization,” *Journal of Controlled Release*, vol. 38, no. 2–3, pp. 219–228, 1996, doi: 10.1016/0168-3659(95)00123-9.

- [182] M. Cultures, P. Effect, S. Lakhota, and E. T. Papoutsakis, "Agitation Induced Cell Injury in Viscosity Is Agitation Intensity Dependent: Experiments and Modeling," *Biotechnology and Bioengineering*, vol. 39, pp. 95–107, 1992.
- [183] U. El-Jaby, M. Cunningham, and T. F. L. McKenna, "Comparison of emulsification devices for the production of miniemulsions," *Industrial and Engineering Chemistry Research*, vol. 48, no. 22, pp. 10147–10151, 2009, doi: 10.1021/ie901005a.
- [184] N. Thakur, G. Garg, P. K. Sharma, and N. Kumar, "Nanoemulsions: A Review on Various Pharmaceutical Application," *Global Journal of Pharmacology*, vol. 6, no. 3, pp. 222–225, 2012, doi: 10.5829/idosi.gjp.2012.6.3.65135.
- [185] M. Stang, H. Schuchmann, and H. Schubert, "Emulsification in High-Pressure Homogenizers," *Engineering in Life Sciences*, vol. 1, no. 4, pp. 151–157, 2001, doi: 10.1002/1618-2863(200110)1:43.0.co;2-d.
- [186] L. W. Phipps, "Cavitation and separated flow in a simple homogenizing valve and their influence on the break-up of fat globules in milk," *Journal of Dairy Research*, vol. 41, no. 1, pp. 1–8, 1974, doi: 10.1017/S0022029900014849.
- [187] S. E. Derenzo, G. Smadja, R. G. Smiths, H. Zaklad, and L. W. Alvarez, "High Precision Charged Particle Detector using Noble Liquids," *Nature*, vol. 233, pp. 617–619, 1971, doi: DOI: 10.1038/233617a0.
- [188] L. W. Phipps, "Some operating characteristics of a simple homogenizing poppet valve; pressure profiles and separation: Zone of fat globule dispersion," *Journal of Dairy Research*, vol. 41, no. 3, pp. 339–347, 1974, doi: 10.1017/S0022029900019786.
- [189] A. Desrumaux and J. Marcand, "Formation of sunflower oil emulsions stabilized by whey proteins with high-pressure homogenization (up to 350 MPa): Effect of pressure on emulsion characteristics," *International Journal of Food Science and Technology*, vol. 37, no. 3, pp. 263–269, 2002, doi: 10.1046/j.1365-2621.2002.00565.x.
- [190] M. B. Schulz and R. Daniels, "Hydroxypropylmethylcellulose (HPMC) as emulsifier for submicron emulsions: Influence of molecular weight and substitution type on the droplet size after high-pressure homogenization," *European Journal of Pharmaceutics and Biopharmaceutics*, vol. 49, no. 3, pp. 231–236, 2000, doi: 10.1016/S0939-6411(00)00069-2.
- [191] J. P. Dhakane, A. Kar, A. Singh Patel, and I. Khan, "Effect of soy proteins and emulsification-evaporation process on physical stability of lycopene emulsions," ~ 1354 ~ *International Journal of Chemical Studies*, vol. 5, no. 5, 2017.
- [192] L. Patil and P. R. Gogate, "Large scale emulsification of turmeric oil in skimmed milk using different cavitation reactors: A comparative analysis," *Chemical Engineering and Processing: Process Intensification*, vol. 126, pp. 90–99, Apr. 2018, doi: 10.1016/j.cep.2018.02.019.
- [193] S. M. Jafari, P. Beheshti, and E. Assadpour, "Emulsification properties of a novel hydrocolloid (Angum gum) for d-limonene droplets compared with Arabic gum," *International Journal of Biological Macromolecules*, vol. 61, pp. 182–188, Oct. 2013, doi: 10.1016/j.ijbiomac.2013.06.028.

- [194] S. M. Jafari, Y. He, and B. Bhandari, "Effectiveness of encapsulating biopolymers to produce sub-micron emulsions by high energy emulsification techniques," *Food Research International*, vol. 40, no. 7, pp. 862–873, Aug. 2007, doi: 10.1016/j.foodres.2007.02.002.
- [195] M. Manea, A. Chemtob, M. Paulis, J. C. de la Cal, M. J. Barandiaran, and J. M. Asu, "Miniemulsification in High-Pressure Homogenizers," *AIChE Journal*, vol. 54, no. 1, pp. 289–297, 2008, doi: DOI 10.1002/aic.11367.
- [196] D. W. Olson, C. H. White, and R. L. Richter, "Effect of pressure and fat content on particle sizes in microfluidized milk," *Journal of Dairy Science*, vol. 87, no. 10, pp. 3217–3223, 2004, doi: 10.3168/jds.S0022-0302(04)73457-8.
- [197] M. Yuh-Fun and C. H. Chung, "Performance of Sonication and Microfluidization for Liquid–Liquid Emulsification," *Pharmaceutical Development and Technology*, vol. 4, no. 2, pp. 233–240, 1999.
- [198] S. Schultz, G. Wagner, K. Urban, and J. Ulrich, "High-pressure homogenization as a process for emulsion formation," *Chemical Engineering and Technology*, vol. 27, no. 4, pp. 361–368, 2004, doi: 10.1002/ceat.200406111.
- [199] A. Maali and M. T. H. Mosavian, "Preparation and Application of Nanoemulsions in the Last Decade (2000-2010)," *Journal of Dispersion Science and Technology*, vol. 34, no. 1, pp. 92–105, 2013, doi: 10.1080/01932691.2011.648498.
- [200] M. Y. Koroleva and E. V Yurtov, "Nanoemulsions: the properties, methods of preparation and promising applications," *Russian Chemical Reviews*, vol. 81, no. 1, pp. 21–43, 2012, doi: 10.1070/rc2012v081n01abeh004219.
- [201] M. S. Alkanawati, F. R. Wurm, H. Thérien-aubin, and K. Landfester, "Large-Scale Preparation of Polymer Nanocarriers by High-Pressure Microfluidization," vol. 1700505, pp. 1–7, 2017, doi: 10.1002/mame.201700505.
- [202] F. J. Preiss, T. Dagenbach, M. Fischer, and H. P. Karbstein, "Development of a pressure stable inline droplet generator with live droplet size measurement," *ChemEngineering*, vol. 4, no. 4, pp. 1–14, 2020, doi: 10.3390/chemengineering4040060.
- [203] M. Nair, C. P. Lusignan, and D. C. Boris, "Preparation of uniform micrometer-sized polymer particles with closed-cell porous architecture made by limited coalescence of a double emulsion," *Colloids and Surfaces A: Physicochemical and Engineering Aspects*, vol. 443, pp. 583–595, 2014, doi: 10.1016/j.colsurfa.2013.11.037.
- [204] B. Mutsch, F. J. Preiss, T. Dagenbach, H. P. Karbstein, and C. J. Kähler, "Scaling of droplet breakup in high-pressure homogenizer orifices. Part ii: Visualization of the turbulent droplet breakup," *ChemEngineering*, vol. 5, no. 2, pp. 1–31, 2021, doi: 10.3390/chemengineering5020031.
- [205] J. Flourey, A. Desrumaux, M. A. V. Axelos, and J. Legrand, "Effect of high pressure homogenisation on methylcellulose as food emulsifier," *Journal of Food Engineering*, vol. 58, no. 3, pp. 227–238, 2003, doi: 10.1016/S0260-8774(02)00372-2.
- [206] J. Flourey, J. Legrand, and A. Desrumaux, "Analysis of a new type of high pressure homogeniser. Part B. study of droplet break-up and recoalescence phenomena,"

- Chemical Engineering Science*, vol. 59, no. 6, pp. 1285–1294, 2004, doi: 10.1016/j.ces.2003.11.025.
- [207] J. Flourey, A. Desrumaux, and J. Legrand, “Effect of ultra-high-pressure homogenization on structure and on rheological properties of soy protein-stabilized emulsions,” *Journal of Food Science*, vol. 67, no. 9, pp. 3388–3395, 2002, doi: 10.1111/j.1365-2621.2002.tb09595.x.
- [208] G. Kolb, K. Viardot, G. Wagner, and J. Ulrich, “Evaluation of a new high-pressure dispersion unit (HPN) for emulsification,” *Chemical Engineering and Technology*, vol. 24, no. 3, pp. 293–296, 2001, doi: 10.1002/1521-4125(200103)24:3<293::AID-CEAT293>3.0.CO;2-0.
- [209] J. Hadžiabdić, E. Vranic, A. Elezovic, and O. Rahic, “Preparation of Nanoemulsions by Hig-Energy and Low-Energy Emulsification Methods,” vol. 62, no. October 2020, 2017, doi: 10.1007/978-981-10-4166-2.
- [210] T. Tadros, P. Izquierdo, J. Esquena, and C. Solans, “Formation and stability of nano-emulsions,” *Advances in Colloid and Interface Science*, vol. 108–109, pp. 303–318, 2004, doi: 10.1016/j.cis.2003.10.023.
- [211] D. Gazolu-Rusanova, I. Lesov, S. Tcholakova, N. Denkov, and B. Ahtchi, “Food grade nanoemulsions preparation by rotor-stator homogenization,” *Food Hydrocolloids*, vol. 102, no. July 2019, p. 105579, 2020, doi: 10.1016/j.foodhyd.2019.105579.
- [212] D. M. Hobbs and F. J. Muzzio, “The Kenics static mixer: A three-dimensional chaotic flow,” *Chemical Engineering Journal*, vol. 67, no. 3, pp. 153–166, 1997, doi: 10.1016/S1385-8947(97)00013-2.
- [213] E. Lobry, F. Theron, C. Gourdon, N. Le Sauze, C. Xuereb, and T. Lasuye, “Turbulent liquid-liquid dispersion in SMV static mixer at high dispersed phase concentration,” *Chemical Engineering Science*, vol. 66, no. 23, pp. 5762–5774, 2011, doi: 10.1016/j.ces.2011.06.073.
- [214] A. Ghanem, T. Lemenand, D. Della Valle, and H. Peerhossaini, “Static mixers: Mechanisms, applications, and characterization methods - A review,” *Chemical Engineering Research and Design*, vol. 92, no. 2, pp. 205–228, 2014, doi: 10.1016/j.cherd.2013.07.013.
- [215] L. F. Albril, *Albright’s Chemical Engineering Handbook*. Boca Raton FL: CRC Press, 2008.
- [216] Z. Anxionnaz, M. Cabassud, C. Gourdon, and P. Tochon, “Heat exchanger/reactors (HEX reactors): Concepts, technologies: State-of-the-art,” *Chemical Engineering and Processing: Process Intensification*, vol. 47, no. 12, pp. 2029–2050, 2008, doi: 10.1016/j.cep.2008.06.012.
- [217] F. Zidouni, E. Krepper, R. Rzehak, S. Rabha, M. Schubert, and U. Hampel, “Simulation of gas-liquid flow in a helical static mixer,” *Chemical Engineering Science*, vol. 137, pp. 476–486, 2015, doi: 10.1016/j.ces.2015.06.052.
- [218] C. D. Armeniades, W. C. Johnson, T. Raphael, and A. D. Little Inc., “Mixing Device,” 1966
- [219] Indiamart, “static-mixer.” <https://www.indiamart.com/fluidyne-instruments/static-mixer.html>

- [220] E. Lobry, F. Theron, C. Gourdon, N. Le Sauze, C. Xuereb, and T. Lasuye, "Turbulent liquid-liquid dispersion in SMV static mixer at high dispersed phase concentration," *Chemical Engineering Science*, vol. 66, no. 23, pp. 5762–5774, 2011, doi: 10.1016/j.ces.2011.06.073.
- [221] "static-mixers @ www.sulzer.com." <https://www.sulzer.com/en/products/static-mixers>
- [222] E. S. Mickaily-Huber *et al.*, "Numerical simulations of mixing in an SMRX static mixer," *Chemical Engineering Journal*, vol. 63, pp. 117–126, 1996.
- [223] D. M. Hobbs and F. J. Muzzio, "Reynolds number effects on laminar mixing in the Kenics static mixer," *Chemical Engineering Journal*, vol. 70, no. 2, pp. 93–104, 1998, doi: 10.1016/S1385-8947(98)00065-5.
- [224] K. Sangtae and J. K. Seppo, *Microhydrodynamics: Principles and Selected Applications*, 1st ed. Dover, 1991.
- [225] P. Sungwornpatansakul, J. Hiroi, Y. Nigahara, T. K. Jayasinghe, and K. Yoshikawa, "Enhancement of biodiesel production reaction employing the static mixing," *Fuel Processing Technology*, vol. 116, pp. 1–8, 2013, doi: 10.1016/j.fuproc.2013.04.019.
- [226] S. A. Jaffer and P. E. Wood, "Quantification of laminar mixing in the Kenics static mixer: an experimental study," *Canadian Journal of Chemical Engineering*, vol. 76, no. 3, pp. 516–521, 1998, doi: 10.1002/cjce.5450760323.
- [227] L. Muruganandam, D. Kunal, and G. O. Melwyn, "Studies on droplet size distribution of oil-in-water emulsion in SMX static mixer," *Journal of Applied Fluid Mechanics*, vol. 11, no. 1, pp. 107–114, 2018, doi: 10.29252/jafm.11.01.28151.
- [228] C. Charcosset, I. Limayem, and H. Fessi, "The membrane emulsification process - A review," *Journal of Chemical Technology and Biotechnology*, vol. 79, no. 3, pp. 209–218, 2004, doi: 10.1002/jctb.969.
- [229] A. J. Gijsbertsen-Abrahamse, A. Van Der Padt, and R. M. Boom, "Status of cross-flow membrane emulsification and outlook for industrial application," *Journal of Membrane Science*, vol. 230, no. 1–2, pp. 149–159, 2004, doi: 10.1016/j.memsci.2003.11.006.
- [230] G. T. Vladislavljević and M. V. Mitrović, "Membrane emulsification - state of the art," *Chemical Industry and Chemical Engineering Quarterly*, vol. 6, no. 4, pp. 523–529, 2000.
- [231] G. T. Vladislavljević, "Structured microparticles with tailored properties produced by membrane emulsification," *Advances in Colloid and Interface Science*, vol. 225, pp. 53–87, 2015, doi: 10.1016/j.cis.2015.07.013.
- [232] S. Van Der Graaf, C. G. P. H. Schroën, and R. M. Boom, "Preparation of double emulsions by membrane emulsification - A review," *Journal of Membrane Science*, vol. 251, no. 1–2, pp. 7–15, 2005, doi: 10.1016/j.memsci.2004.12.013.
- [233] M. M. Dragosavac, R. G. Holdich, G. T. Vladislavljević, and M. N. Sovilj, "Stirred cell membrane emulsification for multiple emulsions containing unrefined pumpkin seed oil with uniform droplet size," *Journal of Membrane Science*, vol. 392–393, pp. 122–129, 2012, doi: 10.1016/j.memsci.2011.12.009.
- [234] D. J. McClements, *Food Emulsions Principles, Practices, and Techniques*. 2004.

- [235] T. Nakashima and M. Shimizu, "Porous glass from calcium alumino boro-silicate glass (in Japanese)," *Cerami Jpn*, vol. 21, pp. 408–412, 1986.
- [236] E. Piacentini, E. Drioli, and L. Giorno, "Membrane emulsification technology: Twenty-five years of inventions and research through patent survey," *Journal of Membrane Science*, vol. 468, pp. 410–422, 2014, doi: 10.1016/j.memsci.2014.05.059.
- [237] A. Mohammed and R. Al-Khateeb, "Application of Emulsion Liquid Membrane Using Green Surfactant for Removing Phenol from Aqueous Solution: Extraction, Stability and Breakage Studies," *Journal of Ecological Engineering*, vol. 23, no. 1, pp. 305–314, Jan. 2022, doi: 10.12911/22998993/143970.
- [238] S. Kwon, K. M. Thomas, and R. Lakerveld, "Integrated membrane emulsification and solution cooling crystallization to obtain a narrow and predictable crystal size distribution," *Chemical Engineering and Processing - Process Intensification*, vol. 171, p. 108751, Jan. 2022, doi: 10.1016/j.cep.2021.108751.
- [239] T. Jiang and C. Charcosset, "Premix membrane emulsification for the preparation of curcumin-loaded nanoemulsions," *Journal of Food Engineering*, vol. 316, Mar. 2022, doi: 10.1016/j.jfoodeng.2021.110836.
- [240] G. T. Vladisavljević and M. V. Mitrović, "Membrane emulsification - state of the art," *Chemical Industry and Chemical Engineering Quarterly*, vol. 6, no. 4, pp. 523–529, 2000.
- [241] T. Nakashima, M. Shimizu, and M. Kukizaki, "Particle control of emulsion by membrane emulsification and its applications," *Advanced Drug Delivery Reviews*, vol. 45, no. 1, pp. 47–56, 2000, doi: 10.1016/S0169-409X(00)00099-5.
- [242] T. Nakashima, M. Shimizu, and M. Kukizaki, "Membrane emulsification by microporous glass," *Inorganic Membranes ICIM2-91*, vol. 62, pp. 513–516, 1991, doi: 10.4028/www.scientific.net/kem.61-62.513.
- [243] C. Charcosset, "Preparation of emulsions and particles by membrane emulsification for the food processing industry," *Journal of Food Engineering*, vol. 92, no. 3, pp. 241–249, 2009, doi: 10.1016/j.jfoodeng.2008.11.017.
- [244] G. T. Vladisavljevic and H. Schubert, "Preparation and analysis of oil-in-water emulsions with a narrow droplet size distribution using Shirasu-porous-glass (SPG) membranes," *Desalination*, vol. 144, no. 1–3, pp. 167–172, 2002, doi: 10.1016/S0011-9164(02)00307-7.
- [245] "Transmembrane Pressure." <https://www.mssincorporated.com/blog/how-to-calculate-transmembrane-pressure/>
- [246] J. Wu, W. Jing, W. Xing, and N. Xu, "Preparation of W/O emulsions by membrane emulsification with a mullite ceramic membrane," *Desalination*, vol. 193, no. 1–3, pp. 381–386, 2006, doi: 10.1016/j.desal.2005.08.026.
- [247] V. Schroder, O. Behrend, and H. Schubert, "Effect of Dynamic Interfacial Tension on the Emulsification Process," *Journal of Colloid and Interface Science*, vol. 340, no. 202, pp. 334–340, 1998.
- [248] C. A. Miller, "Spontaneous Emulsification Produced by Diffusion - A Review," *Colloids and Surfaces*, vol. 29, no. 1, pp. 89–102, 1988, doi: 10.1016/0166-6622(88)80173-2.

- [249] J. Gad, *Zur Lehre von der Blutrache/ in German*. Arch Anat Physiol, 1878.
- [250] C. Solans, D. Morales, and M. Homs, "Spontaneous emulsification," *Current Opinion in Colloid and Interface Science*, vol. 22, pp. 88–93, 2016, doi: 10.1016/j.cocis.2016.03.002.
- [251] S. A. Vitale and J. L. Katz, "Liquid droplet dispersions formed by homogeneous liquid-liquid nucleation: 'The ouzo effect,'" *Langmuir*, vol. 19, no. 10, pp. 4105–4110, May 2003, doi: 10.1021/la026842o.
- [252] D. Carteau, D. Bassani, and I. Pianet, "The 'Ouzo effect': Following the spontaneous emulsification of trans-anethole in water by NMR," *Comptes Rendus Chimie*, vol. 11, no. 4–5, pp. 493–498, Apr. 2008, doi: 10.1016/j.crci.2007.11.003.
- [253] C. Goubault *et al.*, "Effect of nanoparticles on spontaneous Ouzo emulsification Effect of nanoparticles on spontaneous « Ouzo » emulsification," 2021, doi: 10.1016/j.jcis.2021.06.104i.
- [254] N. Anton and T. F. Vandamme, "The universality of low-energy nano-emulsification," *International Journal of Pharmaceutics*, vol. 377, no. 1–2, pp. 142–147, 2009, doi: 10.1016/j.ijpharm.2009.05.014.
- [255] S. Nishimura and Y. Murakami, "Precise Control of the Surface and Internal Morphologies of Porous Particles Prepared Using a Spontaneous Emulsification Method," *Langmuir*, vol. 37, no. 10, pp. 3075–3085, 2021, doi: 10.1021/acs.langmuir.0c03311.
- [256] D. J. McClements, "Edible nanoemulsions: Fabrication, properties, and functional performance," *Soft Matter*, vol. 7, no. 6, pp. 2297–2316, 2011, doi: 10.1039/c0sm00549e.
- [257] J. C. López-Montilla, P. E. Herrera-Morales, S. Pandey, and D. O. Shah, "Spontaneous Emulsification: Mechanisms, Physicochemical Aspects, Modeling, and Applications," *Journal of Dispersion Science and Technology*, vol. 23, no. 1–3, pp. 219–268, 2002, doi: 10.1080/01932690208984202.
- [258] D. Schuster, *Encyclopedia of Emulsion Technology: Basic Theory*, Volume 4. CRC Press, 1983.
- [259] M. Parent, C. Nouvel, M. Koerber, A. Sapin, P. Maincent, and A. Boudier, "PLGA in situ implants formed by phase inversion: Critical physicochemical parameters to modulate drug release," *Journal of Controlled Release*, vol. 172, no. 1. pp. 292–304, 2013. doi: 10.1016/j.jconrel.2013.08.024.
- [260] N. Anton, P. Gayet, J. P. Benoit, and P. Saulnier, "Nano-emulsions and nanocapsules by the PIT method: An investigation on the role of the temperature cycling on the emulsion phase inversion," *International Journal of Pharmaceutics*, vol. 344, no. 1–2, pp. 44–52, 2007, doi: 10.1016/j.ijpharm.2007.04.027.
- [261] K. Shinoda and H. Saito, "The effect of temperature on the phase equilibria and the types of dispersions of the ternary system composed of water, cyclohexane, and nonionic surfactant," *Journal of Colloid And Interface Science*, vol. 26, no. 1, pp. 70–74, 1968, doi: 10.1016/0021-9797(68)90273-7.
- [262] Z. Li *et al.*, "Advances of spontaneous emulsification and its important applications in enhanced oil recovery process," *Advances in Colloid and Interface Science*, vol. 277, p. 102119, 2020, doi: 10.1016/j.cis.2020.102119.

- [263] K. Shinoda and H. Saito, "The Stability of O/W type emulsions as functions of temperature and the HLB of emulsifiers: The emulsification by PIT-method," *Journal of Colloid And Interface Science*, vol. 30, no. 2, pp. 258–263, 1969, doi: 10.1016/S0021-9797(69)80012-3.
- [264] T. Forster, F. Schambil, and H. Tesmann, "Emulsification by the phase inversion temperature method: the role of self-bodying agents and the influence of oil polarity," *International Journal of Cosmetic Science*, vol. 12, no. 5, pp. 217–227, 1990, doi: 10.1111/j.1467-2494.1990.tb00537.x.
- [265] K. Roger, B. Cabane, and U. Olsson, "Emulsification through surfactant hydration: The PIC process revisited," *Langmuir*, vol. 27, no. 2, pp. 604–611, 2011, doi: 10.1021/la1042603.
- [266] G. M. Whitesides, "The origins and the future of microfluidics," *Nature*, vol. 442, no. 7101, pp. 368–373, 2006, doi: 10.1038/nature05058.
- [267] F. Bally *et al.*, "Improved size-tunable preparation of polymeric nanoparticles by microfluidic nanoprecipitation," *Polymer (Guildf)*, vol. 53, no. 22, pp. 5045–5051, Oct. 2012, doi: 10.1016/j.polymer.2012.08.039.
- [268] F. Bally, C. A. Serra, C. Brochon, N. Anton, T. Vandamme, and G. Hadziioannou, "A continuous-flow polymerization microprocess with online GPC and inline polymer recovery by micromixer-assisted nanoprecipitation," *Macromolecular Reaction Engineering*, vol. 5, no. 11–12, pp. 542–547, Dec. 2011, doi: 10.1002/mren.201100047.
- [269] S. W. Kim, K. H. Hwangbo, J. H. Lee, and K. Y. Cho, "Microfluidic fabrication of microparticles with multiple structures from a biodegradable polymer blend," *RSC Advances*, vol. 4, no. 87, pp. 46536–46540, 2014, doi: 10.1039/c4ra05864j.
- [270] J. Warner, "Microelectronics: Its unusual origin and personality," *IEEE Transactions on Electron Devices*, vol. 48, no. 11, pp. 2457–2467, 2001, doi: 10.1109/16.960368.
- [271] L. Jiang and N. S. Korivi, *Microfluidics: Technologies and applications*. Woodhead Publishing Limited, 2013. doi: 10.1533/9780857098757.424.
- [272] F. Yu, W. Hunziker, and D. Choudhury, "Engineering microfluidic organoid-on-a-chip platforms," *Micromachines (Basel)*, vol. 10, no. 3, 2019, doi: 10.3390/mi10030165.
- [273] M. Vauthier, M. Schmutz, and C. A. Serra, "One-step elaboration of Janus polymeric nanoparticles: A comparative study of different emulsification processes," *Colloids and Surfaces A: Physicochemical and Engineering Aspects*, vol. 626, no. May, p. 127059, 2021, doi: 10.1016/j.colsurfa.2021.127059.
- [274] H. A. Stone, A. D. Stroock, and A. Ajdari, "Engineering flows in small devices: Microfluidics toward a lab-on-a-chip," *Annual Review of Fluid Mechanics*, vol. 36, no. January 2004, pp. 381–411, 2004, doi: 10.1146/annurev.fluid.36.050802.122124.
- [275] C. A. Serra and Z. Chang, "Microfluidic-assisted synthesis of polymer particles," *Chemical Engineering and Technology*, vol. 31, no. 8, pp. 1099–1115, 2008, doi: 10.1002/ceat.200800219.
- [276] I. Kobayashi, K. Uemura, and M. Nakajima, "Formulation of monodisperse emulsions using submicron-channel arrays," *Colloids and Surfaces A: Physicochemical and*

- Engineering Aspects*, vol. 296, no. 1–3, pp. 285–289, 2007, doi: 10.1016/j.colsurfa.2006.09.015.
- [277] A. A. Maan, A. Nazir, M. K. I. Khan, R. Boom, and K. Schroën, “Microfluidic emulsification in food processing,” *Journal of Food Engineering*, vol. 147, pp. 1–7, 2015, doi: 10.1016/j.jfoodeng.2014.09.021.
- [278] C. A. Serra and Z. Chang, “Microfluidic-assisted synthesis of polymer particles,” *Chemical Engineering and Technology*, vol. 31, no. 8, pp. 1099–1115, 2008, doi: 10.1002/ceat.200800219.
- [279] N. Convery and N. Gadegaard, “30 Years of Microfluidics,” *Micro and Nano Engineering*, vol. 2, no. November 2018, pp. 76–91, 2019, doi: 10.1016/j.mne.2019.01.003.
- [280] R. K. Shah *et al.*, “Designer emulsions using microfluidics,” *Materials Today*, vol. 11, no. 4, pp. 18–27, 2008, doi: 10.1016/S1369-7021(08)70053-1.
- [281] T. Hessberger, L. B. Braun, C. A. Serra, and R. Zentel, “Microfluidic Preparation of Liquid Crystalline Elastomer Actuators,” *Journal of Visualized Experiments*, no. 135, pp. 1–8, 2018, doi: 10.3791/57715.
- [282] S. Xu *et al.*, “Generation of monodisperse particles by using microfluidics: Control over size, shape, and composition,” *Angewandte Chemie - International Edition*, vol. 44, no. 5, pp. 724–728, 2005, doi: 10.1002/anie.200462226.
- [283] J. Boleininger, A. Kurz, V. Reuss, and C. Sönnichsen, “Microfluidic continuous flow synthesis of rod-shaped gold and silver nanocrystals,” *Physical Chemistry Chemical Physics*, vol. 8, no. 33, pp. 3824–3827, 2006, doi: 10.1039/b604666e.
- [284] Zhihong Nie, Shengqing Xu, Minseok Seo, Patrick C. Lewis, and Eugenia Kumacheva, “Polymer Particles with Various Shapes and Morphologies Produced in Continuous Microfluidic Reactors,” *2006 NSTI Nanotechnology Conference and Trade Show - NSTI Nanotech 2006 Technical Proceedings*, vol. 2, no. 16, pp. 686–689, 2006.
- [285] M. Bouquey, C. Serra, N. Berton, L. Prat, and G. Hadziioannou, “Microfluidic synthesis and assembly of reactive polymer beads to form new structured polymer materials,” *Chemical Engineering Journal*, vol. 135, no. SUPPL. 1, pp. 93–98, 2008, doi: 10.1016/j.cej.2007.07.043.
- [286] C. Serra, N. Berton, M. Bouquey, L. Prat, and G. Hadziioannou, “A predictive approach of the influence of the operating parameters on the size of polymer particles synthesized in a simplified microfluidic system,” *Langmuir*, vol. 23, no. 14, pp. 7745–7750, 2007, doi: 10.1021/la063289s.

CHAPTER II

MATERIALS AND METHODS

OUTLINE

Preface.....	117
<i>A</i> Emulsification Devices	117
1. Some Theoretical and Historical Aspects of the Elongational-Flow Emulsification	117
2. Micro Elongational-Flow Reactor and Mixer (μ RMX)	121
3. Pneumatic Elongational-Flow Reactor and Mixer (pRMX)	125
4. Rotor-Stator Mixer	130
<i>B</i> Thiol-Ene Miniemulsion Formulation	131
1. Coarse Emulsion Preparation	133
1.1 Ambient Atmosphere.....	133
1.2 Inert Atmosphere.....	133
2. Miniemulsion Preparation	134
<i>C</i> Thiol-Ene Miniemulsion Photopolymerization	134
1. Linear Photoreactor (LP).....	135
2. Coiled Tube Photoreactor (CTP)	137
<i>D</i> Characterization Techniques	139
1. Dynamic Light Scattering (DLS).....	139
2. Proton Nuclear Magnetic Resonance (^1H NMR).....	140
<i>E</i> Bibliography	141

Preface

In order to achieve the different goals listed in the conclusion of the previous chapter, use of common emulsification devices, adaptation of existing ones and development of a new one was considered. This chapter therefore presents the different devices that were used in this thesis work for i) the production of thiol-ene miniemulsions, ii) their subsequent photopolymerization to reach size-control poly(thioether) nanoparticles and iii) the characterization of the different miniemulsions and nanosuspensions produced.

A Emulsification Devices

1. Some Theoretical and Historical Aspects of the Elongational-Flow Emulsification

There is an increased interest for emulsification devices that are friendly for the environment, and which require low energy input. Researchers have developed elongational flow devices that are able to provide improved dispersive mixing with the least energy consumption. In 1934 a pioneering work was reported from Taylor, who observed the droplet deformation under simple shear and two-dimensional extensional flow, which occurs in an elongational-flow-based device [1]. His theory proves that in the simple shear, droplet breakup happens only until the viscosity of the dispersed phase is 4 times less the viscosity of the suspending fluid. However, when the viscosity becomes higher, the droplet cannot be deformed further and a steady shape, that might be also slightly deformed, is obtained. On the contrary, it is shown that in the two-dimensional extensional flow, the droplets can rupture in any viscosity ratio provided that the strain rate, the deformation of a material under the evolution of time [2], has a value higher than a critical point (Figure 2.1).

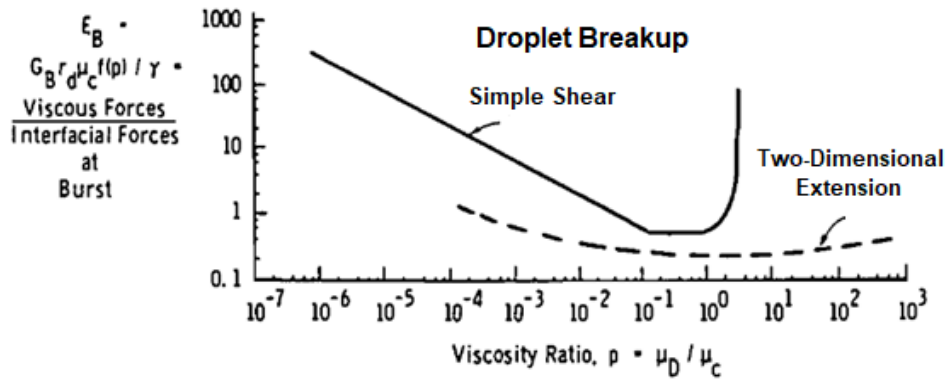


Figure 2.1. Effect of viscosity ratio in simple shear and two-dimensional extensional flow [3].

A very important value that can predict the droplet breakup is the capillary number [4], which is the ratio of the viscous forces divided by the interfacial forces expressed for an elongational flow with the elongational strain rate, $\dot{\epsilon}$ as follows:

$$Ca = \frac{\mu \dot{\epsilon} D_d}{2 \sigma} \quad (2.1)$$

where μ is the viscosity of the emulsion, $\dot{\epsilon}$, the elongational strain rate, D_d the droplet diameter and σ the interfacial tension between the dispersed and continuous phases. As mentioned before and according to the Taylor theory, when this capillary number reaches a critical value, Ca_c , depending on the overall emulsion viscosity, the droplets rupture from one big drop into smaller droplets is observed. In the case that the newly formed droplets have a diameter that can allow the new value of the capillary number to be equal or higher to the Ca_c , they will break up again and form smaller droplets.

In an elongational-flow based device the restriction plays one of the most important roles since it is the parameter that will elongate the droplets and the flow of the emulsion will undergo a strong elongational strain rate, $\dot{\epsilon}$, which will cause the deformation of the droplets. Assuming that the emulsion is a Newtonian liquid, and following Cogswell analysis [5], the elongational strain rate can be defined as:

$$\dot{\epsilon} = \frac{2 \tau_w \dot{\gamma}_w}{3 \Delta P_e} \quad (2.2)$$

where τ_w is the shear stress at the wall of the restriction, $\dot{\gamma}_w$ the shear rate at the wall and ΔP_e is the pressure drop by passing the entrance of the restriction. To

have a better understanding on the parameters that can influence the droplet rupture it is important to develop further the equation 4.

Using the Newtonian law of viscosity one can determine the shear rate as:

$$\dot{\gamma}_w = \frac{\tau_w}{\mu} \quad (2.3)$$

where μ , the overall emulsion viscosity. By combining the two equations 4 and 5, the elongational strain rate becomes:

$$\dot{\epsilon} = \frac{2\tau_w^2}{3\mu\Delta P_e} \quad (2.4)$$

In case the restriction has a cylindrical shape, the shear stress can be expressed as:

$$\tau_w = \frac{D_h \Delta P_h}{4 L_h} \quad (2.5)$$

where D_h is the diameter of the bore of the restriction, ΔP_h the pressure drop across the restriction and L_h is the length of the restriction.

The pressure drop, ΔP_h for Newtonian fluids that are in the laminar regime inside the chambers can be expressed according to Hagen-Poiseuille law as:

$$\Delta P_h = \frac{128 \mu L_h q}{\pi D_h^4} \quad (2.6)$$

where q refers to the flow rate of the emulsion. While in the turbulent flow it is described as:

$$\Delta P_h = \frac{32 f L_h \rho q^2}{\pi^2 D_h^5} \quad (2.7)$$

where f is the Fanning friction factor, which is usually described as a function of the Reynolds number.

Referring to the pressure drop at the entrance of the restriction it can be expressed as:

$$\Delta P_e = K_f \frac{\rho \langle u \rangle^2}{2} \quad (2.8)$$

where K_f is the loss coefficient of the restriction and is determined as

$$K_f = 0.45 \left[1 - \left(\frac{D_h}{D_t} \right)^2 \right] \quad (2.9)$$

where D_t is the inner diameter of the tubing or chamber that is connected to the restriction, $\langle u \rangle$ the mean velocity through the restriction and defined as:

$$\langle u \rangle = \frac{4q}{\pi D_h^2} \quad (2.10)$$

By having a quick look of the aforementioned equations one can understand that the droplet rupture depends on many different factors such as the geometry of the chamber and the restriction, the flow rate and the pressure drop across the restriction [6].

Y. Suzaka in 1979 [7], was the first one to patent a mixing device based on an elongational flow and used to mix polymeric melts. The device is shown in Figure 2.2, where the material is pushed through a series of chambers with a very narrow path which promotes the elongation of the droplets and causes their breakup.

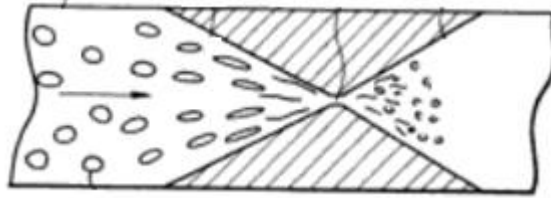


Figure 2.2. Elongational-flow mixing device [7].

Later in 1995, X. Q. Nguyen *at al.* [8], wanted to improve the device developed by Y. Suzaka so they designed a similar device where one of the restrictions could be controlled to adjust the stress applied to the system so as to achieve the desired droplet size depending on the application (Figure 2.3).

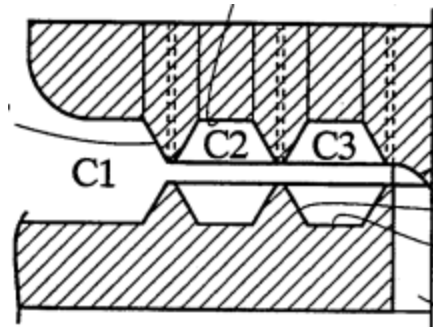


Figure 2.3. Extensional flow mixer [8].

At the same time M. R. Mackley *et al* [8], developed a device called “multipass rheometer” where a fluid is placed in a chamber where two servo-hydraulically driven pistons are moving simultaneously so as the fluid passes through a very narrow capillary and the droplets elongate and rupture (Figure 2.4). The pressure that forces the pistons to move was approximately 210 bar. They claim that this device can be used in rheo-optics, mixing and reactions.

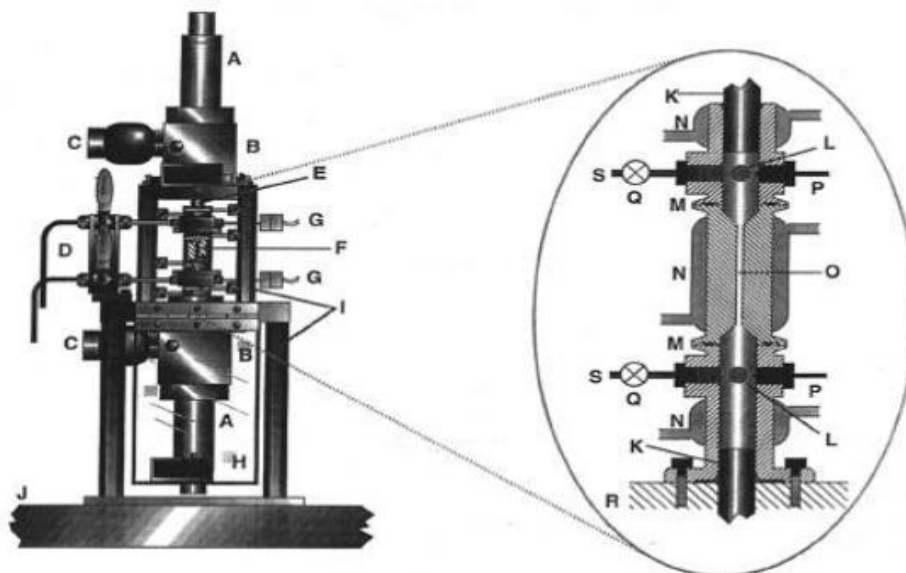


Figure 2.4. Multipass rheometer [8].

Our group got inspired from this work and recently developed a novel mixing device based on the elongational flow [9]. In the following section, all the emulsification devices that were used are reported and commented.

2. Micro Elongational-Flow Reactor and Mixer (μ RMX)

This device combines the elongational-flow reactor and mixer with microfluidics, since a microchannel is used for the elongation of the droplets. This device is mentioned before from our group [10] and is called micro elongational-flow reactor and mixer (μ RMX) (Figure 2.5). It comprises two mid pressure (2.5 bar) syringe pumps (neMESYS Mid Pressure Module, Cetoni), two 25 mL stainless steel syringes (Cetoni), an elongational-flow micromixer and a PolyEtherEtherKetone (PEEK) tee (Valco Vici).

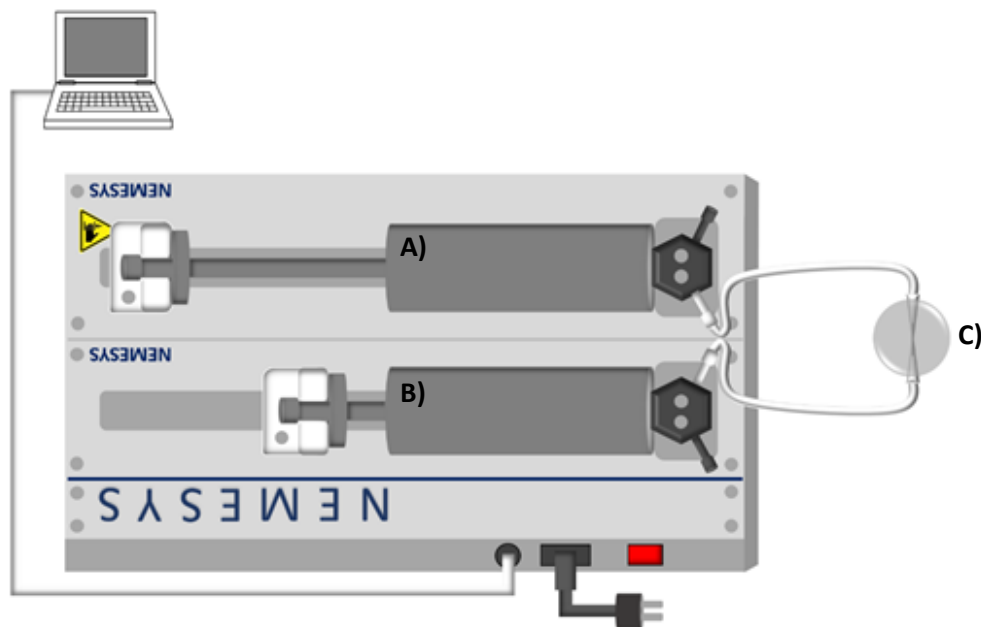


Figure 2.5. Micro Elongational-Flow Reactor and Mixer (μ RMX), A) withdrawing syringe, B) infusing syringe, C) micromixer.

To operate the syringes the supplier provided a software that is able to move the syringe pumps independently to inject or withdraw, work in tandem (withdraw/withdraw, infuse/infuse), or in opposite phase (withdraw/infuse). The micromixer that was used was composed of three or four drilled microchannels with two different bore sizes, 150 or 250 μm . To connect the micromixer with the stainless-steel syringes, two Polytetrafluoroethylene (PTFE) tubing (1.06 mm internal diameter (ID) x 1.68 mm outer diameter (OD)) were used and placed in opposite port positions (180°) in the micromixer. The rest of the microchannels were closed during the experiment but one was open after finishing in order to recover the miniemulsion.

The material to be mixed is introduced in a plastic syringe, whose volume can be varied between 5 and 25 mL, without pre-mixing. The filled syringe and a second empty syringe are placed on the syringe pump older and connected to the micromixer by means of a PTFE tubing. Then through the software, the two syringes are forced to work in opposite phase. Thus, the filled syringe pump starts infusing the solution through the mixer and at the same time the empty syringe starts to withdraw at same flow rate. One back and forth movement of the syringe will count for one cycle. The software allows to adjust different parameters such as

the flow rate and the number of cycles. After the prescribed number of cycles, the device stops and the miniemulsion is recovered for further processing.

Research has already been conducted from our group to evaluate the droplet size of a miniemulsion produced as well as the polydispersity index. W. Yu *et al* [6], worked with methyl methacrylate (MMA) to produce miniemulsion with tunable droplet size. The effect of the process parameters as well as the chemical parameters that can change the droplet diameter was studied (Figure 2.6). They first proved that the droplet diameter was decreasing when the number of cycles was increasing from 100 to 800 number of cycles. While a significant decrease was observed when the flow rate was increasing, and the bore size of the micromixer decreased as a result in both cases an increased value of the strain rate ($\dot{\epsilon}$). Overall, they managed to obtain a droplet size between 500 nm down to 50 nm.

Among the other parameters, they investigated also the effect of the surfactant concentration on the droplet size. A decrease of the droplet size was obvious by increasing the amount of surfactant from 0.5 wt% up to 3.5 wt% referring to the monomer concentration. This can be explained by the fact that the surface tension decreases when the amount of surfactant increases, and it is inversely proportional to the capillary number that was previously discussed. Finally, comparison was made with simple shear rotor-stator device, and it was successfully proven that the μ RMX gave rise to smaller droplets as well as smaller polydispersity due to the elongational flow that was applied to the droplets during mixing. These results were in a very good agreement with Taylor's theory mentioned before and reached a steady state value corresponding to the critical capillary number.

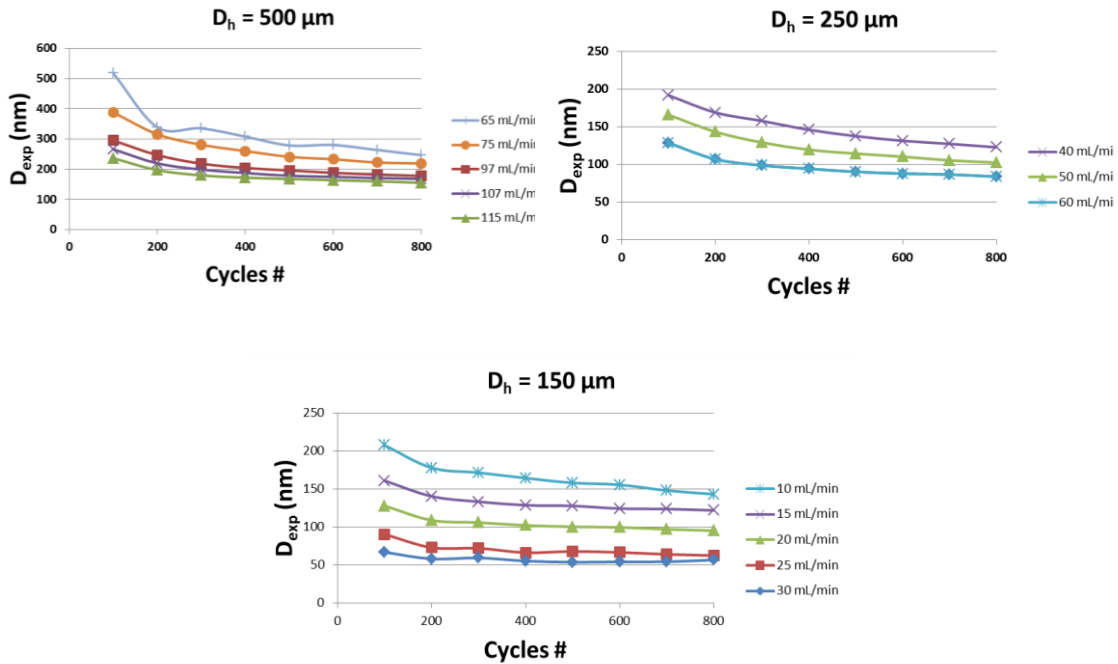


Figure 2.6. Variation of nanodroplet size with respect to the number of cycles for different flow rates and three different micromixers [6].

Following this study, M. Vauthier *et al.* [11], further used the μ RMX device to produce Janus polymeric nanoparticles. This time a solution of two different polymers was directly mixed with water in the device and comparison was made between μ RMX and other more conventional emulsification devices, i.e. rotor-stator and ultrasound generator. An overall investigation was made with all the devices to evaluate the particle size (Figure 2.7). Among all the parameters studied, it was shown that a particle diameter decrease occurs in higher emulsification times while the polydispersity index in some cases was decreasing below 0.2 [12], for which a system can be considered as monomodal. Another important parameter that played a crucial role on the particle size was the volume fraction of the dispersed phase. When the latter was high the particle diameter was also big for the three devices. What is worth mentioning is that when rotor-stator was used and the dispersed phase was 30 wt% of the total volume, the viscosity of the dispersed phase was too high, and lead to a viscosity ratio of dispersed to continuous phase more than 4. This, according to Taylor theory described before, does not allow the droplets to further breakup. In this way they proved that μ RMX can provide small and monomodal nanoparticles as compared to the other two devices.

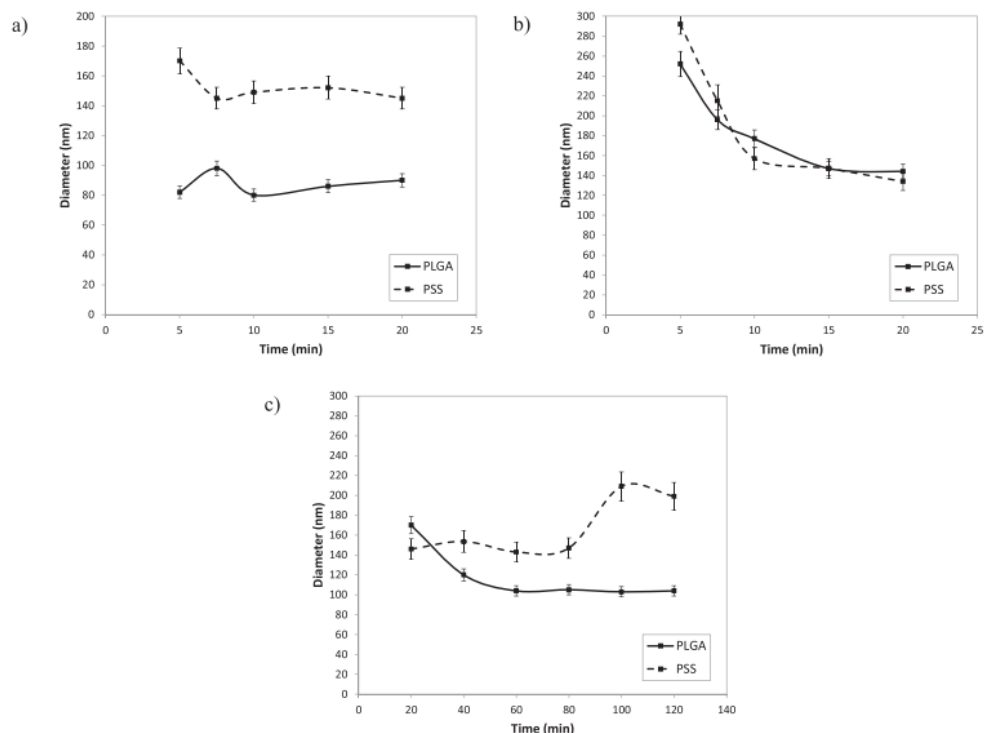


Figure 2.7. Evolution of nanoparticles' diameter regarding to the emulsification time for a) ultrasonicator, b) rotor-stator mixer and c) elongational-flow micromixer [11].

In this thesis experiments were conducted using μ RMX, Ultra-Turrax as well as a novel pneumatic elongational-flow reactor and mixer. The influence of different chemical and process parameters, such the number of cycles, the flow rate and the bore size of the micromixer and will be discussed in the following chapter.

3. Pneumatic Elongational-Flow Reactor and Mixer (pRMX)

A novel low-energy elongational-flow-based device was mainly used in order to produce thiol-ene miniemulsions. The device is called pneumatic elongational-flow reactor and mixer (pRMX) (Figure 2.8) and was developed from our group. The operating principle is based on the reciprocating flow of the material through an

abrupt contraction which generates a strong elongational flow, leads to a highly efficient dispersive mixing even at moderate pressures [13].

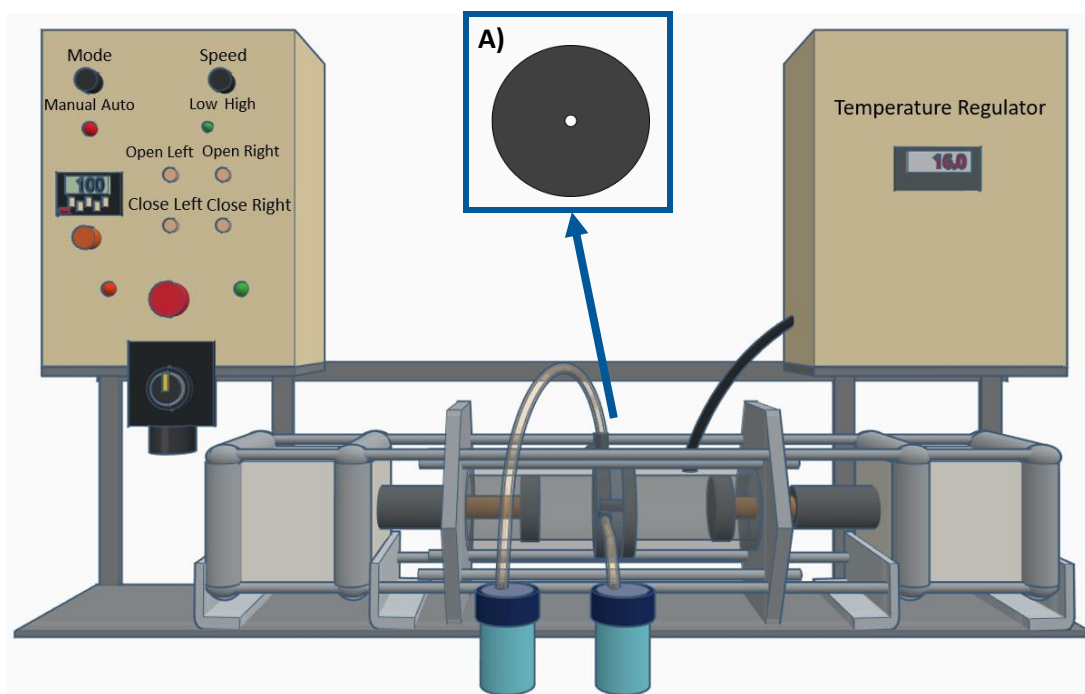


Figure 2.8. Pneumatic Elongational-Flow Reactor and Mixer (pRMX) and static mixing element (A).

It is well known that the elongational flow is more efficient, when it comes to droplet rupture into smaller ones, compared to shear flow. The biggest privilege of using this device is that it works at moderate pressures (approximately 6 bar) unlike the high-pressure homogenizer. One drawback that can potentially limit some applications, is the increase of the local temperature due to the highly turbulent flow regime through the restriction [14].

The device is composed of two cylindrical chambers that come in contact with a static mixing element, which is placed in the center and is responsible for the mixing due to the elongation flow. The two cylindrical chambers are surrounded by a double jacket in which tap water can run through in order to cool down the system. In both sides of the chambers there are two pistons that are placed inside and are pneumatically operating alternately pushing from one chamber to the other through the static mixing element [15] (Figure 2.9). This means that compressed air is used in order to control the movement of the pistons, while a pressure valve allows the control of the air provided to the system, which corresponds to the flow rate or the pistons [16].

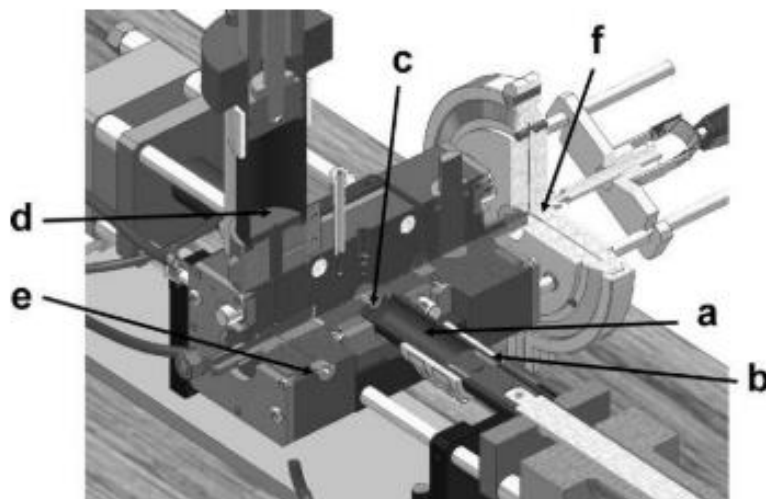


Figure 2.9. Three-dimensional view of the mixer: (a) chamber, (b) piston with seal, (c) mixing element, (d) feeding unit for melts, (e) feeding channel for liquids, and (f) mold [15].

The process can be divided in three steps, the feeding, mixing and outlet of the miniemulsion. The feeding process of the macro-emulsion takes place on the left chamber of the device. To be able to fill the chamber it needs to be fully open, which happens by pushing the button on the control panel so as the piston is moved to the left and the chamber is open and ready to be filled. More specifically, there is a channel, which is connected to a vial containing the macro-emulsion and allows it to flow inside the left chamber. The vial is closed and connected with two channels one for gas and one for feeding. The gas channel is used in order to increase the pressure inside so that the macro-emulsion will flow in the chamber. In the same left chamber, there is also the exit channel. While feeding the left chamber, the right chamber is fixed in position that is close to the mixing element to make sure that no material flows on that direction. The position of the pistons is fixed so the total volume is 35 mL.

Next step is the mixing. During mixing both feeding, and outlet channels are closed. The two pistons are pneumatically driven by compressed air at controlled pressure of 6 bar, which corresponds to the flow rate (q) given to the pistons to move. By changing the pressure one can control the flow rate. The position of the pistons can also be modified so as to control the volume of the materials inside and can be varied in the range of 10-100 cm³. The velocity of the pistons (v) as well as the number of cycles (N) define the mixing sequence [15]. One cycle is

considered as one back and forth movement of the pistons [17]. An experiment can be comprised of several continuous sequences at different flow rates.

The static mixing element (Figure 2.10), which is placed between the pistons, is easy to remove, change the geometry, clean, and place it back. It is made of stainless-steel plate where there are different number of holes of adjustable diameter. Changes on the number of holes of the mixing element, affect the flow rate of the pistons. Two different geometries were investigated in the present work. One was having 4 holes of 1 mm diameter in the front part and one hole, $D = 1$ mm, in the back part. In between there was a space, which was corresponding to a dead volume that was remaining there during the whole experiment. The flow rate, defined as the total volume passed through the restriction per unit of time [18], can roughly be calculated by the following equation:

$$q = \frac{2 \times N \times V}{t} \quad (2.11)$$

where N is the number of cycles, V the volume inside the chamber and t the time to complete one cycle. In the case of the first mixing element the flow rate was found to be $q = 1400$ mL/min. A second static mixing element geometry was designed, which had a simpler design with just one hole through the whole element, $D = 1$ mm. The flow rate with that mixing element became higher, $q = 4200$ mL/min, which can be explained due to the less resistance to the flow caused by the mixing element. In other words, when the pressure drop is constant, the flow can more easily go through one hole as compared to the previous 4 holes mixing element.

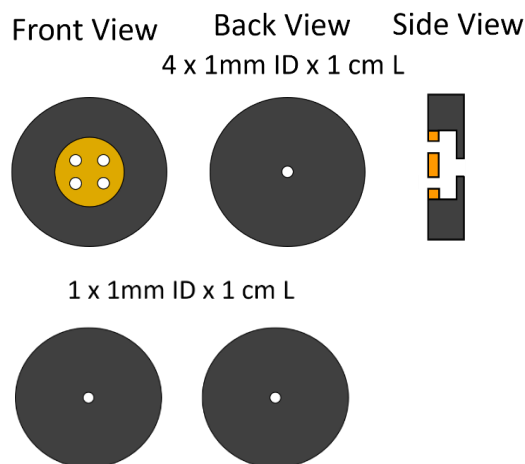


Figure 2.10. Static mixing elements.

On the outer wall of the right chamber there is a pressure detector which measures the pressure during the experiment. There is also a temperature sensor installed to monitor the change of the temperature throughout the experiment. Finally, on the left chamber there is displacement sensor which captures the position of the pistons each moment. All these sensors are connected with a computer which records all the values that are useful to calculate the flow rate each moment.

Finally, after several cycles all the material is pushed to the right chamber where the outlet channel is connected. The valve opens and the final product is recovered in a vial.

When this device was developed the main use was in mixing polymeric blends and in 2012, I. Souilem *et al.* [13], used pRMX to produce methyl methacrylate (MMA) miniemulsion. They first evaluated the droplet diameter when the emulsification time was increasing and observed that the diameter from 100 nm went down to 30 nm, while the miniemulsions were all monomodal (Figure 2.11).

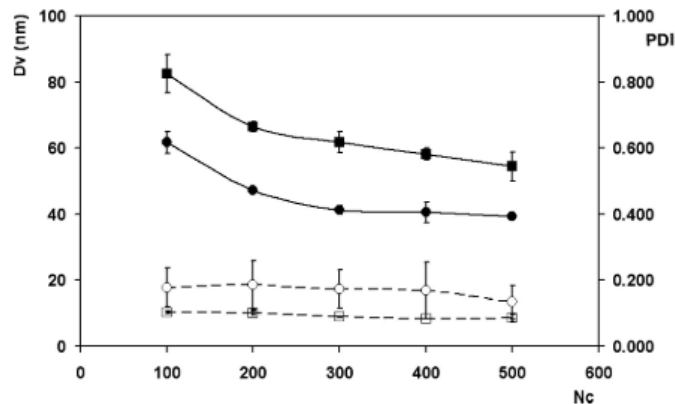


Figure 2.11. Evolution of volume-average drop diameter D_v (black dots) and PDI (white dots) [13].

A very important observation was made referring to the capillary number. They wanted to estimate if the droplet breakup was happening due to elongation or simple shear mechanism. For this reason, they estimated the capillary number by varying the pressure drop, ΔP , during the experiment, and compared with the simple shear and elongation (Figure 2.12). Surprisingly the result showed that the capillary number of the pRMX experiments follows the same trend with the pure elongational flow.

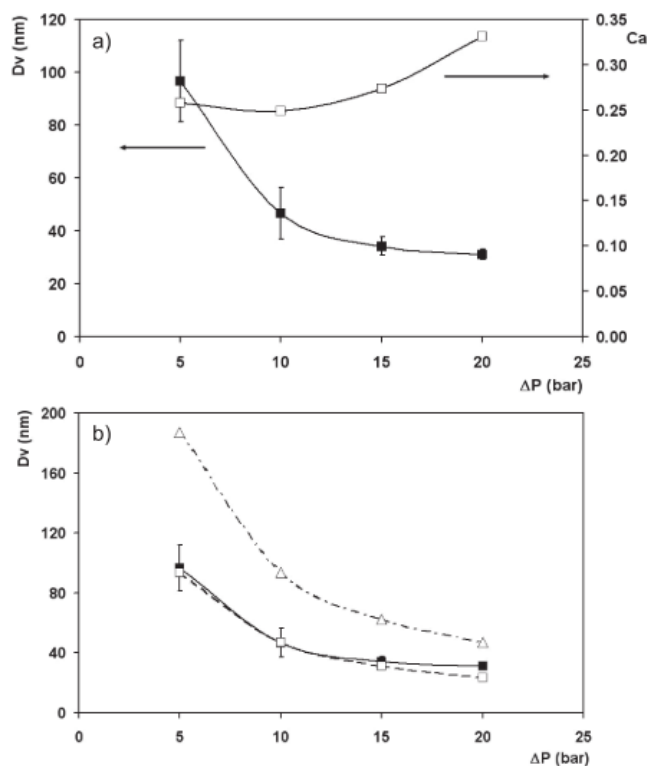


Figure 2.12. (a) Evolution of volume-average drop diameter D_v and capillary number as a function of the pressure drop after 500 cycles. (b) Evolution of D_v as a function of pressure drop (solid lines): RMX after 500 cycles, (\square : dashed lines) for pure elongational flow, (Δ : dashed lines) for pure shear flow [13].

The work made during the present thesis will focus on the variation of the chemical composition of the emulsion as well as the process parameters, mixing element geometry and number of cycles.

4. Rotor-Stator Mixer

In order to compare the droplet size and polydispersity of the miniemulsions that formed the two elongational-flow reactors and mixers along with a rotor-stator mixer were employed. The rotor-stator device was described in detail in chapter I. In this work an Ultra-Turrax T 25 basic (IKA) was used and equipped with a S 25 N – 8 G dispersing element. A total volume of 15 mL was prepared where 80 wt% was the continuous phase and 20 wt% the dispersed phase. The two phases were premixed for 5 min using a magnetic stirrer and then Ultra-Turrax was applied. In order to achieve a better control of the temperature rise during emulsification and diminish the premature polymerization, the vial was placed inside an ice batch whose temperature was monitored and kept constant during the whole experiment.

The influence of the rotational speed was evaluated, where six different speeds, 6500, 9500, 13500, 17500, 21500 and 24000 round per minute (rpm), were tested for 10 min of emulsification. For each speed the samples were emulsified, and three samples were prepared and analyzed so as to obtain a representative average droplet size and polydispersity and evaluate the reproducibility of the method.

Β Thiol-Ene Miniemulsion Formulation

2,2'-(Ethylenedioxy)diethanethiol (EDDT, 98%), 1,2-Ethanedithiol (EDT, 99%), diallyl phthalate (DAP, 98%), Hexadecane (HD, 98%), Diphenyl (2,4,6-trimethylbenzoyl) phosphine oxide (DTPO, 98%), Lithium Phenyl (2,4,6-trimethylbenzoyl) phosphinate (LAP, 98%) and Sodium dodecyl sulfate (SDS, 97%) were obtained from TCI Chemicals and used without further purification. Pentaerythritol tetrakis(3-mercaptopropionate) (PETMP, 95%) was supplied by Bruno Bock. Distilled water was used for the preparation of the continuous phase of the miniemulsion. The chemical structures and amounts that used of all the components can be seen in the following figure.

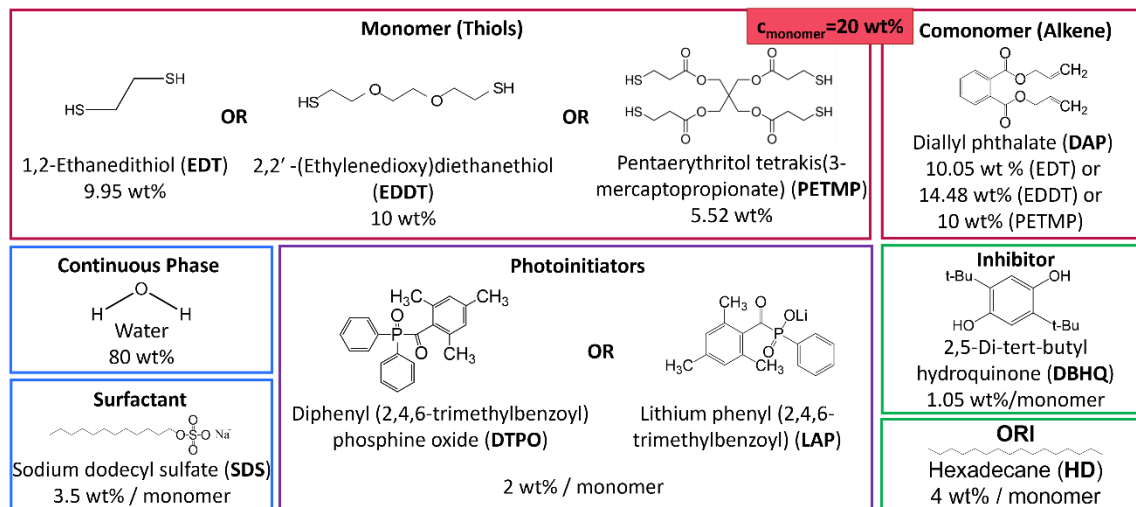


Figure 2.13. Chemical structures and concentrations of all the compounds used for the experiments.

A standard recipe followed to prepare the miniemulsion comprises 80 wt% continuous phase and 20 wt% of dispersed phase (Table 2.1). In more details, the continuous phase was 80 wt% water mixed with SDS at a concentration of 3.5 wt%/C_{monomer}. This solution can be prepared in a bigger quantity to use it for

several experiments. Ideally every week a new continuous phase stock solution was prepared. As for the dispersed phase the two monomers, thiol and alkene, with stoichiometric ratios of the thiol and ene functional groups were mixed. Also, Hexadecane was used as Ostwald ripening inhibitor at concentration of 4 wt%/C_{monomer}, while radical inhibitor of 1 wt%/C_{monomer} was also added to the system to prevent the premature starting of polymerization. Finally, an oil soluble photoinitiator, DTPO, was used (2 wt%/C_{monomer}) so as to perform the photopolymerization later. Unless indicated differently this would be the reference formulation for the miniemulsion.

Table 2.1. Standard miniemulsion formulation.

Continuous Phase	Dispersed Phase
Continuous Phase Distilled Water 80 wt%	Thiol (Ethylenedioxy)diethanethiol (EDDT) 10 wt%
Surfactant Sodium Dodecyl Sulfate (SDS) 3.5 wt% / C _{monomer}	Alkene Diallyl phthalate (DAP) 10 wt%
	Photoinitiator Diphenyl (2,4,6-trimethylbenzoyl) phosphine oxide (DTPO) 2 wt% / C _{monomer}
	Ostwald Ripening Inhibitor Hexadecane (HD) 4 wt% / C _{monomer}
	Radical Inhibitor 2,5-Di-tert-butyl hydroquinone (DBHQ) 1.05 wt% / C _{monomer}

Since the ITN Photoemulsion project is connecting different institutions and industries, the standard miniemulsion formulation was first studied from C. M. Q. Le and A. Chemtob [19], our colleagues at Institut de Science des Matériaux de Mulhouse, IS2M in Mulhouse. They worked on the development of a stable miniemulsion using Ultra-Turrax and Sonicator. Our job was to use this chemistry and apply it on our elongational-flow devices, in order to scale up the process and reach to the industrial application of the thiol-ene miniemulsions.

1. Coarse Emulsion Preparation

A premixing of all the components is required to obtain a homogeneous coarse emulsion in order to make sure that the composition does not vary before entering the emulsification device.

1.1 Ambient Atmosphere

Before miniemulsification with μ RMX, pRMX or Ultra-Turrax a coarse emulsion was prepared. This procedure was established for all the experiments and 5 min of magnetic stirring was applied once all the compounds were added to the vial. There was a specific sequence of the addition of the compounds: starting with the addition in a vial of the photoinitiator and the radical inhibitor, followed by the Ostwald ripening inhibitor, the alkene and the thiol. Few moments were allowed for the powders to be solubilized before adding the continuous phase.

1.2 Inert Atmosphere

An important observation was made that oxygen can react and oxidize the thiol, which means that polymerization takes place as soon as oxygen comes in contact with the thiol [20]. It has been found that a diradical oxygen from the atmosphere can abstract the hydrogen atom from the thiol, generating the radical and start the reaction of thiol with the alkene following the free-initiator thiol-ene click reaction (Figure 2.14).

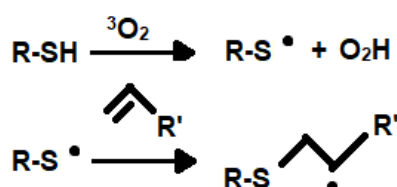


Figure 2.14. Thiol reaction with oxygen [20].

To avoid this unwanted polymerization, experiments were conducted by removing the oxygen. To do so first the compounds with the specific order, as mentioned before, were added to the vial and vacuum was applied to the system for 10 min along with the magnetic stirring. Then, since the oxygen was removed, nitrogen

was applied to the system, to obtain an inert atmosphere. The nitrogen gas was introduced inside the solution to ensure that oxygen that was trapped in between the liquid was totally replaced by nitrogen. In this way, by conducting ^1H NMR, it was observed that the pre-polymerization during the preparation step was zero.

2. Miniemulsion Preparation

After preparing the coarse emulsion with either ambient or inert atmosphere and obtaining a homogeneous solution, the three miniemulsification devices were used, Micro Elongational-Flow Reactor and Mixer (μRMX), Pneumatic Elongational-Flow Reactor and Mixer and Ultra-Turrax. Variation of process and chemical parameters occurred for all the devices to estimate the changes on the droplet and particle diameter as well as polydispersity.

Thiol-Ene Miniemulsion Photopolymerization

After emulsification with one of the aforementioned emulsification devices (μRMX , pRMX, Ultra-Turrax) the obtained miniemulsion was photopolymerized so as to acquire a stable latex. It is very important in this chapter to analyze the polymerization mechanism in miniemulsion. First, the droplets created in the miniemulsion have to be small and as much homogeneous as possible, this will allow them to behave as precursor materials, which will be transferred, through polymer reactions, to the final polymeric particles, also called latexes. To obtain the same droplet and particle size the initial droplets need to maintain their identity with limited exchange of monomer between droplets through the continuous phase. To achieve that, the droplets during polymerization must be the primary locus of the reaction. In the case where a water-soluble initiator is used, the initiation stage will cause the decomposition of the initiator and the formation of radicals in the aqueous phase will follow. The generated radicals are hydrophilic which does not allow them to enter to the hydrophobic oil phase, so they start reacting with the few monomers present in the continuous phase forming oligomers in the aqueous phase. For the droplet nucleation to occur, once these oligomers become hydrophobic, which means that when these oligomers reach a critical chain length they start to become hydrophobic and thus no more soluble in

the water phase. This way they get stabilized by the surfactant and the particles continue to grow by incorporating monomer. This is often called nanoreactor state, since the droplets behave as individual nanoreactor and does not get influenced by the surrounding environment. Termination also occurs in the droplet and ideally the final latex particles will have almost the same size as the droplets.[21], [22] In the case where an oil-soluble initiator is used, when the polymerization is triggered, the reaction starts from the beginning in the droplets. An Ostwald ripening inhibitor is thus added to the oil phase to avoid the possible transfer of monomer through the continuous phase induced by the difference in chemical potential resulting from droplets of different sizes.

In this thesis, free radical thiol-ene click miniemulsion photopolymerization reaction was used to produce thioether latex particles. The free radical thiol-ene reaction was described in detail in chapter I. Two in-line photopolymerization reactors were used and compared during the experiments, one linear and helically one.

1. Linear Photoreactor (LP)

Our group has already developed this linear photoreactor and among all the different applications it was also used to UV irradiate MMA miniemulsion [23]. This device comprises of a syringe pump (PHD 2000, Harvard Apparatus) where a plastic single-use syringe, containing the miniemulsion and covered with aluminum foil to prevent light penetration and the premature polymerization, was placed and kept stable (Figure 2.15). The tip of the syringe is connected with a PTFE tube of a specific diameter, 1.06 mm ID x 1.68 OD, and the miniemulsion is forced to flow inside by adjusting the flow rate of the pump. This PTFE tubing is coaxially fixed in a stainless-steel tube, whose inner diameter was 4mm and the length was 22 cm, and two T-junction UV sources (Lightningcure LC8, Hamamatsu) were placed at both ends of the stainless steel tube. The wavelength of the UV irradiation was kept constant in all experiments at $\lambda = 365$ nm, which was in a good agreement with the absorbance of the photoinitiator that was used. Taking into account the length of the stainless-steel tube as well as the flow rate, which was set at 0.025 mL / min, the residence time was calculated to be 7 min, using the following equation:

$$\tau = \frac{V}{q} \quad (2.12)$$

where q is the flow rate and V is the internal volume of the PTFE tube in stainless-steel tube and can be defined by:

$$V = \pi \frac{ID^2}{4} L \quad (2.13)$$

where ID is the inner diameter of the PTFE tube and L is its length.

This residence time was found to be sufficient enough to achieve the maximum photopolymerization rate. After this time the final latex particles were collected in a beaker and characterized for the particle size and conversion.

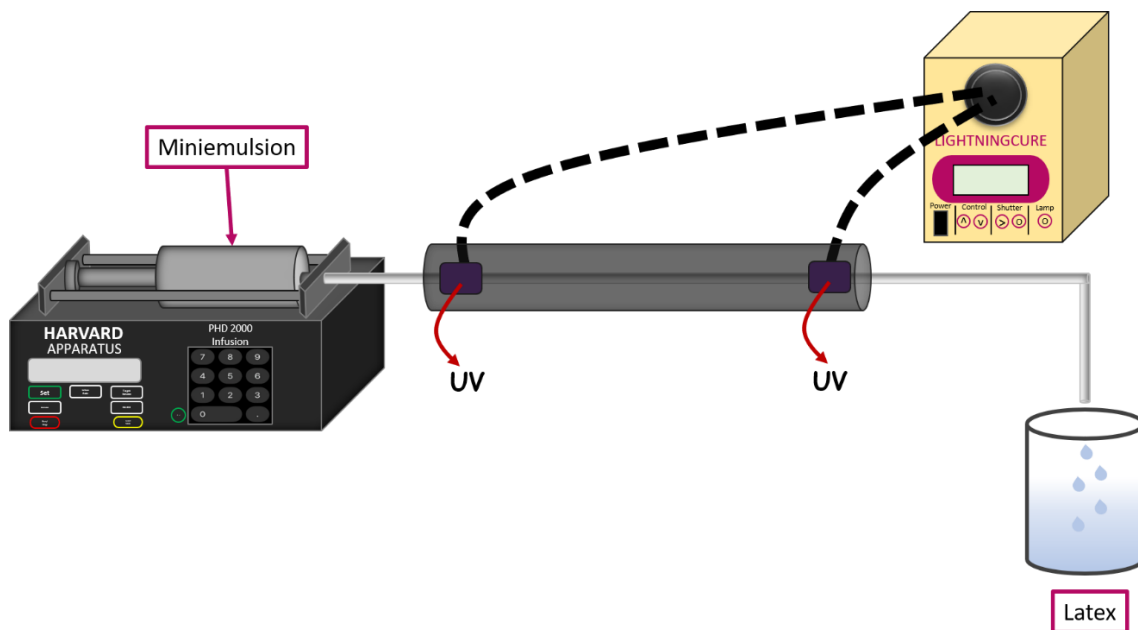


Figure 2.15. Linear Photoreactor.

W. Yu *et al.* [14], observed that the particles had a bigger diameter than the initial droplets. They assume that this can happen due to the difference of the chemical potential of the droplets, meaning that the small droplets have a higher chemical potential than the big ones and the system wants to go to an equilibrium state by monomer diffusion through the water phase from the bigger to the small droplets. This can happen if the monomers are slightly soluble in the water phase. The described phenomena occurs because the UV does not have enough space to penetrate and nucleate the droplets that are in the center of the PTFE tube which

leads in the end to bigger particle sizes (Figure 2.16). In order to avoid this monomer diffusion, they diluted the miniemulsion so as the droplets will have more space in between each other, and the UV irradiation can more easily access all the droplets even the ones that are in the center of the tube and nucleate them. Fortunately, after adding a big amount of solvent, water, they observed that the particle size was identical to the droplet size.

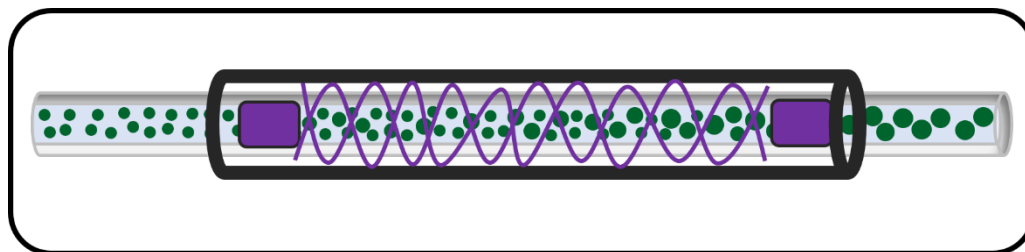


Figure 2.16. Schematic drawing of the UV arrangement, green circles represent the droplets, purple squares the two entrances of UV light, purple waves the propagation of UV light through the stainless- steel tube (black).

2. Coiled Tube Photoreactor (CTP)

For comparison purposes a coiled tube photoreactor was designed in our lab (Figure 2.17). The goal was to bring back the droplets in the center of linear photoreactor to the wall for better change to be nucleated. The new setup includes the same syringe pump (PHD 2000, Harvard Apparatus) as before, where the miniemulsion was placed in a single-use plastic syringe, whose tip was connected with the same PTFE tube (1.06 mm ID x 1.68 OD). This time the design of the photoreactor was constituted of a stainless-steel rod which is placed in the middle, on the wall of this rod 6 m of the PTFE tube are wrapped around. Then a quartz tube was placed in the outer diameter of the PTFE tube, which was further wrapped with an LED strip (ledxon RIBBONFLEX 2000056, solder connections 12V 90 cm, CONRAD, $\lambda = 365$ nm, Orizzonte, LED Lighting, $\lambda = 385$ nm), where the wavelength of the UV irradiation was either $\lambda = 365$ or 385 nm. Finally, a stainless-steel tube was used to keep all the system in place and provide UV protection. The residence time was 7 min, which corresponds to the same residence time with the linear photoreactor and was calculated using equations 14 and 15 and would allow the comparison between the devices.

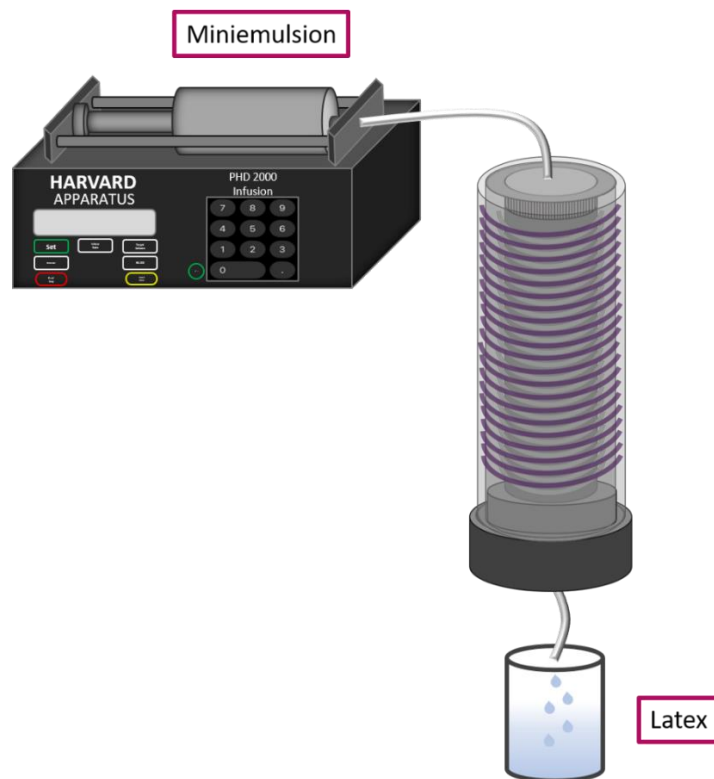


Figure 2.17. Coiled tube photoreactor.

By using the coiled tube photoreactor it is believed that due to the centrifugal force, that is applied to the droplets, more droplets will have the chance to reach the walls of the PTFE tubing where the UV irradiation can reach and nucleate them (Figure 2.18). This way the final latex particles will have the same diameter with the droplets without the need of dilution.

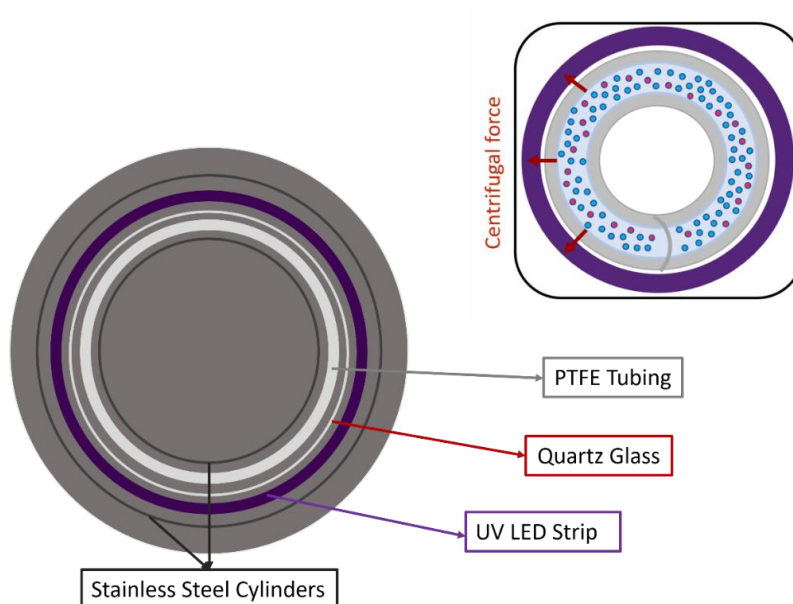


Figure 2.18. Coiled tube photoreactor.

The described coiled tube photoreactor was inspired by a former work from our group. D. Parida *et al.* [24], compared the polymerization conversion of 2-(Dimethylamino)ethyl methacrylate) (DMAEMA) in batch, and using coiled tube reactors. It became obvious that with the coil tube reactor the polymerization started in less time while at the same time the reaction rate appeared to be higher than the batch reaction (Figure 2.19).

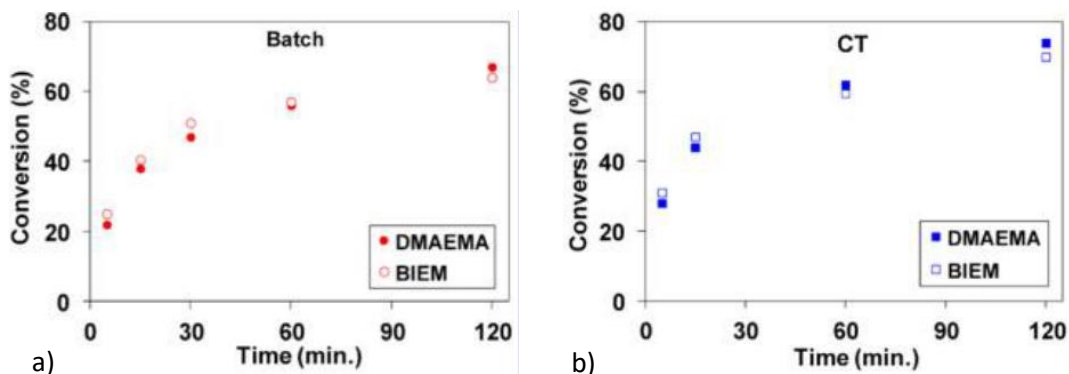


Figure 2.19. Relative conversions in batch (a) and coiled tube (b) reactors [24].

D Characterization Techniques

1. Dynamic Light Scattering (DLS)

Dynamic light scattering (DLS) was used to characterize the droplet and latex diameter as well as the polydispersity index. A DLS, Zetasizer, Nano Series from Malvern was used at a fixed 173° scattering angle. A very important value that needs to be added to the software in order to calculate properly the diameter and the polydispersity is the reflecting index of the monomers that are used. All the samples were prepared in the same way in order for the results to be comparable. First 9 mL of water were added in a vial and 2 drops of freshly prepared miniemulsion, or latex were mixed. To assure that the dilution will be the same in all the experiments the 2 drops that were added, their weight in milligrams was noted. The dilution plays a very important role since it controls the turbidity of the solution and in this way, coalescence can be prevented. From this fresh diluted miniemulsion or latex, 1.5 mL were added to a DLS cuvette, and each sample was automatically measured three times at room temperature. Due to the sensitivity of

the miniemulsion the DLS measurements had to be taken right after emulsification and this time had to be constant for all the experiments. In this way reproducibility is ensured. The important information retrieved directly from the device is the number-, volume and intensity- diameter of the droplets and particles. In this study only the droplet and particle number will be used, since it can provide information about emulsions that have more than one diameter population of droplets/particles. Finally, the polydispersity index of the miniemulsion and latex were obtained automatically and the values that were below 0.2 will be considered as monomodal systems.

2. Proton Nuclear Magnetic Resonance (^1H NMR)

Proton nuclear magnetic resonance (^1H NMR) spectra was recorded in a Bruker Avance I 400 MHz, equipped with Ultrashield magnet, and used to evaluate the polymerization conversion before and after photopolymerization. All the samples were measured mainly after miniemulsification but before photopolymerization. This happened because the different mixing devices provide increase of the temperature of the miniemulsion which could initiate the polymerization. Latex samples were also analyzed, and the results will be discussed in the following chapter. To prepare the miniemulsion and latex sample, 30 μL were mixed with 0.5 mL of dimethyl sulfoxide- d_6 , deuterated DMSO, and poured in an NMR tube. The scans were adjusted to 32 in order to allow the solution more time to be scanned so as the picks to be more identical and not overlap.

Ξ Bibliography

- [1] G. I. Taylor, "The formation of emulsions in definable fields of flow," *Proceedings of the Royal Society of London. Series A, Containing Papers of a Mathematical and Physical Character*, vol. 146, no. 858, pp. 501–523, 1934, doi: 10.1098/rspa.1934.0169.
- [2] D. Askeland, *The science and engineering of materials*, 7th ed. Boston MA: Cengage Learning, 2016.
- [3] P. Taylor and H. P. Grace, "Dispersion Phenomena in High Viscosity Immiscible Fluid Systems and Application of Static Mixers As Dispersion Dispersion Phenomena in High Viscosity Immiscible Fluid Systems and Application O F Static Mixers As Dispersion Devices in Such Systems," *Science (1979)*, vol. 6445, no. 912873516, pp. 37–41, 2009, doi: 10.1080/00986448208911047.
- [4] I. Delaby, B. Ernst, Y. Germain, and R. Muller, "Droplet deformation in polymer blends during uniaxial elongational flow: Influence of viscosity ratio for large capillary numbers," *Journal of Rheology*, vol. 38, no. 6, pp. 1705–1720, Nov. 1994, doi: 10.1122/1.550568.
- [5] M. Vauthier and C. A. Serra, "One-step production of polyelectrolyte nanoparticles," *Polymer International*, vol. 70, no. 6, pp. 860–865, 2021, doi: 10.1002/pi.6178.
- [6] W. Yu *et al.*, "Development of an Elongational-Flow Microprocess for the Production of Size-Controlled Nanoemulsions: Batch Operation," *Macromolecular Reaction Engineering*, vol. 11, no. 1, pp. 1–11, 2017, doi: 10.1002/mren.201600024.
- [7] Y. Suzaka, "Mixing Device," 104,100, 1979
- [8] C. D. Han, *Multiphase flow in polymer processing*, 1st ed. Academic Press, 1981.
- [9] R. Muller, M. Bouquey, and J. Terrisse, "A new mixing device based on elongational flows," 2007
- [10] W. Yu *et al.*, "Development of an Elongational-Flow Microprocess for the Production of Size-Controlled Nanoemulsions: Batch Operation," *Macromolecular Reaction Engineering*, vol. 11, no. 1, Feb. 2017, doi: 10.1002/mren.201600024.
- [11] M. Vauthier, M. Schmutz, and C. A. Serra, "One-step elaboration of Janus polymeric nanoparticles: A comparative study of different emulsification processes," *Colloids and Surfaces A: Physicochemical and Engineering Aspects*, vol. 626, no. May, p. 127059, 2021, doi: 10.1016/j.colsurfa.2021.127059.
- [12] T. F. L. M. Gholamali Farzi, Elodie Bourgeat-Lami, "Miniemulsions Using Static Mixers: A Feasibility Study Using," *Journal of Applied Polymer Science*, vol. 116, no. 5, pp. 2658–2667, 2010, doi: 10.1002/app.
- [13] I. Souilem *et al.*, "A Novel Low-Pressure Device for Production of Nanoemulsions," *Chemical Engineering and Technology*, vol. 35, no. 9, pp. 1692–1698, 2012, doi: 10.1002/ceat.201100676.
- [14] W. Yu, "Development of an Elongational-Flow Microprocess for the Production of Size-Controlled Nanoemulsions: Application to the Preparation of Composite and Hybrid Polymeric Microparticles," Universite de Strasbourg, 2009.

- [15] M. Bouquey, C. Loux, R. Muller, and G. Bouchet, "Morphological Study of Two-Phase Polymer Blends During Compounding in a Novel Compounder of the Basis of Elongational Flows," *Applied Polymer Science*, vol. 21, no. 7, pp. 482–490, 20010, doi: 10.1002/app.32645.
- [16] Heeresh Mistry, *Fundamentals of Pneumatic Engineering*. Creat Space e-Publication, 2013.
- [17] I. Souilem *et al.*, "A Novel Low-Pressure Device for Production of Nanoemulsions," *Chemical Engineering and Technology*, vol. 35, no. 9, pp. 1692–1698, 2012, doi: 10.1002/ceat.201100676.
- [18] P. P. Urone and R. Hinrichs, *Introduction to Science and the Realm of Physics, Physical Quantities, and Units*, 1st ed. XanEdu Publishing Inc, 2012.
- [19] F. Jasinski *et al.*, "Thiol-Ene Linear Step-Growth Photopolymerization in Miniemulsion: Fast Rates, Redox-Responsive Particles, and Semicrystalline Films," *Macromolecules*, vol. 49, no. 4, pp. 1143–1153, 2016, doi: 10.1021/acs.macromol.5b02512.
- [20] R. O. McCourt and E. M. Scanlan, "Atmospheric Oxygen Mediated Radical Hydrothiolation of Alkenes," *Chemistry - A European Journal*, vol. 26, no. 68, pp. 15804–15810, 2020, doi: 10.1002/chem.202002542.
- [21] K. Landfester, "Synthesis of colloidal particles in miniemulsions," *Annual Review of Materials Research*, vol. 36, pp. 231–279, 2006, doi: 10.1146/annurev.matsci.36.032905.091025.
- [22] J. Asua, "Miniemulsion polymerisation," *Progress in Polymer Science*, vol. 27, no. 27, pp. 1283–1346, 2002, doi: 10.1016/S0079-6700(02)00010-2.
- [23] W. Yu *et al.*, "Development of an Elongational-Flow Microprocess for the Production of Size-Controlled Nanoemulsions: Application to the Preparation of Monodispersed Polymer Nanoparticles and Composite Polymeric Microparticles," *Macromolecular Reaction Engineering*, vol. 11, no. 1, pp. 1–10, 2017, doi: 10.1002/mren.201600025.
- [24] D. Parida *et al.*, "Coil flow inversion as a route to control polymerization in microreactors," *Macromolecules*, vol. 47, no. 10, pp. 3282–3287, 2014, doi: 10.1021/ma5001628.

CHAPTER III

FROM THIOL-ENE MINIEMULSION TO THIOETHER LATEX NANOPARTICLES

Outline

Preface.....	147
<i>A</i> Introduction	147
<i>B</i> Thiol-Ene Miniemulsification and Photopolymerization	149
1. Proton Nuclear Magnetic Resonance (¹ H NMR): Spectra Interpretation 149	
2. Miniemulsions with tetra-functional thiol and bi-functional alkene.....	154
2.1 Pneumatic Elongational-Flow Reactor and Mixer: Effect of Process Parameters and Surrounding Atmosphere	155
2.1.1 Four-Holes Static Mixing Element and Ambient Atmosphere	156
2.1.2 One-Hole Static Mixing Element and Inert Atmosphere	160
2.2 Pneumatic Elongational-Flow Reactor and Mixer: Effect of Chemical Parameters.....	162
2.3 System Stability.....	166
2.4 Rotor-Stator Mixer.....	168
3. Bi-Functional Thiol and Bi-Functional Alkene	170
3.1 1,2-Ethanedithiol (EDT) and Diallyl phthalate (DAP)	170
3.1.1 Micro Elongational-Flow Reactor and Mixer (μRMX).....	172
3.1.2 Pneumatic Elongational-Flow Reactor and Mixer (pRMX).....	174
3.1.3 Rotor-Stator Mixer	175
3.2 2,2'-(Ethylenedioxy)diethanethiol (EDDT) and Diallyl phthalate (DAP) 176	
3.2.1 Pneumatic Elongational-Flow Reactor and Mixer: Effect of Process Parameters	178

3.2.2 Pneumatic Elongational-Flow Reactor and Mixer: Effect of Chemical Parameters	180
3.2.3 System Stability	185
3.2.4 Pneumatic Elongational-Flow Reactor and Mixer: Temperature Control 187	
3.2.5 Rotor-Stator Mixer	189
3.3 Thiol-Ene Photopolymerization and Miniemulsification	191
<i>C</i> Conclusions	193
<i>D</i> Bibliography	195

Preface

The two elongational-flow based devices that were described in the previous chapter, along with the two photoreactors, were used to produce monomodal size-controlled thiol-ene based nano-droplets and -particles. In this chapter the results obtained with these devices will be described in detail. The effect of the process as well as chemical parameters on the droplet and particle diameter will extensively be explained. Finally, comparison will be done using a conventional rotor-stator mixer so as to evaluate the different processes.

A Introduction

A system in which distributed droplets or particles of one material are dispersed in a continuous phase of another material is called dispersion [1]. Dispersions can be classified by the combination of the dispersed phase and the medium phase where the particles are suspended in [1]. First type is the gel, which is defined as a non-fluid colloidal network or polymer network that is expanded throughout its whole volume by a fluid [2]. Second is the emulsion, which is a mixture of two or more liquids that are normally immiscible (unmixable or unblendable). Last class of dispersions is the aerosol, which consists of fine solid particles or liquid droplets in air or another gas [2]. In the presented work, focus will be given to oil-in-water (o/w) emulsions between two phases: the oil (dispersed) phase and the aqueous (continuous) phase. Emulsions are thermodynamically unstable, and consequently tend to destabilize over time in order to minimize the interfacial area between the aqueous and oil phase [3]. This break down happens due to various physicochemical mechanisms, including gravitational separation, flocculation, coalescence, Ostwald's ripening and phase separation [3], [4]. In these conditions, the use of the emulsifying agent (surfactant) is essential to obtain a stable emulsion, by forming a thin film around the globules of dispersed phase [5], [6]. Therefore, to enhance emulsions long-term stability, different stabilizers can also be incorporated in emulsion formulations apart from emulsifier, such as texture modifiers, ripening inhibitor and weighting agents. There was always an increased interest in o/w emulsions formation and on the control of the droplet diameter according to the application. Huge amount of research is based on the biomedical

field, for instance Delmas *et al.* [7], aim at extending the stability of miniemulsion produced from soybean oil mixed with water, using ultrasounds. Basically, they detect the droplet size and distribution while emulsifying and found that both decreased after 5 min of emulsification and remained constant from 12 to 30 min. Furthermore, they changed the power of the sonicator and discovered that the droplet size decreased with increase of energy the first approximately 10 min and then it reached a plateau value. Ashokkumar's team then observed the droplet growth by increasing the oil phase volume quantity [8]. But in both studies, overprocessing effect (uncontrolled increase of the system's temperature) occurred, that is unwanted when the droplets' reactivity is high, such as with thiol-ene reaction.

Thiol-ene reaction was first communicated in 1950 by Posner that described the reaction of a thiol with an alkene that form a thioether [9]. Thiol-ene polymerization is often mentioned in the literature as click-chemistry reaction, which refers to a process where simple, efficient reactions that yield in a single product are required. Kolb and his coworkers were the first ones to establish the term 'click-chemistry' by combining small heteroatom units in order to produce modular "blocks" for both small- and large-scale applications [10]. These reactions possess several characteristics, among which the high polymerization conversion with no side products, the insensibility to water and oxygen, provided that the amount of oxygen is less than the amount of thiol, the abstention of solvents since most of the time water is used as well as the stereospecificity and regiospecificity. Overall, thiol-ene chemistry is used in a broad range of applications [11]–[13] since it is known to form rapidly a homogeneous polymeric network due to the polymerization step which can be tailored by step- and chain-growth mechanism [14].

Investigating thiol-ene droplets emulsions and poly(thioether) latex are thus highly challenging with the classic emulsification devices (shear mixer or sonicator) due to the poor stability over time at room temperature [15]. This is why, in this work, we propose an alternative to conventional devices: a pneumatic elongational-flow reactor and mixer. Elongational-flow devices are indeed known to have some unmeet advantages, in comparison with more conventional emulsification

equipments (sonicator and shear devices) [16]–[18]. It allows in particular to control the droplets and latex particles' size and the size distribution from highly viscous solutions (e.g. polymers) with viscosity ratios higher than 4, which is the limiting value according to Grace's theory for the shear devices [19].

➤ Thiol-Ene Miniemulsification and Photopolymerization

1. Proton Nuclear Magnetic Resonance (^1H NMR): Spectra Interpretation

In this section a detailed description will be given on how to interpret the ^1H NMR spectra in order to be able to calculate the polymerization conversion right after emulsification as well as after photopolymerization. It is very important to evaluate if the emulsification process can initiate the polymerization. In that case, the main reason is the increase of the temperature while emulsifying. This increase can either be observed with a thermometer, or in the case where the overall temperature is controlled, the phenomena that can occur is that, in the place close to the mixing element, the temperature is slightly rising but not much so as to be captured by the thermometer. This temperature though might be enough to start the polymerization while using the emulsification devices.

In the rest of the manuscript, miniemulsion will be called the emulsion that was recovered from the different emulsification devices, before flowing in the photopolymerization arrangement. Irrelevantly of the potential presence of the latex particles that may rise from a pre-mature polymerization during the emulsification step. While latex is defined the suspension collected in the end of the photoreactor.

In order to be able to understand a complicated spectrum obtained by the miniemulsion, one needs to first observe the spectra of each compound added in the miniemulsion separately and identify which peaks correspond to which proton of the compound. In this work three different thiols were combined with one bi-functional alkene. Two different types of inhibitors were used, one to control the polymerization, which is the radical inhibitor, and one inhibitor to control Oswald's ripening phenomena. Also, two different photoinitiators were added to the solution.

All the aforementioned compounds were characterized with ^1H NMR (400 MHz) and discussed in detail.

Starting with the different thiols, it is worth mentioning that the bi-functional thiol called 1,2-ethanedithiol (EDT) did not undergo NMR characterization because of the limitation due to the strong smell, details will be discussed in the following chapter devoted to this thiol. Referring to the tetra-functional thiol, pentaerythritol tetrakis(3-mercaptopropionate) (PETMP), the ^1H NMR spectra as well as the chemical structure can be seen in Figure 3.1. It becomes clear that there are many small peaks in the spectra which are due to the impurities contained in the monomer, since it was delivered with 95% purity. Overcoming these small peaks, a very strong peak at $\delta = 2.5$ ppm is this from the deuterated solvent, DMSO- d_6 , while the second strong peak at $\delta = 3.3$ ppm corresponds to water. Indeed, it is well-known that DMSO- d_6 is highly hydroscopic and for this reason a water peak is always coming along with DMSO- d_6 . These two peaks appear in all the spectra that will be shown in this thesis.

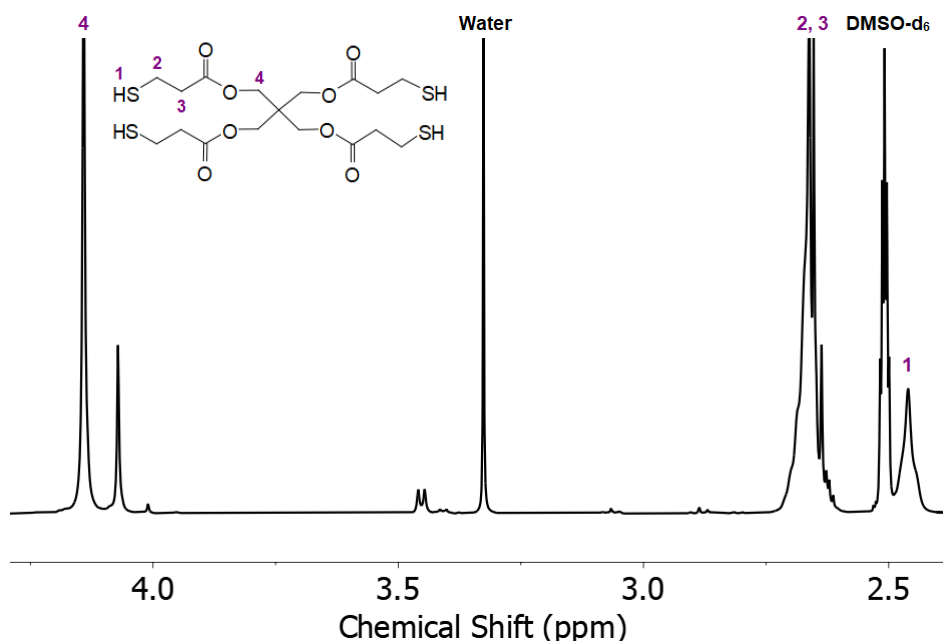


Figure 3.1. Chemical structure and ^1H NMR spectrum of the tetra-functional thiol, pentaerythritol tetrakis(3-mercaptopropionate) (PETMP).

The most important peak and the one that will be followed in order to evaluate the polymerization conversion is the -SH functional group. In the tetra-functional thiol

this group appears at 2.4 ppm (peak n°1), followed by the protons of the -CH₂ groups that are close to the sulfur groups at 2.6 ppm and finally, at 4.13 ppm the -CH₂ protons in the center show a characteristic peak [20].

A bi-functional thiol that is called 2,2'-(ethylenedioxy)diethanethiol (EDDT) was used and the spectra can be seen in Figure 3.2. The characteristic proton of the -SH group is found at 2.2 ppm, the proton of the -CH₂ group that is next to the -SH group can be seen at 2.6 ppm, while the protons that correspond to the -CH₂ groups surrounding the oxygen are seen at 3.5 ppm [21].

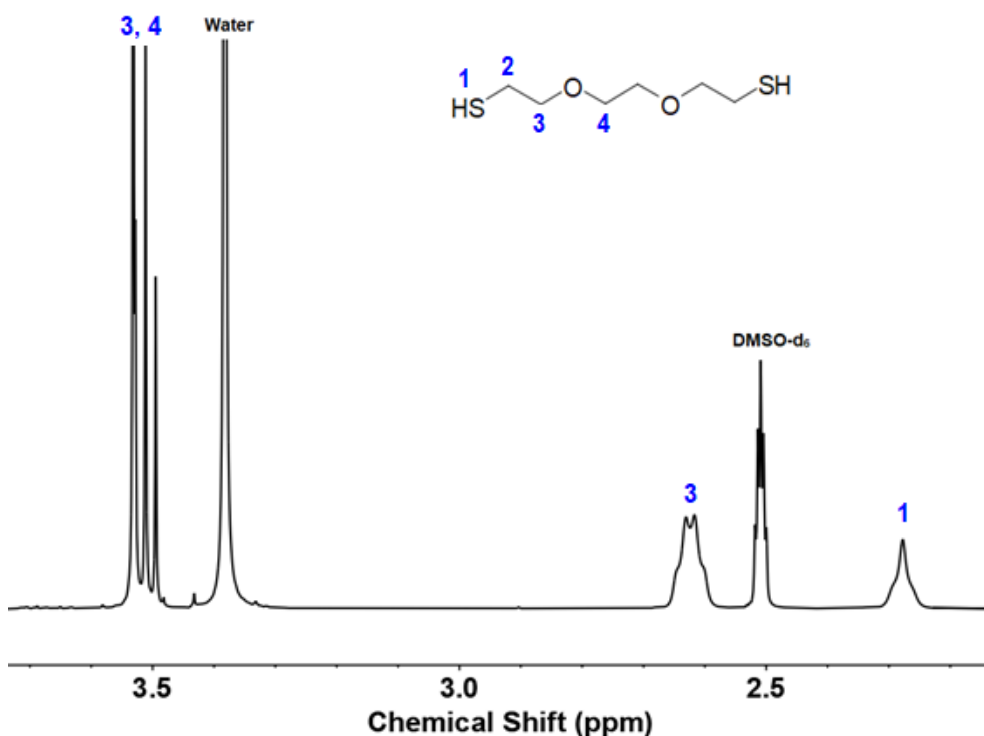


Figure 3.2. Chemical structure and ¹H NMR spectrum of the bi-functional thiol, 2,2'-(ethylenedioxy)diethanethiol (EDDT).

When it comes to the alkene, the only one used for conducting the experiments, the diallyl phthalate (DAP), whose molecular structure and ¹H NMR spectra are presented in Figure 3.3. In this case, the functional group that will be monitored through the experiments is the ending protons of the double bond, =CH₂, which appear at 5.33 ppm. The protons that are next to the double bond, =CH-, are seen at 5.9 ppm, while the protons that are close to the oxygen appear at 4.7 ppm. Finally, the protons of the benzoyl are gathered at 7.7 ppm [22].

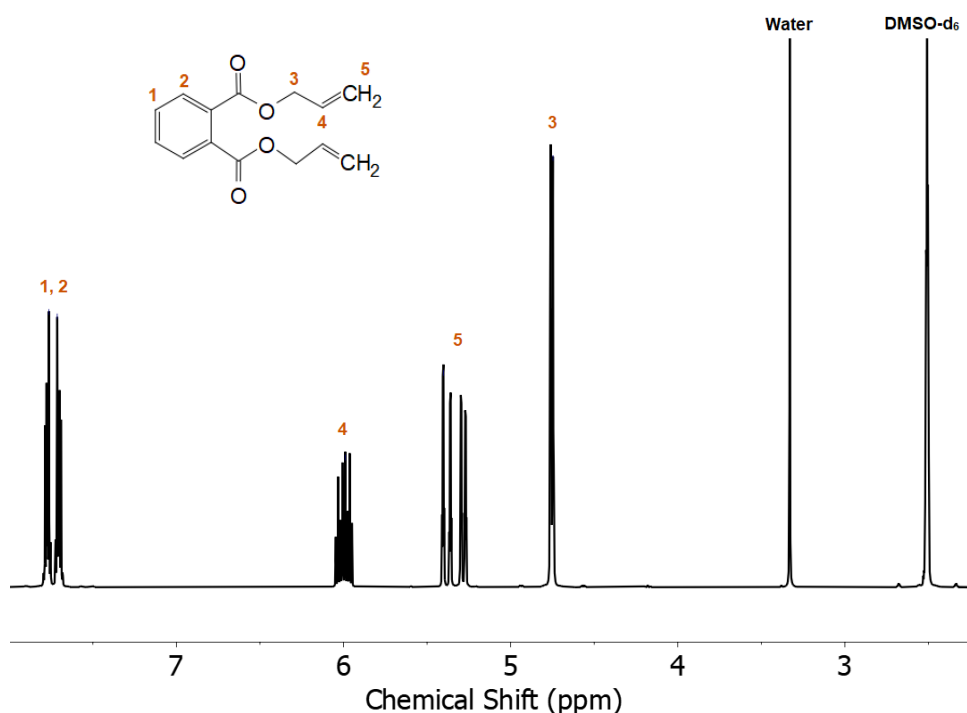


Figure 3.3. Chemical structure and ^1H NMR spectrum of the bi-functional alkene, diallyl phthalate (DAP) .

Once the monomers are mixed and in order to be able to calculate the conversion, a reference peak is needed. This peak has to be the one of a molecule that will be added in the solution, but it will not participate in the reaction. This will allow the calculations to be correct, reproducible and comparable for each experiment. In this case hexadecane, that works as an Ostwald ripening inhibitor, is added to the solution and does not react with any of the components, for this reason it will serve as reference for all the experiments (peaks at 1.2 ppm and 0.8 ppm). The following spectra will be discussed as a representative example of a miniemulsion.

In this spectrum, one can identify all the peaks that were previously described for the two monomers: the tetra-functional thiol (Figure 3.1) and bifunctional alkene (Figure 3.3). It is completely reasonable to assume that the water peak ($\delta = 3.3$ ppm) becomes broader than in previous spectra because the majority of the miniemulsion is water. As mentioned, the two peaks at $\delta = 1.2$ ppm and $\delta = 0.8$ ppm correspond to hexadecane, for protons of $-\text{CH}_2$ group and $-\text{CH}_3$ respectively [23] and since the reference peak to evaluate the polymerization conversion has to be identical and no overlapping with other peaks, the one at 0.8 ppm will be used. The protocol that will be described for this chemical system will be the same with all the different thiols

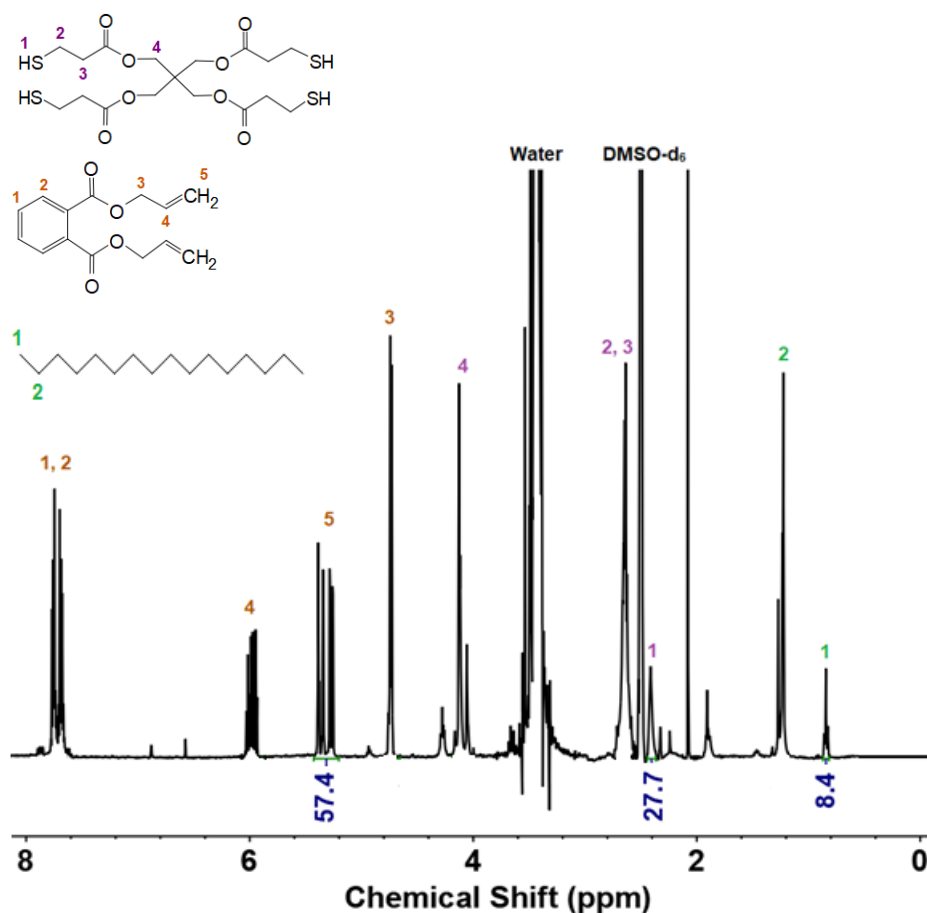


Figure 3.4. Chemical structures of pentaerythritol tetrakis(3-mercaptopropionate) (PETMP), diallyl phthalate (DAP) and hexadecane ^1H NMR spectrum of PETMP-DAP miniemulsion prepared using pneumatic elongational-flow reactor and mixer (pRMX) (400 cycles, (4 holes of 1mm micromixer, room temperature). The continuous/dispersed phase volume ratio was equal to 80/20.

Once all the peaks are identified, and since the concentration of each compound is known the only three functional groups that are important for calculating the conversion are, $-\text{SH}$ of thiol, $=\text{CH}_2$ of alkene and $-\text{CH}_3$ of hexadecane. To start the calculations, one needs the amount of the aforementioned compounds in moles (n), which can be calculated by knowing the mass (m) and molecular weight (M) of those: $n = m/M$. Then, in order to estimate how many protons are in the miniemulsion, simply multiply the molar amount of the compound with the protons of the related functional group:

- Hexadecane: the molar amount of hexadecane that is in the miniemulsion corresponds to $n = 1.4$ mmol. The protons of the group that will be monitored (two $-\text{CH}_3$ groups in hexadecane) are six. This will forecast that the expected protons in the solution will be $1.4 \times 6 = 8.4$ H, which is equivalent with the integration of this peak in the NMR spectra (Figure 3.4).

- Thiol and alkene: Since the reference peak is fixed at 8.4 integration, the same calculations for the thiol and alkene functional groups one can expect, if there is zero polymerization, that the integration of the thiol peak corresponding to the protons of the -SH group will be $8 \times 4 = 32$ H ($n = 8$ mmol, 4 H) and the integration of the alkene peak corresponding to the protons of the =CH₂ group will be equal to $20 \times 4 = 80$ H ($n = 8$ mmol, 4 H).

Taking a look at figure 3.4, one can see the peak at 2.4 ppm (-SH) and the one at 5.3 ppm (=CH₂) have correlated integrations equal to 27.7 and 57.4. Since the amounts are less than the expected ones, calculated before, means that polymerization took place during emulsification. To estimate the percentage of the conversion, the following equation was used:

$$Yield = \frac{\text{Theoretical peak integration} - \text{Peak integration of product}}{\text{Theoretical peak integration}} \times 100 \quad (3.1)$$

As an example, in the previously evocated case of the tetra-functional thiol, the yield corresponds to $[(32 - 27.7) / 32] \times 100 = 13\%$. This means that 87 % of thiol remains in the miniemulsion, and the rest 13 % were consumed, polymerized.

Following this example, all the polymerization conversions that will be mentioned will be calculated by using this protocol and by referring to the thiol, -SH, group consumption.

2. Miniemulsions with tetra-functional thiol and bi-functional alkene

A tetra-functional thiol, pentaerythritol tetrakis(3-mercaptopropionate) (PETMP), was combined with a bi-functional alkene, diallyl phthalate (DAP), to form a polymeric network. This network can be formed due to the multiple functional groups of thiols as well as the alkenes. A standard miniemulsion was prepared as can be seen in Table 2. The continuous phase was 80 wt% of the total volume and the rest 20 wt% was the dispersed phase, where the Ostwald ripening inhibitor, radical inhibitor and photoinitiator were added to the mixture along with the two monomers. In general, two different procedures of producing the coarse emulsion were established as they were described in the previous chapter, and in this

chapter the experimental results will be analyzed to evaluate which method is more suitable to work with. Also, the influence of the design of mixing element, the number of cycles as well as the chemical parameters will be reviewed.

Table 3.1. Miniemulsion formulation with pentaerythritol tetrakis(3-mercaptopropionate) (PETMP)- diallyl phthalate (DAP) “/Cmonomer “stands for “regarding to the monomers concentrations”.

Continuous Phase	Dispersed Phase
Deionized Water 80 wt%	Monomers <u>Thiol</u> : pentaerythritol tetrakis(3-mercaptopropionate) (PETMP) 5.52 wt% <u>Alkene</u> : Diallyl phthalate (DAP) 14.48 wt%
Surfactant Sodium Dodecyl Sulfate (SDS) 3.5 wt% / C _{monomers}	Photoinitiator Diphenyl (2,4,6-trimethylbenzoyl) phosphine oxide (DTPO) 2 wt% / C _{monomers}
	Ostwald Ripening Inhibitor Hexadecane (HD) 4 wt% / C _{monomers}
	Radical Inhibitor 2,5-Di-tert-butyl hydroquinone (DBHQ) 1.05 wt% / C _{monomers}

2.1 Pneumatic Elongational-Flow Reactor and Mixer: Effect of Process Parameters and Surrounding Atmosphere

Experiments have been done using the pneumatic elongational-flow reactor and mixer (pRMX) in order to assess the impact of the process parameters as well as the atmosphere, under which the experiments were performed, on the droplet size and polydispersity. The process parameters that could be altered were the number of cycles and the static mixing element design.

As described in the literature, the flow rate was another important process parameter that leads to a decrease of the droplet diameter by its increase [5]. However, in the case of pRMX, the flow rate could not be directly monitored because it strongly depended on:

- The pressure of the compressed air that is moving the pistons. When this pressure was decreasing, the pistons were not able to move because the energy provided to them was not enough since the viscosity of the miniemulsion was quite

high. This meant that during all experiments the pressure had to be fixed at $p = 6$ bar.

- The number of holes on the mixing element. It can indeed be expected that the flow rate can increase by decreasing the number of holes, meaning that less friction and resistance to the flow apply when the number of holes is less.

Finally, the atmosphere under which the coarse emulsion was prepared will be evaluated. It is already explained that oxygen is a key factor when it comes in contact with the thiol, since it can initiate the polymerization [24].

2.1.1 Four-Holes Static Mixing Element and Ambient Atmosphere

First experiments were conducted using the pneumatic elongational-flow reactor and mixer (pRMX) which was equipped with a four-hole static mixing element that can be seen in Figure 3.5.

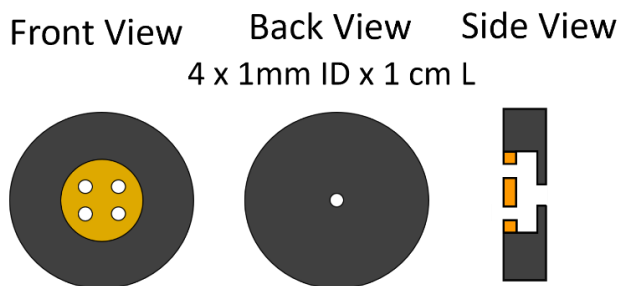


Figure 3.5. Front, back and side view of the four-holes static mixing element.

The coarse emulsion was prepared under ambient atmosphere while mixing the compounds (Table 2) using magnetic stirrer for 5 min. This way it was ensured that the composition of the solution entered the device was constant and homogeneous. The flow rate when this mixing element was used, was approximately $q = 1400$ mL/min. The effect of the number of cycles was investigated, ranging from 100 to 400 (Figure 74).

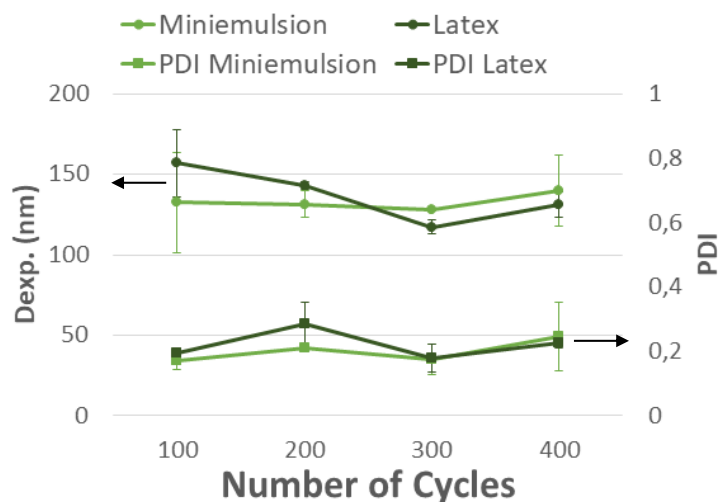


Figure 3.6. Effect of number of cycles on the droplet diameter (Dexp) and polydispersity (PDI) with pneumatic elongational-flow reactor and mixer (pRMX) (coarse emulsion under ambient atmosphere, 4-holes static mixing element).

As it can be seen in Figure 3.6 (light green curves), the average droplet diameter was found to be 132 nm after 100 cycles, while the average droplet diameter decreased down to 127 nm by increasing the number of cycles up to 300. This can indicate that the more time the droplets experience the elongation the more the droplet rupture occurred, and smaller droplets can be generated after each increase of number of cycles. The same behavior was also reported in the literature [16]. Surprisingly, the droplet diameter along with the polydispersity of the miniemulsion increase after 300 cycles. This could happen due to increased coalescence between the droplets, that may be explained by the “over-processing” of the miniemulsions. Indeed, since the emulsification time was longer, the temperature rise close to the mixing element was higher than after a smaller number of cycles. It is worth mentioning that tap water was used to cool down the walls of the pRMX, in order to achieve better control of the temperature. Unfortunately, the energy provided to the system during mixing combined with the high reactivity of the two monomers did not allow the further decrease of the diameter.

The photopolymerization was then conducted using the linear photoreactor that was described in the previous chapter (Chapter II, part C1). For low number of cycles, it is observed that the particles had bigger diameter than the droplets (Figure 3.6 – dark green curves). Previously our group [7] discovered that a

potential diffusion of monomer (methyl methacrylate, MMA) through the water phase from the smaller droplets to the bigger ones can occur with the same UV photoreactor [25]. This could also be the explanation in the thiol-ene chemistry case, since both thiol and alkene are slightly soluble in water, so this diffusion can actually take place and increase the particle size. This phenomenon gave rise to the polydispersity of the latex and in some cases the PDI was close to 0.3.

Table 3.2 shows the polymerization yields for each experiment after miniemulsification, before and after photopolymerization. The polymerization reached more than 60% conversion before photopolymerization and, in some cases the miniemulsion was already fully polymerized after the miniemulsification with pRMX. Finally, the ^1H NMR spectra disclose the complete consumption of both monomers, thiol and alkene, after their exposure to UV light.

Table 3.2. ^1H NMR polymerization conversion after miniemulsification with pneumatic elongational-flow reactor and mixer (pRMX) (coarse emulsion under ambient atmosphere).

	Number of Cycles	100	200	300	400
Before Photopolymerization	thiol conversion (%)	63	99	97	97
	alkene conversion (%)	78	91	91	86
After Photopolymerization*	thiol conversion (%)	100	100	100	100
	alkene conversion (%)	100	100	100	100

* All the latexes were 100% polymerized but cross-links led to an overlapping broad peak.

During all these experiments several problems were encountered. One of the major issues was the clogging of the static mixing element of the pRMX. This meant that polymer, agglomerated particles, were stuck together in the mixing element and the pistons were not able to move anymore. The point where this problem was observed was the empty space between the four holes that combine and led to a single hole (Figure 3.7, red circle). This part was serving as a reservoir in every experiment, so the emulsion was gathered at the “dead volume” parts of the mixing element, where the emulsion stream to be mixed could not penetrate and caused the temperature increase close to the mixing element and start the polymerization.



Figure 3.7. Side view of the four-holes static mixing element, red circle indicates the space of the “dead volume”.

Along with clogging, leakage on the back of the pistons was also observed in almost each experiment. This indicated that the PTFE shields, that were used to ensure that the solution remained in between the pistons and did not flow outside from the device, were not tight enough and allowed the emulsion to exit the device from the space between the piston and the chamber. To solve those problems and at the same time to clean the polymeric particles, the device needed to be disassembled and each part to be removed, thoroughly cleaned and placed again back in the correct position. Once the different pieces such as, pistons, chambers, and static mixing element were arranged back, several tests with only water needed to be done to ensure that there is no leakage in any part of the device. If again leakage was found the device needed to be tightened more. All these cleaning steps took from 1 day up to 1 month in order for the device to be fixed and be able to work again. Several times leakage was inspected also in the mixing element, since it is a separate piece and very accurate movements need to be done, it can very often be misplaced even though it was not noticeable by naked eye but only by testing.

After confronting clogging and dripping during every experiment, and by evaluating the obtained results, decision was made to design a new static mixing element, which was composed of a single hole across its width. In this way, less or zero polymerization due to the temperature increase was expected. At the same time, concern was rising regarding to the atmospheric oxygen that was surrounding the coarse emulsion. This was confirmed by ^1H NMR, where the spectra showed that the coarse emulsion prepared under ambient atmosphere was already polymerized right after mixing with the magnetic stirrer for 5 min. The polymerization yield was above 70% before even starting the emulsification (Table 3)! This let us decide to remove oxygen and replace it by nitrogen. The results will be discussed in the following section.

2.1.2 One-Hole Static Mixing Element and Inert Atmosphere

First, the previous experiments showed that the oxygen of the surrounding atmosphere, while preparing the coarse emulsion, was enough to catalyze the reaction of thiol with alkene and start the polymerization that reached up to 70% yield. Thus, nitrogen was injected in the solution to replace all the oxygen and prevent polymerization. The ^1H NMR spectra in Figure 3.8 revealed that the preparation of coarse emulsion under inert atmosphere was the best way to avoid polymerization in this step since it was completely diminished, down to zero.

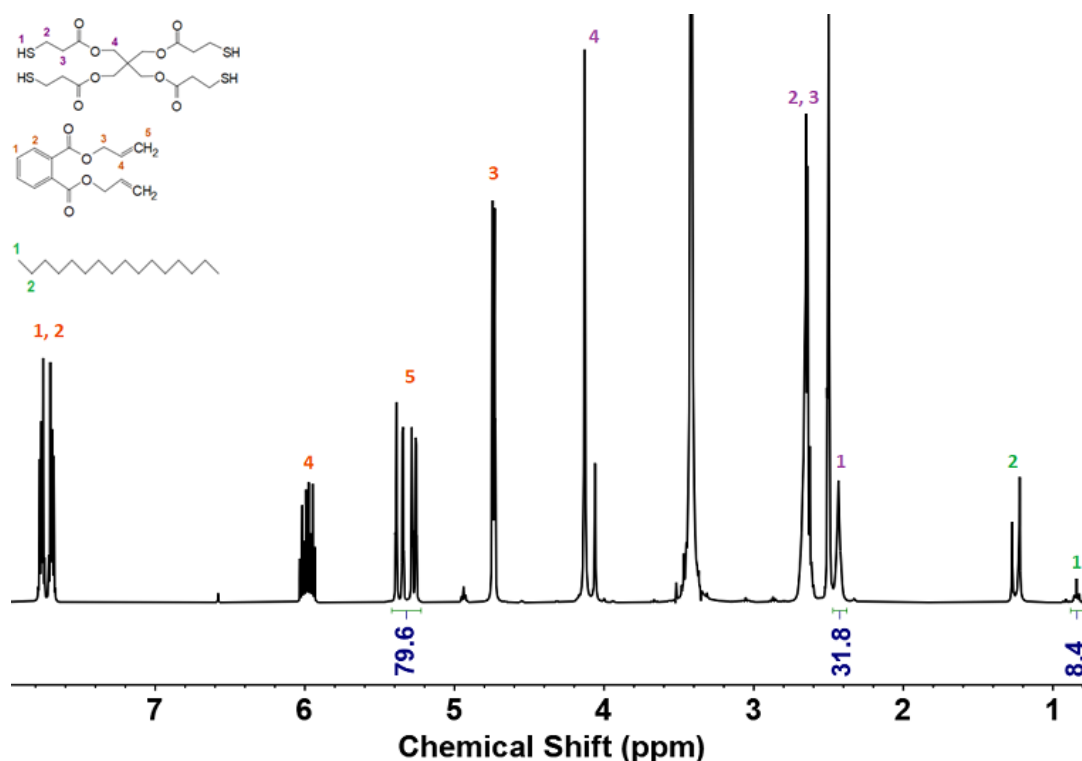


Figure 3.8. ^1H NMR spectrum of the coarse emulsion under inert atmosphere.

Moreover, since the four-hole static mixing element gave rise to polymerization during emulsification, a new design of mixing element was produced with a single hole and no dead volumes in between (Figure 3.9). Since this mixing element had only one hole, the flow rate was ($q = 4200$ mL/min) much higher than the previous one (1400 mL/min).

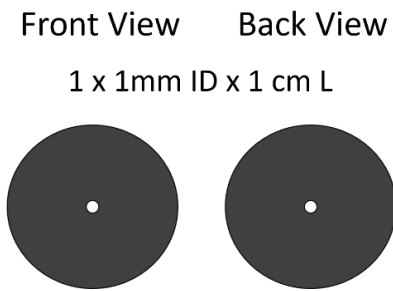


Figure 3.9. Front and back view of the one-hole static mixing element.

Another concern was that the number of cycles: 100 cycles were maybe already too much for the PETMP-DAP miniemulsion to undergo a high yield of polymerization as well as agglomeration. This premature polymerization was not desired during emulsification. Consequently, for this set of experiments, a smaller number of cycles ranging from 5 to 100, were performed (Figure 3.10) and the polymerization conversion was evaluated by ^1H NMR spectroscopy (Table 3.3).

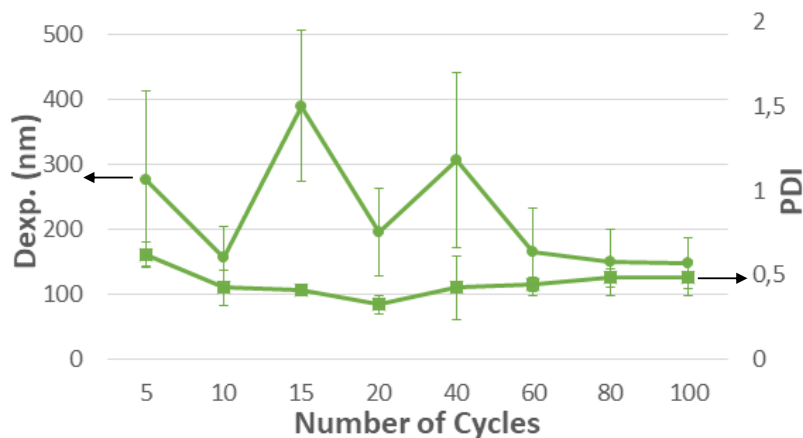


Figure 3.10. Effect of number of cycles on the droplet diameter (Dexp) and polydispersity (PDI) with pneumatic elongational-flow reactor and mixer (pRMX) (coarse emulsion under inert atmosphere, 1-hole static mixing element).

In figure 3.10, the droplets' size experienced many fluctuations and a PDI above 0.3 below 40 cycles. This behavior was probably due to the high reactivity of the two monomers since the polymerization reached up to 60% (Table 3.3) and the system did not reach a steady state. After increasing the number of cycles, the droplet diameter decreased down to 140 nm when the cycles were at maximum 100. However, the polydispersity index as well as the polymerization yield increased by the longer emulsification time. The high polydispersity indicates that

the miniemulsions had not a single droplet diameter, which can dictate that the emulsification time was not enough to achieve monomodal size distribution.

Nevertheless, the polymerization conversion was already high before even conducting photopolymerization, which was a restrictive factor to proceed in a higher number of cycles.

Table 3.3. Polymerization conversion after pentaerythritol tetrakis(3-mercaptopropionate) (PETMP)- diallyl phthalate (DAP) miniemulsification with pneumatic elongational-flow reactor and mixer (pRMX) obtained by ^1H NMR.

Number of Cycles	5	10	15	20	40	60	80	100
Thiol Conversion (%)	44	44	37	30	61	27	18	50
Alkene Conversion (%)	45	59	49	39	74	48	49	70

A very important observation was made at this point, that the clogging of the device was not so often as compared with the previous mixing element, but still happened. Referring to the dripping problem, it was still arising, and the tightening of the piston shields was often mandatory.

Worth mentioning is that in this set of experiments no UV polymerization occurred since focus was give on improving first the miniemulsification's procedure. This included (i) the coarse emulsion preparation along with (ii) the geometry change of the mixing element and (iii) the decrease of number of cycles. As expected, the polymerization yield was lower than with the previous conditions but still in most of the experiments exceeded the 40%. Sadly, this was a limitation to the proper evaluation of the droplet diameter and polydispersity. For this reason, the chemical parameters were examined in the following part, in order to observe any variation on the droplet size.

2.2 Pneumatic Elongational-Flow Reactor and Mixer: Effect of Chemical Parameters

The composition of the emulsion was altered so as to estimate the droplet size and polydispersity. The parameters that changed were the amount of surfactant, the addition and absence of radical inhibitor. This set of experiments were conducted

before changing the static mixing element design, which was the four-holes mixing element together with ambient atmosphere.

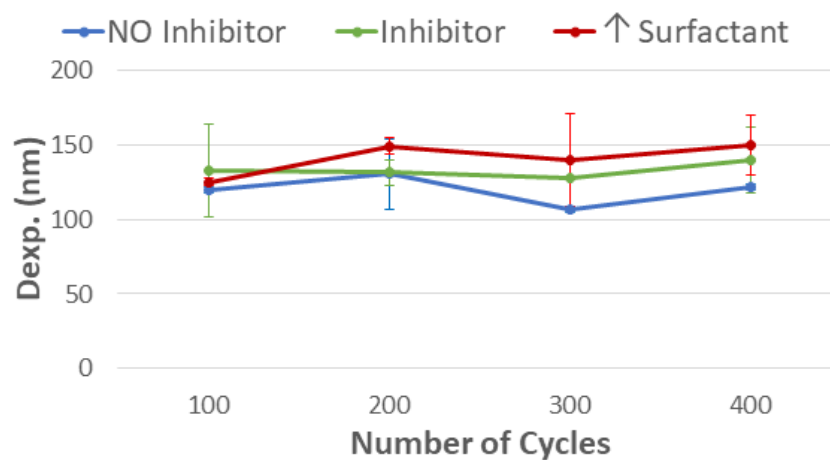


Figure 3.11. Effect of number of cycles and chemical parameters on the droplet diameter with pneumatic elongational-flow reactor and mixer (pRMX) (coarse emulsion under ambient atmosphere, 4-holes static mixing element).

In Figure 3.11, the green line corresponds to the standard miniemulsion that was described in detail in part 2 (Table 3.3). The blue line represents experiments that were done without the use of radical inhibitor. As it is shown in the graph, the diameter undergoes several fluctuations and there is not a specific trend observed. In the majority of the experiments the PDI was below 0.2, which indicates that the miniemulsion had a single droplet size and can be referred as monomodal [26]–[28]. However, an almost complete polymerization occurred during emulsification (yield = 98 %, Table 3.4), which can explain the ups and downs of the droplet diameter. There are two major explanations for this behavior. Starting with the very rapid reaction of thiol with alkene, that was already initiated from the atmospheric oxygen. The polymerization was enhanced by the heat rise during emulsification, which meant that the Brownian motion in the emulsion was high enough for the droplet's coalescence.

Table 3.4. ¹H NMR polymerization conversion after miniemulsification of pentaerythritol tetrakis(3-mercaptopropionate) (PETMP) - diallyl phthalate (DAP) with pneumatic elongational-flow reactor and mixer (pRMX), no radical inhibitor.

Number of Cycles	100	200	300	400
Thiol Conversion (%)	98	98	97	97
Alkene Conversion (%)	97	99	98	99

Appraising these results, allows us to make to conclusion that the radical inhibitor is mandatory for this process, since the polymerization was a bit lower when the radical inhibitor was present.

Another set of experiments was performed using a bigger amount of surfactant (Figure 3.11, red line). Instead of the standard concentration, 3.5 wt%/C_{monomer} *i.e.* 35 mmol/L, the amount was increased up to 5 wt%/C_{monomer} (50 mmol/L), both values were above the critical micelle concentration (CMC) of SDS, which is equal to 8 mmol/L. Generally, according to the literature [26]–[28], a decrease of the droplet diameter is observed when the amount of surfactant is increased. This is due to the parallel decrease of the surface tension, which strongly depends on the capillary number which becomes higher; thus the droplet size is expected to be smaller.

In our study, the droplet diameter first decreased, from 133 nm for the standard miniemulsion to 125 nm with higher surfactant amount, as expected from the theory. In the contrary, a further increase of the number of cycles led to an increase on the droplet diameter, up to 150 nm. As mentioned from different research groups [29], [30], when the amount of surfactant used is not enough to cover and stabilize the oil droplets, they tend to coalesce thus the droplet size increases. This lack of surfactant, even though the amount is higher than the CMC, probably gave rise to the coalescence of the droplets, along with the droplet diameter. Another explanation for this coalescence may stand in the increase of the temperature during emulsification which could lead to the destabilization of the miniemulsion. Even though the droplets were bigger, the polydispersity index did not exceed 0.2, which meant that the miniemulsion was monomodal.

Finally, the polymerization yield (Table 3.5) was close to 80%, which is still very high but less as compared with the previous results (Table 3.4). This could potentially be explained by the increased amount of surfactant that was able to provide better stability against coalescence to the system.

Table 3.5. ^1H NMR polymerization conversion after miniemulsification of pentaerythritol tetrakis(3-mercaptopropionate) (PETMP)- diallyl phthalate (DAP) with pneumatic elongational-flow reactor and mixer (pRMX), $[\text{SDS}] = 5 \text{ wt\%/}C_{\text{monomer}}$.

Number of Cycles	100	200	300	400
Thiol Conversion (%)	88	71	75	70
Alkene Conversion (%)	76	58	74	66

After miniemulsification using pRMX, each experiment was placed under UV, using the linear continuous photoreactor as described in chapter II. The wavelength was fixed at $\lambda = 365 \text{ nm}$ and the residence time at $\tau = 7 \text{ min}$. Another important reminder is that once the miniemulsion was obtained, directly the polymerization begun so as to reassure that the miniemulsion did not have time to potentially destabilize through time.

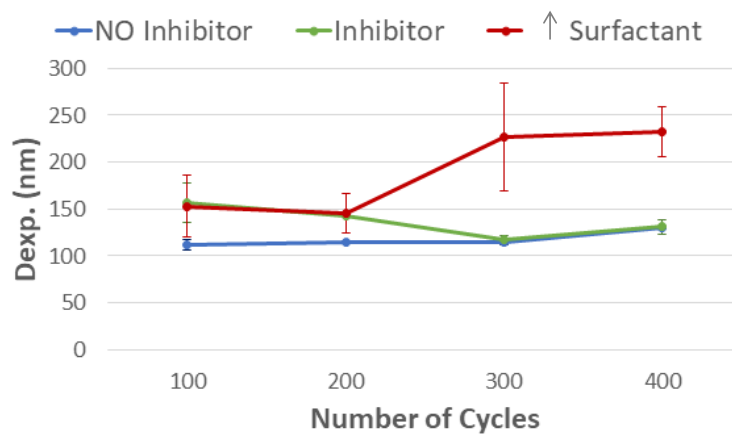


Figure 3.12. Effect of number of cycles and chemical parameters on the latex particle diameter after emulsification with pneumatic elongational-flow reactor and mixer (pRMX) (coarse emulsion under ambient atmosphere, 4-holes static mixing element) and photopolymerization UV at 365 nm.

In Figure 3.12, most of the experiments showed a particle diameter that was approximately identical with the droplet diameter. When higher amount of surfactant was used, an increase of the particle's diameter was observed for 300 and 400 number of cycles. This particle diameter increase was approximately 90 nm higher than the produced droplets. As reported in chapter II, W. Yu *et al.* [16], attributed this behavior to the slight solubility of the two monomers in the water, that allows their diffusion through the continuous phase from the smaller to the bigger droplets during photopolymerization. The difference of the chemical potential between the droplets is the driving force for this mechanism. As described

previously, this can lead to an increased polydispersity of the latex, where in some cases the PDI was close to 0.3.

Regardless the droplet size and polydispersity, the ^1H NMR spectra disclose the complete consumption of both monomers, thiol and alkene, after their exposure to UV light. It can also be observed that for low number of cycles and in absence of inhibitor, latex particles size was smaller than in the presence.

Unluckily, the clogging problems of the pRMX were continuously arising during most of the experiments and most of the time it was long with the leakage on the back of the pistons. This was now followed by frequent clogging of the photoreactor, which happened due to the stacking of particles on the walls of the PTFE tube, which caused the diameter of the tube to block and the miniemulsion could not flow further. That meant that the PTFE tubing needed to be changed and to be replaced by a new one and start the whole procedure from the beginning. Considering all the presented results and difficulties, it was found very useful for this research to assess the stability of the standard miniemulsion, whose composition can be seen in Table 3.3, and to compare it with the emulsion where no inhibitor was used.

2.3 System Stability

It was important to know the stability of the miniemulsions and to evaluate the time the system could stay unchanged. For this purpose, miniemulsions were produced and several samples through time were taken and analyzed by DLS. The main goal was to observe any changes of the diameter of the droplets and the polydispersity index. Two different miniemulsions were studied, one prepared under the standard conditions (Table 3.1) and a second one prepared without using any radical inhibitor. These two miniemulsions were manipulated under ambient atmosphere and by using pRMX device equipped with the four-holes static mixing element, for 200 number of cycles. This number of cycles was chosen since the produced emulsions showed the maximum reproducibility (small error bar, Figure 3.6) among the rest of the experiments. It is worth mentioning that these

emulsions were already described and analyzed in the previous chapter for their droplet sizes, polydispersity, and premature polymerization during emulsification.

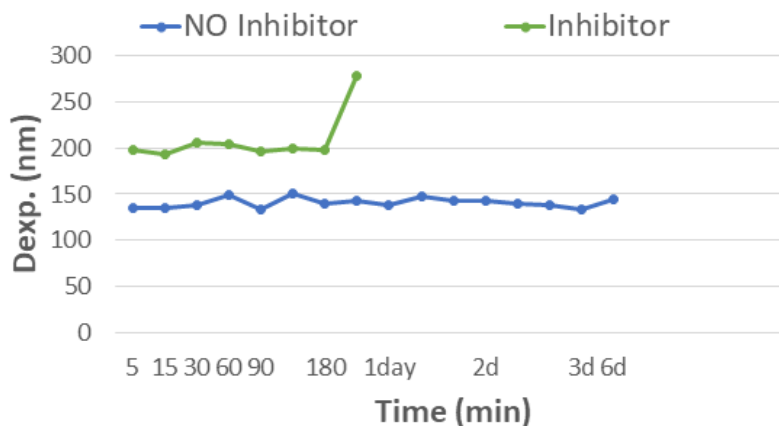


Figure 3.13. Miniemulsions stability by investigating the evolution of the droplets' diameter after emulsification with pneumatic elongational-flow reactor and mixer (pRMX) (coarse emulsion under ambient atmosphere, 4-holes static mixing element, 200 cycles), blue line) no radical inhibitor was used, polymerization yield = 99%, green line) addition of radical inhibitor, polymerization yield = 90%.

The droplets' diameter was studied for 6 days, while during the first 24 hours the measurements were very frequent as compared to the next days. The frequency of the measurements was more crucial the first 24 h since it was more luckily that the miniemulsion will be destabilized, because of the high reactivity of the thiol and the alkene as well as the heat rise during emulsification.

As it can be seen in Figure 3.13, the miniemulsion without the radical inhibitor was stable during the 6 days of continuous characterization. This can be explained by the fact that this miniemulsion was already polymerized, up to 99% conversion (Table 3.4), due to the heat along with oxygen during emulsification. The latex that was formed remained stable through time with very minor fluctuations on the polydispersity, while remaining below 0.2.

On the other hand, the miniemulsion prepared with the addition of radical inhibitor was stable for the first day, but then a huge increase of almost 100 nm on the droplet size was observed. The droplet diameter reached 280 nm, while the polydispersity increased more than 0.3. This could be a strong indication that the miniemulsion was destabilized and led to the agglomeration of the droplets to form bigger and more disperse emulsion. In addition, this miniemulsion was found to be 90% polymerized, meaning that this played a very crucial role on the destabilization, since 10% of the monomers were still unreacted. These remained

monomers could be already initiated but once the heat during emulsification faded the polymerization needed more time to occur, thus the increase of the droplet size after 24 h.

It can be concluded that the miniemulsion could be stable for less than 24 h, as evaluated by DLS. Unfortunately, premature polymerization could not be controlled in this step, and this was a catalytic factor for the miniemulsion destabilization.

2.4 Rotor-Stator Mixer

Comparison was made between pRMX and rotor-stator mixer, both methods were evaluated in terms of droplet size and distribution. The rotor-stator mixer was used for 10 min at different rotational speed, ranging from 6500 rpm to 24000 rpm, to emulsify the thiol-ene miniemulsion without the use of radical inhibitor and under ambient atmosphere. The choice of not adding the radical inhibitor was done in order to estimate the polymerization conversion during emulsification and compare with the same results obtained using pRMX. Right after emulsification the miniemulsions were placed in the linear UV photoreactor to photopolymerize. Results are presented in Figure 3.14.

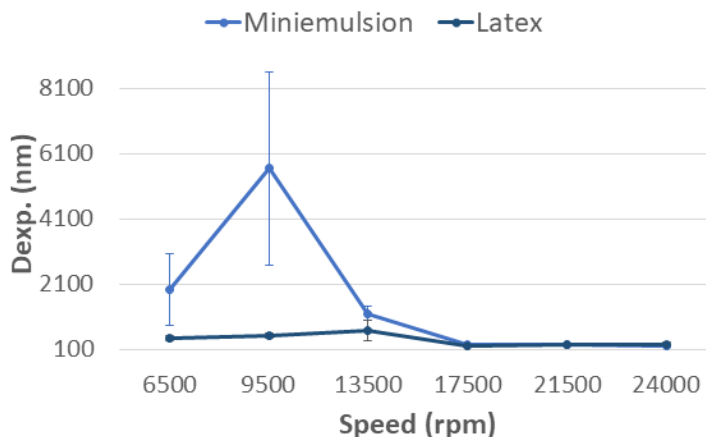


Figure 3.14. Effect of rotational speed on the droplet and particle diameter.

Starting with the results of the miniemulsion (light blue curve), before 9500 rpm, the droplet size was above 2 μm with very broad error bar. These two results must be taken with caution because these droplet sizes were much bigger than the measurement size range given for the DLS device used (20 - 900 nm). An explanation for these very big droplet diameters can be that the device when

operated in low speeds was not able to provide enough shear to the droplets to rupture. And this can be confirmed by the following experiments when the speed increased further at 17500 rpm the droplet diameter significantly dropped down to 230 nm and the PDI followed this trend a bit below than 0.2. As it can be seen in Figure 3.14, a further increase of the rotational speed did not provide any further significant decrease on the droplet while the PDI was increased a bit above 0.2 for 24000 rpm. This could be the beginning of the “over-processing” of the miniemulsion, since the energy given to the system was quite high, the temperature of the miniemulsion was increased even though an ice bath was used. This could lead to the coalescence of the droplets, thus the increased polydispersity.

Taking a look on the table with the ^1H NMR conversions (Table 3.6), it became clear that the higher the rotational speed the more polymerization during emulsification occurred. This was expected due to the temperature increase during emulsification which led to the beginning of the polymerization, even more than 90% yield. The increased yield was also due to the increased reactivity between the two monomers that got enhanced when the heat during emulsification started to increase.

Table 3.6. ^1H NMR polymerization conversion after miniemulsifications of pentaerythritol tetrakis(3-mercaptopropionate) (PETMP)- diallyl phthalate (DAP) with rotor-stator mixer.

Rotational Speed (RPM)	6500	9500	13500	17500	21500	24000
Thiol Conversion (%)	41	0	69	98	99	87
Alkene Conversion (%)	31	27	70	92	95	84

Regarding the photopolymerization, the yield was always equal to 100% indicating that the monomers were fully consumed. In Figure 3.14, the latex particles had identical sizes with the droplets apart from the particles that were produced using the minimum rotational speed. For the later particles, the diameter returned from the DLS measurements were way above the size measurement range of the device. For this reason, these values are not considered accurate.

Comparing the aforementioned results with the one obtained with the pRMX (Figure 3.6), it can be seen that miniemulsion produced using the latter had better

characteristics (Table 3.7): the miniemulsion produced with the pRMX had smaller droplet size, approximately 120 nm, while the miniemulsion produced with the shear mixer had 270 nm droplet diameter. As for the polydispersity in pRMX experiments, under the same conditions with the rotor-stator mixer, was monomodal, contrary with the Ultra-Turrax that the PDI was in most of the cases above 0.2.

Table 3.7. Lowest droplet size and polydispersity index obtained with two devices to produce pentaerythritol tetrakis(3-mercaptopropionate) (PETMP)- diallyl phthalate (DAP) miniemulsions and latexes.

Device	Lowest Droplets' Size (nm)	Lowest Droplets' PDI (nm)	Lowest Latex Particles' Size (nm)	Lowest Latex PDI (nm)
pRMX	107	0.12	112	0.17
Rotor-stator mixer	229	0.17	229	0.14

As it has been described previously from our group [13], comparison between these two devices, using methyl methacrylate, showed the same trend, that the miniemulsion prepared with pRMX was smaller in size and monodisperse as compared with the shear mixer [18].

3. Bi-Functional Thiol and Bi-Functional Alkene

Different types of thiols were examined during this research, which had different number of functional groups and molecular weights. When the tetra-functional thiol was used, it was expected that cross links will be formed between the thiol and the bifunctional alkene, while using a bi-functional thiol can form linear polymeric chains [34]. The main purpose was to compare the different chemistries in terms of droplet and particle size, polydispersity, as well as stability through time.

3.1 1,2-Ethanedithiol (EDT) and Diallyl phthalate (DAP)

The first experiments were conducted using 1,2-ethanedithiol (EDT) combined with diallyl phthalate (DAP) (Figure 3.15).

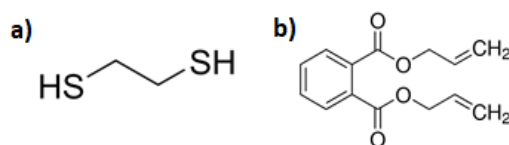


Figure 3.15. Topologic representation of a) 1,2-ethanedithiol and b) diallyl phthalate.

In this part, three different devices were used to prepare the miniemulsion: micro elongational-flow reactor and mixer (μ RMX), pneumatic elongational-flow reactor and mixer (pRMX) and rotor-stator mixer. Comparison was done between the three devices to evaluate the different processes along with the droplet and particle sizes. The photopolymerization took place right after emulsification, where the miniemulsion was flowing in the continuous linear photoreactor that was described previously.

The miniemulsion that was produced had the same formulation (Table 3.8) and consistency for all the devices:

- First the radical inhibitor was added in a vial, along with the Oswald ripening inhibitor and the two monomers, thiol and alkene.
- Then the water phase was prepared mixing distilled water, surfactant, and the water-soluble photoinitiator.
- Finally, the two phases were mixed with a magnetic stirrer for 5 min under ambient atmosphere and introduced in the different devices.

Table 3.8. Miniemulsion formulation with 1,2-ethanedithiol (EDT) - diallyl phthalate (DAP). "/C_{monomer}" stands for "regarding to the monomers concentrations".

Continuous Phase	Dispersed Phase
<p>Deionized Water 80 wt%</p>	<p>Monomers <u>Thiol</u>: pentaerythritol tetrakis(3-mercaptopropionate) (PETMP) 5.52 wt% <u>Alkene</u>: Diallyl phthalate (DAP) 14.48 wt%</p>
<p>Surfactant Sodium Dodecyl Sulfate (SDS) 3.5 wt% / C_{monomer}</p>	<p>Ostwald Ripening Inhibitor Hexadecane (HD) 4 wt% / C_{monomer}</p>
<p>Photoinitiator Lithium Phenyl (2,4,6- trimethylbenzoyl) phosphinate (LAP, 98%) 2 wt% / C_{monomer}</p>	<p>Radical Inhibitor 2,5-Di-tert-butyl hydroquinone (DBHQ) 1.05 wt% / C_{monomer}</p>

A very important and limiting factor to work with this thiol was the high volatility of the EDT, due to the very low molecular weight. This was a catalytic factor since the ventilation was not enough to limit the smell of the toxic thiol. For this reason, only few experiments were conducted using this thiol. It can be seen in the graphs that will be presented that there are no error bars, this is because only one experiment for each parameter and device was conducted.

3.1.1 Micro Elongational-Flow Reactor and Mixer (μ RMX)

The research started with the use of the micro elongational-flow reactor and mixer (μ RMX). The micromixer that was used for the experiments had bore size equal to 150 μm , while the flow rate was constant at 30 mL/min. Keeping the same restriction and flow rate, the influence of the number of cycles on the droplet and particle diameter and polydispersity was investigated (Figure 3.16). In comparison with pRMX the flow rate was drastically reduced since the restriction in μ RMX was much smaller ($d_{\text{hole, pRMX}} = 1 \text{ mm}$, $d_{\text{hole, } \mu\text{RMX}} = 150 \mu\text{m}$), which results in higher pressure that exceeded the syringe pump capability.

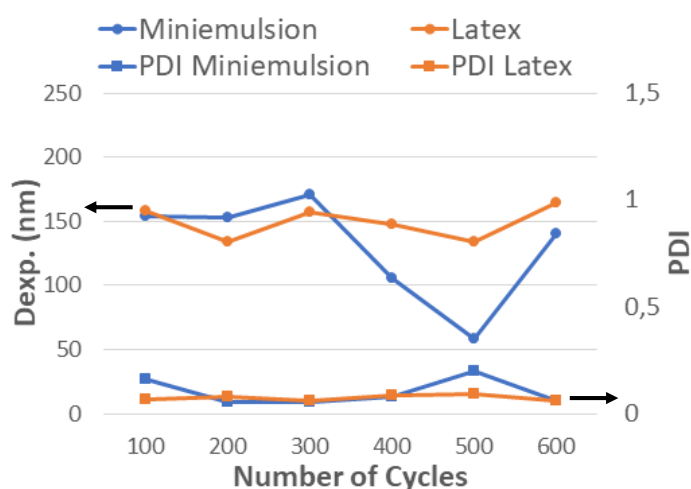


Figure 3.16. Effect of number of cycles of the micro elongational-flow reactor and mixer (μ RMX) (150 μm , 30 mL/min) on the droplet and particle diameter (Dexp) and polydispersity (PDI).

As expected, when the number of cycles increased from 100 to 500, the droplet size decreased from 160 nm down to 60 nm. The small increase on the diameter after 300 cycles could be an experimental error since the experiments were only conducted once. Then, after 600 cycles, a strong increase was observed on the droplet diameter, up to 140 nm. Possibly, this was the limitation of the specific chemical system, that led to the “over-processing” of the miniemulsion thus the beginning of the coalescence of the droplets. However, this possible explanation has to be taken with care, given that it was not possible to replicate the experiments due to the aforementioned problem indicated by the high volatility of EDT.

Following the emulsification, photopolymerization was conducted at $\lambda = 365 \text{ nm}$ and the results for the latex can be seen in Figure 3.16 “latex”. In low number of

cycles, the latex seemed to show a bit smaller diameter than the miniemulsion. As mentioned before, the experiments were performed only one time due to the strong limitation of the smell of this thiol. This could potentially explain this small variation on the diameters before and after polymerization, due to the lack of more experimental values in order to have an average diameter. However, it has been reported that when a water-soluble initiator was used, the polymerization mechanism occurred differently. According to this research [32], the water-soluble initiator will enhance the formation of oligomers in the aqueous phase, and they grow through mass transfer from the non-nucleated monomer droplets that behave as a reservoir. This is the same mechanism with the emulsion polymerization. This mechanism leads to a smaller particle size as compared with the droplets (Figure 3.17).

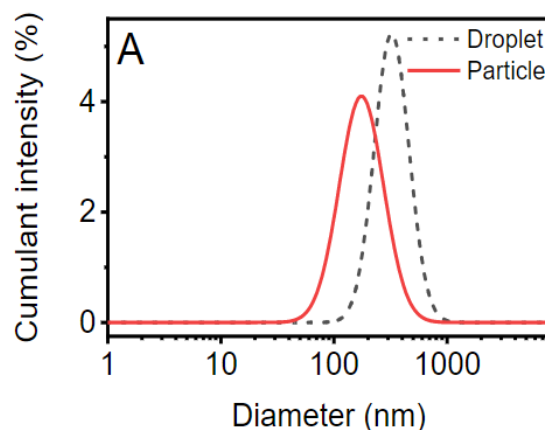


Figure 3.17. Size distributions in a 2,2'-(ethylenedioxy)diethanethiol (EDDT)- diallyl phthalate (DAP) miniemulsion photopolymerization using water soluble photoinitiator [32].

On the contrary, in higher number of cycles the latex revealed bigger diameter than the miniemulsion. A potential explanation here could be the slight solubility of the two monomers into the water, where the monomer diffuses through the continuous phase, from the smaller droplets to the bigger. This diffusion happens due to the difference in chemical potential as it is already described in the previous chapters. Some important remarks were that the polydispersity for both miniemulsion and latex was below 0.2, which meant that the solutions were monomodal. However, due to the very strong odor of the thiol, NMR spectroscopy could not be conducted, which means that the polymerization conversion during emulsification and after photopolymerization was unknown.

Despite the restrictions due to smell, it can clearly be observed a decreasing trend on the droplet diameter by the increase of the number of cycles. This was also observed by researchers that used the same device [16] and can be attributed to the elongational strain rate that is responsible for the droplet rupture as described in chapter II.

3.1.2 Pneumatic Elongational-Flow Reactor and Mixer (pRMX)

The pneumatic elongational-flow reactor and mixer (pRMX) was used in order to produce miniemulsion that would then flow under UV in the continuous photoreactor to obtain the latex. The pRMX was equipped with the four-holes static mixing element (Figure 3.5) and experiments were conducted under ambient atmosphere.

In Figure 3.18 one can see the diameter and polydispersity of the systems.

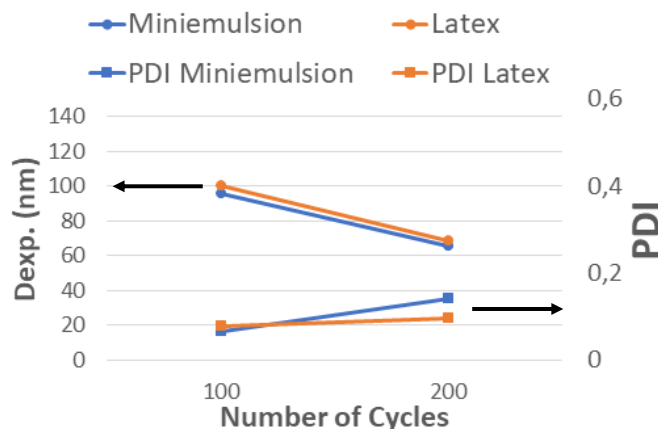


Figure 3.18. Effect of number of cycles of the pneumatic elongational-flow reactor and mixer (pRMX) (ambient atmosphere, 4-holes static mixing element) on the droplet and particle diameter (Dexp) and polydispersity (PDI).

The miniemulsions exhibited a strong decrease (from 97 nm to 68 nm) when the number of cycles increased from 100 to 200. The same decrease was followed by the latex particles, with values that were approximately the same as the droplets. Regarding the polydispersity all the experiments showed a unique diameter, which was concluded by the PDI value that was below 0.2.

Finally, during these experiments the device was clogged again, this time not only in the mixing element but also in the entrance of the PTFE tubing. Also, it was unfortunate that pRMX device was very big and could not be placed under the fume hood in the lab. This limited the research to only few results since the strong smell of thiol could not be extracted and eliminated.

3.1.3 Rotor-Stator Mixer

A rotor-stator mixer was finally used to produce EDT-DAP miniemulsions and to compare the results with the two aforementioned elongational-flow-based devices. In Figure 3.19, all the different device's rotational speeds along with the diameters and polydispersity of the systems are presented.

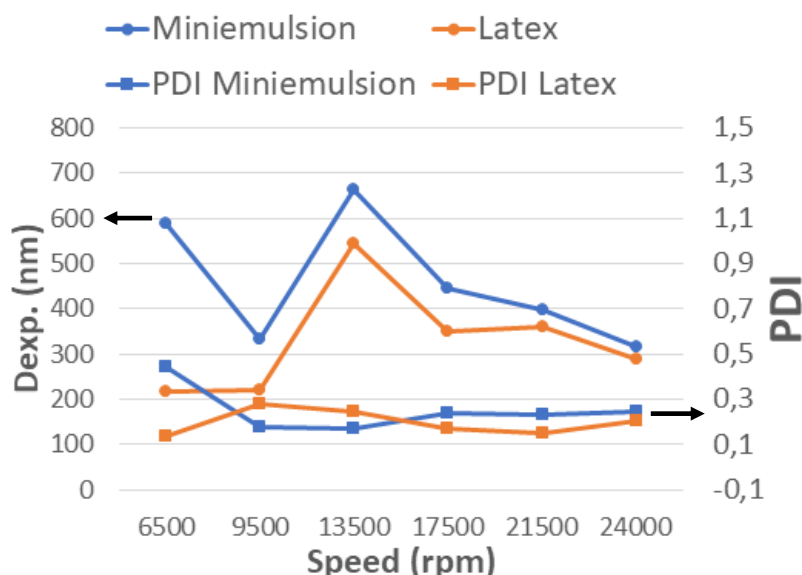


Figure 3.19. Effect of rotational speed on the droplet and particle diameter and polydispersity.

In low rotational speed, below 13,500 rpm, large fluctuations of droplet and latex particles' size were observed. This could be due to the polymerization that could occur since the heat during emulsification was increased. Another factor that could start the polymerization of thiol with the alkene was the oxygen of the atmosphere, which is impossible to avoid when using rotor-stator mixers.

A further increase of the rotational speed up to 24,000 rpm led to the decrease of the droplet diameter from 662 nm down to 317 nm and to the decrease of polydispersity index from 0.4 to below 0.2.

Comparing the results of the three emulsification devices (Table 3.9), one can estimate that the pRMX was the device that produced the smallest and monodisperse droplets and particles, followed by the μ RMX and finally the rotor-stator mixer. These variations can be explained by the fact that the flow rate that is applied to the system using pRMX, $q = 1400$ mL/min, is at least 47 times stronger than the one of μ RMX ($q = 30$ mL/min). This displays that the higher the flow rate, the smaller the diameter of the droplets and particles, which comes in an agreement with a previous work done by our group [16]. Finally, Ultra-Turrax was the least effective device to produce monomodal and small droplets and latex, as compared with the elongational-flow-based devices, as expected by the Taylor theory [19].

Table 3.9. Lowest droplet size and polydispersity index obtained with three devices to produce 1,2-ethanedithiol (EDT) - diallyl phthalate (DAP) miniemulsions and latexes.

Device	Lowest Droplets' Size (nm)	Lowest Droplets' PDI (nm)	Lowest Latex Particles' Size (nm)	Lowest Latex PDI (nm)
μ RMX	58	0.05	134	0.06
pRMX	68	0.07	68	0.08
Rotor-Stator Mixer	289	0.17	217	0.14

Unfortunately, the strong smell and volatility of this bi-functional thiol was determinant factor to the termination of this set of experiments. Another bi-functional thiol that was less volatile and with a smell that could be controlled was decided to work with for the rest of the experiments and will be presented in the following part.

3.2 2,2'-(Ethylenedioxy)diethanethiol (EDDT) and Diallyl phthalate (DAP)

A less volatile bi-functional thiol (2,2'-(ethylenedioxy)diethanethiol-EDDT, Figure 3.2) was used, whose molecular weight was higher than the previous one. This thiol was easier to handle during experiments since the odor was less strong. The miniemulsion was composed of the disperse phase, where the thiol, alkene, radical

inhibitor, Ostwald ripening inhibitor along with the photoinitiator were mixer, and the continuous phase of water and surfactant (Table 3.10).

Table 3.10. Miniemulsion formulation with 2,2'-(ethylenedioxy)diethanethiol (EDDT)- diallyl phthalate (DAP)/ C_{monomer} stands for “regarding to the monomers concentrations”.

Continuous Phase	Dispersed Phase
Deionized Water 80 wt%	Monomers <u>Thiol</u> : 2,2'-(Ethylenedioxy)diethanethiol (EDDT) 10 wt% <u>Alkene</u> : Diallyl phthalate (DAP) 14.48 wt%
	Photoinitiator Diphenyl (2,4,6-trimethylbenzoyl) phosphine oxide (DTPO) 2 wt% / C_{monomer}
Surfactant Sodium Dodecyl Sulfate (SDS) 3.5 wt% / C_{monomer}	Ostwald Ripening Inhibitor Hexadecane (HD) 4 wt% / C_{monomer}
	Radical Inhibitor 2,5-Di-tert-butyl hydroquinone (DBHQ) 1.05 wt% / C_{monomer}

Experiments were conducted using rotor-stator mixer and pneumatic elongational-flow reactor and mixer (pRMX) equipped with a static mixing element with one hole throughout its length. The pRMX flow rate was constant, $q = 4200 \text{ mL/min}$, during all experiments and the oxygen was removed and replaced by nitrogen, in order to prevent premature polymerization. In the case of pRMX the influence of the number of cycles as well as the variation of the chemical composition of the miniemulsion were investigated.

Finally, since the premature polymerization during emulsification, that was already described in all the different cases, was too high, decision was made to focus on improving the emulsification process and reducing the polymerization yield. For this reason, no photopolymerization occurred after emulsification for majority of the experiments and main focus was give on the mixing process. Only the optimized set of experiments was investigated under the continuous coiled tube photoreactor using $\lambda = 365 \text{ nm}$ wavelength and will be discussed in the following section.

3.2.1 Pneumatic Elongational-Flow Reactor and Mixer: Effect of Process Parameters

The impact of the number cycles on the droplet diameter and size dispersity was investigated using pRMX with the one-hole mixing element. Since the experiments conducted with the tetra-functional thiol PETMP under inert atmosphere revealed that the polymerization during preparation of the coarse emulsion was zero when the oxygen was removed from the system (Figure 3.8), this bi-functional thiol was manipulated under inert atmosphere only. In Figure 3.20, the effect of the number of cycles, ranging from 5 to 300, on the droplet size and polydispersity is presented.

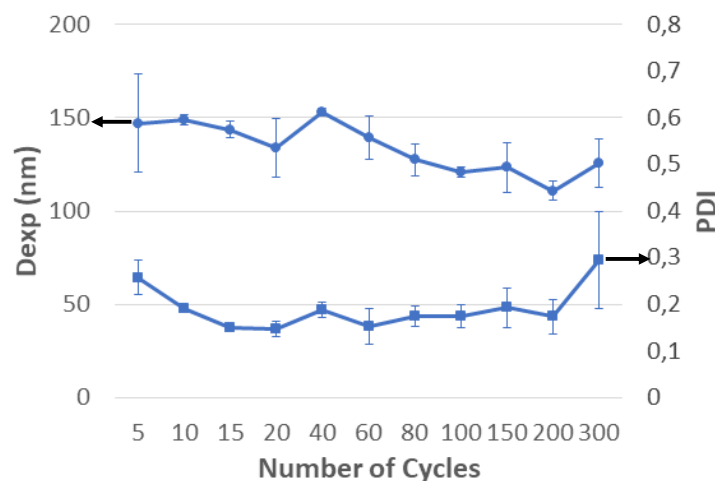


Figure 3.20. Effect of number of cycles on the droplet diameter and polydispersity after emulsification with pneumatic elongational-flow reactor and mixer (pRMX) (inert atmosphere, 1-hole static mixing element).

One can observe that starting from 5 cycles the diameter was 147 nm and increasing the number of cycles to 200 the droplet diameter slightly decreased for approximately 40 nm. It is worth mentioning that in the first 5 cycles the polydispersity was higher than 0.2, which indicated that the miniemulsion was not yet monomodal. At 40 cycles, an experimental artefact led to an increase of the droplet size, of the PDI along with an increase of the polymerization during emulsification, yield = 35 % (Table 3.11). Taking in to account the increased values of the polymerization yield at 40 number of cycles, along with the increase of the diameter (Figure 3.20), one could attribute this to an experimental artefact. Considering also that a further increase of the number of cycles, decreased the droplet diameter, the assumption of an experimental error is the most logical explanation.

Nonetheless, further increase after 300 cycles revealed an increase on the droplet diameter (approximately 20%) as well as the polydispersity. This could be the starting point of the “over-processing” effect applied to the miniemulsion. In other words, the emulsification time was too long for the specific chemical system and the coalescence of the droplets was more likely to happen.

Table 3.11. Polymerization conversion after miniemulsification of 2,2'-(ethylenedioxy)diethanethiol (EDDT)-diallyl phthalate (DAP) with pneumatic elongational-flow reactor and mixer (pRMX) obtained by ^1H NMR.

Number of Cycles	5	10	15	20	40	60	80	100	200	300
Thiol Conversion (%)	27	20	27	30	35	29	29	29	36	23
Alkene Conversion (%)	43	35	40	42	45	40	37	40	41	25

In this point and after discussing the results of both tetra- and bi- functional thiols, a comparison of the two is important to assess which of the two was able to provide smaller droplet diameter and narrower size distribution. The comparison was done between the two miniemulsion prepared with one-hole mixing element and under ambient atmosphere, so as to ensure that the only difference in the process was the thiol molecule. In Figure 3.21, the two graphs of EDDT-DAP and PETMP-DAP droplets size and PDI regarding to the pRMX number of cycles are combined in one.

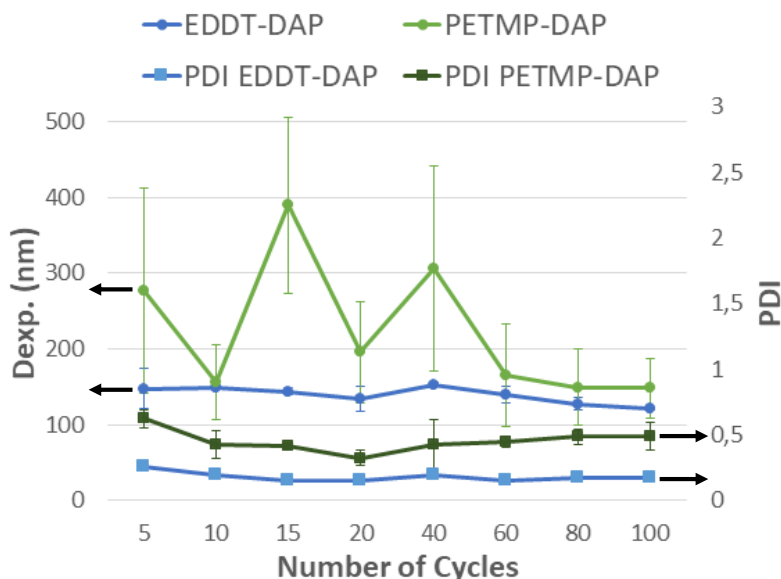


Figure 3.21. Comparison of 2,2'-(ethylenedioxy)diethanethiol (EDDT)-diallyl phthalate (DAP) (blue curves) and pentaerythritol tetrakis(3-mercaptopropionate) (PETMP)-diallyl phthalate (DAP) (green curves) miniemulsion droplets and polydispersity after emulsification with pneumatic elongational-flow reactor and mixer (pRMX) (inert atmosphere, 1-hole static mixing element).

A clear difference between the two different thiols is observed in Table 3.12 for the smallest nanoparticle size that could be achieved. The tetra-functional thiol, PETMP, revealed a droplet size higher (390 - 148 nm) than the bi-functional thiol, EDDT (155 - 120 nm), during all the number of cycles that were examined. This could be explained:

- By the size of each molecule: PETMP is a bigger molecule than EDDT, or
- By the PDI values: the polydispersity of the PETMP-DAP miniemulsion was always above 0.2, which meant that the miniemulsion was polydisperse, contrary to the monomodal EDDT-DAP miniemulsions. The increased polydispersity could lead to the destabilization of the system, thus the coalescence of the droplet, which is highly implied for the PETMP-DAP miniemulsion.
- By the difference of reactivity between PETMP and EDDT. Indeed, a premature polymerization can strongly affect the composition as well as the viscosity of the dispersed phase [33], leading to the changes on the droplet rupture [19], along with size and size distribution. An improvement was found on the polymerization yield during emulsification using the bi-functional thiol. In the case of EDDT-DAP miniemulsion the yield was close to 30%, while experiments with PEMTP-DAP miniemulsion had a higher yield, approximately 40 %.

Table 3.12. Lowest droplet size and polydispersity index obtained with two different thiols tetra-functional pentaerythritol tetrakis(3-mercaptopropionate) (PETMP) and 2,2'-(ethylenedioxy)diethanethiol (EDDT) combined with diallyl phthalate (DAP) using pneumatic elongational flow reactor and mixer (pRMX).

Thiol	Lowest Droplets Size (nm)	Lowest Droplets PDI (nm)
Tetra-functional (PETMP)	148	0.32
Bi-functional (EDDT)	120	0.15

3.2.2 Pneumatic Elongational-Flow Reactor and Mixer: Effect of Chemical Parameters

Once evaluating the process parameters, the influence of the chemical parameters was investigated. The aim was to assess the droplet diameter and polydispersity along with the premature polymerization keeping a constant number of cycles, equal to 80. This choice was due to the smallest droplet size and polydispersity,

combined with the smallest polymerization conversion during emulsification. The amount of surfactant, radical inhibitor, Oswald ripening inhibitor as well as of the photoinitiator were varied so as to monitor the droplet diameter (Figure 3.22). The standard miniemulsion formulation can be seen in Table 3.10, where the reference concentrations C_0 are reported. The variations of the concentration of the aforementioned compounds were done referring to the standard ones.

For example, in the case where the amount of surfactant was altered, the reference concentration of SDS $C_{0(\text{SDS})}$ was 3.5 wt%/C_{monomer} (blue spots), half the concentration $C_{0(\text{SDS})}/2$ (green spots) responded to 1.75 wt%/C_{monomer} of SDS, zero concentration (yellow spots) refers to the complete absence of SDS, and finally double concentration $2 \cdot C_{0(\text{SDS})}$ (red spots) describes the double amount of surfactant, 7 wt%/C_{monomer}. The same concept was followed for the rest of the chemical parameters.

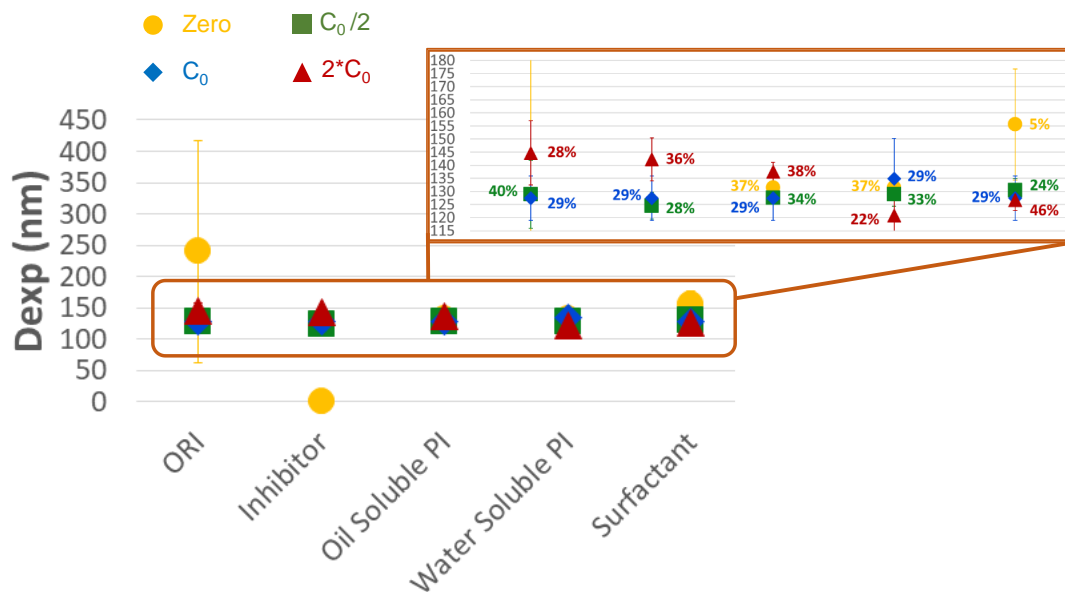


Figure 3.22. Effect of the variation of chemical parameters on the droplet size and polymerization conversion referring to -SH consumption. The miniemulsions were produced with the pneumatic elongational-flow reactor and mixer (pRMX) (inert atmosphere, 1-hole static mixing element, 80 cycles).

Starting with the Ostwald ripening inhibitor (ORI), its role is to provide equilibrium of the chemical potential between the droplets of the miniemulsion. It is proven that the less soluble in the water is this inhibitor, the more efficient against Ostwald ripening it is [34]. In Figure 3.22, the absence of ORI led to a strong increase on

the droplet size, which was expected since the system was not stabilized and Oswald ripening (i.e. merging of small droplets into bigger ones) occurred rapidly. This also result in a very broad size distribution, above 0.5. Adding half of the reference amount of ORI to the system was able to stabilize it and reduce the droplet diameter down to 129 nm. Taking a look on the reference (blue rhombus) becomes obvious that the increased amount of ORI led to a further decrease of the droplet size, 127 nm, along with the polydispersity, which was below 0.2. This proved that the miniemulsion droplets were able to equilibrate the difference of the chemical potential and provide a single size distribution. However, doubling the amount of ORI showed an increase on the diameter (from 127 nm to 250 nm) as well as the PDI = 0.22. This could potentially happen due to the limited solubility of the ORI used, hexadecane, in the disperse phase when a bi-functional thiol was used. A research group that worked with the same set of monomers [32] described that in high amounts of hexadecane, the insolubility increased and a thin layer of hexadecane was present on the surface of the droplets (brighter colour in Figure 3.23).

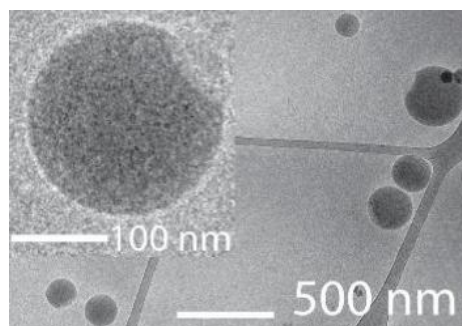


Figure 3.23. Cryo-TEM image of an 2,2'-(ethylenedioxy)diethanethiol (EDDT)- diallyl phthalate (DAP) miniemulsion containing DBHQ [32].

Regarding the radical inhibitor concentration, an increase of the droplet size and polydispersity was observed by increasing the amount of inhibitor. One potential reason for the increase of the diameter could be that the higher the amount of the inhibitor the higher the droplet load, thus the increased diameter. However, taking a closer look to the polymerization conversion, it is also increasing with the increased inhibitor concentration. Thus, the radical inhibitor maybe did not allow the droplets to stabilize against coalescence, which was enhanced during emulsification due to the temperature increase. Even though, the number of cycles

was the same for all the experiments, the only parameter that might change and its weather dependent, is the temperature of the cooling jacket. As mentioned already, the water that flows in the cooling jacket comes from the tap and is affected from the temperature outside. A warm day could limit the temperature control thus starting of the polymerization due to heat easier.

On one hand, when using an oil soluble photoinitiator (Figure 3.24 a) the droplets appear to increase in size, while the polydispersity remains below 0.2 for all experiments. This behavior could probably be explained by the fact that the premature reaction of the two monomers was increased when the amount of photoinitiator increased. The higher yield means that probably the radical inhibitor amount was not enough to fully prevent the radical formation during emulsification. Additionally, since the amount of photoinitiator was increased, the radicals formed were not able to inhibit by the less amount of inhibitor, thus the polymerization started to take place. This could be also enhanced by the fact that the photoinitiator was soluble only in the disperse phase and the radicals were initiated there, which led the increase of the droplet size. Additionally, the more components added to the dispersed phase, the larger the droplet diameter that was formed (Figure 3.24 a).

On the other hand, the use of a water-soluble initiator (Figure 3.24.b) showed the reverse behavior. This might happen due to the different polymerization mechanism that is followed when this type of initiator is used. It can be observed that the polymerization yield during emulsification was above 22%, which means that the radicals started to form. As described in the literature [32] and explained previously, the monomer droplets in the case of the water-soluble initiator oligomers were formed in the aqueous continuous phase, thus the monomer droplets serve as reservoir and the monomer was diffused through the continuous phase to the oligomers. This caused the particles to have a smaller diameter as compared with the droplets, as shown in Figure 3.24. Even though the photopolymerization did not take place, the heat rise close to the mixing element during emulsification was enough to initiate the polymerization.

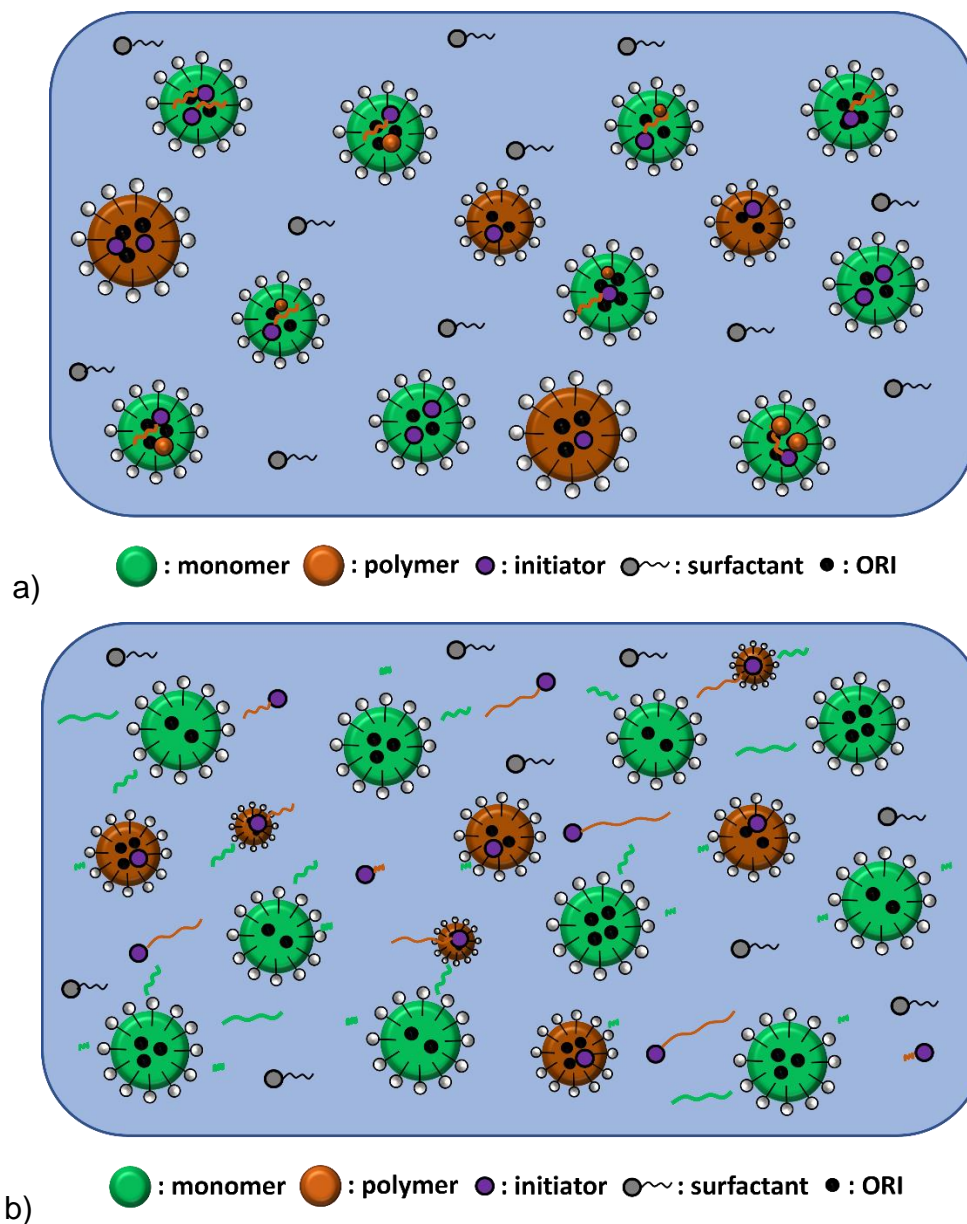


Figure 3.24. Photopolymerization mechanism when a) oil soluble and b) water soluble photoinitiator was used.

Worth mentioning is that by the absence of initiator (Figure 3.22, yellow spots) the miniemulsion revealed the maximum polymerization yield (37%). As reported several times in this manuscript, the temperature rise in the pRMX device plays the most crucial role for initiating the premature polymerization. This is the case even by the absence of initiator.

Finally, the influence of the surfactant, SDS, concentration was inspected. A quite clear trend was recovered for the droplet diameter. The increase of the amount of SDS decreased the droplet size as well as the polydispersity. It has already been

explained in literature that small amounts of surfactant are not able to cover the surface of the droplets and stabilize them [34]. This leads to the coalescence of the droplets, followed by an increase of the diameter and polydispersity. Furthermore, the surface tension decreases when the amount of surfactant increases, thus the capillary number described in previous chapter increases and leads to a smaller droplet diameter.

Overall, the effect of the different chemical parameters on the droplet size and polydispersity was investigated. It was found that the limit on the concentration of the Oswald ripening inhibitor was close to 4 wt%/C_{monomer} and a further increase causes the increase of the droplets due to the hydrophobicity of hexadecane. On the contrary, the increased inhibitor amount led to a higher droplet size, which could be either due to the increase of the load of the droplets or by the polymerization that occurred during emulsification. As for the two different photoinitiator the yield was noticeable, and it is believed that the difference on the droplet diameter emanates from the two different polymerization mechanisms that were analyzed. Eventually, the increase of the surfactant concentration was critical to the decrease of the diameter.

3.2.3 System Stability

In this point and after several changes on different parameters, it was considered very important to study the stability through time of the standard miniemulsion. For this reason, a miniemulsion using pRMX, equipped with one-hole mixing element, at 80 number of cycles, under inert atmosphere, and with the standard concentrations (Table 3.10) was formulated. During the stability test, the same time samples were taken for DLS (Figure 3.25) and ¹H NMR (Table 3.13) measurements. In this way the droplet size, polydispersity and polymerization yield were monitored. The first sample was characterized 5 minutes right after the emulsification and the droplet size was 138 nm with a narrow size distribution (PDI < 0.2). The premature reaction between the two monomers started with a yield of 22%. The EDDT-DAP miniemulsion was stable in droplet diameter and polymerization which did not exceed the yield = 25%. After one day the miniemulsion started to destabilize and the diameter increased up to 216 nm and

the polydispersity index was a bit above 0.2. This time the polymerization rose to almost 60%. After one day, the miniemulsion started to further polymerize and the droplets coalescence until after one week the diameter reached 220 nm and the PDI was 0.21. In one week, the polymerization conversion reached almost yield = 100%.

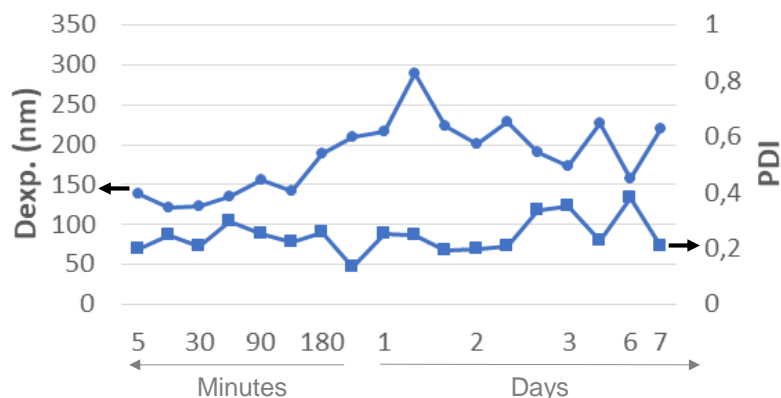


Figure 3.25. 2,2'-(ethylenedioxy)diethanethiol (EDDT)- diallyl phthalate (DAP) miniemulsion stability after its production with the pneumatic elongational-flow reactor and mixer (pRMX) (inert atmosphere, 1-hole static mixing element, 80 cycles).

Table 3.13. Polymerization conversion after miniemulsification of 2,2'-(ethylenedioxy)diethanethiol (EDDT)-diallyl phthalate (DAP) with the pneumatic elongational-flow reactor and mixer (pRMX) obtained by ^1H NMR.

Time	5 (min)	60 (min)	180 (min)	1 (d)	2 (d)	3 (d)	6 (d)	7 (d)
Thiol conversion (%)	22	21	25	59	76	89	92	99

In Figure 3.25, the droplet diameter as well as polydispersity experience several fluctuations after the passing of one day. This could be either due to the destabilization of the miniemulsion or due to statistical error. The latter can be explained because this stability test was done only one time and not several times in order to obtain the average values.

Even though the premature polymerization during emulsification started, the EDDT-DAP miniemulsion showed a relative stable profile approximately one day. This could be helpful in case of further photopolymerization was conducted.

3.2.4 Pneumatic Elongational-Flow Reactor and Mixer: Temperature Control

In all the previous parts, the main issue that was described refers to the very rapid reaction between the thiol and the alkene that was enhanced during emulsification. This happened due to the increase of the heat close to the mixing element of pRMX. For all the experiments, a cooling jacket was used to achieve a control on the temperature rise. At the same time, the temperature was monitored using a sensor that was installed on the walls of the chamber of pRMX. It was observed this temperature was still rising even after using that tap water to cool down the device. It is mentioned previously that this water was strongly depending on the weather and the temperature could not be further controlled. This is probably why, even after several changes and improvements on the preparation of the miniemulsions, the thiol-ene polymerization still took place.

For this reason, a chiller was installed and connected with the cooling jacket of pRMX. Isopropanol was used to cool down the device close to 10 °C, contrary with the already used tap water ($T > 20$ °C). Even from the first experiments the dripping problem was becoming stronger, while some grey particles were obtained along with the miniemulsion. After few experiments with the standard recipe of the EDDT-DAP miniemulsions, the whole emulsion was grey instead of white (Figure 3.26), which after few days was becoming reddish. This started rising questions about what could be wrong.



Figure 3.26. Miniemulsion containing metallic particles after adding a chiller to the system.

To examine and understand what the grey particles could be, several experiments were performed, where every time the same grey solution was obtained. Parallel with that, a closer look on the back part of the pistons (Figure 3.27) revealed some black materials, which had a gluey texture.



Figure 3.27. Back side of the pneumatic elongational-flow reactor and mixer (pRMX) piston.

Elemental analysis confirmed that these grey particles, coming from the back part of the pRMX pistons, had metallic origin (Table 3.14). It is important to mention that the whole device was made of stainless-steel, only the back part of the piston was made of brass. Brass is an alloy of copper and zinc, which can easily be oxidized. Another crucial measurement was the pH of the miniemulsion, which was found to be very acidic, pH = 4.

Table 3.14. Elemental analysis of emulsion and grey gluey material

Réf. Externe	Emulsion		Contamination	
Réf. ECPM	21-03-08-CS-EK-01	unité	21-03-08-CS-EK-02	unité
Al	0,60 ± 0,01	mg/kg	4332 ± 70	mg/kg
Ca	0,57 ± 0,01	mg/kg	406 ± 8	mg/kg
Cr	0,223 ± 0,002	mg/kg	482 ± 7	mg/kg
Cu	11,52 ± 0,08	mg/kg	6,9 ± 0,2	% (m/m)
Fe	1,95 ± 0,02	mg/kg	1,65 ± 0,03	% (m/m)
K	0,456 ± 0,003	mg/kg	156 ± 2	mg/kg
Mg	0,073 ± 0,001	mg/kg	41 ± 3	mg/kg
Mn	0,40 ± 0,01	mg/kg	2739 ± 36	mg/kg
Na	431 ± 7	mg/kg	1659 ± 24	mg/kg
Ni	0,140 ± 0,002	mg/kg	376 ± 3	mg/kg
P	155 ± 2	mg/kg	2893 ± 461	mg/kg
S	1,26 ± 0,04	% (m/m)	12,6 ± 0,3	% (m/m)
Si	0,37 ± 0,02	mg/kg	875 ± 29	mg/kg
Zn	3,91 ± 0,07	mg/kg	2,69 ± 0,05	% (m/m)

Finally, the main problem was that by installing the chiller ($T = 10^{\circ}\text{C}$), the shields that were used to reassure the tightness between the piston and the chamber, were shrunken due to the cold temperature. This caused the acidic miniemulsions to flow a bit outside of the device from the back position of the pistons, leading to the corrosion of the brass part of the piston, which was eventually polymerizing the miniemulsion and forming small particles combined with the brass, black gluey particles. For this reason, no further experiments could be performed using pRMX, because the miniemulsions obtained was contaminated with metallic particles and any characterization technique would not have been accurate to evaluate the droplets size and polydispersity.

3.2.5 Rotor-Stator Mixer

In this point, just like it has been done with PETMP-DAP system, comparison of two emulsification devices (shear mixer and pRMX) was crucial to compare the droplet diameter along with the polydispersity. The composition of miniemulsions were the same standard recipe with the EDDT-DAP miniemulsion (Table 3.6). Photopolymerization followed after emulsification, at wavelength $\lambda = 365 \text{ nm}$ and residence time $\tau = 7 \text{ min}$, using the coiled tube photoreactor.

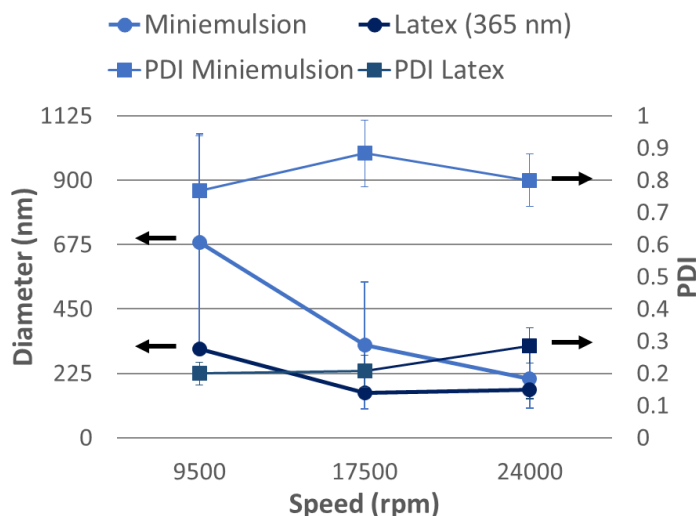


Figure 3.28. Effect of rotational speed on the droplet and particle diameter and polydispersity.

In Figure 3.28 is observed that for low rotational speed, the droplet diameter appeared to be 683 nm, while increasing the speed the size decreased down to 323 nm. Additional increase of the speed to maximum showed a further decrease

of the droplet diameter, 207 nm. However, the polydispersity index measured by DLS was above 0.8, which meant that different droplet sizes appear in the miniemulsion indicating that was polydisperse. Regarding the polymerization yield during emulsification, it was very low, below 15%, for all the experiments (Table 3.15).

Table 3.15. ¹H NMR polymerization conversion after miniemulsification of 2,2'-(ethylenedioxy)diethanethiol (EDDT)- diallyl phthalate (DAP) with rotor-stator mixer.

Rotational Speed (rpm)	9500	17500	24000
Thiol Conversion (%)	6	12	2
Alkene Conversion (%)	5	15	1

The same decreasing trend was observed for the latex when the rotational speed was increased. Nevertheless, the particle size appeared to be much smaller than the droplet size, more than 300 nm difference. This could potential be attributed to different factors: (i) the miniemulsion and latex was not stable through time and a face separation occurred by the end of the day, (ii) that maybe when the sample for the DLS was taken, the bigger, heavier particles sedimented on the bottom of the vial and (iii) the smaller particles were the ones, whose droplet size was measured.

Comparing those results with the results described previously for the same chemical system prepared with the pRMX (Figure 3.20), the pRMX was, once more, able to provide better mixing in terms of droplet diameter and polydispersity. In all the experiments the pRMX miniemulsion was monomodal alike the rotor-stator mixer which was polydisperse. The same occurred to the diameter, since the one obtained from pRMX was below 150 nm, contrary to the minimum 207 nm of shear mixer (Table 3.16). These observations allowed to conclude that pRMX could deliver improved control on the droplet diameter and polydispersity, despite the 20% of polymerization yield.

Table 3.16. Lowest droplet size and polydispersity index obtained with two devices to produce 2,2'-(ethylenedioxy)diethanethiol (EDDT)-diallyl phthalate (DAP) miniemulsions.

Device	Lowest droplets' size (nm)	Lowest droplets' PDI (nm)
pRMX	110	0.15
Rotor-stator mixer	207	0.88

3.3 Thiol-Ene Photopolymerization and Miniemulsification

Since many problems were encountered during miniemulsification, as mentioned, premature polymerization, clogging and finally corrosion of the pRMX, a new procedure was established to produce latex particles. Unfortunately, due to lack of time, since this new idea came almost in the end of this research project, only few preliminary experiments were conducted using this new method.

During these experiments, the two monomers (EDDT and DAP) along with the oil soluble photoinitiator were first mixed in a vial. Then, a given amount of acetone was added in order to control the viscosity of the solution. The main goal was to inject this solution in the coiled tube photoreactor, $\lambda = 365$ nm and $\tau = 7$ min, and photopolymerize it. Once the polymer was obtained, it was mixed with water and surfactant, which was the continuous phase, using magnetic stirrer for 10 min. Then, the solution (Table 3.17) was introduced in the pRMX equipped with one-hole mixing element, to obtain a latex.

Indeed, since the poly(ether) was stable at temperatures close to 30°C, the pRMX could be used without using the chiller. The number of cycles was set at 100 so as to achieve a homogeneous latex. Worth mentioning is that trials were done at lower number of cycles, but no homogeneous latex could be obtained, thus the 100 cycles was found to be the least one to provide homogenous latex. It was challenging to achieve a stable latex, because the disperse phase was very viscous and the particles formed were more dense than the continuous phase. This was the driving force for the destabilization of the latex. Thus, longer emulsification time slowed down this destabilization.

Table 3.17. Latex formulation based on 2,2'-(ethylenedioxy)diethanethiol (EDDT)- diallyl phthalate (DAP).
"/Cmonomer "stands for "regarding to the monomers concentrations".

Polymeric Solution
Poly(thioether) 10 wt% 2,2'-(Ethylenedioxy)diethanethiol (EDDT) + 10 wt% Diallyl phthalate (DAP)
Photoinitiator Diphenyl (2,4,6-trimethylbenzoyl) phosphine oxide (DTPO) 2 wt% / Cmonomer
Solvent Acetone Different concentrations

Continuous Phase	Dispersed Phase
Distilled Water 80 wt%	Polymeric Solution Poly(thioether)
Surfactant Sodium Dodecyl Sulfate (SDS) 3.5 wt% / Cmonomer	

The acetone that was trapped in the droplets, was diffused to the aqueous phase, since it was soluble to water and evaporated by stirring the solution for 1 hour before leaving the latex under the fume hood overnight. The next day the latex was characterized for the particle diameter and polydispersity (Figure 3.29).

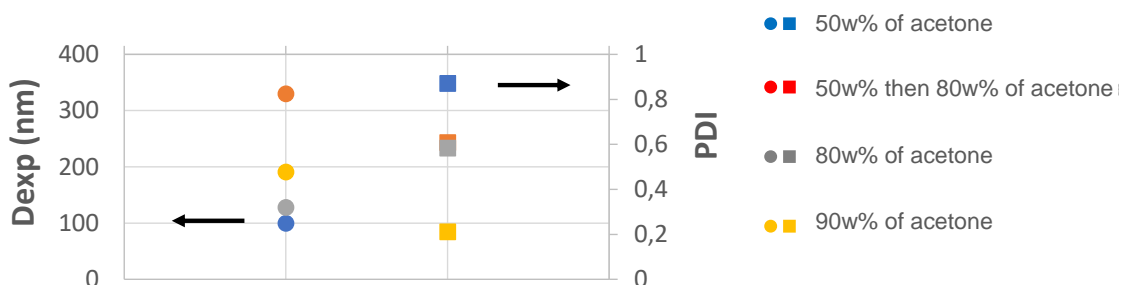


Figure 3.29. Effect of solvent concentration on the droplet diameter (circles) and polydispersity (squares) at fixed number of cycles, 100.

Different concentrations of acetone were tested, ranging from 50w% to 90w%, in order to observe the particle size and polydispersity. The particle diameter obtained the smallest by adding 50w% of acetone (100 nm), but the polydispersity was close to 0.9, which meant that the latex completely polydisperse. Further, it was observed that the latex was not stable, and sedimentation took place few hours after terminating the stirring for the solvent evaporation. An attempt to decrease the polydispersity was done by preparing the polymer with 50 wt% acetone and after emulsification to dilute the 40 mL of latex in 80 wt% of water. This led the particles to increase the size while the dispersity was still very high, above 0.6.

It was again observed that the latex particles were very viscous, which made them dense, thus the destabilization of the latex occurred rapidly. For this reason, the amount of acetone was increased up to 90 wt%. This last preparation condition gave encouraging results since the diameter was a bit below 200 nm and the polydispersity close to 0.2, which indicated that the latex had a monomodal size

distribution. More investigations need thus to be done, but increasing the solvent amount to decrease the particles' size, in order to achieve a stable latex with a tunable particle size.

↻ Conclusions

Different emulsification devices were used to produce thiol-ene miniemulsions. Two homemade elongational-flow emulsification devices (μ RMX and pRMX) which were compared with a simple shear rotor-stator mixer. Among the three, the shear mixer showed the poorest diameter and dispersity control.

Additionally, the composition of the miniemulsion was investigated by using different types of thiols: one tetra-functional and two-bifunctional ones. It was shown that the bi-functional thiol, 2,2'-(Ethylenedioxy)diethanethiol (EDDT), was the one providing the smallest diameter and polydispersity. Furthermore, the droplets' size decreased steadily when the number of cycles was increased. Therefore, the droplets' size could easily be targeted by adjusting the number of cycles. The amount of surfactant, photoinitiator, radical and Oswald ripening inhibitor was also investigated, proving that the smallest diameter ($d = 121$ nm) was obtained when water soluble initiator with twice the standard concentration was used. On the contrary, the largest diameter ($d = 156$ nm) was observed when no surfactant was added in the miniemulsion. The latter result was expected since the droplets could not stabilize against coalescence. This variation of parameters provided a droplet diameter control according to what was varying. For the tetra-functional thiol, the number of cycles did not change the droplets' size, but it was found that the diameter was highly sensitive to the mixing element (1-hole vs 4-holes) and the presence of oxygen during the preparation of the solutions. This complies well with the increased reactivity of higher functional monomers.

Unfortunately, due to the acidic nature of the miniemulsion many problems occurred. Starting with clogging during emulsification, while at the same time leakage on the back part of the chambers was observed. This dripping was enough to corrode the pRMX piston, which was made of brass, and metallic particles appeared in the solution. Finally, this corrosion was a restrictive factor to further

work with thiol-ene solutions in the pRMX, when the temperature was below room temperature.

This led to a new experimental procedure, where the monomers were mixed with photoinitiator and acetone, in different concentrations. The solution was flowed in the coiled tube photoreactor, and the polymer solution was obtained before introducing it into the pRMX. Interesting results were obtained with this procedure when the monomer solution was mixed with 90 wt% acetone, since the diameter was equal to 200 nm and the latex appeared monomodal. This technique needs further improvement and investigation.

D Bibliography

- [1] S. Slomkowski *et al.*, "Terminology of polymers and polymerization processes in dispersed systems (IUPAC recommendations 2011)," *Pure and Applied Chemistry*, vol. 83, no. 12, pp. 2229–2259, 2011, doi: 10.1351/PAC-REC-10-06-03.
- [2] R. G. Jones *et al.*, "Compendium of Polymer Terminology," *International Union of Pure and Applied Chemistry (IUPAC)*, 2008.
- [3] B. Novales, P. Papineau, A. Sire, and M. A. V. Axelos, "Characterization of emulsions and suspensions by video image analysis," *Colloids and Surfaces A: Physicochemical and Engineering Aspects*, vol. 221, no. 1–3, pp. 81–89, 2003, doi: 10.1016/S0927-7757(03)00102-X.
- [4] D. J. McClements and S. M. Jafari, "Improving emulsion formation, stability and performance using mixed emulsifiers: A review," *Advances in Colloid and Interface Science*, vol. 251, pp. 55–79, 2018, doi: 10.1016/j.cis.2017.12.001.
- [5] M. M. Robins, A. D. Watson, and P. J. Wilde, "Emulsions - Creaming and rheology," *Current Opinion in Colloid and Interface Science*, vol. 7, no. 5–6, pp. 419–425, 2002, doi: 10.1016/S1359-0294(02)00089-4.
- [6] B. A. Khan *et al.*, "Basics of pharmaceutical emulsions: A review," *African Journal of Pharmacy and Pharmacology*, vol. 5, no. 25, pp. 2715–2725, 2011, doi: 10.5897/AJPP11.698.
- [7] T. Delmas *et al.*, "How to prepare and stabilize very small nanoemulsions," *Langmuir*, vol. 27, no. 5, pp. 1683–1692, 2011, doi: 10.1021/la104221q.
- [8] T. S. H. Leong, T. J. Wooster, S. E. Kentish, and M. Ashokkumar, "Minimising oil droplet size using ultrasonic emulsification," *Ultrasonics Sonochemistry*, vol. 16, no. 6, pp. 721–727, 2009, doi: 10.1016/j.ultsonch.2009.02.008.
- [9] T. Posner, "Zum Schluss darf ich es nicht unterlausen, nieuen Aasisteuteii Hrn. / In German," *Ber. Dtsch. Chem. Ges.*, vol. 38, no. 1, pp. 646–657, 1905.
- [10] H. C. Kolb, M. G. Finn, and K. B. Sharpless, "Click Chemistry: Diverse Chemical Function from a Few Good Reactions," *Angewandte Chemie - International Edition*, vol. 40, no. 11, pp. 2004–2021, 2001, doi: 10.1002/1521-3773(20010601)40:11<2004::AID-ANIE2004>3.0.CO;2-5.
- [11] T. O. Machado, P. B. Cardoso, P. E. Feuser, C. Sayer, and P. H. H. Araújo, "Thiol-ene miniemulsion polymerization of a biobased monomer for biomedical applications," *Colloids and Surfaces B: Biointerfaces*, vol. 159, pp. 509–517, 2017, doi: 10.1016/j.colsurfb.2017.07.043.
- [12] J. Kumpfmüller, K. Stadlmann, Z. Li, V. Satzinger, J. Stampfl, and R. Liska, "Two-photon-induced thiol-ene polymerization as a fabrication tool for flexible optical waveguides," *Designed Monomers and Polymers*, vol. 17, no. 4, pp. 390–400, 2014, doi: 10.1080/15685551.2013.840515.
- [13] Y. Rong, S. Ali, Q. Ouyang, L. Wang, B. Wang, and Q. Chen, "A turn-on upconversion fluorescence sensor for acrylamide in potato chips based on fluorescence resonance

- energy transfer and thiol-ene Michael addition,” *Food Chemistry*, vol. 351, no. January, p. 129215, 2021, doi: 10.1016/j.foodchem.2021.129215.
- [14] Madhusa, “Difference Between Chain Growth and Step Growth Polymerization.” <https://pediaa.com/difference-between-chain-growth-and-step-growth-polymerization/>
- [15] G. Kühne, J. S. Diesen, and E. Klemm, “New results of the self-initiation mechanism of SH/En addition polymerization,” *Angewandte Makromolekulare Chemie*, vol. 242, pp. 139–145, 1996, doi: 10.1002/apmc.1996.052420109.
- [16] W. Yu *et al.*, “Development of an Elongational-Flow Microprocess for the Production of Size-Controlled Nanoemulsions: Batch Operation,” *Macromolecular Reaction Engineering*, vol. 11, no. 1, Feb. 2017, doi: 10.1002/mren.201600024.
- [17] M. Vauthier, M. Schmutz, and C. A. Serra, “One-step elaboration of Janus polymeric nanoparticles: A comparative study of different emulsification processes,” *Colloids and Surfaces A: Physicochemical and Engineering Aspects*, vol. 626, no. May, p. 127059, 2021, doi: 10.1016/j.colsurfa.2021.127059.
- [18] I. Souilem *et al.*, “A Novel Low-Pressure Device for Production of Nanoemulsions,” *Chemical Engineering and Technology*, vol. 35, no. 9, pp. 1692–1698, 2012, doi: 10.1002/ceat.201100676.
- [19] P. Taylor and H. P. Grace, “Dispersion Phenomena in High Viscosity Immiscible Fluid Systems and Application of Static Mixers As Dispersion Dispersion Phenomena in High Viscosity Immiscible Fluid Systems and Application O F Static Mixers As Dispersion Devices in Such Systems,” *Science (1979)*, vol. 6445, no. 912873516, pp. 37–41, 2009, doi: 10.1080/00986448208911047.
- [20] John Wiley & Sons and Inc. SpectraBase, “Compound ID=7qu3qeDCtNc SpectraBase Spectrum ID=2kdCneBr7IX.”
- [21] F. Jasinski *et al.*, “Supporting Information (SI) Thiol-ene Linear Step-Growth Photopolymerization in Miniemulsion: Fast Rates, Redox-Responsive Particles, and Semi-Crystalline Films.”
- [22] Chemical Book, “Diallyl phtalate (131-17-9) 1H NMR.”
- [23] Chemical Book, “N-Hexadecane 1H NMR.”
- [24] R. O. McCourt and E. M. Scanlan, “Atmospheric Oxygen Mediated Radical Hydrothiolation of Alkenes,” *Chemistry - A European Journal*, vol. 26, no. 68, pp. 15804–15810, 2020, doi: 10.1002/chem.202002542.
- [25] W. Yu *et al.*, “Development of an Elongational-Flow Microprocess for the Production of Size-Controlled Nanoemulsions: Batch Operation,” *Macromolecular Reaction Engineering*, vol. 11, no. 1, pp. 1–11, 2017, doi: 10.1002/mren.201600024.
- [26] M. Vauthier and C. A. Serra, “One-step production of polyelectrolyte nanoparticles,” *Polymer International*, vol. 70, no. 6, pp. 860–865, 2021, doi: 10.1002/pi.6178.
- [27] N. Anton *et al.*, “A new microfluidic setup for precise control of the polymer nanoprecipitation process and lipophilic drug encapsulation,” *Soft Matter*, vol. 8, no. 41, pp. 10628–10635, Nov. 2012, doi: 10.1039/c2sm25357g.

- [28] S. Ding, N. Anton, T. F. Vandamme, and C. A. Serra, "Microfluidic nanoprecipitation systems for preparing pure drug or polymeric drug loaded nanoparticles: an overview," *Expert Opinion on Drug Delivery*, vol. 13, no. 10, pp. 1447–1460, 2016, doi: 10.1080/17425247.2016.1193151.
- [29] J. Bibette, D. Roux, and B. Pouligny, "Creaming of emulsions: the role of depletion forces induced by surfactant," *Journal de Physique II*, vol. 2, no. 3, pp. 401–424, 1992, doi: 10.1051/jp2:1992141.
- [30] L. L. Hecht, C. Wagner, K. Landfester, and H. P. Schuchmann, "Surfactant concentration regime in miniemulsion polymerization for the formation of MMA nanodroplets by high-pressure homogenization," *Langmuir*, vol. 27, no. 6, pp. 2279–2285, 2011, doi: 10.1021/la104480s.
- [31] I. Souilem, C. A. Serra, R. Muller, Y. Holl, and M. Bouquey, "Dimensional Analysis of a Novel Low-Pressure Device for the Production of Size-Tunable Nanoemulsions Ines," *AIChE Journal*, vol. 61, no. 1, pp. 23–30, 2015, doi: 10.1002/aic.14690.
- [32] S. Kentish, T. J. Wooster, M. Ashokkumar, S. Balachandran, R. Mawson, and L. Simons, "The use of ultrasonics for nanoemulsion preparation," *Innovative Food Science and Emerging Technologies*, vol. 9, no. 2, pp. 170–175, 2008, doi: 10.1016/j.ifset.2007.07.005.
- [33] K. Y. Hernández-Giottonini *et al.*, "PLGA nanoparticle preparations by emulsification and nanoprecipitation techniques: Effects of formulation parameters," *RSC Advances*, vol. 10, no. 8, pp. 4218–4231, 2020, doi: 10.1039/c9ra10857b.
- [34] F. Alves and I. Nischang, "Radical-mediated step-growth: Preparation of hybrid polymer monolithic columns with fine control of nanostructural and chromatographic characteristics," *Journal of Chromatography A*, vol. 1412, pp. 112–125, Sep. 2015, doi: 10.1016/j.chroma.2015.08.019.
- [35] C. M. Q. Le, L. Vidal, M. Schmutz, and A. Chemtob, "Droplet nucleation in miniemulsion thiol – ene step photopolymerization," 2021, doi: 10.1039/D1PY00139F.
- [36] M. Manea, A. Chemtob, M. Paulis, J. C. de la Cal, M. J. Barandiaran, and J. M. Asu, "Miniemulsification in High-Pressure Homogenizers," *AIChE Journal*, vol. 54, no. 1, pp. 289–297, 2008, doi: DOI 10.1002/aic.11367.
- [37] K. Landfester, N. Bechthold, F. Tiarks, and M. Antonietti, "Formulation and stability mechanisms of polymerizable miniemulsions," *Macromolecules*, vol. 32, no. 16, pp. 5222–5228, 1999, doi: 10.1021/ma990299+.

CHAPTER IV

DEVELOPMENT OF A CONTINUOUS PNEUMATIC ELONGATIONAL-FLOW REACTOR AND MIXER

OUTLINE

Preface.....	201
<i>A</i> Continuous Pneumatic Elongational-Flow Reactor and Mixer (cpRMX) .	201
<i>B</i> Forecasted Experiments	205
<i>C</i> Operating Software Manual	208
Preparation:.....	209
<i>D</i> Bibliography	213

Preface

Two batch elongational flow reactor and mixers along with a linear and coiled tube photoreactors were developed in the previous chapter. It was observed that droplet and particle diameter control could be achieved by adjusting either process or chemical parameters. In this chapter an innovative elongational-flow based device will be described. This device works in a continuous mode and in a larger industrial scale as compared with the previously described devices.

A Continuous Pneumatic Elongational-Flow Reactor and Mixer (cpRMX)

A novel device was built under the scope of this PhD. The device is called continuous pneumatic elongational-flow reactor and mixer (cpRMX) (Figure 4.1). The working principal is based on the elongation of the droplets, which also occurred in the micro elongational-flow reactor and mixer (μ RMX) and pneumatic elongational-flow reactor and mixer (pRMX) that were described in the previous chapters. In more detail, in all these devices, an elongational reciprocating flow is created due to the movement of the pistons which breaks the droplets into smaller ones in each passing through the restriction.

The cpRMX device comprises of two pistons that are aligned vertically and come in contact in the center with the mixing element. In this RMX, the mixing element is small, and it can easily be removed, cleaned and placed back in place without the need to dismount the whole device. The mixing element that is designed has 3 holes of 1 cm diameter each, but the number of holes can be modified depending on the need of each application. Compressed air is the driving force to pneumatically move both pistons. The pressure can be tuned between 10 and 100 bar. However, a minimum pressure of 10 bar is required to move the pistons and thus will be considered the working pressure. At first, pressure is directed to the bottom chamber which was previously filled with the raw solution to be emulsified, the upper chamber pressure is at atmospheric pressure. Thus, the bottom piston starts to move upwards. When it reaches the mixing element, the pressure is directed to the upper chamber while the pressure is released in the bottom

chamber. Thus, the upper piston starts to move downwards while the bottom piston moves freely. This procedure counted as one cycle.

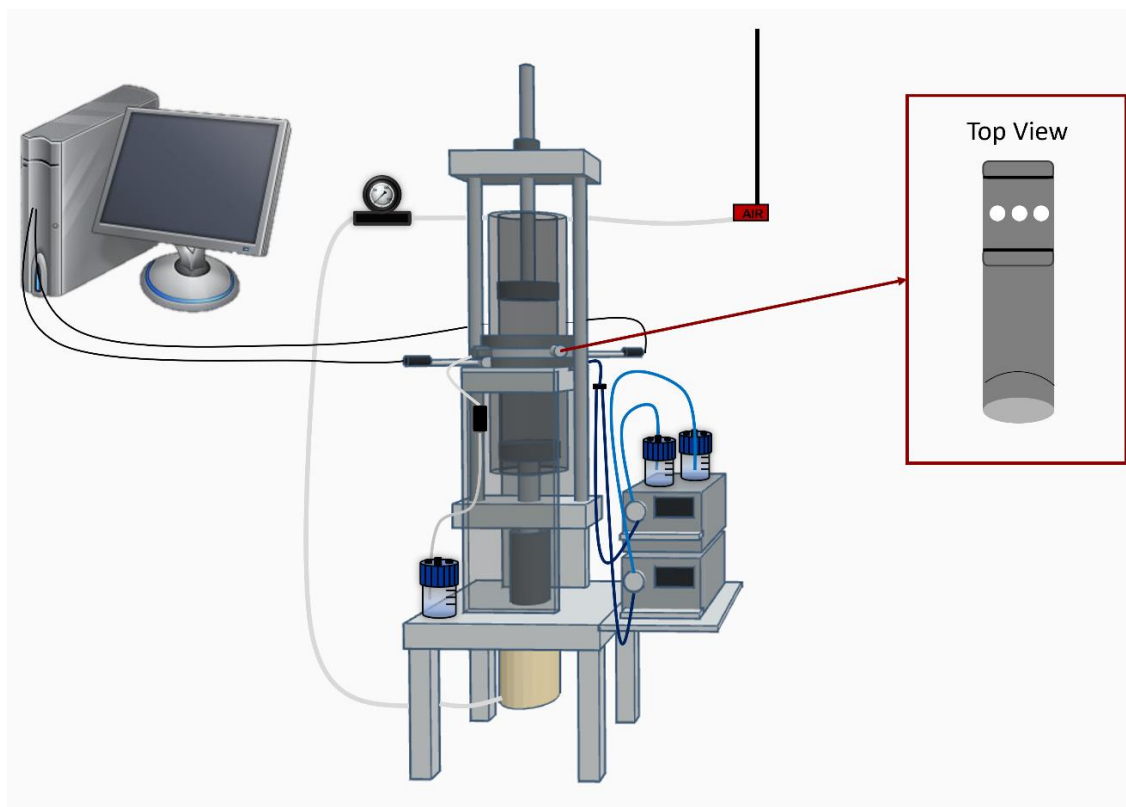


Figure 4.1. Schematic drawings of the continuous pneumatic elongational-flow reactor and mixer (cpRMX, left) and mixing element (right).

The main goal of the cpRMX is the continuous production of miniemulsion, which will be photopolymerized to finally obtain a latex with tunable diameter. For this reason, the process was divided in four steps: the feeding, mixing, photopolymerization and outlet. Starting with the feeding two high pressure piston pumps (MX-Class Pump) were installed which were connected with the continuous and dispersed phase respectively. The two phases were flowing in two different PTFE tubes that were coming in contact, with the help of a T-junction, right before the mixing element. This was to ensure that the two phases would not come in contact before emulsification, so as to avoid any premature reaction between the different components.

To start the cpRMX, a software is mandatory to operate. A detailed manual of the operating software in English will be given by the end of this chapter. This software controls the pressure provided to the piston to move, the volume and the number of cycles for each experiment. The software collects the values from the two

pressure sensors that are antipodally installed. One sensor is connected to the upper chamber and the second to the bottom chamber. To adjust the volume, between 5 and 113 mL, the “remote” mode needs to be selected on the operating box. In this way the pressure is released and only the gravity force is applied to the pistons. Then the screw-rod that is on the top of the device can be tighten or loosen to as to obtain the desired volume, that can be seen on the software. Once this step is done, the mode can be switched to “local” from the corresponding box and the bottom “up-down” can be pressed so as to reassure that both pistons are calibrated to the desired volume. This volume will correspond to the position of the bottom piston once the mode “remote” is selected.

To fill the cpRMX the mode has to be in “local” and the outlet valve open and both pistons in zero position (*i.e.* in contact with the mixing element). Then the flowrate on both high-pressure piston pumps is adjusted close to 7 mL/min, so as to fill the upper chamber quickly. Once the liquid is flowing to the outlet it means that the chamber is filled with the desired volume that was adjusted previously. For the continuous operation of cpRMX the outlet valve can be closed and one waits until the pressure becomes higher than 20 bar on the software. This will allow the chamber to be completely filled. Then outlet valve opens again, and the flowrates of the high-pressure piston pumps can be modified depending on the desired flowrate.

For the mixing step, the mode has to be again switched to “remote” in order for the liquid to flow under pression to the bottom chamber. The flowrate of the pistons can be adjusted by the “Speed SetPoint” box, while the duration of the experiment can also be controlled. The duration will indicate the number of cycles that will be done during the experiment. Finally, the cpRMX is ready to run according to the parameters given to the software. The emulsion flows from the bottom chamber through the mixing element to the upper chamber with the help of the compressed air.

While mixing the high-pressure piston pumps work and continuously feed the cpRMX chamber with fresh dispersed and continuous phase solutions. This will force the miniemulsion that was already mixed in the device to the exit the device though the mixing element. The flowrate of the exit has to be equal with the

combined flowrates of dispersed and continuous phases given to the high-pressure piston pumps. For example, if the continuous phase flowrate is $q_c = 0.4$ mL/min and the disperse phase flowrate is $q_d = 0.1$ mL/min, the outlet flowrate will be $q_{\text{outlet}} = 0.5$ mL/min. The outlet PTFE tube is connected with a coiled tube photoreactor that was described in the previous chapter. This means that the outlet flowrate will determine the residence time, the time that the miniemulsion will stay under UV. For the same example, when the $q_{\text{outlet}} = 0.5$ mL/min the residence time will be 8 min. In the case that the outlet flowrate is not equal to the combined inlet flowrates a setting valve is added after the outlet valve in order to achieve a better control on the outlet flowrate. Finally, the latex is collected in a vial which is connected with the outlet tube of the coiled tube photoreactor.

In case where the photopolymerization is not desired the photoreactor can be removed from the outlet and the freshly prepared miniemulsion can be collected instead.

There is the possibility of the cpRMX to work in a batch mode. In this case both high-pressure valves stop once the chamber is filled, and at the same time the outlet valve is also closed. This operation will be the same as the pRMX operation but in a vertical direction. The operating flowrate and duration can be adjusted again from the same software.

The main purpose of this newly built device is to produce miniemulsion and latex in a continuous way, while it is fully automated and only a software is needed to operate the device. This can allow the use of cpRMX on a larger industrial scale. Using the continuous mode several advantages are expected against the batch one. Starting with a high production rate, since there is no dead time between charging, discharging the solution and cleaning the device. This will also allow to obtain a constant quality of the product over time with the same particle size and polydispersity. These can be adjusted by varying the flowrate and/or the duration of each experiment. The particle size and polydispersity can be tuned depending on the application of the final product. Finally, the improved design of cpRMX as compared with pRMX allows the easy modification of the static mixing element by simply unscrewing it without the need of dismounting the whole device as for the pRMX.

Unfortunately, during the time this research lasted no successful experiments could be conducted with the cpRMX. This was due: 1) to the time requested to design the device, to fabricate and assemble all its different parts and to adjust them (roughly one year) and 2) the late delivery of the software (roughly one year as a consequence of the Covid situation) which was mandatory to operate the device safely. It is worth mentioning that this software was designed by the technical support provided from our institute. Once the software was delivered, several trials were conducted with water to troubleshoot the software while at the same time the tightness of the cpRMX was assessed. During these tests one pressure sensor broke, and the device could not be operated, for safety reasons, until it was replaced by the new one which took almost 3 months. Furthermore, many leaking problems were encountered from the beginning, which will necessitate to redesign the setup and more precisely the piston seal and seal holder.

➤ Forecasted Experiments

In this point, and since no successful experiments could be conducted, some forecasted experiments will be described using cpRMX. After evaluation of the several advantages explained in the previous part, the predicted experiments that could be performed will be discussed.

1. Calibration of the high-pressure piston pumps. One has to estimate that the flowrate that is shown on the device is identical with the outlet flowrate. This has to be done for all possible flowrates. By drawing the calibration curve of the pumps one can estimate and adjust accordingly the desired flowrate. Worth mentioning is that the specific high-pressure piston pumps (MX-Class Pump), provide the possibility of changing the pump performance (%) so as to be correctly calibrated.

2. Calibration of the cpRMX device. This has to be adjusted according to the solution that will be introduced. There is the need to evaluate the inlet and outlet flowrate. In more detail, the combined flowrate of the dispersed and continuous phases flowrates have to be identical with the flowrate in the outlet tube. To assess this, the upper chamber of cpRMX has to be filled and the inlet and outlet valves

to be open. Additionally, the two pumps will continuously pump the liquid, starting with the smallest flowrate possible, and the time and volume of the outlet flowrate will be observed. This has to be done for all the possible flowrates and changes have to be done accordingly. These changes could be on the high-pressure piston pumps directly, or by modifying the position of the setting valve.

3. After completing the calibration of both pumps and cpRMX and reassure their accurate performance, the experiments that could be done in order to evaluate the possibility to control the droplet and particle diameter are:

-The variation of process parameters:

i) change of the flowrate through the mixing element by means of the piston driving pressure which can be done from the software. It is expected that the higher the flowrate, the smaller the droplet/particle diameter [1]

ii) change of the geometry of the mixing element. Since the latter has been designed to be easily exchanged, it will be possible to investigate the effect of the geometry of that element, namely the number and diameter of the holes. Since cpRMX is a continuous process, the pistons will operate continuously thus no control of the number of cycles is required.

iii) change of the feed flowrate by adjusting the individual flowrate of the two piston pumps. It is expected that the higher the feed flowrate, the lower the droplets size. Possibly one can also investigate asymmetric piston flowrates to get access to different monomer ratios in final emulsion.

-The variation of photoreactor parameters:

i) change the UV lamp intensity and wavelength

ii) change of the residence time in flow photoreactor to get access to different polymerization times. This could be obtained by using a third piston pump delivering water that will modulate the flowrate at the entrance of the photoreactor.

iii) alternatively, the residence time can also be changed by using PTFE tubings of different inner diameters.

-The variation of chemical parameters:

i) changing the composition of the emulsion, meaning the amount of surfactant, of Ostwald's ripening and radical inhibitors, of initiator and monomer molecular structure, monomer and comonomer ratios.

There are many factors that can influence the droplet and particle diameter. The most important ones have been described and it is expected that the droplet diameter could be tuned depending on the desired application. This way a larger industrial scale process operating at low pressure could be operated continuously.

Operating Software Manual



Figure 4.2. Pictures of the continuous pneumatic elongational-flow reactor and mixer (cpRMX, left) and the mixing element (right).

Preparation:

- 1) After turning on the computer and the control box (switch on the large box), open the “RMX vertical” software.



- 2) Check that the graphics acquire values continuously.
- 3) Adjust the pressure regulator to sufficient pressure (it can be adjusted to 6 bar).



1st Initialization of the cpRMX:

The aim is to get the zero, it corresponds to the top stop of the RMX. For this operation, the mode selector must be on "remote".

Click on "initialize".

Remark:

- 1) The RMX go up stop then go down stop in order to take the corresponding position measurements.
- 2) After this operation, the “Start RMX” button becomes active.
- 3) This operation is mandatory at least once when restarting the "RMX_vertical" program.

Adjusting the volume of the cpRMX chamber:



The RMX chamber is theoretically empty for this operation.

On the control box:

- 1) Set the mode selector to "local".
- 2) Press the "up - down" button until the mechanism comes to a stop upwards, then to a stop downwards. These positions can be called "top dead center" and "bottom dead center". In this way, both pistons remain in contact with the mixing element.
- 3) Set the mode selector to "remote". In this way, the drive mechanism goes down by gravity.
- 4) Loosen the lock nut on the adjustment rod above the cpRMX.
- 5) Adjust the screw to the desired volume indicated on the RMX program.
- 6) Re-tighten the lock nut.
- 7) Perform the following actions: 1) and 2) in order to check the minimum and maximum volume indication. Correct the setting if necessary. The measurement error should not be more than $\pm 0.1 \text{ cm}^3$.

2nd Initialization of the cpRMX:

The aim is to get the value of the volume corresponding to the bottom stop of the RMX which will be used during the operation of the RMX.

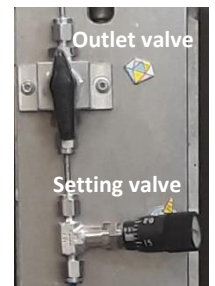
For this operation, the mode selector must be on "remote".

- 1) Click on "initialize".

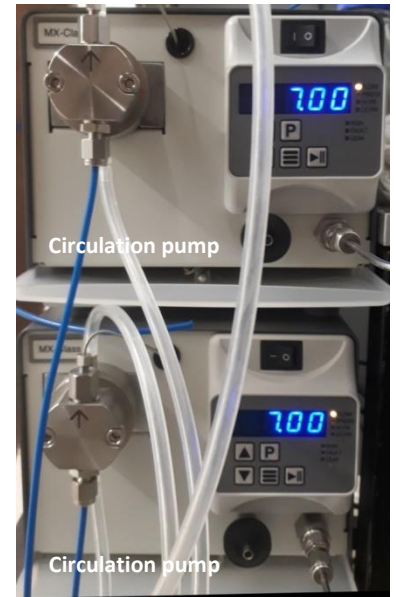
Filling the RMX:

For this operation the method selector will preferably be on "local", the mechanism brought into abutment downwards.

- 1) Open the outlet valve.
- 2) Sufficiently open the regulating valve.
- 3) Put each circulation pumps inlet pipe in a container containing the part of the sample provided. As well as the outlet pipe in another container.



- 4) Ensure that the pressures maximum circulation pumps are set to 100bar.
- 5) Switch on the pumps with the flowrate ratio required to obtain the right mixture by selecting high flowrates in order to reduce the filling time.
- 6) Wait for the sample to start coming out of the RMX.
- 7) Close the valve at the RMX outlet.
- 8) Wait until the pressure exceeds 20 bar in the RMX chamber.
- 9) Open the outlet valve.
- 10) Adjust the flowrates of the circulation pumps to the operating values.
- 11) Turn the adjusting valve knob to obtain a residual pressure of approx. 10 to 20 bar.



Stop the circulation pumps.

RMX works:

For this operation, the method selector must be on "Remote".

- 1) If necessary, change the destination folder and / or the name of the recording file using the "folder \ file" field. The name of the file will automatically be time stamped.
- 2) In "Speed SetPoint" set the piston displacement speed setpoint in cm^3/min .
- 3) In "dTime measure" set the time interval between measurements in ms. The minimum increment is 10 ms.
- 4) In "Duration" set the maximum time of the experiment in seconds.
- 5) The "Number of measures per cycle" field is for information only. If you want to change this value, you have to act on "dTime measure". To start up circulation pumps (the debits planned for the experiment must be settled beforehand).
- 6) Wait for the pressure in the RMX chamber to stabilize.
- 7) Click on "Start RMX".
- 8) Check for a few minutes that the "Valve" indication does not reach 100% (indicated by the "Valve saturation" indicator).

If this happens, speed can't anymore be regulated. This is due to too high a "Speed SetPoint" value.

The mechanism goes back and forth at the prescribed speed until the maximum time of the experiment, or until you click on "Stop RMX".

Dysfunction:

The program fails to communicate with the control box:

- 1) Check if the control box is switched on.
- 2) Check whether the USB cable is properly connected between the control box and the pilot computer.
- 3) If necessary, press on the "Reset" button located on the control box.

The program loses communication with the control unit:

- 1) Find and open: "Gestionnaire de périphérique" (Device Manager).
- 2) Unwind: "Contrôleur de bus USB" (USB bus controller).
- 3) Right click on "dispositif de stockage de masse USB" → "désactiver l'appareil" (USB mass storage device → deactivate the device).
- 4) If necessary, press on the "Reset" button located on the control box.

The indication "Valve" hit 100% (indicated by the "Valve saturation" indicator):

Set the pressure regulator to a higher pressure or choose a "Speed SetPoint" lower value.

The "Local" mode has erratic operation:

It can happen after an emergency stop.

- 1) Execute a "Start RMX" or "Initialize" sequence in "remote" mode.
- 2) If necessary, stop and restart the "RMX_vertical" program and / or press the small "reset" button on the control box.

D Bibliography

- [1] W. Yu *et al.*, “Development of an Elongational-Flow Microprocess for the Production of Size-Controlled Nanoemulsions: Batch Operation,” *Macromolecular Reaction Engineering*, vol. 11, no. 1, Feb. 2017, doi: 10.1002/mren.201600024.

CHAPTER V

MICROFLUIDIC DEVICE FOR THIOETHER MICRON SIZE PARTICLES

OUTLINE

Preface.....	217
<i>A</i> Introduction	217
<i>B</i> Materials and Methods.....	219
1. Co-Flow Microfluidic Device for Production of Microparticles	219
2. Co-Flow Microfluidic Device for Production of Microrods.....	221
3. Control of particle size	222
4. Thiol-Ene Solution Formulation and Particles Characterization	223
<i>C</i> Results and Discussion.....	224
1. Thioether Microparticles.....	225
2. Thioether Microrods.....	232
<i>D</i> Conclusion	233
<i>E</i> Bibliography	235

Preface

In the previous chapters the formation of miniemulsion and latex was described by using elongational-flow devices and comparing with conventional simple shear device. In this chapter different morphologies of thioether particles are developed. Instead of nanoparticles, in the case of latex, microparticles and microrods are discussed in this chapter using microfluidic devices. The effect of viscosity of the continuous phase, along with the continuous and disperse phase flow rates on the particle diameter will be discussed.

A Introduction

Thiol-ene Thiol-ene click chemistry has received an extensive interest due to several advantages, which were extensively discussed in Chapter I. Among the benefits of this chemistry [1] is the very fast reactivity between the two monomers which can allow the rapid production of poly(thioether) particles. Another important advantage is the high polymerization yield with no side products.

Only few research groups decided to work with thiol-ene click chemistry in microfluidics. A first report was found in 2010 [2], where thiol-ene and thiol-yne microporous and nonporous functional beads were produced. They developed a homemade microfluidic device (Figure 5.1) and obtained monodisperse beads having a size between 210 and 600 μm (Figure 5.2). The continuous phase was either light mineral oil mixed with silicon-based non-ionic surfactant (ABIL EM-90) for the nonporous particles or water with SDS for the porous particles. While the disperse phase was a mono- or tetra-functional thiol combine with mono-, bi- or tri-functional alkene or mono-, bi-functional alkyne.

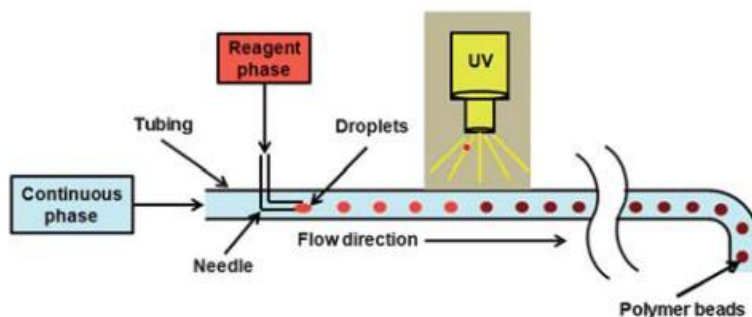


Figure 5.1. Schematic drawing of the microfluidic setup [2].

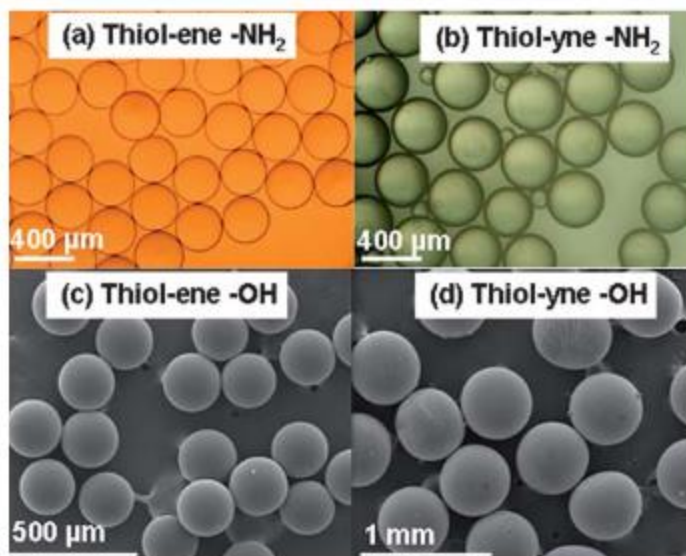


Figure 5.2. Optical (top) and SEM (bottom) images of the nonporous functional beads [2].

Later in 2017 D. V. Amato *et al.* [3], used microfluidics to produce microcapsules with thiol-ene click chemistry (Figure 5.3). They used a tri-functional thiol and either bi- or tri-functional alkene along with a photoinitiator as the dispersed shell phase. On the other hand, the material encapsulated was anhydride monomers, while the outer continuous phase was water with surfactant. The reaction was triggered under UV irradiation and the diameter of the microcapsules was found to be 300 μm .

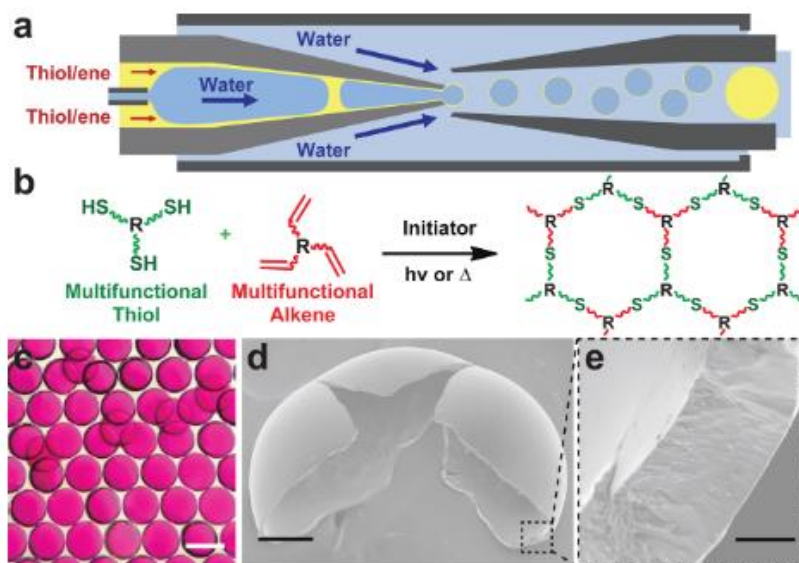


Figure 5.3. a) Glass capillary microfluidic device, b) thiol-ene reaction, c) optical microscope image, d, e) SEM images of dried microcapsules [3].

Finally, in 2021 a research group [4] developed a co-axial microfluidic chip and produced different morphologies of thiol-ene chemistry by applying UV irradiation (Figure 5.4). Starting with particles that had a diameter of approximately 0.6 mm, followed by fibers of approximately 0.4 mm diameter and finally thioether rods of 2 mm length and 0.5 mm diameter (Figure 5.5).



Figure 5.4. Co-axial microfluidic chip [4].

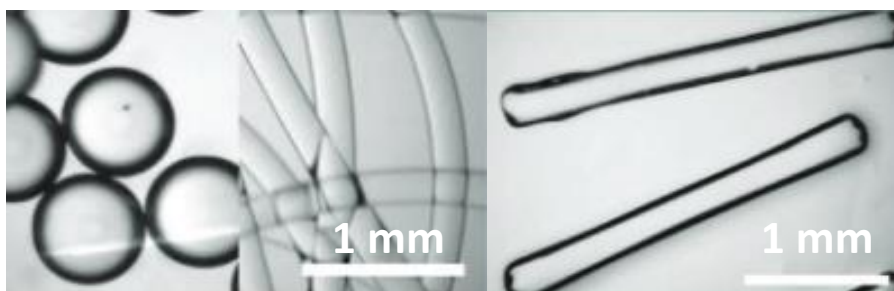


Figure 5.5. Optical microscope images of microparticles and microfibers [4].

➤ Materials and Methods

1. Co-Flow Microfluidic Device for Production of Microparticles

The co-flow microfluidic device that was used for the production of microparticles is presented in figure 5.6. It comprises of two syringe pumps (PHD 200, Harvard Apparatus) one for the continuous phase and a second one for the disperse phase. Each syringe was connected with a PTFE tube (ID 1.06 mm) that was coming in contact with the other one using a T-junction (P-728-01). In the T-junction the PTFE tube of the dispersed phase was connected with a fused silica capillary in order to achieve a smaller particle diameter. Two different capillaries were used and evaluated, one of 75 μm and one 100 μm inner diameter. The exit of the capillary was fixed on the left side of the T-junction, while the continuous phase was flowing from the top of it. The two phases were coming in contact in the outlet PTFE tube, where the tip of the glass capillary was centralized. To reassure that the capillary was correctly centralized, and the droplets were able to form, an optical microscope (Eclipse 80i, Nikon) was used. When the dispersed

phase exited the glass capillary, it came in contact with the continuous phase. This resulted to the shearing of the disperse phase by the continuous phase and ultimately led to the droplet formation. Once the droplets are formed thanks to the droplet generator (T-junction), the downstream PTFE tube is placed inside a linear flow photoreactor, that was described in Chapter II. This photoreactor comprises of a 22 cm stainless steel tube, which accommodates two T-junctions on both ends, where the UV light is applied. The UV light (Lightning-cure LC8, Hamamatsu) wavelength was fixed at 360 nm and was chosen to be compatible with the photoinitiator that was used. Further information about the residence time in relation with the flow rate adjusted on the syringe pump can be found in Chapter II.

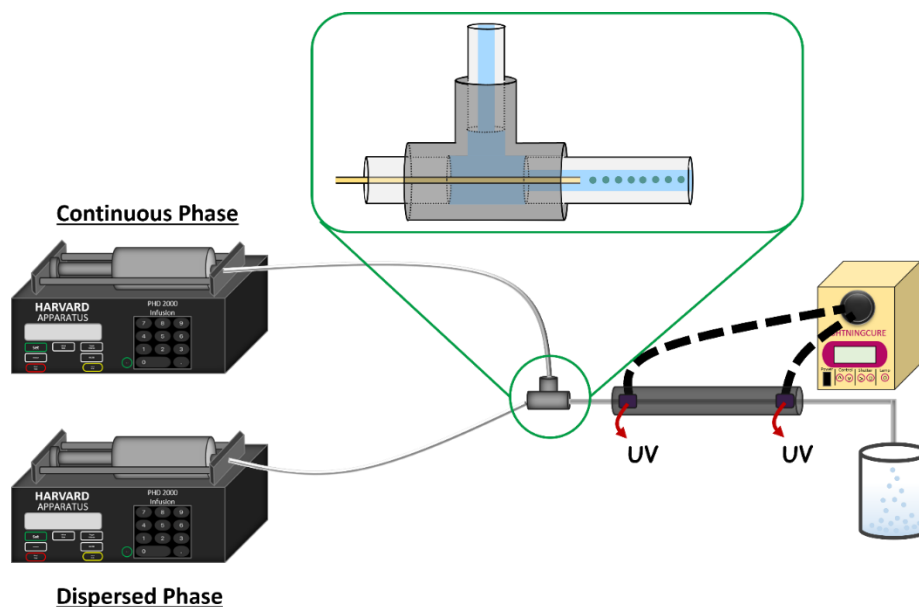


Figure 5.6. Co-flow microfluidic device for production of microparticles.

Two dimensionless numbers are crucial for the droplet formation, the Reynolds number and the capillary number. Both are already described in Chapter I. As a reminder the equations are shown below. Starting with the Reynolds number:

$$Re = \frac{\rho v D}{\mu} \quad (5.1)$$

where ρ is the density of the fluid, v the mean velocity of the fluid, D the characteristic dimension of the flow, usually the width of the channel, and μ is the dynamic viscosity of the fluid. While the capillary number is defined as:

$$Ca = \frac{\mu V}{\sigma} \quad (5.2)$$

where σ is the interfacial tension between the two fluids. Any change on the aforementioned measures can influence the particle size.

2. Co-Flow Microfluidic Device for Production of Microrods

By slightly altering the design of the device, it is possible to obtain microrods instead of microparticles. Keeping the same two syringe pumps and T-junction, the dispersed phase was forced to flow in a fused silica capillary (Postnova) of 100 μm inner diameter. Conversely to the previous device, the exit tube is by now connected with a second PTFE tube (OD 1.6 mm, ID 0.3 mm) so as the inner diameter of the former be equal with the outer diameter of the second tube (Figure 5.7). In this way once the droplets were formed at the tip of the capillary, they were forced to flow in the smallest diameter PTFE tube. This causes the deformation of the droplets which results in the production of elongated droplets. The latter are then polymerized in line using the linear photoreactor that was described before to form nanorods (Figure 5.7).

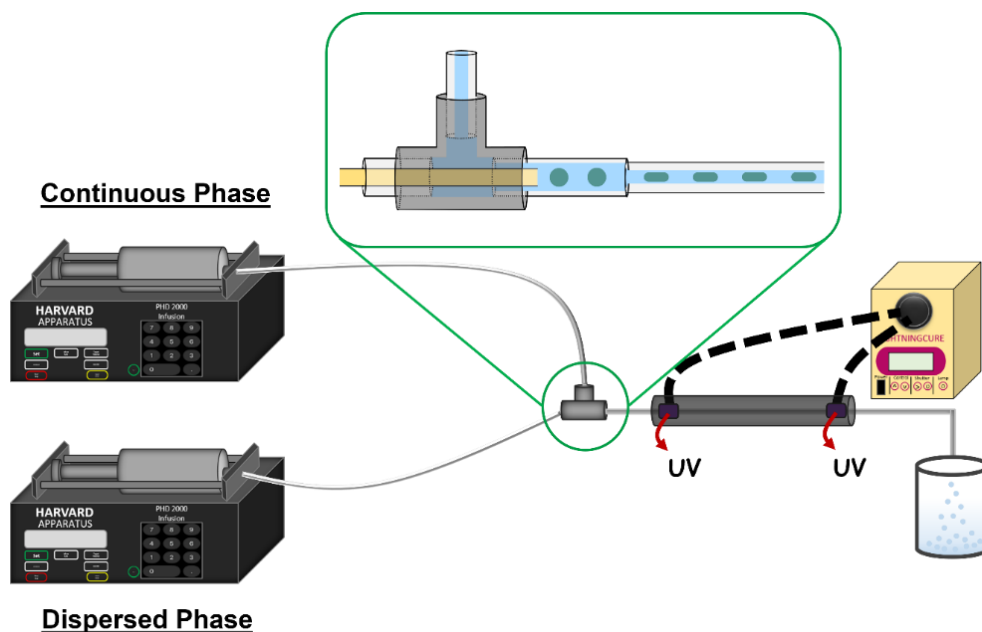


Figure 5.7. Co-flow microfluidic device for production of microparticles.

3. Control of particle size

Although not directed to the production of thioether micron size particles, our group developed a microfluidic process for the production of size controlled microdroplets as precursors for polymeric microparticles. This process was adapted as mentioned above for the production of thioether micron size particles. Thus, it seems interesting to highlight here some key aspects of the control of particle size. On the foremost, the capillary number ratio between the continuous and disperse phases (Ca_c / Ca_d) was found to have the strongest effect on the particle size [5]. Indeed, particles of methyl methacrylate (MMA) mixed with glycidyl methacrylate (GMA), along with dimethacrylate ethylene glycol (DIMAEG), were produced using different concentrations of methyl cellulose in water as continuous phase. Figure 5.8 shows the effect of Ca_c / Ca_d on the particle diameter. Different viscosities of the continuous phase were also tested and for all of them it was obtained a master curve that exhibits a decrease in particle size when the capillary number ratio increases.

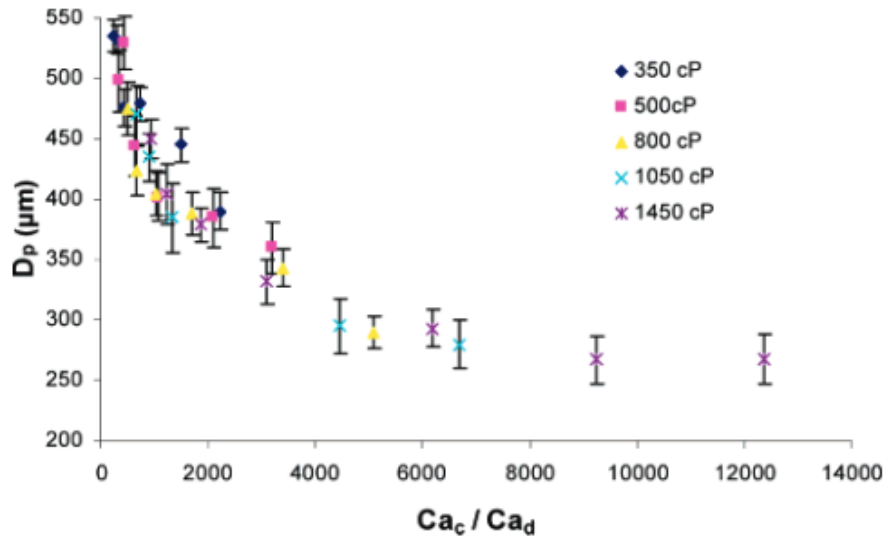


Figure 5.8. Influence of the capillary number ratio of the continuous and disperse phase for different viscosities [5].

Hence, taking into consideration the ratio Ca_c / Ca_d , one can foresee the particle diameter behavior.

$$\frac{Ca_c}{Ca_d} = \frac{\mu_c V_c}{\mu_d V_d} \quad (5.3)$$

The fluids mean velocity is defined as:

$$v = \frac{Q}{A} \quad (5.4)$$

Q is the flow rate and A is the inner cross-section of either the PTFE tube (continuous phase) or capillary (disperse phase) that:

$$A = \frac{\pi d^2}{4} \quad (5.5)$$

where d is the inner tube or capillary diameter.

4. Thiol-Ene Solution Formulation and Particles Characterization

For all the experiments a trifunctional thiol (trimethylolpropane tris(3-mercaptopropionate), TMPTMP, Sigma-Aldrich, 95%) along with a bifunctional alkene (diallyl phthalate, DAP, TCI Chemicals, 98%), and the photoinitiator (diphenyl (2,4,6-trimethylbenzoyl), DTPO, TCI Chemicals). The choice of these two multifunctional monomers was done in order to obtain solid crosslinked particles. Concerning the continuous phase, distilled water was admixed with a viscosifier, hydroxyethyl cellulose (Mw= 720,000 g/mol), in different concentrations such as to change its viscosity and evaluate its influence on particle size. The table below shows the experimental formula.

Table 5.1. Solution formulation.

Continuous Phase	Dispersed Phase
Continuous Phase Distilled Water	Thiol Trimethylolpropane Tris(3-mercaptopropionate) (TMPTMP) 10 wt%
Viscosifier Hydroxyethyl cellulose Different concentrations 0.5 – 1.5 wt%	Alkene Diallyl phthalate (DAP) 10 wt%
	Photoinitiator Diphenyl (2,4,6-trimethylbenzoyl) phosphine oxide (DTPO) 2 wt% / C _{monomers}

The increased number of functional groups is expected to form more stable particles due to the high crosslinking density between the three functional thiol and the bifunctional alkene.

A numerical microscope Keyence, VHX-J100T, was used to observe the microparticles and microrods as well as to measure their sizes.

Additionally, the viscosities of the different phases under study (continuous phases of various viscosifier amounts and dispersed phase) were measured at 19°C (temperature controller CT52, Schott) using a viscosity measuring unit AVS 360 (Schott) monitored by an electronic controller (Schott TITRONIC universal). Various viscometers were needed to measure the kinematic viscosities (Table 5.2). This method was based on the determination of the time required for the solution to flow through a capillary. Each measurement was repeated eight times and a mean value for the flow time was taken. This time was then correlated to the kinematic viscosity ν as follows:

$$\nu = K (t-H) \quad (5.6)$$

where K is a constant related to the capillary (mm^2/s^2), t the average flow time (s) and H the Hagenbach correction of time (here, $H = 0$ s).

Table 5.2. Viscometer used to measure the kinematic viscosities of the different solutions of this project.

Viscometer Type	K (mm^2/s^2)	Maximum Kinematic Viscosity Measurable (mm^2/s)
Micro-Oswald	0.01064	1.2
Micro-Ubbelohde	1.039	10
Ubbelohde	3.079	3000

The values of the dispersed and continuous phases dynamic viscosities, μ_d and μ_c respectively, were then easily determined from their respective volumetric mass (ρ) since $\mu = \rho \nu$.

Results and Discussion

In this thesis, focus will be given on producing thioether micron size particles using the previously described microfluidic device. The impact of the continuous and

dispersed phase flow rate as well as the viscosity of the continuous phase on the particle size will be discussed.

1. Thioether Microparticles

Since the thiol-ene chemistry was never tested before with our microfluidic process, the influence of the flow rate of continuous (Q_c) and disperse (Q_d) phases was investigated. To have a better estimation of the overall effect of both flow rates and understand which one plays the most crucial role on the droplet diameter, the ratio Q_c / Q_d was plotted in all figures.

A first set of experiments were conducted using a 100 μm inner diameter capillary. In order to be able to understand which flow rate has a higher impact on the particle diameter control, one flow rate was kept constant and the second one was changing. Figure 5.9 represents the experiments that were conducted when the dispersed phase flow rate was constant $Q_d = 3 \mu\text{L}/\text{min}$ and the continuous phase flow rate was changing. Variations on the latter were done from $Q_c = 150 \mu\text{L}/\text{min}$ up to $Q_c = 700 \mu\text{L}/\text{min}$.

Figure 5.9 revealed the decrease of the size down to 275 μm , from 442 μm , when Q_c was increasing from 150 $\mu\text{L}/\text{min}$ to 700 $\mu\text{L}/\text{min}$. This complies well with the fact that the droplet size results from the competition of the shear force imposed by the flow of the continuous phase and the surface tension. Note that the latter has a fixed value for a given continuous and disperse phases system. The higher the former, the lower is the particle size. Thus, when the Ca_c / Ca_d increases, e.g. when the continuous phase flow rate is increased, the shear force imposed on droplet formation is higher which induces the production of smaller particles. This means that the particle size can be controlled just by adjusting the flow rate of the continuous phase.

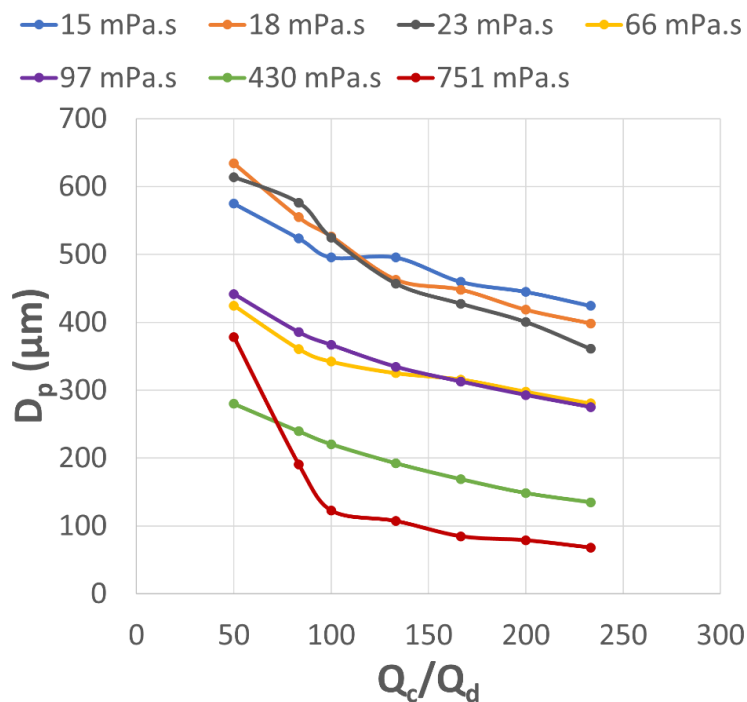


Figure 5.9. Evolution of the mean particle diameter by keeping the dispersed phase flow rate constant and varying the dynamic viscosity (μ_c) and flow rate of the continuous phase, $Q_d = 3\mu\text{L}/\text{min}$, capillary inner diameter = $100\mu\text{m}$.

Another way to control the particle diameter was to change the viscosity of the continuous phase. For this reason, viscosity measurements were performed, and the dynamic and kinematic viscosities were determined and reported in Table 5.3. It is observed that the higher the mass concentration of hydroxyethyl cellulose in the aqueous continuous phase, the higher is the viscosity. Indeed, high molecular weight polymers are known to be efficient viscosifiers in food industry for instance.

Table 5.3. Dynamic and kinematic viscosity the continuous and dispersed phases

Continuous Phase		
Hydroxyethyl cellulose concentration c (wt%)	Dynamic viscosity μ_c (mPa.s)	Kinematic viscosity ν (mm^2/s)
0.5	15	$1.6 \cdot 10^{-2}$
0.6	18	$1.8 \cdot 10^{-2}$
0.7	23	$2.3 \cdot 10^{-2}$
0.8	66	$6.7 \cdot 10^{-2}$
1	97	$1.5 \cdot 10^{-1}$
1.2	430	$4.3 \cdot 10^{-1}$
1.5	751	$7.7 \cdot 10^{-1}$
Dispersed Phase		
	Dynamic viscosity μ_d (mPa.s)	Kinematic viscosity ν (mm^2/s)
	5.7	$4.8 \cdot 10^3$

As such, at a given value of Q_c / Q_d (*i.e.* 233), one observes in Figure 5.9 a strong decrease of the particle diameter from roughly 400 to 100 μm . This observation complies well with the increased shear force when the continuous phase viscosity is increasing. Indeed, the shear force exerted on the forming droplet is simply proportional to the viscosity.

The mean particle size reported in Figure 5.9 was evaluated thanks to a numerical microscope and reported in Table 5.4. As an example, Figure 5.10 presents two images of the diameter determination of a bunch of particles produced under two different concentrations of viscosifier (0.6 and 1.5 wt%). In addition to showing that the particle diameter is dependent of the continuous phase viscosity, this image reveals that all particles are highly monodisperse in size as it can be seen also in Figure 5.11.

Table 5.4. Flow rates and particle diameter for different concentrations of hydroxyethyl cellulose and an inner capillary diameter of 100 μm (data reported in Figure 109)

Flow Rates ($\mu\text{L}/\text{min}$)			Diameter (μm)						
Q_c	Q_d	Q_c/Q_d	C=0.5 wt%	C=0.6 wt%	C=0.7 wt%	C=0.8 wt%	C=1 wt%	C=1.2 wt%	C=1.5 wt%
150	3	50	575	634	614	424	442	280	378
250	3	83	523	555	576	361	385	239	191
300	3	100	496	527	525	342	367	220	123
400	3	133	496	463	457	325	334	192	107
500	3	167	459	448	427	316	313	169	85
600	3	200	445	418	400	298	293	148	79
700	3	233	424	398	361	280	275	135	68

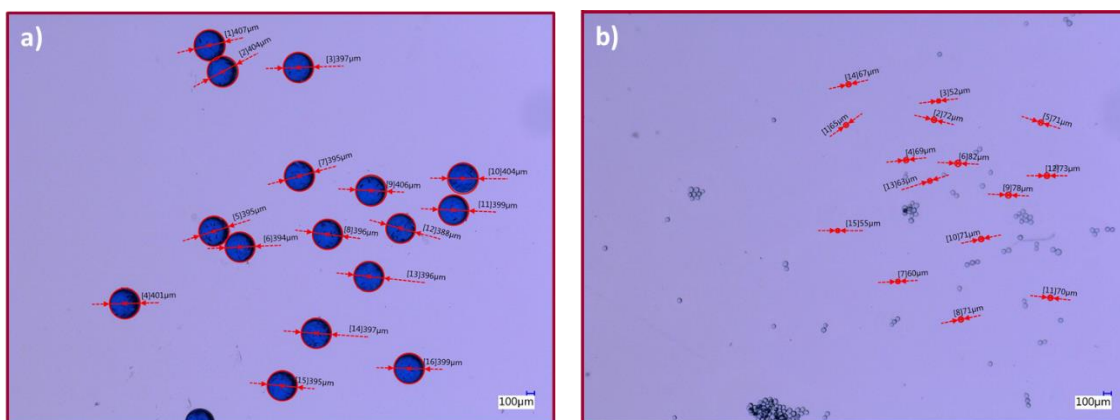


Figure 5.10. Numerical image of thioether microparticles produced with capillary ID = 100 μm , $q_d = 3 \mu\text{L}$, $q_c = 700 \mu\text{L}/\text{min}$ and a) C = 0.6 wt%, PDI = 0.12 and b) C = 1.5 wt%, PDI = 0.09.

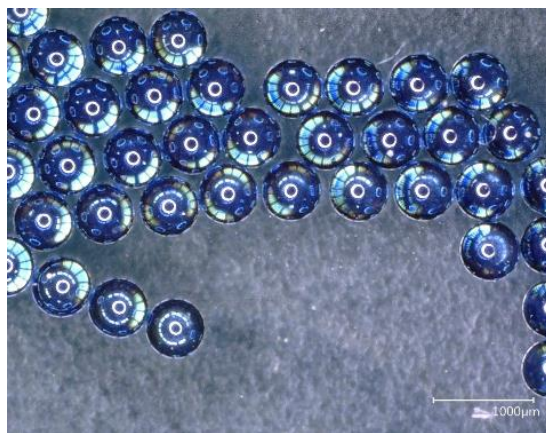


Figure 5.11. Numerical image of thioether 575 μm microparticles PDI = 0.04 ($Q_d = 3 \mu\text{L}/\text{min}$, $Q_c/Q_d = 50$, $C = 0.5 \text{ wt}\%$)

As mentioned in the previous part, the capillary number strongly depends on the viscous and interfacial forces. Research has shown that the particle diameter changes when the ratio Ca_c / Ca_d varies [5]–[7] (Equation 5.3). For this reason, Figure 5.12 presents the variation of the data reported in Figure 5.9 as a function of Ca_c / Ca_d . It is observed that independently of the continuous phase viscosity, all the obtained particle diameters fall down on a single master curve. This comes in agreement with previous research conducted by our group on another chemical system (free radical polymerization) (Figure 5.8). Thus, it is highlighted that despite its own specificities the thiol-ene chemistry can be implemented in droplet and that the resulting droplet size is only affected by the hydrodynamic conditions.

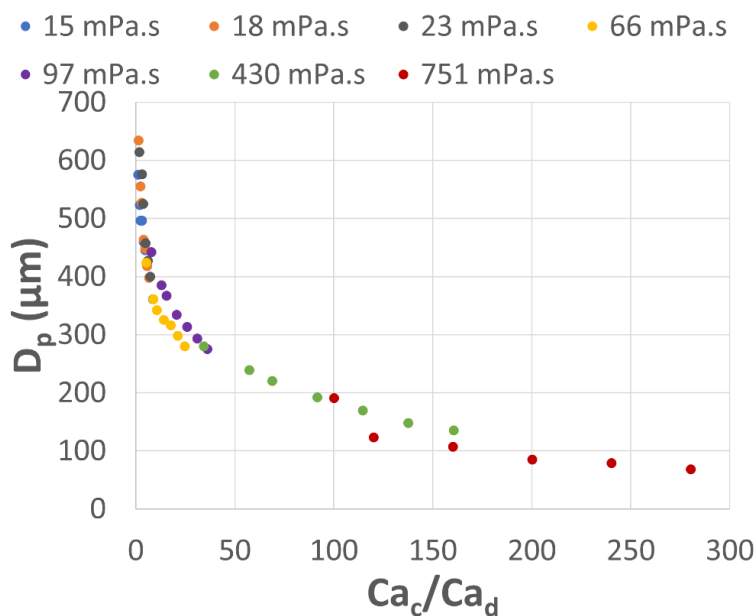


Figure 5.12. Master curve of the droplet diameter in relation with the capillary number ratio Ca_c/Ca_d , for different dynamic viscosities (μ_c) of the continuous phase, $Q_d = 3 \mu\text{L}/\text{min}$, capillary inner diameter = $100 \mu\text{m}$

It was observed from Figure 5.12 that the particle diameter was strongly influenced by the ratio Ca_c / Ca_d . In more detail, the higher the capillary number ratio the smaller is the particle diameter. However, we can question ourselves about the effect of the capillary diameter.

Therefore, a smaller capillary (ID = 75 μ m) was used. The flow rate of the continuous phase was the one parameter that was varying while the other parameter was the viscosity of the continuous phase. Regarding the first one, different Q_c were tested, and the ratio of Q_c / Q_d was altered in order to observe the particle size (Figure 5.13). The same trend as with the bigger capillary was observed. More specifically, for the 1 wt% concentration of hydroxyethyl cellulose the initial particle size was 381 μ m, while increasing Q_c led to a strong decrease down to 149 μ m (Figure 5.14).

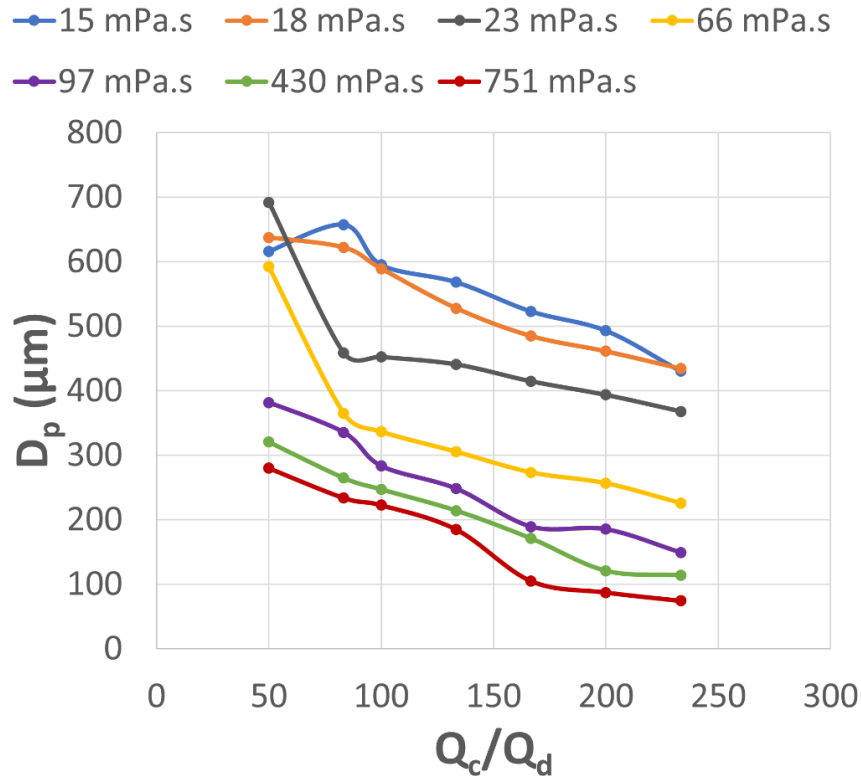


Figure 5.13. Evolution of the particle diameter by keeping the dispersed phase flow rate constant and varying the dynamic viscosity (μ_c) and flow rate of the continuous phase, $Q_d = 3\mu\text{L}/\text{min}$, capillary inner diameter = 75 μm .

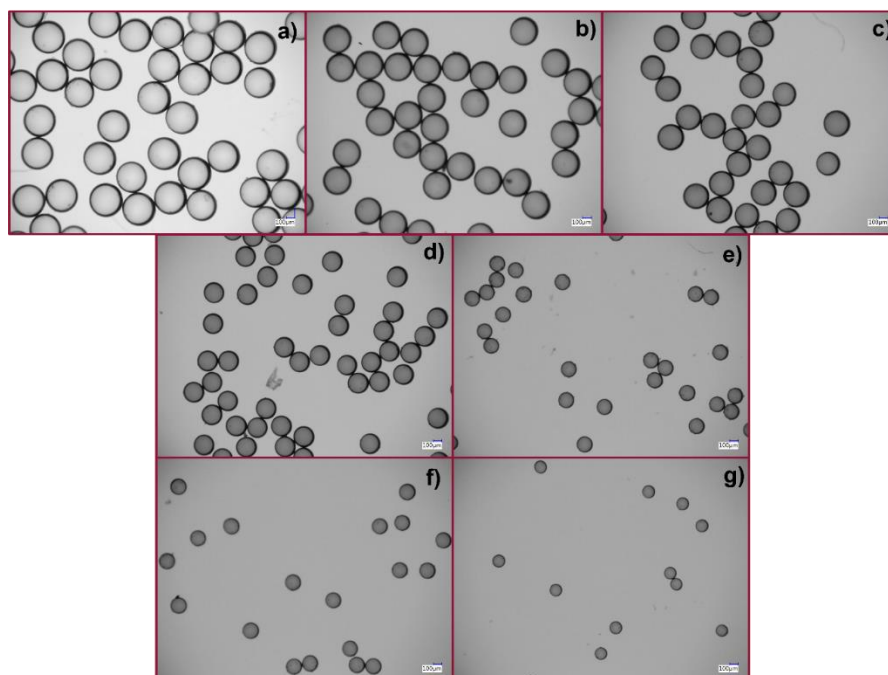


Figure 5.14. Numerical images of particles produced for a hydroxyethyl cellulose concentration of 1wt%, a disperse phase flow rate of 3 $\mu\text{L}/\text{min}$ and different flow rate ratios: 50 (A), 83 (B), 100 (C), 133 (D), 167 (E), 200 (F) and 233 (G).

Following the variation of Q_c , the amount of hydroxyethyl cellulose in the continuous phase was increased in order to plot the diameter behavior. The same solutions as before was used, whose viscosities can be found on Table 5.5. A decreasing trend of the particle size when the viscosity was increased was observed especially in higher Q_c / Q_d ratios. The highest diameter was found to be at 434 μm for 0.5 wt% of hydroxyethyl cellulose, while the smallest was at 74 μm corresponding to the highest viscosity and Q_c / Q_d values. The minimum diameter obtained was roughly equal to the inner diameter of the capillary, which could indicate the beginning of a threshold zone. In this zone the diameter of the particles does not get affected from a further increase of Q_c / Q_d and a plateau is expected to be reached. This threshold zone is strongly depending on the inner diameter of the capillary. Indeed, for the 100 μm capillary, the threshold value of the flowrate ratio was around 100, while for the 75 μm it appears around 167. The Table 5.5 comprises all the diameters and flow rates obtained with all the different viscosities and flow rates.

Table 5.5. Flow rates and particle diameter for different concentrations of hydroxyethyl cellulose and an inner capillary diameter of 75 μm (data reported in Figure 113).

Flow Rates ($\mu\text{L}/\text{min}$)			Diameter (μm)						
Q_c	Q_d	Q_c/Q_d	C=0.5 wt%	C=0.6 wt%	C=0.7 wt%	C=0.8 wt%	C=1 wt%	C=1.2 wt%	C=1.5 wt%
150	3	50	616	637	692	592	381	320	280
250	3	83	657	622	458	365	335	265	234
300	3	100	595	589	452	336	283	247	222
400	3	133	568	528	441	305	248	214	185
500	3	167	523	485	414	273	189	171	105
600	3	200	493	461	393	256	185	121	87
700	3	233	430	434	368	226	149	114	74

Since experiments showed an important relation of the particle diameter with the capillary number ratio Ca_c / Ca_d for capillary inner diameter 100 μm , the same graph was also conducted for capillary inner diameter 75 μm (Figure 5.15).

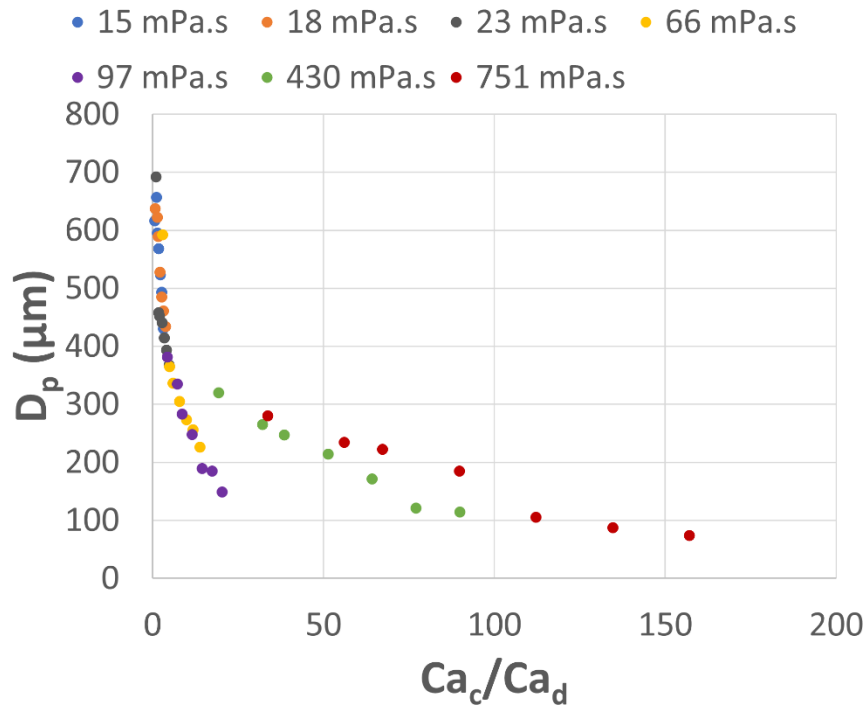


Figure 5.15. Master curve of the droplet diameter in relation with the capillary number ratio Ca_c/Ca_d , for different dynamic viscosities (μ_c) of the continuous phase, $Q_d = 3\mu\text{L}/\text{min}$, capillary inner diameter = 75 μm .

Figure 5.15 revealed the same dependence of the ratio Ca_c / Ca_d on the particle diameter, as with the capillary of inner diameter 100 μm . The particle diameter was decreasing when the ratio of capillary number was increasing. However, for the two higher viscosities ($\eta = 430$ and 850 mPa.s) the curves do not align with other lower viscosities curves. This behavior could potentially be attributed to some experimental or diameter determination errors.

The comparison between the results obtained with the two different capillary diameters reveals that the smallest particle size is obtained with the 75 μm capillary when all other parameters are kept the same (continuous phase viscosity and Q_c / Q_d). For example, for 1.2 wt% concentration of hydroxyethyl cellulose and the highest $Q_c = 700 \mu\text{L}/\text{min}$, the particles prepared using the 75 μm ID capillary had a diameter of 114 μm . On the contrary, the particles prepared with the 100 μm capillary have a higher size, close to 135 μm . This observation complies well with the fact that at a given flow rate ratio, the smaller the capillary inner diameter, the higher is the velocity of the dispersed phase.

To conclude, two capillaries with 75 and 100 μm inner diameters were used so as to achieve a control on the particle size. Two parameters played a key role, the flow rate ratio, Q_c / Q_d , and the continuous phase viscosity. Both parameters affect the size in a way that their increase globally lowered the particle diameter. Finally, the ratio of the capillary number, Ca_c / Ca_d , was also crucial to the diameter control since any increase of this ratio led to a decrease of the particle diameter.

2. Thioether Microrods

A different morphology of thioether micron size particles was attempted by slightly modifying the design of the process (Figure 5.7). To the best of our knowledge only one group reported thioether microrods so far and decision was made to evaluate whether thioether microrods can be produced with the specific chemical system under study. The system was the same as for the microparticles and can be seen on Table 5.1. Several clogging problems were encountered during the experiments but ultimately microrods were successfully produced. The obtained microrods appeared to be resistant to any solvent (*i.e.* acetone, ethanol and dichloromethane) and all exhibited the same length and width distribution. More specifically, the average length and width were kept constant to 1551 and 350 μm respectively (Figure 5.16).

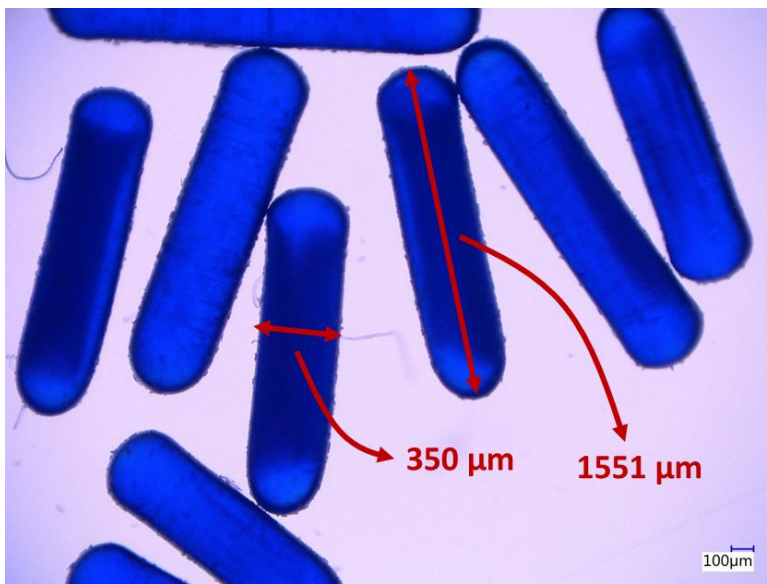


Figure 5.16. Thioether microrods produced with $Q_c = 400 \mu\text{L}/\text{min}$ and $Q_d = 15 \mu\text{L}/\text{min}$.

It has been previously reported from our group [8] that the characteristics of the rods can be tuned by altering the dispersed phase flow rate. It is expected that thiol-ene click chemistry could provide the same control but the fast reactivity between the thiol and alkene needs to be carefully monitored in order to avoid any clogging problems.

D Conclusion

Microfluidics have been used in order to produce thioether micron size particles. A specific process developed in our lab was described for the production of thioether microparticles and microrods. A single device was used for both morphologies that were obtained upon a light modification in the design of the droplet generator. Regarding the microparticles, two capillaries of different size were used and compared. In both cases the effect of the continuous phase flow rate and viscosity were investigated. The smallest capillary (I.D. $75 \mu\text{m}$) was the one providing the smallest particles. An identical tendency of the particle diameter was observed for both capillaries. More specifically, the particle diameter showed a decreasing behavior when the continuous phase flow rate was higher, while the same behavior appeared with the increase of the viscosity of the continuous phase. Combining the two effects in a single operating parameter expressed as the continuous to dispersed capillaries ratio gives a master curve. The latter can be used to predict

the particle diameter for a given set of operating parameters or to set these parameters at specific values to target a given particle size.

Finally, in the case of microrods, a first attempt was made to obtain thioether microrods that had an elongated shape. Despite the clogging difficulties that were fixed at the very end, the microrods produced using thiol-ene chemistry give a promising perspective for further investigations.

Ξ Bibliography

- [1] H. C. Kolb, M. G. Finn, and K. B. Sharpless, "Click Chemistry: Diverse Chemical Function from a Few Good Reactions," *Angewandte Chemie - International Edition*, vol. 40, no. 11, pp. 2004–2021, 2001, doi: 10.1002/1521-3773(20010601)40:11<2004::AID-ANIE2004>3.0.CO;2-5.
- [2] R. A. Prasath, M. T. Gokmen, P. Espeel, and F. E. du Prez, "Thiol-ene and thiol-yne chemistry in microfluidics: A straightforward method towards macroporous and nonporous functional polymer beads," *Polymer Chemistry*, vol. 1, no. 5, pp. 685–692, Jul. 2010, doi: 10.1039/c0py00041h.
- [3] D. v. Amato, H. Lee, J. G. Werner, D. A. Weitz, and D. L. Patton, "Functional microcapsules via thiol-ene photopolymerization in droplet-based microfluidics," *ACS Applied Materials and Interfaces*, vol. 9, no. 4, pp. 3288–3293, Feb. 2017, doi: 10.1021/acsami.6b16382.
- [4] J. Jiang, G. Shea, P. Rastogi, T. Kamperman, C. H. Venner, and C. W. Visser, "Continuous High-Throughput Fabrication of Architected Micromaterials via In-Air Photopolymerization," *Advanced Materials*, vol. 33, no. 3, Jan. 2021, doi: 10.1002/adma.202006336.
- [5] C. Serra, N. Berton, M. Bouquey, L. Prat, and G. Hadziioannou, "A predictive approach of the influence of the operating parameters on the size of polymer particles synthesized in a simplified microfluidic system," *Langmuir*, vol. 23, no. 14, pp. 7745–7750, 2007, doi: 10.1021/la063289s.
- [6] M. Seo, Z. Nie, S. Xu, P. C. Lewis, and E. Kumacheva, "Microfluidics: From dynamic lattices to periodic arrays of polymer disks," *Langmuir*, vol. 21, no. 11, pp. 4773–4775, May 2005, doi: 10.1021/la050070p.
- [7] D. F. Zhang and H. A. Stone, "Drop formation in viscous flows at a vertical capillary tube," *Physics of Fluids*, vol. 9, no. 8, pp. 2234–2242, 1997, doi: 10.1063/1.869346.
- [8] Z. Chang, C. A. Serra, M. Bouquey, L. Prat, and G. Hadziioannou, "Co-axial capillaries microfluidic device for synthesizing size- and morphology-controlled polymer core-polymer shell particles," *Lab on a Chip*, vol. 9, no. 20, pp. 3007–3011, 2009, doi: 10.1039/b913703c.

CONCLUSIONS AND PERSPECTIVES

A Context and Objectives

A variety of emulsification devices were reported in the literature. Ultrasound generators, rotor-stator mixers, static mixers and high-pressure homogenizers are widely known for their use in laboratory and industrial scales. However, several disadvantages can be reported, such as the unavailability of ultrasound generators in larger scale productions, poor diameter control for the rotor-stator mixers, pressure drop problems in the case of static mixers and high energy consumption using high-pressure homogenizers.

On the contrary, elongational flow-based devices shown an increased interest. It is already reported that these devices are able to provide better mixing and diameter control by consuming a smaller amount of energy, i.e. by working under low pressure, as compared to the conventional emulsification devices.

Thiol-ene click chemistry was used in this research so as to maintain a droplet and particle diameter control with the least energy requirements. Thiol-ene click chemistry provides several benefits among which the fast reactivity and the absence of side products during the reaction.

In this thesis, four objectives have been successfully achieved:

- The diameter control of thiol-ene miniemulsion and poly(thioether) latex by using an elongational-flow emulsification device in conjunction with the flow photoreactors,
- The production of thioether latex by a low energy consumption device that is friendlier to the environment as compared to the conventional emulsification devices,
- The design and building of a continuous elongational-flow emulsification device
- The use of a microfluidic device to acquire thioether microparticles and microrods with tunable particle diameter.

➤ Results

1. Chapter 3: From thiol-ene miniemulsion to thioether latex nanoparticles

The main goal of this research was to develop low energy emulsification devices in order to produce monomodal size-controlled (60 – 400 nm) poly(thioether) latex. **Two novel elongational-flow reactor and mixers** were used (Figure 6.1). Both devices had the same working principle which described a reciprocating elongational flow, that goes through an abrupt contraction and leads to a strong elongational flow. This allowed the **highly efficient dispersive mixing** of the emulsion even at moderate pressures. One of the main differences between the two devices relies on the operating pressure, on the micro elongational-flow reactor and mixer the operating pressure was 2 bar, while it was 6 bar on the pneumatic elongational-flow reactor and mixer. The latter could easily be used to scale up the process since the volume that could be added was almost two times more than the former one.

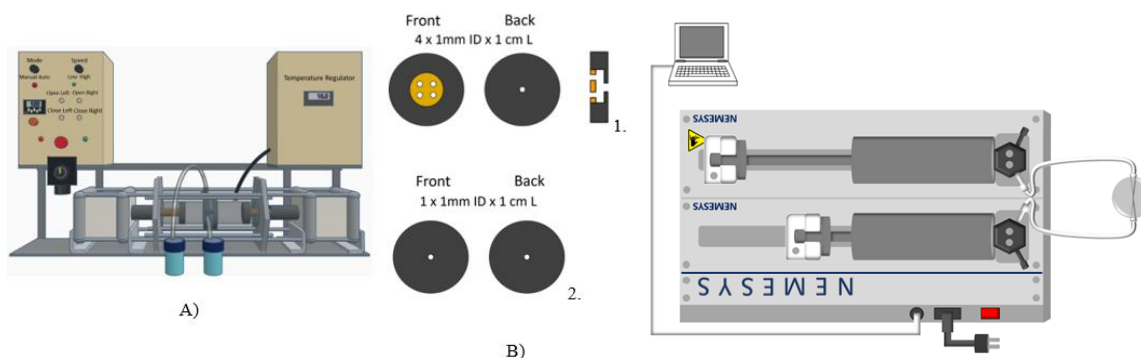


Figure 6.1. (left) Pneumatic elongational-flow reactor and mixer (pRMX) with the different mixing elements, (right) Micro elongational-flow reactor and mixer (μ RMX).

Three different thiol monomers were compared and described. A tetra-functional pentaerythritol tetrakis(3-mercaptopropionate) (PETMP) as well as two bi-functional thiols 1,2-Ethanedithiol (EDT) and 2,2'-(Ethylenedioxy)diethanethiol (EDDT) were mixed with a bi-functional alkene diallyl phthalate (DAP). With the pneumatic elongational-flow reactor and mixer (pRMX), two different mixing element geometries were investigated, one with four holes on the front and one hole on the back and a second one with a single hole throughout the width of the

mixing element (Figure 6.1. left). Finally, the influence of the oxygen of the atmosphere was also investigated by changing the experimental atmosphere from ambient to inert.

Starting with the **tetra-functional thiol PETMP**, that was more prone to develop crosslinked materials when combined with the bi-functional alkene, the effect of the number of cycles on the droplet size was investigated.

When the **four-holes mixing element** and ambient atmosphere was used a control of the diameter was achieved with the minimum droplet size to be close to 120 nm, while the droplets did not exceed 150 nm in size. Experiments were also conducted by changing the composition of the miniemulsions in order to investigate the influence of the amount of radical inhibitor and surfactant on the droplets' diameter. All experiments revealed a maximum of 150 nm while the minimum diameter was close to 100 nm. It was also found that some latex had a diameter close to the one of the droplets, while other had a higher size.

However, since clogging problems were encountered and a premature polymerization (with sometimes 100% of polymerization yield) occurred during emulsification, some changes needed to be done.

An improvement of the process was established by changing the mixing element and using the one with the **single hole**. Additionally, the ambient atmosphere was changed into inert atmosphere in order to avoid the presence of oxygen that can react with the thiol and initiate the free radical polymerization. The resulted thiol-ene miniemulsion showed a less premature polymerization during emulsification with maximum 60 % yield. However, a lower number of cycles was tested, and it was found that the droplet diameter was reduced when the cycles were above 40, with a minimum of 145 nm diameter.

Two **linear thiols** were used but the EDT was much more volatile as compared to the EDDT, which limited its research. The more volatile thiol was mixed using the micro elongational-flow reactor and mixer (μ RMX, Figure 6.1) as well as the pRMX

with 4-holes mixing element. Experiments showed that the pRMX and μ RMX were capable to obtain droplet sizes very similar ($d_{\mu\text{RMX}} = 58 \text{ nm}$ and $d_{\text{pRMX}} = 68 \text{ nm}$). Concerning the particle diameter obtained with pRMX it was found identical to the droplet size, while for μ RMX potential coalescence during polymerization led to the increase of the particle's diameter. In both cases the increase of the number of cycles allowed the droplets and particles to decrease in size.

Finally, the less volatile thiol (EDDT) was examined using the pRMX that was equipped with the single hole mixing element. All the experiments were conducted under ambient atmosphere, since it was found to limit the premature polymerization due to the absence of the oxygen. The droplet diameter significantly decreased (from 170 nm to 119 nm) by the increase of the number of cycles from 5 to 300. Coalescence of the droplets was observed for the maximum number of cycles which could indicate that the miniemulsion was subject of the "over-processing" effect. The influence of the concentration of the Ostwald ripening and radical inhibitor, surfactant along with the type of the photoinitiator on the droplet diameter was also described. It is worth mentioning that the diameter was between 120 and 250 nm for all the experiments. Furthermore, the premature polymerization was calculated and found to be less than 35 % for all the experiments, what was very encouraging.

Comparison between this bi-functional thiol and the tetra-functional showed that the latter had a higher polymerization conversion. However, all thiol-ene systems appeared to be stable for one day of storage.

It was also important to compare all these results with the one obtained by using a more conventional emulsification device. As expected, the rotor-stator mixer gave rise to the larger droplet diameter ($d > 200 \text{ nm}$) and polydispersity ($\text{PDI} > 0.2$), which allowed to conclude that the elongational-flow devices were the most appropriate for controlling the size and reducing the polydispersity of the latex. Indeed, as it was described by Taylor, the simple shear flow (rotor-stator) is less effective in the droplet breakup as compared to the elongational flow.

2. Chapter 4: Development of a continuous pneumatic elongational-flow reactor and mixer

Development of a novel elongational-flow based device was done (Figure 6.2). This device had the same working principle than the pneumatic elongational-flow reactor and mixer, but with many differences. The main purpose was to develop a device that would be able to continuously infuse monomer solution, emulsify and then photopolymerize the droplets in order to obtain the latex. This home-made device was operating with the help of a software that was prepared in our lab. Unfortunately, due to many delays in the manufacture and software delivery induced by the Covid situation and some leakage problems, the device was not yet fully operational before the end of this thesis.

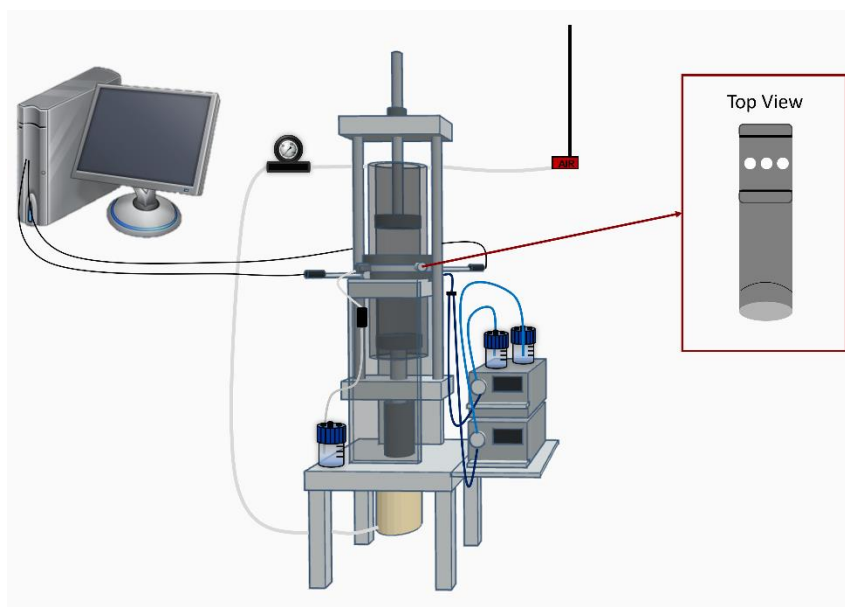


Figure 6.2. Left) schematic representation of the continuous pneumatic elongational-flow reactor and mixer (cpRMX), right) mixing element.

3. Chapter 5: Microfluidic device for thioether micron size particles

Finally, different thioether morphologies were produced by using a microfluidic process. Thioether microparticles with tunable sizes were synthesized. The two main parameters that influence the size were the flow rate and viscosity of the continuous phase. Two different capillaries were used (Inner Diameter = 100 and

75 μm) and the particles appeared slightly smaller when the smallest capillary was used, with the lowest diameter of 74 μm , which was equal to the capillary inner diameter. Additionally, a strong dependence on the capillary number ratio of the particle diameter was found. The higher the Ca_c / Ca_d (c: continuous phase, d: dispersed phase), the smaller were the particle diameter.

A successful attempt was also made to produce thioether microrods of 1551 μm length and 350 μm width (Figure 3).

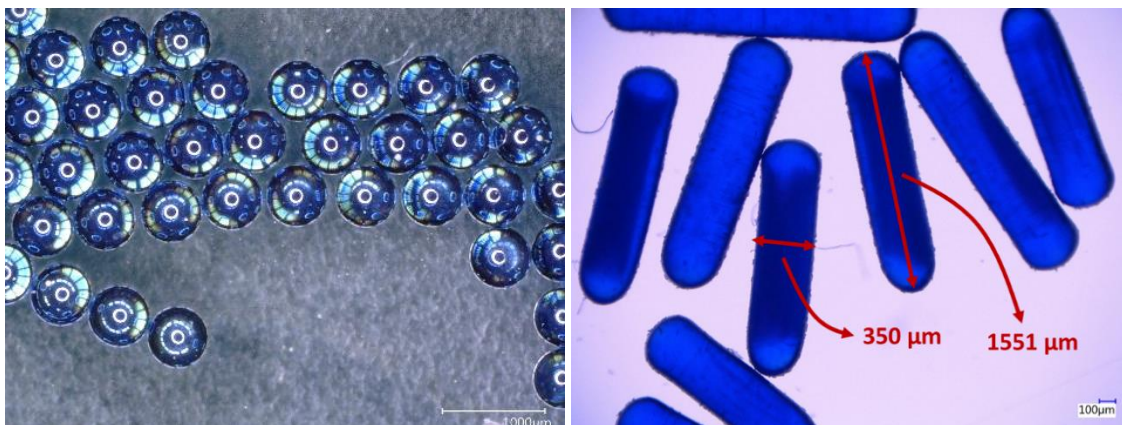


Figure 3. left) Numerical image of thioether 575 μm microparticles ($Q_d = 3 \mu\text{L}/\text{min}$, $Q_c/Q_d = 50$, $C = 0.5 \text{ wt}\%$); right) thioether microrods produced with $Q_c = 400 \mu\text{L}/\text{min}$ and $Q_d = 15 \mu\text{L}/\text{min}$

In summary, this thesis research showed the production of thiol-ene based **nano- and micro-droplets** whose size could be controlled by adjusting different process and chemical parameters. The elongational-flow devices that were developed in our lab also provide highly efficient emulsification as compared to a conventional rotor-stator mixer.

Perspectives

The elongational-flow based emulsification devices have significant advantages that could be used on laboratory as well as **industrial scale**. The improved diameter control can be achieved by consuming less energy as compared to conventional emulsification devices. The materials to be mixed can vary depending on the application, which could be either cosmetics, drugs or food.

A very promising method to simplify the process is the **continuous pneumatic elongational-flow reactor and mixer** that was developed. This way the production time will be reduced by operating in continuous mode, and the quality of the final product will be the same, since one raw material batch will be used. The solutions to be mixed can be of any of the aforementioned fields by tuning the final size of the product.

Beneficial could also be the online characterization of the miniemulsion and latex. For example, a Dynamic Light Scattering or Raman probe would be useful for the inspection of the characteristics of the product without the need of separate sampling. In this was a fully automated environmentally friendly process can be developed.

Finally, promising preliminary results were obtained with the used of coiled tube photoreactor to obtain a poly(thioether) solution and then emulsifying using the elongational-flow based device. This could allow the production of poly(thioether) latex without with a strict temperature control.

SCIENTIFIC PRODUCTION

A Articles

- (1) Eirini Skoufa, Christophe A. Serra, Michel Bouquey, Madeline Vauthier, Production of poly(thioether) nanoparticles using an elongational flow low energy miniemulsion process, Macromolecular Reaction Engineering, to be submitted

B Oral Communications

- (1) Eirini Skoufa, Madeline Vauthier, Michel Bouquey, Christophe A. Serra, Low energy miniemulsification device, International Colloquium of the French Polymer Society – GFP 2019, Mulhouse (France), November 2019
- (2) Eirini Skoufa, Madeline Vauthier, Michel Bouquey, Christophe A. Serra, Low energy elongational-flow device for the production of monomodal miniemulsions, PacificChem_2020, Honolulu (Hawaii), December 2021
- (3) Eirini Skoufa, Madeline Vauthier, Michel Bouquey, Christophe A. Serra, Low energy miniemulsification device, 1st Consortium Meeting ITN PHOTO-EMULSION, Mulhouse (France), October 2018
- (4) Eirini Skoufa, Madeline Vauthier, Michel Bouquey, Christophe A. Serra, Low energy miniemulsification device, 2nd Consortium Meeting ITN PHOTO-EMULSION, Mainz (Germany), October 2019
- (5) Eirini Skoufa, Madeline Vauthier, Michel Bouquey, Christophe A. Serra, Low energy miniemulsification device, 3rd Consortium Meeting ITN PHOTO-EMULSION, Freiburg (Germany), October 2020
- (6) Eirini Skoufa, Madeline Vauthier, Michel Bouquey, Christophe A. Serra, Low energy miniemulsification device, 4th Consortium Meeting ITN PHOTO-EMULSION, Mainz (Germany), October 2021

C Science Dissimination

- (1) Eirini Skoufa Fête de la Science, Strasbourg (France), November 2021

Poly(thioether) micro- and nanoparticles produced by low energy emulsification devices and continuous-flow photopolymerization

Résumé

Les nanoparticules de poly(thioéther) constituent une classe de nanomatériaux qui pourraient convenir à de nombreuses applications telles que la nanomédecine, les revêtements ou l'analyse. Cependant, leur développement est limité par le faible contrôle de leur taille et de leur dispersité induit par les dispositifs conventionnels de cisaillement utilisés pour l'étape d'émulsification. Au cours de cette thèse, deux nouveaux dispositifs d'émulsification cyclique discontinue travaillant à basse pression et basés sur un écoulement élongationnel d'une solution thiol-ène/eau ont été utilisés pour produire, en conjonction avec un photoréacteur à flux continu, des nanoparticules monomodales en taille. Une étude approfondie a été menée pour quantifier les variations des caractéristiques des nanoparticules en fonction des paramètres matériaux (fonctionnalité et nature du thiol, quantité de photoamorceur, d'inhibiteurs de maturation d'Ostwald et de radicaux) ainsi que des paramètres de procédé (géométrie de l'élément de mélange, nombre de cycles). En outre, un nouveau dispositif à flux continu a été conçu, qui pourrait permettre la production de latex de thioéther en des quantités pré-industrielles. Enfin, un dispositif microfluidique a été utilisé pour obtenir des microparticules et des microbâtonnets de thioéther de taille contrôlable. Des recommandations ont pu être extraites des expériences pour aider au réglage des paramètres du procédé afin d'obtenir des particules d'une taille spécifique.

Mots-clés : thioether, microfluidique, flux élongationnel, micromélange, microparticules, nanoparticules, microbâtonnets, latex

Abstract

Poly(thioether) nanoparticles composed a class of nanomaterials which could be suitable for many applications such as nanomedicine, coating or analytics. However, their development is impeded by the poor control on their size and dispersity induced by the conventional emulsification shear devices use for the emulsification step. In this research two batch novel cycling emulsification devices working under low pressure and based on the elongational-flow of a thiol-ene/aqueous solution were used to produce, in conjunction with a continuous-flow photoreactor, monomodal nanoparticles. A thorough study was conducted to quantify the variations of nanoparticles' characteristics with changes in material parameters (functionality and nature of the thiol, amount of photoinitiator, of Ostwald ripening and radical inhibitors) as well as process parameters (geometry of the mixing element, number of cycle). Additionally, a novel continuous flow device was designed that could allow the production of thioether latex in pre-industrial scales. Finally, one microfluidic device was used to obtain thioether microparticles and microrods with controllable sizes. Useful guidelines were returned to tune the process parameters for targeting a specific particle's size.

Keywords: thioether, microfluidics, elongational-flow, micromixer, microparticle, nanoparticle, microrod, miniemulsion, latex